Biosynthesis and characterization of polymers from cider by-products. Bacterial cellulose-based nanocomposites

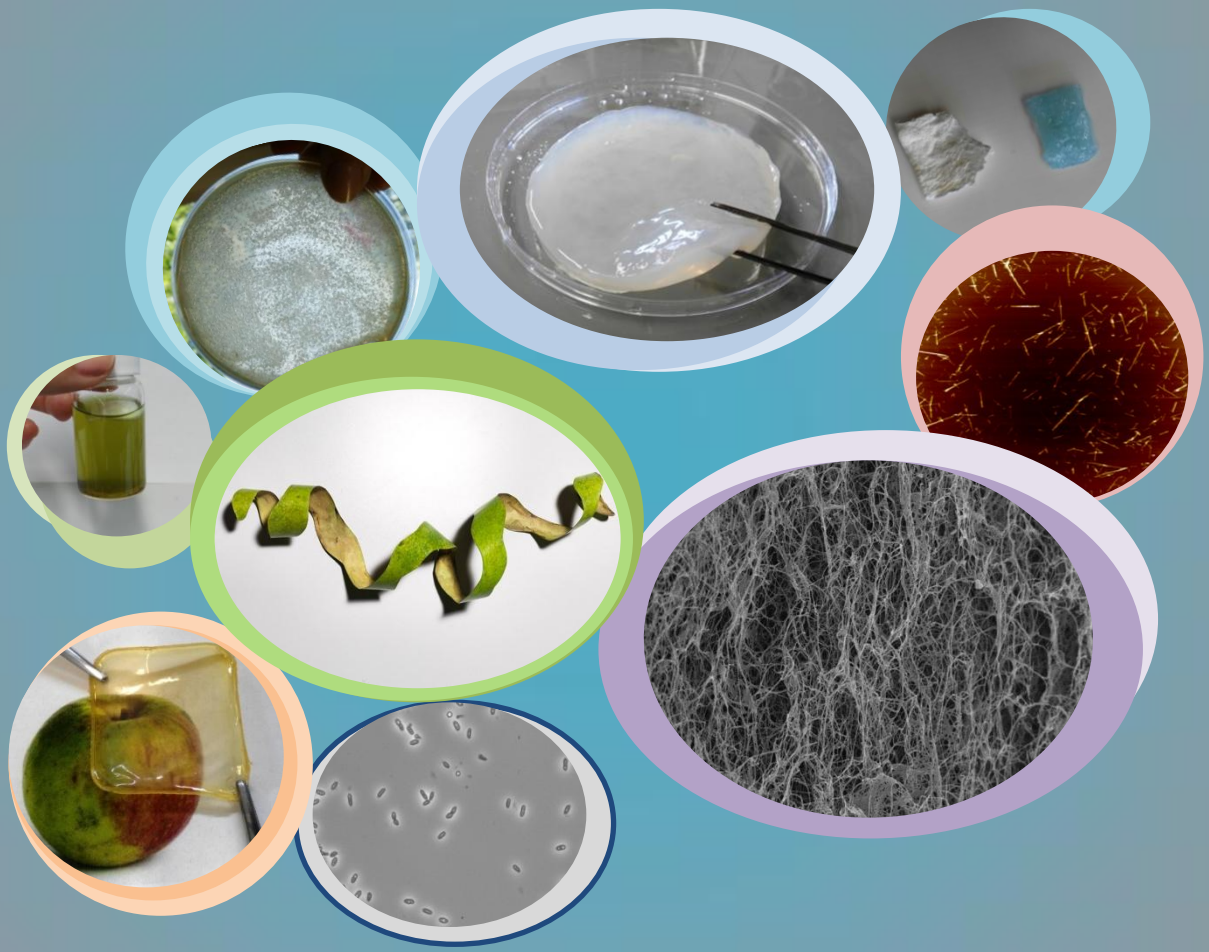

Universidad del País Vasco
Euskal Herriko Unibertsitatea

Leire Urbina Moreno

Donostia-San Sebastian, 2018

BIOSYNTHESIS AND CHARACTERIZATION OF POLYMERS FROM CIDER BY-PRODUCTS. BACTERIAL CELLULOSE-BASED NANOCOMPOSITES

PhD Dissertation presented by

LEIRE URBINA MORENO

Under the supervision of

Dr. MARIA ANGELES CORCUERA

Dr. ALOÑA RETEGI

Donostia-San Sebastian, December 2018

Ackowledgements

Ahora que me toca escribir esta parte de la tesis y hago balance de estos años, me he dado cuenta de que me llevo muchas personas y buenas experiencias. Este trabajo me ha ayudado a desarrollarme profesionalmente, pero mucho más de forma personal, y por ello quiero agradecer a toda la gente que ha estado conmigo de una u otra forma durante el camino.

En primer lugar, quisiera agradecer a mis directoras de tesis la Dra. Maria Angeles Corcuera y la Dra. Aloña Retegi por haberme brindado su confianza para llevar a cabo este trabajo y por haberme ayudado con sus conocimientos y experiencia durante estos años.

Por otra parte, me gustaría agradecer al Gobierno Vasco tanto por la ayuda económica concedida para realizar esta tesis doctoral (PIF PRE_2015_2_0009), como por la concesión de la beca de movilidad.

Asimismo, quisiera agradecer al Departamento de Ingeniería Química y del Medio Ambiente por facilitarme el uso de las instalaciones necesarias para llevar a cabo este trabajo y a los Servicios Generales (SGIker) de la UPV/EHU por el apoyo técnico proporcionado a lo largo de estos años. Especialmente quiero agradecer a la Dra. Loli Martín, técnico del servicio de Macroconducta-Mesoestructura-Nanotecnología, por su compromiso tanto técnico como humano, y por estar siempre dispuesta a echarme un cable.

Me gustaría agradecer a la Dra. Maria Auxiliadora Prieto del Grupo de Biotecnología de Polímeros, del Centro de Investigaciones Biológicas (CIB) del CSIC, por su apoyo técnico y humano durante mi estancia en su grupo de investigación. Quiero darle las gracias también a Ana, porque durante mi estancia en Madrid me ayudó muchísimo.

Igualmente quisiera dar las gracias al Dr. James Winterburn de la Escuela de Ingeniería Química y Ciencia Analítica de la Universidad de Manchester por haberme dado la oportunidad de trabajar en su grupo de investigación y haberme ayudado tanto durante mi estancia en Manchester. A todos mis compañeros durante mi estancia en Manchester por hacerme sentir una más. Especialmente a Anna, por ser un apoyo tan importante y estar siempre dispuesta a ayudarme y a Phavit, por esos momentos tan buenos en el laboratorio.

Quiero darle gracias a Marina por su ayuda tanto fuera como dentro del laboratorio y a Arantxa, por enseñarme los rincones de Alicante y por tratarme como una amiga, realmente fue lo que me llevé de allí.

Me gustaría también agradecer a todos mis compañeros del laboratorio, tanto los de mi Grupo "Materiales+Tecnologías" (GMT) del Departamento de Ingeniería Química y del Medio Ambiente (UPV/EHU) como los que no lo son, por su apoyo, risas y por ayudarme durante estos años. No voy a nombraros a todos, pero os tengo en mente. Tania, Jone y Alaitz, gracias por esos momentos divertidos durante las comidas que amenizan el día a día.

A mi amiga Vero, gracias por entenderme en cada momento de la tesis, por los pintxopotes, por los planes improvisados en Donosti y por hacer la vida fuera de casa mucho más fácil.

A mi amiga Olatz, gracias por ser mi apoyo constante. Porque hemos trabajado codo con codo, porque hemos pasado tanto lo bueno como lo malo de esta tesis juntas y cuando ha hecho falta nos hemos tomado unas cañas para verlo todo con otros ojos. Sin ti esto no hubiera sido lo mismo. Al resto de mis amigas, Ale, Yaiza y Nere, por hacer los buenos momentos el doble de buenos y darme la vida en los malos, porque sois uno de mis grandes apoyos en la vida. Parte de esta tesis es para vosotras cuatro.

Y por último quiero agradecer a toda mi familia, mis tíos y tías, mi amama... por el apoyo y la confianza que han tenido en mí durante esta etapa tan importante en mi vida. Recordaré siempre la pregunta que me han repetido en varias ocasiones y que siempre me ha sacado una sonrisa "¿qué tal van tus manzanas?". A Izaskun por saber escuchar, entenderme y darme siempre buenos consejos. A mis chicos, mi hermano y mi Aita, por apoyarme en cada paso del camino y por ser uno de mis motores para todo. Gracias por escucharme en todo momento y por intentar entender lo que os cuento aunque os suene un poco a chino. A tí Aita, que casi te hace más ilusión esta tesis que a mí. Parte de este trabajo es vuestro también.

A toda mi gente

Para mi Ama

SUMMARY

This work is focused on the utilization of by-products derived from cider production to obtain value-added products applying biotechnology concepts. The apple pomace has been used as a cheap and sustainable carbon substrate in bacterial fermentation processes to obtain biopolymers. Moreover, the obtained biopolymers have been fully characterized and used to prepare nanocomposites for different applications.

On the one hand, bacterial cellulose, an extracellular bacterial polysaccharide, was biosynthesized using *Komagataeibacter medellinensis* ID13488 bacterial strain. The optimal culture conditions to produce bacterial cellulose membranes using apple residues and sugar cane were investigated. The culture medium was analyzed in terms of pH, sugar and oxygen consumption. Bacterial cellulose membranes were characterized and their properties were compared to the ones obtained in commercial culture media.

Moreover, bacterial cellulose membranes were used for the development of different nanocomposites with tailored properties with potential applications in different areas: water cleaning processes, biomedicine and food packaging. Bacterial cellulose-based nanocomposites were developed by different techniques, i.e. *ex situ* and *in situ* modifications, infiltration and coating with other polymers. Furthermore, bacterial cellulose membranes were used as a source of cellulose nanocrystals. These were isolated by acid hydrolysis for the preparation of nanocomposites.

In addition, cider by-products were used to biosynthesize polyhydroxyalkanoates, bacterial intracellular polyesters, using *Psedomonas putida* KT2440 bacterial strain. Different strategies were used in

order to increase the biopolymer production and the extracted product was characterized. This polyhydroxyalkanoate was used as an hydrophobic coating in bacterial cellulose-based films with possible applications in food packaging.

Furthermore, cider by-products were used as a source of natural extracts with antioxidant properties. Apple extracts were extracted using different solvents and their antioxidant capacity was evaluated. In addition, these extracts were used for the development of bacterial cellulose-based films with antioxidant properties which could be suitable for food related applications.

The present work would imply an integral use and valorization of cider by-products to obtain value added materials. The proposed approach would provide viable and economically competitive processes for the production of bacterial polymers, which in turn, would result in low-cost and environmentally-friendly materials for advanced applications.

INDEX

CHAPTER 1

CHAPTER 2

CHAPTER 6

CHAPTER 7

CHAPTER 1

INTRODUCTION

1. INTRODUCTION

1.1 MOTIVATION

Nowadays, the development of the next generation of materials, products and processes is governed by the sustainability, green chemistry and eco-efficiency. Biopolymers and biodegradable plastics based on renewable agricultural and biomass feedstock can be considered a sustainable and eco-efficient alternative in markets currently dominated by products derived exclusively from fossil sources.

Bacteria can synthesize a wide range of biopolymers that serve diverse biological functions and have suitable properties for applications in numerous fields such as drug delivery, biomedicine, food products, environment and agriculture. Concretely, bacterial polysaccharides, such as bacterial cellulose (BC) and bacterial polyesters, such as polyhydroxyalkanoates (PHAs) exhibit physical and chemical characteristics that confer them diverse functional properties, non-toxicity, biodegradability and biocompatibility.

On the one hand, bacterial cellulose is an extracellular biopolymer produced by some kind of bacteria. These bacteria are capable to convert glycerol, glucose and other organic substrates into BC. It has some remarkable properties such as excellent mechanical properties due to the 3D network-like structure formed by cellulose nanofibers during its biosynthesis, high water holding capacity, high crystallinity and purity. In recent years, the investigation and utilization of BC in functional materials has been the focus of numerous research studies, as this material gives the oportunity to develop BC-based nanocomposites.

On the other hand, polyhydroxyalkanoates represent an important group of biodegradable plastics. These are produced by various bacteria as intracellular carbon and energy storage compounds and they differ in composition, molecular weight and other parameters. Concretely, *Pseudomonas* strains can use glucose, glucanoate, fructose and glycerol as carbon sources to produce medium-chain-length PHAs (mcl-PHAs) that contain 6–14 carbon atoms in their monomeric units. These mcl-PHAs exhibit elastomeric and adhesive properties, and also are biodegradable and biocompatible, features that make them interesting as biomaterials for several applications.

However, despite the enormous potential of these bacterial derived polymers in various applications, the high cost of production is the main drawback that hinders industrial implementation. Therefore, one of the major challenges to address in bacterial derived polymer technology is to find suitable carbon sources as substrates that are cheap and do not compete with food production for achieving large scale industrial applications. In this context, apple pomace is the main by-product of apple juice and cider production. The wet apple pomace is biodegradable and a voluminous waste with high water and fermentable sugar contents, so this induces a quick spoilage in landfills, and therefore, its disposal causes serious environmental problems. The apple pomace contains minerals and also a large amount of carbohydrates. Taking these features into account, cider by-products could be considered a good substrate for BC and mcl-PHA production. Additionally, apples are known as good sources of polyphenolic compounds (phenolic acid derivatives and flavonoids) with high antioxidant capacity and antimicrobial properties of great interest in active packaging.

Therefore, in this work, the viability of cider by-products from the Basque Country as a cheap and sustainable carbon substrate for BC and mcl-PHA production was demonstrated. The obtained biopolymers were characterized and used for the preparation of materials with tailored properties for specific applications in different fields. Additionally, the extraction of polyphenolic compounds was performed to develop films with antioxidant properties with potential applications in food packaging. The aim of the present work is to provide an alternative for the valorization of by-products from cider production by the development of an integrated procedure to obtain high value-added biopolymers applying biotechnology concepts.

1.2 CELLULOSE

1.2.1 Structure of cellulose

Cellulose is regardered as the most abundant biopolymer in nature. It is the main structural component in plants, but it can be found in animals and other microorganisms. It is defined as a semicrystalline polysaccharide macromolecule, a linear homopolymer of D-anhydroglucopyranose ($C_6H_{11}O_5$) units linked together by β-(1→4)-glycosidic bonds. Each glucose monomer of cellulose consists of three hydroxyl groups positioning at C_6 for the primary hydroxyl groups while at C_2 and C_3 for the secondary hydroxyl groups that can form intra and intermolecular hydrogen bonds. Therefore, due to this chemical constitution and spatial conformation cellulose presents highly ordered structure [1]. The molecular structure of cellulose is illustrated in **Figure 1.1**. As it is a semicrystalline biopolymer, it consists of both crystalline and amorphous regions. Crystalline organization and crystalline

degree strongly affect mechanical properties of cellulose fibers, the more crystalline the material, the higher mechanical performance. Depending on the source (wood cellulose, cotton cellulose, cellulose from natural fibers or cellulose from bacterial fermentation), arrangements of crystals in each cellulose fiber are different and thus, the mechanical properties of these fibers differ from one to each other [1].

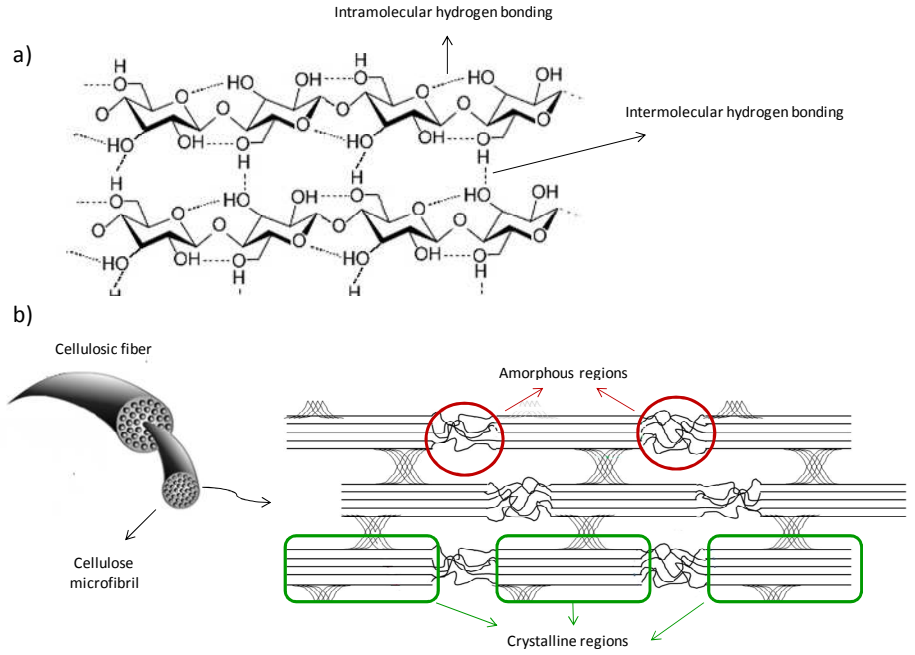

Figure 1.1 a) Molecular structure of cellulose and b) cellulose fibers arrangement.

In terms of crystallinity, cellulose displays six different polymorphs, namely, I, II, III_I, III_{II}, IV_I and IV_{II} with the possibility of conversion from one to the other as it can be observed in **Figure 1.2** [2]. Cellulose type I is the most abundant form in nature. The crystalline structure of cellulose I is a mixture

of two distinct crystalline structure forms: cellulose I_α (triclinic) and cellulose I_β (monoclinic). I_α is metastable and can be converted into I_β, and the conversion is usually accomplished through hydrothermal heating. Depending on the source of the cellulose, the relative abundance ratio of these two allomorphs varies. Cellulose I_β is the main constituent of the cellulose from plants, such as cotton, wood and ramie, while the cell walls of the green algae and bacteria are rich in the I_α allomorph [3]. Cellulose II can be prepared by two different distinct routes: mercerization (alkali treatment) and regeneration (solubilization and subsequent recrystallization) and, as it is energetically more stable than cellulose I, the process is irreversible. Celluloses III_I and III_{II} can be formed by treatment with liquid ammonia, and the reaction is reversible. Celluloses IV_I and IV_{II} can be obtained by heating celluloses III_I and III_{II}, respectively [4].

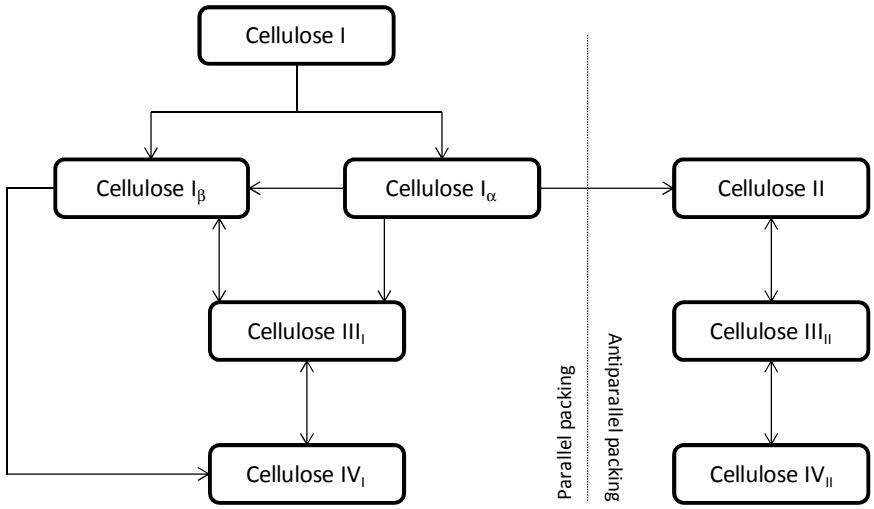

Figure 1.2 Conversion of cellulose polymorphs from one to the other.

1.2.2 Sources of cellulose

Cellulose is a promising material for the production of chemicals and cellulose-derived monomers and can be obtained from different sources. As commented above, cellulose is an important structural component of the cell walls of plants. In fact, vascular plants are the main industrial sources of cellulose. Textile fibers are usually isolated from cotton plant while most paper products originate from wood pulp [5]. There are other sources of cellulose such as natural fibers: sisal, hemp, corn, yute, flasks, rice and wheat straw. However, cellulose from lignocellulosic biomass forms a native composite material with lignin, hemicelluloses and pectin. Hemicellulose is strongly bound to cellulose fibrils presumably by hydrogen bonds, so the isolation of cellulose is achieved by strong chemical treatments that can affect cellulose structure [6].

Moreover, cellulose is also present in a wide variety of other living species such as algae, fungi and in some sea animals such as tunicates. Concretely, there is a type of cellulose named bacterial cellulose (BC) which is produced by some bacterial strains and it is attracting special attention. BC and plant cellulose present identical chemical structure, but BC presents higher purity and higher degree of crystallinity than plant cellulose. Moreover, BC forms characteristic ribbon-like fibrils which result in a morphology with interesting properties, especially outstanding mechanical properties [7]. These interesting features make BC promising for a wide variety of applications, therefore this work is centered in the biosynthesis of this type of cellulose.

1.2.3 Bacterial cellulose biosynthesis

BC is an extracellular biopolymer produced by Gram negative bacteria (characterized by their cell envelopes, which are composed of a thin peptidoglycan cell wall sandwiched between an inner cytoplasmic cell membrane and a bacterial outer membrane), strictly aerobic (require oxygen) and non-photosynthetic. Genera of BC producers include *Acetobacter, Rhizobium, Sarcina, Agrobacterium, Alcaligenes*, etc. They are usually found in fruits, vegetables, vinegar and alcoholic beverages and use glucose, glycerol and other organic subtrates for BC production [8,9]. BC is produced as a film in the air-liquid interface and it confers mechanical, chemical and biological protection within the natural habitat, so that the cells are trapped in the polymer network, which keeps the bacterial population at the air-liquid interface and thus allows the microorganism, a strict aerobic, to be close to the air.

Komagataeibacter (Acetobacter) xylinus (previously named as *Gluconacetobacter xylinus*) has been considered as model microorganism for basic and applied studies on cellulose [10]. Due to its ability to produce relatively high levels of polymer, it is the most commonly studied source of bacterial cellulose. In this work *Komagataeibacter medellinensis* strain was used, which is a parental strain. In these kind of bacteria, the cellulose synthesis occurs in two main stages: the first is the conversion of the carbon source in uridine diphosphoglucose (UDPGlc), which is the substrate used to produce cellulose and the second stage is the formation of cellulose and its secretion into the culture medium. The first step involves a specifically regulated multi-step process, involving a large number of individual enzymes and complex of catalytic and regulatory proteins [11]. The process starts with the formation

of UDPGlc, followed by glucose polymerization into the β-1→4 glucan chain and a nascent chain which forms ribbon-like structure of cellulose chains formed by hundreds or even thousands of individual cellulose chains. These are extruded out through tiny pores present on their cell envelope. These chains combine and form fibrils which further aggregate to form cellulose ribbons (nanofibers). Then, the ribbons generate a 3D network with plenty of spaces between the nanofibers that lead to a highly porous matrix with an expanded surface area [12]. **Figure 1.3** shows a schematic representation of BC biosynthesis process.

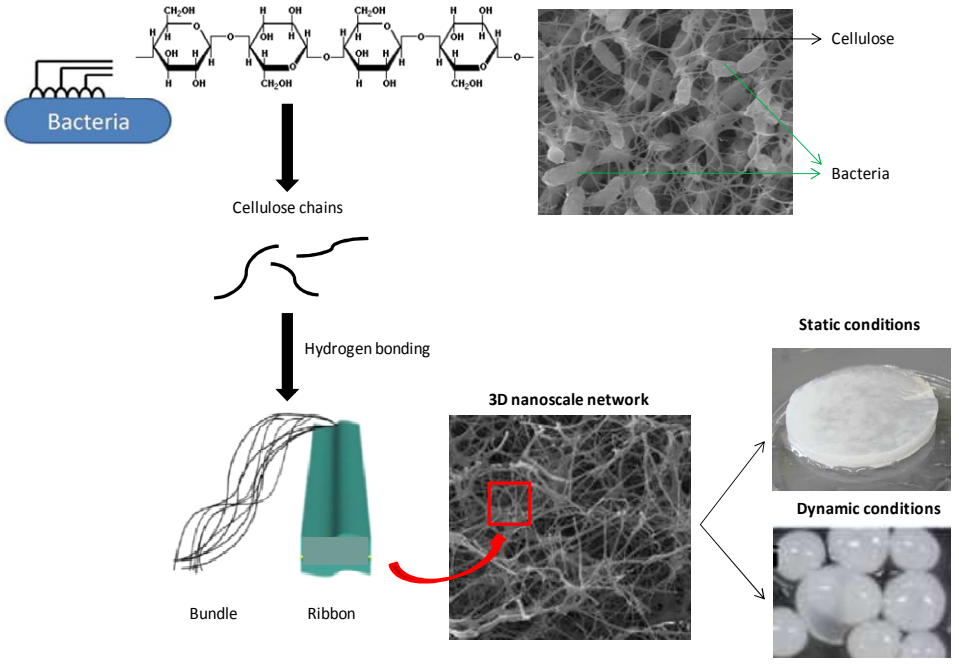

Figure 1.3 Schematic representation of BC biosynthesis.

The chemical structure of BC is composed by (1→4)-D-anhydroglucopyranose chains bounded through β-glycosidic linkages and its geometry is determined by the intramolecular and intermolecular hydrogen bonding network. Besides, the well arranged nanofiber conformation gives to BC interesting properties: high mechanical strength even at wet state, high crystallinity and water holding capacity and broad chemical modifying ability. Additionally, BC is chemically pure and biocompatible and biodegradable and offers the possibility to be molded into dimensional structures depending on the vessel shape used during its biosynthesis [13].

Among cellulose producer bacteria, a huge diversity can be found along the cellulose biosynthesis pathways, as well as differences in the nanostructure of the polymer or its chemical properties and crystallinity. From the genetic point of view, BC biosynthesis is due to four-gene bcsABCD (bcsA, bcsB, bcsC and bcsD) operon which was initially identified in *Komagataeibacter (Acetobacter) xylinus*. An operon is a functioning unit of DNA made of linked genes which regulates other genes responsable for protein synthesis. Products of the first two genes, bcsA and bcsB are essential for BC production. However, all four gene products are required for maximal cellulose production *in vivo*, indicating that bcsC and bcsD are involved in exporting the glucan molecules and packing them at the cell surface. There are genomic data reporting a great diversity of cellulose synthase operons which indicate significant differences in cellulose secretion mechanisms [14]. It has been reported that *Gluconacetobacter spp*. produces crystalline cellulose while *Salmonella typhimurium* and *Escherichia coli* produce amorphous cellulose as a component of their extracellular matrix [15].

1.2.4 Bacterial cellulose cultivation methods and conditions

In terms of cultivation method, there are two main fermentation techniques which provide BC with different morphologies: static and dynamic cultivation conditions. In static conditions, BC is produced as a gelatinous membrane at the air/liquid interface on the surface of culture medium, in which the cellulose is approximately 1% of the total weight. In contrast, in dynamic conditions, pellets or agglomerations of cellulose can be obtained with different shapes depending on the reactor and fermentation conditions [16]. Different morphologies depending on the cultivation method can be observed in **Figure 1.3**. In terms of productivity, static conditions usually give higher yields and higher crystalline BC, so this work is focused on the BC production in static mode.

Regarding culture conditions, BC production is a function of the oxygen supply, pH, temperature and the substrate used (carbon sources, which generally are saccharides). Fermentation process is normally carried out at around 28–30 °C and pH 3-6. Until date, the most used culture medium for BC production is the one developed by Hestrin and Schramm, known as H-S medium or standard medium, composed by D-glucose, peptone, yeast extract, sodium phosphate dibasic (Na_2HPO_4) and citric acid [17]. However, although traditionally BC is produced from culture media containing glucose as carbon source, the use of glucose and other commercial nutrient sources is not economically viable since results in high production costs, which limits the production at industrial scale and applications of BC. For this reason in recent years the studies have been focused on the developement of cost-effective carbon feedstocks from agroindustrial by-products and residues. Different residues have been tested for BC

production such as dry olive mill residues [18], wheat straw [19], waste beer yeast [20] and cheese whey, sulfite pulping liquor and crude glicerol [21], among others. Specifically, the use of fruit residues has resulted interesting for BC production as they contain high contents of carbohydrates. Pineapple wastes, grape pomace extract, papaya, orange, apple and pear juices have been used for BC production [22-25].

Furthermore, apart from making the BC production process more economic, the use of these residues has also a positive impact in the corresponding industry and in local and national economies since helps to decrease environmental problems associated with the disposal of the wastes and it can be considered a waste valorization alternative. Taking this into account, in this work the feasibility of using cider by-products for BC biosynthesis has been studied.

1.2.5 Applications of BC

As explained above, BC presents amazing physicochemical properties which make it interesting for a wide range of applications.

On the one hand, it can be considered a promising material in the production of a great variety of nanocomposites with designed functional properties. BC can be used as the whole membrane or as a source of nanoreinforcements such as nanofibers (CNFs) and nanocrystals (CNCs) [26,27]. CNCs and CNFs differ in terms of their production processes and structures, and can generally be isolated from a given cellulose source by mechanical, chemical, a combination of mechanical and chemical, or enzymatic processes [7]. CNCs concretely, are usually obtained by acid

hydrolysis with HCl or H_2SO_4. The acid treatment leads to the removal of the amorphous domains that are distributed along the fibers, and leads to the formation of cellulose nanocrystals (isolated from crystalline regions of cellulose represented **Figure 1.1**). As it is commonly known, the use of cellulose nanocrystals as a reinforcement in nanocomposites has numerous advantages and leads, in the proper concentration and dispersion, to an enhacement of the mechanical properties.

Furthermore, BC membrane possesses hydroxyl groups on the surface, so it can be easily modified with other polymers or additives to obtain different surface characteristics such as lipophilic or hydrophilic, magnetic and optical properties.

Besides, it has the possibility to be modified through *ex situ* and *in situ* methods. *Ex situ* methods consist on the modification of the purified BC by the impregnation technique to trapp, fix, coat or infiltrate the additive/polymer in the spaces between the nanofibers of the BC membrane. Using i*n situ* methods, BC-based composites can be obtained by the addition of some additives or soluble polymers to the culture medium so that the additive is incorpored into the BC growing nanofiber network during its biosynthesis. Some examples of additives or polymers are polyethylene glycol (PEG), poly(vinyl alcohol) (PVA), starch, chitosan, aloe vera and carbon nanotubes [28,13]. In presence of these additives, the pore size, elasticity or water holding capacity of the BC membrane can be modified. Algar et al. [30] prepared *in situ* BC/montmorillonite hybrid nanocomposites with improved thermal stability and water vapor and oxygen gas barrier properties with respect to neat BC membranes. Saibuatong and Phisalaphong [31] prepared *in situ* BC/aloe vera composite films and they

observed improved mechanical strength, crystallinity, water absorption capacity and water vapor permeability in comparison with the neat BC film.

Taking into account these interesting features and all the posibilities that BC offers, BC-based materials have been studied in many fields. In the food industry it has been considered a raw material for food as a water-binding, stabilizing and gelling agent and also a potential food packaging material [32]. Also, as it offers the possibility of being modified, sterification reaction or impregnation methods have been applied to obtain BC-based materials for food related applications with proper and enhanced barrier properties [33].

In the biomedical field, BC has also been studied for in *vitro* and *in vivo* applications in regenerative medicine, as wound dressing device, artificial blood vessels and tissue engineering [34]. In this area, it has been also used to develop transdermal or local delivery systems by loading different drugs into the BC structure [35]. Nonetheless, BC has no activity against bacterial infections so in order to achieve antimicrobial activity, different strategies have been developed such as the incorporation of silver nanoparticles [36].

Additionally, it has been proposed as a nanomaterial for sensors, photocatalytic nanomaterials, optoelectronic materials and devices, and magnetically responsive membranes [13].

Moreover, due to its three-dimensional network structure, BC may be better than plant cellulose in adsorption of heavy metal ions, so it has been studied for aplications in water cleaning processes for copper, lead, zinc or iron removal. In this case, in order to enhance the adsorption ability to heavy metal ions, different chemical modifications have been applied to BC. For

example, in order to incorporate functional groups or to enhance the substitution degree, grafting of diethylenetriamine and phosphorylation reaction have been applied to BC [37,38].

1.3 POLYHYDROXYALKANOATES

1.3.1 Biosynthesis of polyhydroxyalkanoates

Polyhydroxyalkanoates (PHAs), are biopolyesters synthesized by microorganisms as lipid inclusions for energy storage in granular forms within the cellular structure. A schematic representation of the biosynthesis process can be observed in **Figure 1.4**. PHA producer bacteria can be divided in two types. The first type of bacteria requires limitation of a nutrient during cultivation such as phosphorous, nitrogen, oxygen or magnesium to accumulate PHAs and they do not accumulate PHAs during the growth phase. In this group bacteria *Ralstonia eutropha*, *Pseudomonas oleovorans* and *Pseudomonas putida* can be found [40]. The second type of bacteria accumulates PHAs during the growth phase and do not require any nutrient limitation such as recombinant *Escherichia coli*.

The microorganism used, culture conditions and carbon source are factors which affect the monomeric composition and thus, influence the properties of these biopolymers [41]. In general, PHAs can be divided in two main groups: short-chain-length PHAs (scl-PHAs) which contain 3-5 carbon atoms and medium-chain-length PHAs (mcl-PHAs) that contain 6-14 carbon atoms in their monomeric units. Until now, most of the research related to the biosynthesis of PHAs has been focused on scl-PHAs, such as poly(3-hydroxybutyrate) (PHB) and related co-polymers. These are produced by a

wide variety of bacterial strains i.e. *Cupriavidus necator*, *Saccharophagus degradans*, *Caldimonas taiwanensis* or *Halopiles* [40]. These scl-PHAs resemble classical thermoplastics; hence, they compete with polyethylene, polypropylene, or polylactic acid. However, due to its crystalline nature, PHB is difficult to process [42]. On the other hand, mcl-PHAs are produced by *Pseudomonas* strains. It has been previously reported that these bacteria can biosynthesize saturated and unsaturated monomers, which in combination with long chains, leads to highly amorphous polymers [43-45]. Moreover, there are several studies that demonstrate the biocompatibility of these polymers [46,47].

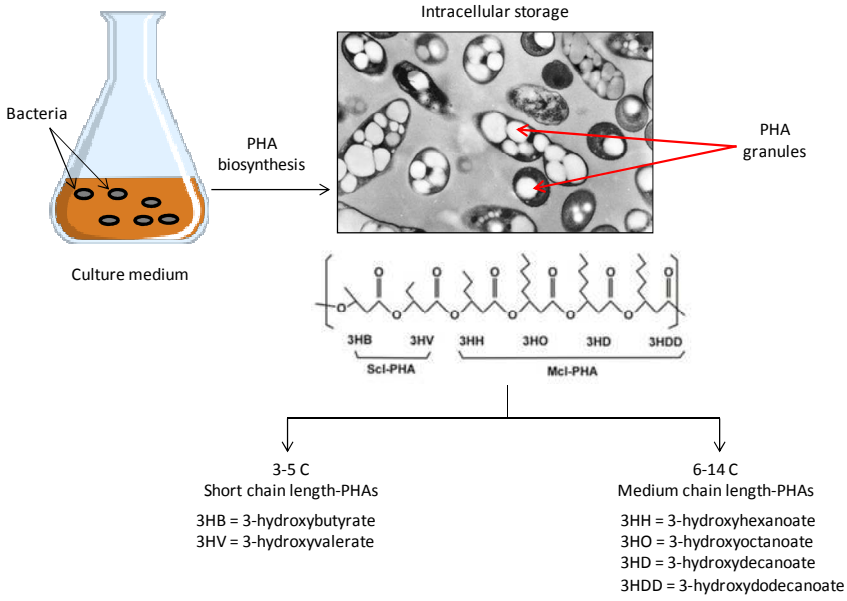

Figure 1.4 Schematic representation of PHA biosynthesis.

Pseudomonas strains show potential as they can assimilate a wide range of both, structurally related (fatty acids) and unrelated (glucose, glucanoate,

fructose and glycerol) carbon sources due to their catabolic versatility and genetic diversity. The structurally unrelated carbon sources are considered less toxic and less expensive than the fatty acids used so far, and their use in PHA biosynthesis can lead to a reduction of production costs opening up the possibility of large scale production [48]. In this context, agrowastes and residues from the food industry are good candidates for PHA production since they offer abundant and inexpensive carbon source. There is a large open field to convert food waste or by-products in PHAs and different wastes have been proposed to date, such as whey, starch, oils, spent coffee grounds, pea-shell slurry, etc [49,50]. Basnett et al. [51] used untreated biodiesel waste as a feedstock for *Pseudomonas mendocina* CH50 to produce PHAs and obtained a PHA yield of 39.5% composed of monomeric units from 6 to 12 carbons. Sugar wastes have also been tested for PHA production [52,53]. Hokamura et al. [54] used soybean wastewater with the recombinant *Pseudomonas sp*. 61-3 strain to produce co-polymers with short and medium length chains. Fruit pomaces and wastes such as apricots, cherries, grapes, date seeds or orange have been also studied for different PHAs production [55-57]. For this reason, in this work the possibility of using cider by-products for mcl-PHA biosynthesis has been analyzed using *Pseudomonas putida* KT2440 bacterial strain as it is the best characterized, nutritionally versatile and plant root-colonizing Gram negative bacterium.

1.3.2 Applications of mcl-PHAs

Until date, scl-PHAs have been more studied than mcl-PHAs, so nowadays the applications of the last are in development. Usually, mcl-PHAs present elastomeric behavior, i.e. present low crystallinity, low tensile strength and

high elongation at break with glass transition temperatures ranging from -50 to -25 °C and melting temperatures ranging from 40 to 65 °C [58]. They are considered as biological rubbers or latexes since they display latex-to resin-like properties and do not become brittle even far below the freezing point [59].

As mentioned above, these bioplastics are biocompatible so this makes mcl-PHAs and its copolymers an attractive alternative in the biomedical field for applications in which elastomeric and flexible materials are needed. scl-PHAs, like PHB, are hard and brittle in nature and are more suitable for hard tissue engineering or bone replacement materials, while mcl-PHAs are more attractive for heart valves, cardiac patches and other vascular applications, skin tissue engineering, wound healing and controlled drug delivery [60,61].

Additionally, PHAs have been studied for applications in nanotechnology. They present better adherence to natural nanofibres compared to conventional polyolefin matrixes so they can be used for the manufacturing of bionanocomposites [39]. In the food packaging area, they are considered an alternative to pretroleum-derived plastics as they are biodegradable. For this reason, mcl-PHAs are suitable for adhesive applications in friendly packaging. In fact, mcl-PHAs have been used for the development of hot melt biodegradable adhesives [62,63]. Based on their sticky character, the application of a thin layer attached on simple paper sheets has been proposed as an alternative to paper-plastic two-layer latex composite sheets as used in retail. Moreover, as they exhibit very low glass transision temperatures they can be interesting for storage of goods like foods under freezing conditions [64].

Finally, mcl-PHAs have been used in blends to improve the toughness and ductility of other polymers such as PHB [65]. Concretely, in the area of agriculture, mcl-PHAs have been used in blends with PHB to develop Nodax™, which can be used to manufacture biodegradable films to use as coatings for fertilizers, insecticides and herbicides [66]. Taking these features into account, in this work the biosynthesized mcl-PHA has been used as a coating for a nanoreinforced paper with possible applications in food packaging.

1.4 NATURAL EXTRACTS WITH ANTIOXIDANT PROPERTIES

As mentioned above, both BC and mcl-PHAs have potential applications in food related applications, as they are biodegradable and non-toxic. These food related applications include food packaging, food coating and encapsulation. Nowadays, the focus of reasearch is the "active packaging" or "intelligent packaging" [67]. This involves the development of packaging systems with advanced functions such as extension of self life or improvement of the quality of the food by the incorporation of components or additives in the packaging.

One of the main causes of spoilage of a great variety of foods, is the lipid oxidation. It causes a loss of both sensorial and nutritional quality of foods and may even lead to the formation of toxic aldehydes. One of the main regarded strategies to avoid this problem is the development of antioxidant active packaging. These antioxidant packages can be designed to act in two different ways: (1) releasing antioxidants to the food and (2) scavenging undesirable compounds from the headspace or from the food. Scavengers are substances that modify, trap or react with substances which are

involved in any step of the oxidation process [68]. Traditionally synthetic antioxidants have been used, but due to the fact that there is risk of potential toxicity from their migration to the food, in recent years the number of investigations related to the extraction and addition of natural extracts to coatings and packaging materials has increased [69-72].

These natural extracts are sources of antioxidant compounds, i.e. polyphenols and flavonoids, and are present in medicinal plants, fruits and vegetables [73]. These bioactive compounds are common constituents of the human diet and are secondary metabolites generally involved in defense against ultraviolet radiation or aggression by pathogens. Moreover, they present potential as dietary or food antioxidants and also have been related with the prevention of diseases associated with oxidative stress, such as cancer and cardiovascular and neurodegenerative diseases [74]. For these reasons, from the point of view of consumer´s health, the use of natural antioxidants and antimicrobials in the packaging is regardered as an alternative to synthetic substances. Concretely, apples are found to be one of the best sources of polyphenolic compounds. For this reason, in this work the extraction of polyphenolic compounds from cider by-products has been performed to evaluate their antioxidant capacity and possible use in food related applications.

1.5 VALORIZATION OF APPLE WASTE

Apples, one of the most consumed fruits worldwide, are among the major sources of phytochemicals and antioxidants in the human diet. The manufacturation of apple juice, cider, jam and vinegar involves considerable amounts of apple and thus, large volumes of residue named apple pomace

are produced [75]. This waste represents around the 25-30% of the weight of the original fresh fruit and consists of peel, core, seeds, calyx, stem, exhausted soft tissue and also discarded apples. On the one hand, wet apple pomace is a voluminous waste with high water and fermentable sugar contents and on the other hand, it is biodegradable with high levels biochemical oxygen demand. This involves a quick spoilage in landfills, so its disposal causes serious environmental problems. Apart from the traditional use as cattle feed (though only a small fraction is used in this manner), different possibilities have been considered to make good use of the apple pomace, such as compost, as a source of aroma an polyphenolic compounds, production of edible products or pectin and xyloglucan extraction [76,77]. Although the composition of the apple pomace varies depending on different factors, i.e. maturation and ripening of the fruits, it contains minerals and also a large amount of carbohydrates, of which about 70% are simple sugars, being fructose the predominant sugar, followed by glucose, sucrose, arabinose, galactose and xylose [78]. This makes apple pomace an interesting carbon substrate for fermentation processes with bacteria. Moreover, as commented above, apples (and their by-products) are known as good sources of phenolic acid derivatives (primarily hydroxycinnamic acid derivatives) and flavonoids (flavonols, flavanols such as catechins and proanthocyanidins, flavanones, flavones, dihydrochalcones and anthocyanins) that can be used in different fields such as cosmetics or food related applications [79]. In cider apples, particularly, these compounds can be found at high concentrations [80,81]. The extraction of these polyphenolic compounds can be performed by different procedures and the efficiency of the process depends on many factors such as extraction technique (Soxhlet, ultrasound, microwave or coventional maceration

method), solvent (acetone, ethanol, methanol, water) and others. Taking all this into account, the non-use or the discard of apple pomace of today's apple processing industry would mean a loss of resources.

In Spain, more than 20,000 tonnes of apple pomace are produced every year as a by-product of cider production, with Asturias being the largest producer, followed by the Basque Country [82]. A great amount of the by-products generated in this sector goes to landfill so, in this work the use of apple pomace as a main nutrient for the biosynthesis of BC and mcl-PHAs has been assessed applying concepts of biotechnology. In addition, the obtained biopolymers have been characterized and BC-based nanocomposites have been developed for different applications. Moreover, the use of this waste as a source of polyphenols could be an alternative for the valorization of by-products of the cider production. For this reason, in this work the extraction of apple polyphenols from cider by-products has been performed and the antioxidant capacity of the extracts has been analyzed. Subsequently, the extracts have been incorporated to films for the development of antioxidant food packaging materials. This would imply an integral use of this waste to obtain value added products. The schematic representation of this work which involves the integral use of cider by-products using biotechnological processes can be observed in **Figure 1.5**.

Figure 1.5 Schematic representation of this work.

1.6 GENERAL OBJECTIVES

The main objectives of this work were to assess the feasibility of using cider by-products from the Basque Country as the main substrate for bacterial cellulose and polyhydroxyalkanoate biosynthesis and the production of bacterial cellulose-based nanocomposites with tailored properties for potential applications in different fields: water cleaning processes, biomedicine and food packaging. Additionally, cider by-products were used to obtain natural extracts with antioxidant properties which were incorporated in BC-based films for possible food related applications.

In chapter 1 a brief introduction has been made to focus the topic of the research and to give an overview of the work. Moreover, the specifications of the employed raw materials and reactants, and characterization techniques used during the work are included in chapter 2. Therefore, the following points, summarize the main objectives of each chapter:

- In chapter 3 a culture process to produce BC using by-products of the cider production from the Basque Country was investigated. *Komagataeibacter medellinensis* strain ID13488 was used for the study. The optimun culture conditions for maximal BC production were stabished. The culture media were characterized in terms of pH, oxygen and sugars consumption. The physicochemical and mechanical properties, microstructure, crystallinity and water holding capacity of the biosynthesized BC membranes were analyzed and compared to those obtained in H-S commercial medium. Additionally, in collaboration with the Polymer Biotechnology Group of the Biological Research Center (CIB-CSIC), the expression level of the operon bcs (genes involved in BC biosynthesis) in apple residue containing medium respect to standard H-S medium was determined.

- In chapter 4 environmentally friendly membranes were prepared by *in situ* and *ex situ* routes based on BC as template and chitosan as functional entity, for the elimination of copper in wastewaters. The mechanical behavior, crystallinity, water holding capacity, morphology and copper removal capacity of these membranes were analyzed.

- In chapter 5 water-activated shape memory nanocomposites were prepared by the infiltration of a waterborne polyurethane dispersion

into BC membranes for biomedical applications. The mechanical performance, thermomechanical properties and water-activated shape-memory behavior were analyzed and the biocompatibility of the nanocomposites was assessed.

- In chapter 6 the technical feasibility of using cider by-products as a substrate for the production of medium chain length polyhydroxyalkanoates (mcl-PHAs) by *Pseudomonas putida* KT2440 was demonstrated. After the optimization of the culture medium, the biopolymer was extracted from the biomass and a detailed characterization was carried out.

- In chapter 7 BC-based films for potential food related applications with improved mechanical properties and hydrophobicity and antioxidant properties were developed. In the first section of this chapter, bacterial cellulose nanocrystals (BCNCs) were isolated from BC membranes. The study of the effect of various acid hydrolysis treatments on the morphology and thermal properties of the obtained BCNCs was carried out. Furthermore, in the second section of the chapter cider-waste extracts were obtained by Soxhlet extraction using different solvents and different pH treatments. The free radical scavenging capacity of the different extracts was assessed. In the last section of the chapter, BCNCs were incorporated into BC membranes by infiltration in order to obtain stiffer reinforced BC nanopapers. Then, the reinforced nanopapers were coated with the mcl-PHA synthesized in chapter 6 with different contents of antioxidant apple extracts. After the preparation of the nanocomposites, the morphological, mechanical and thermal

characterization was performed and the antioxidant capacity of the films was assessed.

- In chapter 8, general conclusions of the work as well as the proposed future works are presented.

1.7 REFERENCES

[1] Jawaid, M., Boufi, S., Khalil, A. (2017) Cellulose-reinforced nanofibre composites. Production, properties and applications. United Kingdom: Elsevier Woodhead.

[2] Azizi Samir, M.A., Alloin, F., Dufresne, A. Review of recent research into cellulosic whiskers, their properties and their application in nanocomposite field. Biomacromolecules 6 (2005) 612-626.

[3] Poma, A.B., Chwastyk, M., Cieplak, M. Coarse-grained model of the native cellulose Iα and the transformation pathways to the Iβ allomorph. Cellulose 23 (2016) 1573-1591.

[4] Park, S., Baker, J.O., Himmel, M.E., Parilla, P.A., Johnson, D.K. Cellulose cystallinity index: measurement techniques and their impact on interprering cellulase performance. Biotechnol. Biofuels. 3 (2010) 1-10.

[5] Lavanya, D., Kulkarni, P.K., Dixit, M., Raavi, P.K., Krishna, L.N.V. Sources of cellulose and their applications- a review. IJDFR. 2 (2011) 19-38.

[6] Li, X., Tabil, L.G., Panigrahi, S. Chemical treatments of natural fiber for use in natural fiber-reinforced composites: A review. J. Polym. Environ. 15 (2007) 25-33.

[7] Shaghaleh, H., Xu, X., Wang, S. Current progress in production of biopolymeric materials based on cellulose, cellulose nanofibers, and cellulose derivatives. RSC Adv. 8 (2018) 825-842.

[8] Castro, C., Zuluaga, R., Álvarez, C., Putaux, J.L., Caro, G., Rojas, O.J., Mondragon, I., Gañán, P. Bacterial cellulose produced by a new acid-resistant strain of *Gluconacetobacter genus*. Carbohydr. Polym. 89 (2012) 1033-1037.

[9] Belgacem, M.N., Gandini, A. (2008) Monomers, polymers and composites from renewable resources. Amsterdam: Elsevier Science.

[10] Lavasani, P.S., Motevaseli, E., Shirzad, M., Modarressi, M.H. Isolation and identification of *Komagataeibacter xylinus* from Iranian traditional vinegars and molecular analyses. Iran. J. Microbiol. 9 (2017) 338-347.

[11] Chawla, P.R., Bajaj, I.B., Shrikant, A.S., Singhal, R.S. Fermentative production of microbial cellulose. Food. Technol. Biotechnol. 47 (2009) 107-124.

[12] Shah, N., Ul-Islam, M., Khattak, W.A., Park, J.K. Overview of bacterial cellulose composites: A multipurpose advanced material. Carbohydr. Polym. 98 (2013) 1585-1598.

[13] Hu, W., Chen, S., Yang, J., Li, Z., Wang, H. Functionalized bacterial cellulose derivatives and nanocomposites. Carbohydr. Polym. 101 (2014) 1043–1060.

[14] Römling, U., Galperin, M.Y. Bacterial cellulose biosynthesis: diversity of operons, subunits, products, and functions. Trends. Microbiol. 23 (2015) 545-557.

[15] Zogaj, X., Nimtz, M., Rohde, M., Bokranz, W., Römling, U. The multicellular morphotypes of *Salmonella typhimurium* and *Escherichia coli* produce cellulose as the second component of the extracellular matrix. Mol. Microbiol. 39 (2001) 1452-1463.

[16] Petersen, N., Gatenholm, P. Bacterial cellulose-based materials and medical devices: current state and perspectives. Appl. Microbiol. Biotechnol. 91 (2011) 1277-1286.

[17] Hestrin, S., Schramm, M. Synthesis of cellulose by *Acetobacler xylinum*: II. Preparation of freeze-dried cells capable of polymerizing glucose to cellulose. Biochem. J. 58 (1954) 345-352.

[18] Gomes, F.P., Silva, N.H.C.S., Trovatti, E., Serafim, L.S., Duarte, M.F., Silvestre, A.J.D., Neto, C.P., Freire, C.S.R. Production of bacterial cellulose by *Gluconacetobacter sacchari* using dry olive mill residue. Biomass. Bioenergy. 55 (2013) 205-211.

[19] Chen, L., Hong, F., Yang, X-X., Han, S-F. Biotransformation of wheat straw to bacterial cellulose and its mechanism. Bioresour. Technol. 135 (2013) 464-468.

[20] Lin, D., Lopez-Sanchez, P., Li, R., Li, Z. Production of bacterial cellulose by *Gluconacetobacter hansenii* CGMCC 3917 using only waste beer yeast as nutrient source. Bioresour. Technol. 151 (2014) 113-119.

[21] Carreira, P., Mendes, J.A.S., Trovatti, E., Serafim, L.S., Freire, C.S.R., Silvestre, A.J.D., Neto, C.P. Utilization of residues from agro-forest industries in the production of high value bacterial cellulose. Bioresour. Technol. 102 (2011) 7354-7360.

[22] Algar, I., Fernandes, S.C.M., Mondragon, G., Castro, C., Garcia-Astrain, C., Gabilondo, N., Retegi, A., Eceiza, A. Pineapple agroindustrial residues for the production of high value bacterial cellulose with different morphologies. J. Appl. Polym. Sci. 132 (2015) 41237 (1-8).

[23] Cerrutti, P., Roldán, P., Martínez-García, R., Galvagno, M.A., Vázquez, A., Foresti, M.L. Production of bacterial nanocellulose from wine industry residues: importance of fermentation time on pellicle characteristics. J. Appl. Polym. Sci. 133 (2016) 43109 (1-9).

[24] Kurosumi, A., Sasaki, C., Yamashita, Y., Nakamura, Y. Utilization of various fruit juices as carbon source for production of bacterial cellulose by *Acetobacter xylinum* NBRC 13693. Carbohydr. Polym. 76 (2009) 333-335.

[25] Zahan, K. A., Hedzir, M. S. A., Mustapha, M. The potential use of papaya juice as fermentation medium for bacterial cellulose

production by *Acetobacter xylinum* 0416. Pertanika J. Trop. Agric. Sci. 40 (2017) 343-350.

[26] Legnani, C., Vilani, C., Calil, V.L., Barud, H.S., Quirino, W.G., Achete, C.A., Ribeiro, S.J.L., Cremona, M. Bacterial cellulose membrane as flexible substrate for organic light emitting devices. Thin. Solid. Films. 517 (2008) 1016-1020.

[27] Vasconcelos, N.F., Feitosa, J.P.A., da Gama, F.M.P., Morais, J.P.S., Andrade, F.K., Filho, M.M., Rosa, M.F. Bacterial cellulose nanocrystals produced under different hydrolysis conditions: Properties and morphological features. Carbohydr. Polym. 155 (2017) 425-431.

[28] Phisalaphong, M., Jatupaiboon, N. Biosynthesis and characterization of bacteria cellulose–chitosan film. Carbohydr. Polym. 74 (2008) 482-488.

[30] Algar, I., Garcia-Astrain, C., González, A., Martin, L., Gabilondo, N., Retegi, A., Eceiza. A. Improved permeability properties for bacterial cellulose/montmorillonite hybrid bionanocomposite membranes by *in-situ* assembling. J. Renew. Mater. 4 (2016) 57-65.

[31] Saibuatong, O-A, Muenduen Phisalaphong, M. Novo aloe vera–bacterial cellulose composite film from biosynthesis. Carbohydr. Polym. 79 (2010) 455-460.

[32] Shi, Z., Zhang, Y., Phillips, G.O., Yang, G. Utilization of bacterial cellulose in food. Food. Hydrocoll. 35 (2014) 539-545.

[33] Liliana C. Tomé, L.C., Brandão, L., Mendes, A.M., Silvestre, A.J.D., Neto, C.P., Gandini, A., Freire, C.S., Marrucho, I.M. Preparation and characterization of bacterial cellulose membranes with tailored properties surface and barrier properties. Cellulose 17 (2010) 1203-1211.

[34] Picheth, G.F., Pirich, C.L., Sierakowski, M.R., Woehl, M.A., Sakakibara, C.N., de Souza, C.F., Martin, A.A., da Silva, R., de Freitas, R.A. Bacterial cellulose in biomedical applications: A review. Int. J. Biol. Macromol. 104 (2017) 97-106.

[35] Stumpf, T.R., Yang, X., Zhang, J., Cao, X. *In situ* and *ex situ* modifications of bacterial cellulose for tissue engineering. Mat. Sci. Eng. 82 (2018) 372-383.

[36] Maneerung, T., Tokura, S., Rujiravanit, R. Impregnation of silver nanoparticles into bacterial cellulose for antimicrobial wound dressing. Carbohydr. Polym. 72 (2008) 43-51.

[37] Jin, X., Xiang, Z., Liu, Q., Chen, Y., Lu, F. Polyethyleneimine-bacterial cellulose bioadsorbent for effective removal of copper and lead ions from aqueous solution. Bioresour. Techol. 244 (2017) 844-849.

[38] Oshima, T., Kondo, K., Ohto, K., Inoue, K., Baba, Y. Preparation of phosphorylated bacterial cellulose as an adsorbent for metal ions. React. Func. Polym. 68 (2008) 376-383.

[39] Raza, Z.A., Abid, S., Banat, I.M. Polyhydroxyalkanoates: Characteristics, production, recent developments and applications. Int. Biodeterior. Biodegradation. 126 (2018) 45-56.

[40] Kourmentza, C., Plácido, J., Venetsaneas, N., Burniol-Figols, A., Varrone, C., Gavala, H. N., Reis, M. A. M. Recent advances and challenges towards sustainable polyhydroxyalkanoate (PHA) production. Bioeng. 4 (2017) 55-98.

[41] Saharan, B.S., Grewal, A., Kumar, P. Biotechnological production of polyhydroxyalkanoates: a review on trends and latest developments. Chin. J. Biotechnol. 2014 (2014) 1-18.

[42] Rydz, J., Sikorska, W., Kyulavska, M., Christova, D. Polyester-based (bio)degradable polymers as environmentally friendly materials for sustainable development. Int. J. Mol. Sci. 16 (2015) 564-596.

[43] Huijberts, G., Eggink, G., de Waard, P., Huisman, G. W., Witholt, B. *Pseudomonas putida* KT2442 cultivated on glucose accumulates Poly(3-hydroxyalkanoates) consisting of saturated and unsaturated monomers. Appl. Environ. Microbiol. 58 (1992) 536-544.

[44] Muangwong, A., Boontip, T., Pachimsawat, J., Napathorn, S. C. Medium chain length polyhydroxyalkanoates consisting primarily of unsaturated 3-hydroxy-5-cis-dodecanoate synthesized by newly isolated bacteria using crude glycerol. Microb. Cell. Fact. 15 (2016) 1-17.

[45] Sánchez, R. J., Schripsema, J., da Silva, L. F., Taciro, M. K., Pradella, J. G.C., Gomez, J.G.C. Medium-chain-length polyhydroxyalkanoic acids (PHAmcl) produced by *Pseudomonas putida* IPT 046 from renewable sources. Eur. Polym. J. 39 (2003) 1385-1394.

[46] Renard, E., Vergnol, G., Langlois, V. Adhesion and proliferation of human bladder RT112 cells on functionalized polyesters. IRBM. 32 (2009) 214-220.

[47] Yang, X., Zhao, K., Chen, G-Q. Effect of surface treatment on the biocompatibility of microbial polyhydroxyalkanoates. Biomaterials 23 (2002) 1391-1397.

[48] Leong, Y. K., Show, P. L., Ooi, C. W., Ling, T. C., Lan, J. C-W. Current trends in polyhydroxyalkanoates (PHAs) biosynthesis: Insights from the recombinant *Escherichia coli*. J. Biotechnol. 180 (2014) 52-65.

[49] Nielsen, C., Rahman, A., Ur Rehman, A., Walsh, M. K., Miller, C. D. Food waste conversion to microbial polyhydroxyalkanoates. Microb. Biotechnol. 10 (2017) 1338-1352.

[50] Patel, S.K.S., Kumar, P., Singh, M., Lee, J-K., Kalia, V.C. Integrative approach to produce hydrogen and polyhydroxybutyrate from biowaste using defined bacterial cultures. Bioresour. Technol. 176 (2015) 136–141.

[51] Basnett, P., Lukasiewicz, B., Marcello, E., Gura, H. K., Knowles, J. C., Roy, I. Production of a novel medium chain length poly (3-hydroxyalkanoate) using unprocessed biodiesel waste and its evaluation as a tissue engineering scaffold. Microb. Biotechnol. 10 (2017) 1384-1399.

[52] Da Silva, D., Antonio, R., Rossi, J., Pena, R. Production of medium-chain-length polyhydroxyalkanoate by *Pseudomonas oleovorans* grown in sugary cassava extract supplemented with andiroba oil. Food. Sci. Technol. 34 (2014) 738-745.

[53] Diniz, S.C., Taciro, M.K., Gomez, J.G.C., Pradella, J.G.C. High-cell-density cultivation of *Pseudomonas putida* IPT 046 and medium-chain-length polyhydroxyalkanoate production from sugarcane carbohydrates. Appl. Biochem. Biotechnol. 119 (2004) 51-70.

[54] Hokamura, A., Yunoue, Y., Goto, S., Matsusaki, H. Biosynthesis of polyhydroxyalkanoate from steamed soybean wastewater by a recombinant strain of *Pseudomonas sp*. 61-3. Bioeng. 4 (2017) 68-78.

[55] Follonier, S., Goyder, M.S., Silvestri, A-C., Crelier, S., Kalman, F., Riesen, R., Zinn, M. Fruit pomace and waste frying oil as sustainable resources for the bioproduction of medium-chain-length polyhydroxyalkanoates. Int. J. Biol. Macromol. 71 (2014) 42–52.

[56] Guzmán, F., Winterburn, J. Effect of limonene on the heterotrophic growth and polyhydroxybutyrate production by *Cupriavidus necator* H16. Bioresour. Technol. 221 (2016) 336–343.

[57] Yousuf, R.G., Winterburn, J. Date seed characterisation, substrate extraction and process modelling for the production of polyhydroxybutyrate by *Cupriavidus necator*. Bioresour. Technol. 222 (2016) 242–251.

[58] Muhr, A., Rechberger, E.M., Salerno, A., Reiterer, A., Schiller, M., Kwiecień, M., Adamus, G., Kowalczuk, M., Strohmeier, K., Schober, S., Mittelbach, M., Koller, M. Biodegradable latexes from animal-derived waste: Biosynthesis and characterization of mcl-PHA accumulated by *Ps. citronellolis*. React. Funct. Polym. 73 (2013) 1391-1398.

[59] Rai, R., Keshavarz, T., Roether, J.A., Boccaccini, A.R., Roy, I. Medium chain length polyhydroxyalkanoates, promising new biomedical materials for the future. Mater. Sci. Eng. R. Rep. 72 (2011) 29-47.

[60] Rai, R., Roether, J.A., Knowles, J.C., Mordan, N., Salih, V., Locke, I.C., Gordge, M.P., McCormick, A., Mohn, D., Stark, W.J., Keshavarz, T., Boccaccini, A.R., Roy, I. Highly elastomeric poly(3-hydroxyoctanoate) based natural polymer composite for enhanced keratinocyte regeneration. Int. J. Polym. Mater. 66 (2017) 326-335.

[61] Renard, E., Vergnol, G., Langlois, V. Adhesion and proliferation of human bladder RT112 cells on functionalized polyesters. IRBM. 32 (2009) 214-220.

[62] Noda, I. Nonwoven materials comprising biodegradable copolymers. WO1997004036 A1. The Procter & Gambre Company. 1997.

[63] Whitehouse, R.S., Zhong, L., Daughtry, S. Compositions comprising low molecular weight polyhydroxyalkanoates and methods employing same. US7094840 B2. Metabolix, Inc. 2006.

[64] Koller, M. Poly(hydroxyalkanoates) for food packaging: application and attempts towards implementation. Appl. Food. Biotechnol. 1 (2014) 3-15.

[65] Philip, S., Keshavarz, T., Roy, I. Polyhydroxyalkanoates: biodegradable polymers with a range of applications. J. Chem. Technol. Biotechnol. 82 (2007) 233-247.

[66] Noda, I., Green, P.R, Satkowski, M.M., Schechtman, L.A. Preparation and properties of a novel class of polyhydroxyalkanoate copolymers. Biomacromolecules 6 (2005) 580-586.

[67] Aguilar, M.R., San Román, J. (2014). Smart polymers and their applications. United Kingdom: Elsevier Woodhead.

[68] Gómez-Estaca, J., López-de-Dicastillo, C., Hernández-Muñoz, P., Catalá, R., Gavara, R. Advances in antioxidant active food packaging. Trends. Food. Sci. Technol. 35 (2014) 42-51.

[69] Medina-Jaramillo, C., Ochoa-Yepes, O., Bernal, C., Famá, L. Active and smart biodegradable packaging based on starch and natural extracts. Carbohydr. Polym. 176 (2017) 187-194.

[70] Manach, C., Scalbert, A., Morand, C., Remesy, C. Jimenez, L. Polyphenols: Food sources and bioavailability. Am. J. Clin. Nutr. 79 (2004) 727-747.

[71] López de Dicastillo, C., Bustos, F., Guarda, A. Galotto, M.J. Cross-linked methyl cellulose films with murta fruit extract for antioxidant and antimicrobial active food packaging. Food. Hydrocol. 60 (2016) 335-344.

[72] Ferreira, A.S., Nunes, C., Alichandra Castro, A., Paula Ferreira, P. Coimbra, M.A. Influence of grape pomace extract incorporation on chitosan films properties. Carbohydr. Polym. 113 (2014) 490-499.

[73] Wang, L., Dong, Y., Men, H., Tong, J. Zhou, J. (2013). Preparation and characterization of active films based on chitosan incorporated tea polyphenols. Food. Hydrocol. 32 (2013) 35-41.

[74] Selvaraj, K., Chowdhury, R., Bhattacharjee C. Isolation and structural elucidation of flavonoids from aquatic fern *Azolla microphylla* and evaluation of free radical scavenging activity. Int. J. Pharm. Pharm. Sci. 5 (2013) 743-749.

[75] Perussello, C.A., Zhang, Z., Marzocchella, A., Tiwari, B.K. Valorization of apple pomace by extraction of valuable compounds. Compr. Rev. Food. Sci. Food. Saf. 16 (2017) 777-796.

[76] Perussello, C., Zhang, Z., Marzocchella, A., Tiwari, B. Valorization of apple pomace by extraction of valuable compounds. Compr. Rev. Food. Sci. Food Saf. 16 (2017) 776-796.

[77] Shalini, R., Gupta, D.K. Utilization of pomace from apple processing industries: a review. J. Food. Sci. Technol. 47 (2010) 365-371.

[78] Kruczek, M., Gumul, D., Kačániová, M., Ivanišhová, E., Mareček, J., Gambuś, H. Industrial apple pomace by-products as a potential source of pro-health compounds in functional food. J. Microbiol. Biotechnol. Food. Sci. 7 (2017) 22-26.

[79] Du, W-X., Olsen, C.W., Avena-Bustillos, R.J., Friedman, M., McHugh, T.H. Physical and antibacterial properties of edible films formulated with apple skin polyphenols. J. Food. Sci. 76 (2011) 149-155.

[80] Zuriarrain, A., Zuriarrain, J., Puertas, A.I., Dueñas, M.T., Ostra, M., Berregi, I. Polyphenolic profile in cider and antioxidant power. J. Sci. Food. Agric. 95 (2015) 2931-2943.

[81] Pingret, D., Fabiano-Tixier, A.S., Bourvellec, C., Renard, C.M.G.C. Chemat, F. Lab and pilot-scale ultrasound-assisted water extraction of polyphenols from apple pomace. J. Food. Eng. 111 (2012) 73-81.

[82] Dineiro, Y., Valles, B., Picinelli, A. Phenolic and antioxidant composition of by-products from the cider industry: Apple pomace. Food. Chem. 117 (2009) 731-738.

CHAPTER 2

MATERIALS AND CHARACTERIZATION TECHNIQUES

2. MATERIALS AND CHARACTERIZATION TECHNIQUES

2.1 INTRODUCTION

In this chapter, the materials employed for the biosynthesis of bacterial cellulose (BC) and the medium-chain-length polyhydroxyalkanoate (mcl-PHA), and the preparation of their nanocomposites are described. The reagents used for the extraction of natural extracts from apple residues and isolation of bacterial cellulose nanocrystals are also described.

Moreover, the characterization techniques used for the analysis of the fermentation media and the determination of the characteristics of the obtained materials from the study of their physicochemical, structural, mechanical, thermal, morphological and other specific properties are detailed.

2.2 RAW MATERIALS AND REAGENTS

The main raw materials used for the biosynthesis of both BC and mcl-PHA were the apple residues (AR) collected from a cider producer of Gipuzkoa (Northen Spain) containing peel, seeds, core, stems, exhausted soft tissue and also discarded apples (**Figure 2.1**). In the case of BC biosynthesis commercial sugarcane (SC) was also used.

The reagents for the preparation of Hestrin & Shramm (H-S) commercial medium used as reference were: D-Glucose ($C_6H_{12}O_6$≥99.0%), yeast extract (≥89.0%), sodium phosphate dibasic (Na_2HPO_4≥99.0%) and citric acid ($C_6H_8O_7$≥99.5%) purchased from Sigma Aldrich (Missouri, USA), and peptone (≥85%) obtained by Panreac Applychem (Spain).

Figure 2.1 Cider by-products used in this work for BC and mcl-PHA biosynthesis.

The reagents for the determination of dissolved oxygen used for Winkled method potassium iodide (KI), normal maize starch, mercury (II) iodide (HgI_2), sodium thiosulphate pentahydrate ($Na_2S_2O_3{\cdot}5H_2O$) were supplied by Sigma-Aldrich (Spain), and sodium hydroxide (NaOH), sulphuric acid (H_2SO_4 96%wt), manganese sulphate monohydrate ($MnSO_4{\cdot}H_2O$) and potassium dichromate ($K_2Cr_2O_7$) were purchased from Panreac Applychem (Spain).

A medium molecular weight chitosan (Ch) (MMW= 6.4 x 10^5 (estimated at 25 °C in 0.3 M acetic acid/0.2 M sodium acetate trihydrated from intrinsic viscosity) with a degree of deacetylation (DD) of 77% (obtained from proton nuclear magnetic resonance (^{1}H NMR)) was used for the preparation of BC/Ch bionanocomposites. Acetic acid glacial (technical grade) and sodium acetate trihydrated were obtained by Panreac Applychem (Spain). Copper (II) nitrate trihydrate ($Cu(NO_3)_2{\cdot}3H_2O$, > 98%) was purchased by Scharlau. Ethylenediaminetetraacetic acid (EDTA, anhydrous, ≥99%) and glutaraldehyde (GA, grade II, 25% in H_2O) were purchased from Sigma-Aldrich (Spain).

Impraperm DL 3746 waterborne polyurethane (WBPU) with 37%wt of solids content and 87.1 ± 0.3 nm particle size and 0.083 ± 0.016 polydispersity

(calculated by light scattering) was kindly supplied by Covestro (Germany) and used for the preparation of BC/WBPU nanocomposites.

Sulphuric acid (H_2SO_4 96%wt) for isolation of bacterial cellulose nanocrystals was purchased from Panreac Applychem (Spain) and solvents for the extraction of apple waste extracts, ethanol (96%wt) and acetone (99%wt), were obtained from Sigma-Aldrich (Spain).

2.3 CHARACTERIZATION TECHNIQUES

2.3.1 Characterization of the fermentation media

2.3.1.1 Bacterial cellulose production

The determination of BC production was performed by gravimetric methods. For this, BC samples were weighted in dry state and values in g L^{-1} respect to the initial volume of culture media were calculated. The values were expressed as average of three measurements.

2.3.1.2 pH

The pH of the culture media for BC production was measured using a pH-meter GLP22 of Crison Instruments, which was calibrated with pH 4.00 and 7.00 buffer solution standards.

2.3.1.3 Winkler method

Winkler method is generally used to determine the concentration of dissolved oxygen (DO) in water samples, in this case in BC culture media. This method involves the treatment of the sample with an excess of

manganese (II),potassium iodide and sodium hydroxide. Oxygen in the water sample oxidizes iodide ion (I^-) to iodine (I_2) quantitatively. The amount of iodine generated is determined by titration with a standard thiosulphate ($S_2O_3^{-2}$) solution. The end point is determined by using starch as a visual indicator. DO is fixed by the addition of Mn (II) under basic conditions, resulting in a brown precipitate, manganic hydroxide ($Mn(OH)_3$). Prior to analysis, the sample is acidified to pH 1.0-2.5 with sulphuric acid. This causes the precipitated hydroxides to dissolve, liberating Mn (III) ions. Mn (III) ions oxidize previously added iodide ions to iodine. Iodine forms a complex (triiodide ion, I^{3-}) with surplus iodide ions. Iodine and the complex exist in equilibrium, thus I^{3-} serves as a reservoir of I_2. The iodine is titrated with thiosulphate. Iodine is reduced to iodide and the thiosulphate is oxidized to tetrathionate. The stoichiometric **Equations 2.1-2.5** for the reactions described above are:

$$Mn^{+2} + 2OH^- \rightarrow Mn(OH)_2 \qquad \textbf{(2.1)}$$

$$2Mn(OH)_2 + \frac{1}{2}O_2 + H_2O \rightarrow 2Mn(OH)_3 \qquad \textbf{(2.2)}$$

oxidation of Mn(II) to Mn(III)

$$2Mn(OH)_3 + 2I^- + 6H^+ \rightarrow 2Mn^{+2} + I_2 + 6H_2O \qquad \textbf{(2.3)}$$

oxidation of I^- to I_2

$$I_2 + I^- \overset{H^+}{\leftrightarrow} I_3^- \qquad \textbf{(2.4)}$$

$$I_3^- + 2S_2O_3^{-2} \rightarrow 3I^- + S_4O_6^{-2} \qquad \textbf{(2.5)}$$

oxidation of $S_2O_3^{-2}$ to $S_4O_6^{-2}$; reduction of I_3^- to I^-

The amount of dissolved oxygen (mg O_2 L^{-1}) in the culture media was calculated from the titration where one mole of O_2 reacts with four moles of

thiosulphate. Three samples of 25 mL were extracted from each culture at different incubation times and the dissolved oxygen was calculated following the **Equation 2.6**:

$$DO\ (mg\ O_2\ L^{-1}) = \frac{V_{thiosulph} \cdot N_{thiosulph}}{V_s} \qquad \textbf{(2.6)}$$

where $V_{thiosulph}$ is the volume of thiosulphate used to titrate the sample, $N_{thiosulph}$ is the normality of the thiosulphate solution and V_s is the volume of the sample.

2.3.1.4 Optical density

Total biomass over time (bacterial growth + PHA production) for PHA production was monitored measuring the optical density (OD_{600}) at 600 nm using a spectrophotometer, UV-mini1240 (Shimadzu, USA). 1-2 mL of the culture sample was transferred to an Eppendorf tube and centrifuged at 13000 rpm for 5 min at room temperature. The supernatant was stored at -20 °C prior to further analysis while the cell pellet was resuspended in 0.7%wt NaCl solution to measure the optical density.

2.3.1.5 Dry cell weight

The total biomass at the end of the fermentation for PHA production was estimated gravimetrically as dry cell weight (DCW). 5-10 mL of fermented broth obtained from shake flasks at the end of the fermentation was centrifuged at 5000 rpm for 15 min. The cell pellet was resuspended in a small quantity of distilled water and dried at 50 °C using labelled, dried and pre-weighted aluminium plates to estimate the final DCW.

2.3.1.6 Total nitrogen

The amount of total nitrogen (TN) in culture media for PHA production was determined using a total nitrogen analyser unit (TNM^{-1}) attached to a TOC-control V organic carbon unit (Shimazdu, Japan). An aliquot of 250 μL of solid-free supernatant extracted at different times from fermentation media of PHA production was diluted with distilled water to a final volume of 20 mL and filtered through 0.45 mm pore nylon filters from Sigma-Aldrich before analysis. Standards of potassium nitrate (KNO_3, from Sigma-Aldrich) were used for calibration.

2.3.2 Physicochemical characterization

2.3.2.1 Chromatographic techniques

2.3.2.1.1 High performance anion-exchange chromatography

The concentrations of glucose, fructose and sucrose in the culture media for BC production were determined using ionic chromatography system of Thermo Fisher Scientific (Dionex Ionic Chormatograph DX600) consisted of a Dionex CarboPac PA10 analytic and protective and IonPac ATC-3 columns and a pulsed amperiometric detection. The injection volume was of 10 μL and the flow rate of 1 mL min^{-1}. High Performance Anion-Exchange Chromatography with Pulsed Amperometric Detection technique (HPAE-PAD) was used for the measurements. The eluent gradient was 100 mM NaOH from 0-10 min, 100–200 mM NaOH from 10-40 min, 200 mM NaOH to 1M NaOH from 40-45 min and 1M NaOH to 100 mM NaOH from 45 to 55 min.

2.3.2.1.2 High performance liquid chromatography

The concentration of glucose and fructose in the supernatant collected from the samples at different cultivation times for PHA production was determined using Dionex Ultimate 3000 high performance liquid chromatography (HPLC) equipment. Samples were filtered using 0.45 μm nylon filters from Sigma-Aldrich prior to analysis. The refractive index intensity of the samples was measured using a RefractoMax 521 (ThermoFisher Scientific, UK) detector, set at 50 °C. Peak area and concentration were correlated using a calibration curve constructed by running standards of known concentration. An Aminex HPX-87H column was used to achieve the separation at a temperature of 50 °C. An isocratic flow of 0.6 mL min^{-1} was used with 5 mM H_2SO_4 as an eluent, and 20 μL injection volume was used.

2.3.2.1.3 Gel permeation chromatography

Gel permeation chromatography (GPC) was used to calculate weight average and number average molecular weights, $\bar{M}_w$ and $\bar{M}_n$, respectively, and polydispersity index (PI) of the biosynthesized PHA. A Thermo Scientific chromatograph, equipped with an isocratic Dionex UltiMate 3000 pump and a RefractoMax 521 refractive index detector was used. The separation was carried out at 30 °C within four Phenogel GPC columns from Phenomenex, with 5 μm particle size and 10^5, 10^3, 100 and 50 Å porosities, respectively, located in a UltiMate 3000 Thermostated Column Compartment. Tetrahydrofuran (THF, purchased by Scharlab) was used as mobile phase at a flow rate of 1 mL min^{-1}. Samples were prepared by dissolving the obtained

PHA films in THF at 1 wt% and filtering using nylon filters with a 0.45 μm pore size. $\overline{M}_w$ and $\overline{M}_n$ were referred to monodisperse polystyrene standards.

2.3.2.1.4 Gas chromatography-mass spectrometry

PHA quantification and monomeric composition was identified by gas chromatograpy-mass spectrometry (GC–MS) analysis of the methanolyzed polymer. Methanolysis was carried out according to modified method reported by Lageveen et al. [1]. In the fermentation experiments to quantify PHA production at the end of the process, 10 mg of final biomass were dissolved in 2 mL of chloroform ($CHCl_3$, purchased by Scharlab) and then 2 mL of a mixture of methanol and sulphuric acid (CH_3OH:H_2SO_4 (85:15 v/v) purchased by Scharlab) were added into the vial and incubated at 100 °C for 140 min, then cooled to room temperature. Around 1 mL of distilled water was added and vigorously vortexed with the resulting solution being allowed to stand for 10 min. The bottom organic layer was separated and filtered (nylon filters of 0.22 μm) into GC vials and remaining H_2O content was removed. To determine the monomeric composition of the PHA, 10 mg of extracted and purified PHA were dissolved in the reagent mixture (2 mL of CH_2Cl_2 and then 2 mL of CH_3OH:H_2SO_4 (85:15 v/v) mixture) and treated as above. About 2 μL of methanolyzed sample was automatically injected into the column (J&W 122-7032: 2724.40537 DB-WAX). Oven temperature was programmed at 40 °C for 2 min and then increased to 240 °C at 5 °C min^{-1} and maintained for 15 min.

2.3.2.2 X-ray diffraction

X-ray diffraction (XRD) patterns of different samples were measured using PHILIPS X'Pert Pro diffractometer, in theta-theta configuration secondary monochromator with CuKα (λ = 0.154 nm) and a solid state pixel detector, operating at 40 kV with a filament of 40 mA. The diffractrograms were collected in the region 2θ = 5° to 50°, where θ is the angle of incidence of the X-ray been on the sample. The crystallinity index (CI^{XRD}) was calculated using the empirical method described by Segal et al. [2] using the **Equation 2.7**.

$$CI^{XRD} = \frac{I_{200} - I_{am}}{I_{200}} \quad \textbf{(2.7)}$$

where I_{200} is the maximum intensity of the (200) lattice diffraction at ~2θ = 22.7° and I_{am} is the intensity scattered by the amorphous part of the sample (the location of the amorphous material intensity considered in this work was at ~2θ = 18°).

In the case of BCNCs, the crystallite size was determined by the Scherrer equation (**Equation 2.8**) using the method based on the width of the diffraction patterns [3]:

$$L_{h,k,l} = \frac{k \cdot \lambda}{\beta \cdot \cos \theta} \quad \textbf{(2.8)}$$

where $L_{h,k,l}$ is the size of crystallite (nm), k is the Scherrer constant (0.9), λ is X-ray wavelength (1.54 Å), β is the width at half height of the selected peak in radians and θ is the Bragg angle [4,5].

2.3.2.3 Viscosimetry

Polymerization degree (PD) of the different BC samples was calculated through intrinsic viscosity value [η] determined using the procedure described in ASTM D1795-96 standard method [6]. All experiments were performed using an Ubbelholde capillary viscosimeter and using cupriethylenediamine (CED, purchased by Sigma-Aldrich) as solvent. The intrinsic viscosity values were transformed to PD according to the Staudinger-Mark-Houwink empirical equation (**Equation 2.9**):

$$[\eta] = K \cdot PD^{a} \qquad \textbf{(2.9)}$$

where constants K and a are dependent on the polymer-solvent system used. For cellulose dissolved in CED these constants are determined as K = 2.28 and a = 0.76 for DP > 950 [7]. Three membranes synthesized in each culture medium were assessed.

2.3.2.4 Fourier transform infrared spectroscopy

Fourier transform infrared (FTIR) spectroscopy was used to identify the characteristic functional groups and hydrogen bonding interactions. This technique is based on irradiating the sample with an infrared light source. In this way the light adsorbed by the sample is reflected in the spectrum at different wavenumbers. Spectra were recorded using a Nicolet Nexus spectrophotometer provided with MKII Golden gate accessory (Specac) with diamond crystal at a nominal incidence angle of 45° and ZnSe lens. Measurements were run after averaging 32 scans with a resolution of 4 cm^{-1} in the range 4000 to 650 cm^{-1}.

Infrarred spectra were also used to estimate the crystallinity indexes (CI^{IR}) and the percentage of I_β allomorph of the BC samples and BCNCs. The crystallinity indexes (CI^{IR}) were estimated as the area ratio of the bands at 1427 and 893 cm^{-1} using the **Equation 2.10** [8].

$$CI^{IR} = \frac{A_{1427}}{A_{893}} \qquad \textbf{(2.10)}$$

where A_{1427} is the integrated area of absorbance band centered at 1427 cm^{-1} and A_{893} is the integrated area of absorbance band centered at 893 cm^{-1}.

The approximate percentage of I_β allomorph was estimated using the **Equation 2.11** [9].

$$I_\beta = \frac{A_{710}}{(A_{710}+A_{750})} \qquad \textbf{(2.11)}$$

where A_{710} is the integrated area of absorbance band centered at 710 cm^{-1} and A_{750} is the integrated area of absorbance band centered at 750 cm^{-1}.

2.3.2.5 Proton and carbon nuclear magnetic resonance spectroscopy

The chemical structure of the PHA was investigated using proton (^1H NMR) and carbon (^{13}C NMR) nuclear magnetic resonance. This technique is based on the application of an electromagnetic field and the analysis of the variation in the frequencies of proton or carbon nucleus. PHA samples were dissolved in deuterated chloroform ($CDCl_3$) prior to analysis. ^{13}C and ^1H NMR measurements were conducted with a Bruker Avance 500 spectrometer, equipped with a BBO probe with gradient in Z axis. The spectrum was recorded using the zg Bruker library at 125.77 MHz. For the ^{13}C NMR

measurements a time domain of 64 K was used in a spectral width of 31000 Hz. An interpulse delay of 2 s was employed for and acquisition time of 1.5 s averaging 32 K scans. For the ^{1}H NMR measurements a time domain of 64 K was used in a spectral width of 10000 Hz. An interpulse delay of 2 s was employed for and acquisition time of 3 s averaging 64 K scans.

2.3.2.6 Physical adsorption

Physical adsorption (physisorption) was used to determine and quantify specific surface area and average pore diameter of the compressed BC membranes and BC/Ch system. BET theory (Brunauer, Emmett and Teller) is based on multilayer physical adsorption of a gas (typically nitrogen) onto the surface of the solid to determine the specific surface area. In the case of porous materials, BJH method (Barrett-Joyner-Halenda) uses the modified Kelvin equation (**Equation 2.12**) to relate the amount of adsorbate removed from the pores of the material, as the relative pressure is decreased from a high to low value, to the size of the pores [10].

$$\frac{P}{P_0} = \exp\left(-\frac{2\sigma \cos \varpi \, V_M}{RT} \cdot \frac{1}{r}\right) \qquad \textbf{(2.12)}$$

where P/P_0 is the relative vapour pressure, σ is the surface tension, ϖ is the contact angle (which is assumed to be zero), V_M is the liquid molar volume, R is the Universal gas constant, T is the temperature and r is the radius of the pore.

Nitrogen adsorption-desorption isotherms were obtained at 77 K over the whole range of relative pressures using BET and BJH methods, respectively.

Samples were characterized using Autosorb 1C/TCD (Quantachrome, USA) after outgassing solid samples at 323 K for 24 h. Total pore volume was calculated at the relative pressure of adsorbate (**Equation 2.13**):

$$\frac{P}{P_0} = 0.976 \qquad \textbf{(2.13)}$$

2.3.2.7 Elemental analysis

Elemental analysis (EA) was performed using a Euro EA3000 Elemental Analyzerof Eurovector to determine: (1) the composition of BC/Ch system (C, H and N %) and (2) the sulphate groups anchored to BCNCs during the hydrolysis process (S %). Samples were measured by SCAB.PE.29.PR.10.02 method in solid state. In this way the sample is combusted in presence of oxygen and the resultant products are analyzed in a chromatographic column. Thereby, a thermal conductivity detector provides a signal of each element and the resulting signals, proportional to the amount of eluted gasses, are analyzed by Callidus® software which automatically provides the sample elemental composition report.

2.3.2.8 Conductometric titration

The concentration of sulphate groups anchored to BCNCs during the hydrolysis process was determined by conductometric titration (CT), using a CrisonEC-Meter GLP 31 conductometer calibrated with 147 µS cm^{-1}, 1413 µS cm^{-1} and 12.88 mS cm^{-1} standards. Samples were measured in triplicate at 25 °C using NaOH and HCl 10 mM for the titration. BCNCs were dispersed by 10 min sonication in a sonicator in a mixture of 25 mL water and 10 mL of 10 mM HCl, and the dispersion was subsequently titrated with 10 mM NaOH

[11]. The consumption of NaOH for the titration of the sample and the blank was measured and **Equation 2.14** was used, based on changes of conductivity, to determine the sulphur content (S (%)):

$$S\ (\%) = \frac{32 \cdot C \cdot V}{W} \times 100 \qquad \textbf{(2.14)}$$

where C is the concentration of NaOH, V is the volume required to titrate the sample (obtained after subtracting the volume required to titrate the blank) and W is the weight of the titrated BCNCs.

2.3.2.9 Ultraviolet–visible spectrophotometry

Opacity of BC/BCNC/PHA-extract systems was determined according to the method of Park et al. [12]. The film absorbance was measured at 600 nm using a UV spectrophotometer Shimadzu (UV-3600). The films were cut into a rectangle pieces and directly placed in a spectrophotometer test cell and an empty test cell was used as the reference. The opacity of the films was calculated by the following **Equation 2.15**:

$$O = \frac{Abs_{600}}{q} \qquad \textbf{(2.15)}$$

where O is the opacity, Abs_{600} is the value of absorbance at 600 nm and q is the film thickness (mm).

2.3.3 Thermal characterization

2.3.3.1 Differential scanning calorimetry

Differential scanning calorimetry (DSC) measurements were carried out in order to analyze thermal behavior of films. This technique is based on heat provided to a sample or a reference for maintaining the same temperature. Thereby, when the sample undergoes a thermal transition, the required heat for the sample will vary respect to the reference, and will be reflected in the thermograms. A Mettler Toledo 822e equipment provided with a robotic arm and an electric intracooler as the refrigerator unit was used. Aluminum pan containing sample (5-10 mg) was heated from -75 to 200 °C at a scanning rate of 10 °C min^{-1} in nitrogen atmosphere. Glass transition temperature (T_g) was determined as the inflection point of the heat capacity change, whereas melting temperature (T_m) and enthalpy (ΔH_m) were established as the maximum and the area under the endotherm peak, respectively.

2.3.3.2 Thermogravimetric analysis

In this technique, the degradation process of the sample was controlled by measuring the mass of the sample in a microbalance during a heating scan. Thereby, the evolution of the mass loss respect to the sample initial mass can be quantified. Measurements were performed by using a TGA/SDTA 851 Mettler Toledo instrument. Tests were run from 25 to 800 °C at a heating rate of 10 °C min^{-1}. These tests were carried out under nitrogen atmosphere in order to prevent the thermoxidative degradation. In the case of apple extracts tests were also carried out under oxygen atmosphere.

2.3.4 Mechanical and thermomechanical characterization

2.3.4.1 Tensile tests

Mechanical behavior of different samples was determined at room temperature. By this tecnique, the sample is subjected to a constant elongation rate where the sample is extended until failure. In this way, the equipment records the force and elongation values for the reflecting in stress-strain curves, where different characteristic properties of the materials are determined: maximum tensile strength (σ_{max}), Young's modulus (E) and elongation at break (ε_b). Depending of the system analyzed different testing machines were used. In all cases at least five samples were tested, being the average values reported.

- BC and BC/Ch system were analyzed in a Minimat 2000, Rheometrics Scientific with a 200 N load cell. Initial grip separation was set at 22 mm, and cross-head rate was set at 1 mm min^{-1} following ASTM D1708-93 standard procedure [13]. The samples were cut in 30 x 5 mm^2 rectangular specimens.

- BC/WBPU system was analyzed in a Universal Testing Machine (MTS Insight 10) with a load cell of 10 kN and pneumatic grips. Samples were cut in 30 x 5 mm^2 rectangular specimens following ASTM D1708-93 standard procedure [13]. For the determination of the Young's modulus (E), a crosshead rate of 0.5 mm min^{-1} was set using a video extensometer. Maximum strength and elongation at break were measured at a crosshead rate of 50 mm min^{-1} using also a video extensometer.

- PHA and BC/BCNC/PHA-extract system were analyzed in a Instron 5967 with a load cell of 500 N and pneumatic grips. Samples were cut in 30 x 5 mm^2 rectangular specimens following ASTM D1708-93 standard procedure [13]. In the case of the PHA, for the determination of the Young's modulus, a crosshead rate of 0.5 mm min^{-1} was set. Maximum tensile strength and elongation at break were measured at a crosshead rate of 20 mm min^{-1}. For the BC/BCNC/PHA-extract system a crosshead rate of 1 mm min^{-1} was used.

2.3.4.2 Dynamic mechanical analysis

In the dynamic mechanical analysis (DMA) a sinusoidal stress is applied and the strain response is measured by varying the temperature of the sample. The phase difference between the stimulus and response are used to determine the storage modulus (E') as well as loss modulus (E''), whose relation result in the tangent of phase angle (Tanδ). The thermomechanical stability of the PHA and BC/WBPU system were analyzed using an Eplexor 100 N analyser, Gabo equipment. Tensile mode measurements were carried out from -100 to 100 °C at a scanning rate of 2 °C min^{-1}. The static strain was established as 0.05 % and the operating frequency was fixed at 1 Hz.

2.3.5 Hydrophilicity

2.3.5.1 Water contact angle

The surface hydrophility of the BC/BCNC/PHA-extract films was anlyzed by static water contact angle (WCA). This technique is based on the deposition of a deionized water drop in the surface of the film in order to analyze the

equilibrium air-water-film contact angle value, which will depend on the chemical interactions between them. Measurements were carried out in a Dataphysics OCA20 equipment at room temperature. At least six contact angle values were averaged by dropping 2 μL of deionized water over the film surface.

2.3.5.2 Water holding capacity

For the swelling study of the different systems, three samples of each system were immersed in deionized water during 24 h at room temperature. At different time intervals, samples were removed from water, wiped with filter paper for free water removal and then weighed. The water holding capacity (WHC) was calculated using the **Equation 2.16**:

$$\text{WHC}\ (\%) = \left(\frac{W_{wet} - W_{dry}}{W_{dry}} \right) \cdot 100 \qquad \textbf{(2.16)}$$

where W_{wet} is the weight of swollen samples at different times and W_{dry} is the weight of the previously dried samples.

2.3.6 Morphological characterization

2.3.6.1 Atomic force microscopy

Atomic force microscopy (AFM) is a technique based on the interactions between the tip and the sample. The tip and sample attractive-repulsion forces create a deflection in the tip and the images are created by mapping the deflections in each point of the sample. This technique was used to determine the morphology of the surface of the BC membranes, BC/Ch

systems and BCNCs. AFM images were obtained using a Nanoscope IIIa scanning probe microscope (MultimodeTM Digital Instruments) with an integrated force generated by cantilever/silicon probes, applying a resonance frequency of about 180 kHz. Cantilevers had a tip radius of 5-10 nm and were 125 μm long. The morphology of BC membranes and BC/Ch system was studied in tapping mode. Samples of the membranes were cut in 5 x 5 mm^2 and stuck in mica. Otherwise, the analysis of the morphology of the BCNCs measurements was performed in peak force mode from spin-coated samples (Spincoater P6700). A drop of BCNC/water suspension was deposited onto mica and prepared by spin coating at 1200 rpm for 130 s. Water was removed before imaging the sample in a vacuum chamber for one week at room temperature. Diameter and length measurements of the samples were carried out from height images by the AFM software.

2.3.6.2 Scanning electron microscopy

Scanning electron microscopy (SEM) consists on irradiating the surface of the sample with a high-energy electron beam, in order to analyze the different signals obtained from the electron sample interactions. SEM was used to obtain images of the cross sections of BC membranes, BC/Ch system and BC/WBPU system. Prior to SEM assay, films were freeze-fractured with liquid nitrogen in order to expose the cross section of the film. Scanning electron microscope JEOL JSM-6400 was used with a wolframium filament operating at an accelerated voltage of 20 kV and at a working distance of 5-10 mm. Samples were coated with approximately 20 nm of chromium using a Quorum Q150 TES metallizer.

2.3.7 Oxygen permeability

The permeability is a property of the material which expresses the ability to let pass a fluid (liquid or gas) through itself. In this work, the barrier properties of the BC/BCNC/PHA-extract system were analyzed in terms of oxygen permeability (OP). The oxygen transmission rate of the samples was determined at 50% relative humidity (RH), 23 °C and 760 mm Hg using an OX-TRAN 2/21 equipment of Mocon following the ASTM 3985-10 [14]. In order to obtain the oxygen permeability, film thickness and gas partial pressure were considered in each case.

2.3.8 Biocompatibility

The *in vitro* biocompatibility of the BC membranes and BC/WBPU system was confirmed by cytotoxicity assay as well as adhesion tests (cell viability (Live/Dead)).

2.3.8.1 Cytotoxicity assay

Short-term cytotoxicity tests were performed in order to evaluate the presence and/or release of toxic degradation products. The extractive method (ISO 10993-11:2009) was used [15]. Cytotoxicity was assessed by PrestoBlue® (Invitrogen, USA), a resazurin-based solution that functions as a colorimetric cell viability indicator. For this assay, murine fibroblasts (L929 cells) were seeded into 96-well plates at a density of 4 x 10^3 cells/well in 100 µL of complete culture medium. After 24 h, the medium was replaced with 100 µL of negative control (complete medium), positive control (DMSO, 10 % in complete medium) or biomaterial´s extractive media and a 10% of PrestoBlue® was added. The optical density (OD) was measured at 570 and

600 nm in a spectrophotometer (Synergy HT spectrophotometer, Biotek, USA) at different time points (0, 24 and 48 h). The viability of the cells was calculated following the **Equation 2.17**:

$$\text{Viability (\%)} = \frac{[\text{Abs}]_{\text{sample}}}{[\text{Abs}]_{\text{negative control}}} \cdot 100 \qquad \textbf{(2.17)}$$

where $[\text{Abs}]_{\text{sample}}$ is the absorbance of the sample cells and $[\text{Abs}]_{\text{negative control}}$ is the absorbance of the negative control cells (in this case high-density polyethylene). All assays were conducted in triplicate and average values and standard deviations were estimated.

2.3.8.2 Cell adhesion

The analysis of cell long term adhesion was carried out by performing Live/Dead assays. Samples of 0.5 cm^2 were prepared (3 replicates for each sample) and prior to analysis the materials were sterilized. Neat BC was sterilized with ethanol 70% for 2 h, while BC/WBPU nanocomposite was sterilized under ultraviolet light for 30 min (to prevent the dissolution of the WBPU). Then, materials were washed 3 times with phosphate buffered saline (PBS from Sigma-Aldrich) and incubated in 500 µL of a complete medium (Dulbecco's modified Eagle's medium (DMEM) supplemented with sodium pyruvate 1mM, 1% of non essential amino acids, 1% penicillin-streptomycin and fetal bovine serum 10%) at 37 °C for 24 h. After pre-wetting, the medium was removed and 50000 cells (Murine fibroblasts L929) were seeded on the materials according to ISO 10993-11: 2009 [15]. After incubating for 90 min to ensure adhesion, PBS was added to the surrounding

wells to prevent drying. Finally, 500 μL of complete medium was added to the wells with materials.

Images of the samples were taken after 72 h, 7 and 14 days. The medium was removed and samples were washed with PBS three times. Subsequently, calcein-AM 4 mM and ethidium homodimer-1 in PBS were added. Calcein-AM ($\lambda_{ex}/\lambda_{em}$: 495/515 nm) reports the esterase activity of living cells emitting in green and homodimer-1 emits in red ($\lambda_{ex}/\lambda_{em}$: 493/630 nm), indicating the loss of integrity of the plasma membrane [16]. After incubating the samples in the dark at 37 °C for 20 min, the analysis was carried out in an Olympus LV500 confocal microscope (Olympus, Japan).

2.3.9 Antioxidant capacity

The antioxidant capacity of the apple extracts and BC/BCNC/PHA-extract system was analyzed by different methods. In the case of the extracts, a previous precipitation and filtration process was carried out prior to antioxidant analysis in order to remove possible insoluble compounds. The method followed was developed by Yang et al. [17] and consists on an ethanol precipitation (95%) for 24 h at 4 °C in order to eliminate possible interferences. 50 mg of each extract were dissolved in 20 mL of ethanol and after vortexing these were stored at 4 °C in the refrigerator for 24 h. Then, the solutions were centrifuged for 15 min at 5000 rpm and 4 °C and the final extracts were stored in a refrigerator until use. The antioxidant capacity of the extracts was determined by DPPH radical scavenging assay, ferric reducing antioxidant power assay (FRAP), ABTS radical scavenging assay and total phenolic content method (TPC) and all measurements were performed in triplicate.

Antioxidant activity of the BC/BCNC/PHA-extract films was determined by DPPH and ABTS assays. Pieces of film (~5 mg) and 2 mL of the working solution depending on the method used, were mixed [18]. All measurements were performed in triplicate. The antioxidant activity was determined by the percentage of inhibition of the DPPH and ABTS.

The absorbance measurements for determining the antioxidant capacity were performed in a spectrophotometer Biomate-3 UV-vis and all the reagents used for the determination of the antioxidant capacity were purchased by Sigma-Aldrich.

2.3.9.1 DPPH radical scavenging activity

The DPPH (2,2-diphenyl-1-picrylhydrazyl) radical assay was performed according to the method previously described by Wang et al. [19]. Trolox (6-hydroxy-2,5,7,8-tetramethylchroman-2-carboxylic acid) was used as a standard in the assay. A calibration curve was prepared in a concentration range of 10-100 mg trolox L^{-1}. 250 µL of extract or standard diluted with ethanol were added to 2 mL of DPPH solution (6.25 x 10^{-5} M) in methanol, and left to stand in the dark for 30 min at room temperature. The absorbance was then measured at 517 nm in 1 mL quartz cuvettes in UV-vis equipment.

In the case of the extracts, the results are expressed in mg trolox equivalent (TE) per g extract (mg TE/g extract) and in the case of the BC/BCNC/PHA-extract films by the percentage of inhibition of the DPPH given as (**Equation 2.18**):

$$\text{DPPH scavenging activity } (\%) = \frac{\text{Abs}_{\text{DPPH}} - \text{Abs}_{\text{s}}}{\text{Abs}_{\text{DPPH}}} \cdot 100 \qquad \textbf{(2.18)}$$

where A_{DPPH} is the absorbance value at 517 nm of the methanol solution of DPPH and A_s is the absorbance value at 517 nm of the DPPH assay solution.

2.3.9.2 FRAP assay

A modified version of the FRAP (ferric reducing antioxidant power) method was used [20]. Trolox was used as a standard in the assay and a calibration curve was prepared in a concentration range of 10–150 mg trolox L^{-1}. The working FRAP reagent was prepared by mixing 2.5 mL of TPTZ (2,4,6-tripyridyl-S-triazine; 10 mM in 40 mM hydrochloric acid), 2.5 mL of ferric chloride hexahydrate (20 mM) and 25 mL of sodium acetate buffer (0.3 mM, pH 3.6). The FRAP assay was carried out at 37 °C. 1800 µL of the FRAP reagent were mixed with 180 µL of water and 60 µL of apple pomace extract or standard diluted with ethanol. After 30 min, the absorbance at 595 nm was measured in UV-vis equipment. The results are expressed in mg trolox equivalent per g extract (mg TE/ g extract).

2.3.9.3 ABTS assay

ABTS radical cation, a blue chromophore, was produced after the reaction of the ABTS (2,2´-azinobis(3-ethylbenzothiazoline-6-sulfonic acid) diammonium salt with a 0.6 mM potassium persulfate solution (1:1) in the dark, for 16 h at room temperature [19]. Then the absorbance of the $ABTS^{\cdot+}$ solution was adjusted to 0.7 at 734 nm with ethanol. Trolox was used as a standard in the assay and a calibration curve was prepared in a

concentration range of 10-50 mg trolox L^{-1}. 250 µL of apple pomace extract or standard diluted with ethanol were mixed with 2 mL of the $ABTS^{\cdot+}$ solution and the absorbance of the samples was measured after 40 min at 734 nm in UV-vis equipment. Trolox was used as a standard in the assay.

In the case of the extracts the results are expressed in mg trolox equivalent per g extract (mg TE/g extract) and by the percentage of inhibition of the ABTS in the case of the BC/BCNC/PHA-extract films given as (**Equation 2.19**):

$$\text{ABTS scavenging activity } (\%) = \frac{\text{Abs}_{\text{ABTS}} - \text{Abs}_{\text{s}}}{\text{Abs}_{\text{ABTS}}} \cdot 100 \qquad \textbf{(2.19)}$$

where A_{ABTS} is the absorbance value at 734 nm of the ABTS control solution and A_s is the absorbance value at 734 nm of the ABTS assay solution.

2.3.9.4 TPC

The TPC (total phenolic content) method was adapted from the developed procedure by Diñeiro et al. [20]. Galic acid (GA) was used as a standard in the assay and the calibration curve was prepared in a concentration range of 5-400 mg GA L^{-1}. In a test tube, 0.1 mL of apple pomace extract or standard diluted with ethanol were mixed with 2 mL of a 20% Na_2CO_3 solution, 5 mL of H_2O and 0.5 mL of Folin-Ciocalteau reagent from Sigma-Aldrich. The absorbance was determined after 30 min at 40 °C at 765 nm by the calibration curve in UV-vis equipment. The results were expressed in mg of galic acid equivalent per g of extract (mg GA/g extract).

2.4 REFERENCES

[1] Lageveen, R.G., Huisman, G.W., Preusting, H., Katelaar, P., Eggink, G., Witholt, B. Formation of polyesters by *Pseudomonas oleovorans*: effect of substrates on formation and composition of poly-(R)-3-hydroxyalkanoates and poly-(R)-3-hydroxyalkenoates. Appl. Environ. Microbiol. 54 (1998) 2924-2932.

[2] Segal, L., Creely, J.J., Martin, A.E., Conrad, C.M. An empirical method for estimating the degree of crystallinity of native cellulose using the X-ray diffractometer. Text. Res. J. 29 (1959) 786-794.

[3] Patterson, A.L. The Scherrer formula for X-ray particle size determination. Phys. Rev. 56 (1939) 978-982.

[4] Sullivan, E.M., Moon, R.J., Kalaitzidou, K. Processing and characterization of cellulose nanocrystals/polylactic acid nanocomposite films. Materials 8 (2015) 8106-8116.

[5] Langford, J.I., Wilson, A.J.C. Scherrer after sixty years: A survey and some new results in determination of crystallite size. J. Appl. Crystallogr. 11 (1978) 102–113.

[6] ASTM, D1795-96 (1996). Test method for intrinsic viscosity of cellulose. Annual Book of ASTM Standards American Society for Testing and Materials, Philadelphia, USA.

[7] Marx-Figini, M. Significance of the intrinsic viscosity ratio of unsubstituted and nitrated cellulose in different solvents. Angew. Makromol. Chem. 72 (1978) 161-171.

[8] Oh, S.Y., Yoo, D.I., Shin, Y., Kim, H.C., Kim, H.Y., Chung, Y.S., Park, W.H., Youk, J.H. Crystalline structure analysis of cellulose treated with sodium hydroxide and carbon dioxide by means of X-ray diffraction and FTIR spectroscopy. Carbohydr. Res. 340 (2005) 2376-2391.

[9] Szymańska-Chargot, M., Cybulska, J., Zdunek, A. Sensing the structural differences in cellulose from apple and bacterial cell wall materials by Raman and FT-IR spectroscopy. Sensors. 11 (2011) 5543-5560.

[10] Sing, K. The use of nitrogen adsorption for the characterisation of porous materials. Colloid. Surf. A. Physicochem. Eng. Asp. 187 (2001) 3-9.

[11] Espinosa, S. C., Kuhnt, T., Foster, E. J., Weder, C. Isolation of thermally stable cellulose nanocrystals by phosphoric acid hydrolysis. Biomacromolecules 14 (2013) 1223-1230.

[12] Park, P., Je, J., Kim, S. Free radical scavenging activities of differently deacetylated chitosans using an ESR spectrometer. Carbohydr. Polym. 55 (2004) 17-22.

[13] ASTM, D1708-93 (1993) Test method for tensile properties of plastics by use of microtensile specimens. Annual Book of ASTM Standards American Society for Testing and Materials, Philadelphia, USA.

[14] ASTM, D3985-10 (2010). Standard test method for oxygen gas transmission rate through plastics film and sheeting using a Coulometric Sensor. Annual Book of ASTM Standards American Society for Testing and Materials, Philadelphia, USA.

[15] ISO, 10993-11-2009 (2009) Biological evaluation of medical devices, Part 11: Tests for systemic toxicity.

[16] Althouse, G.C., Hopkins, S.M. Assesments of boar sperm viability using a combination of two fluorophores. Theriogenology 43 (1995) 595-603.

[17] Yang, X., Yang, S., Guo, Y., Jiao, Y., Zhao, Y. Compositional characterisation of soluble apple polysaccharides, and their antioxidant and hepatoprotective effects on acute CCl_4-caused liver damage in mice. Food. Chem. 138 (2013) 1256-1264.

[18] Riaz, A., Lei, S., Akhtar, H.M.S., Wan, P., Chen, D., Jabbar, S., Abid, M., Hashim, M.M., Zeng, X. Preparation and characterization of chitosan-based antimicrobial active food packaging film incorporated with apple peel polyphenols. Int. J. Biol. Macromol. 114 (2018) 547–555.

[19] Wang, X., Li, C., Liang, D., Zou, Y., Li, P., Ma, F. Phenolic compounds and antioxidant activity in red-flesh apples. J. Funct. Foods. Part B. 18 (2015) 1086-1094.

[20] Diñeiro, Y., Suarez, B., Picinelli, A. Phenolic and antioxidant composition of by-products from the cider industry: Apple pomace. Food. Chem. 117 (2009) 731–738.

CHAPTER 3

BACTERIAL CELLULOSE BIOSYNTHESIS

3. BACTERIAL CELLULOSE BIOSYNTHESIS

3.1 INTRODUCTION

As explained in chapter 1, the high production costs derived from the expensive culture media traditionally used (commercial cultures such as Hestrin and Schramm medium (H-S)) for bacterial cellulose (BC) biosynthesis limit its applications. Therefore, the search of cheap carbon and nutrient sources is essential to overcome this limitation. The main objective of this chapter is to give an insight into agricultural waste utilization for BC biosynthesis. The optimal culture conditions to produce BC using by-products of the cider production from the Basque Country have been investigated applying concepts of biotechnology to relate the biosynthesis parameters with the characteristics of the obtained products.

The apple residue (AR) was mixed with sugar cane (SC) (AR/SC medium) in different ratios to analyze the BC production. Then, a complete study of the culture medium in terms of optimal pH and sugar and oxygen consumption was performed and the results were compared to those obtained in commercial cultures (H-S medium). Additionally, in collaboration with the Polymer Biotechnology Group of the Biological Research Center (CIB-CSIC), a microbiological study was performed to analyze differences in the expression level of genes involved in BC biosynthesis in AR/SC and H-S media. This chapter also includes the physicochemical, mechanical and morphological characterization of the BC obtained in AR/SC medium and the comparative study of its properties with the BC obtained in H-S medium.

The proposed approach could provide an economically competitive process for the production of BC in presence of cider waste which in turn, will

provide a potentially low-cost, environmentally-friendly material for advanced applications.

3.2 EXPERIMENTAL

3.2.1 BC biosynthesis

There are several bacterial strains which have the capacity to biosynthesize BC. In this work a bacterium from genera *Acetobacter* was used. *Komagataeibacter medellinensis* (*K. medellinensis*) strain ID13488 (CECT 8140) was isolated from vinegar broth fermentation [1] and kindly supplied by New Materials Research Group, Pontificia Bolivariana University of Medellin, Colombia. It was stored at 3 °C prior to reactivation and use in experiments. For the preparation of inocula, cells were reactivated in 80 mL of H-S standard medium, which was grown at 28 °C for 4 days. The H-S medium is composed of 2% (w/v) D-glucose, 0.5% (w/v) peptone, 0.5% (w/v) yeast extract, 0.27% (w/v) sodium phosphate dibasic (Na_2HPO_4) and 0.12% (w/v) citric acid. This medium was then transferred to 250 mL of identical medium in Erlenmeyer flasks, incubated as above and used to inoculate the apple waste juice media.

Prior to media preparation all the material was sterilized in the autoclave for 15 min at 121 °C. All the experiments were conducted in Erlenmeyer shake flasks with a working volume of 1/3 of the Erlenmeyer volume.

For standard growth conditions, bacterial cells were grown in Hestrin and Schramm medium. Apple residues/sugar cane medium was prepared dissolving sugar cane in distilled water at room temperature and mixing with apple residue filtered juice obtained from washed, crushed and squeezed apple residues collected from a cider producer of Gipuzkoa.

Culture media were sterilized as described above. BC membranes were biosynthesized in both, standard H-S and AR/SC media at 28 °C and pH 4 (H-S medium was adjusted with citric acid and AR/SC medium with acetic acid) for 13 days, under static conditions using 1% (v/v) of inoculum of the working volume. Then, BC membranes were purified by treating with KOH (2 wt%), for 24 h at room temperature in agitation, in order to remove non-cellulosic compounds. Finally BC membranes were thoroughly washed under running water until a complete neutralization (pH = 7) and stored at 5 °C in deionized water until utilization. The BC production procedure followed in this work is shown in **Figure 3.1**.

Finally, BC membranes were dried in an oven at 60 °C for 3 days between two teflon plates in order to avoid shrinkage and to completely remove the water before their characterization. All the samples were stored in a desiccator until use.

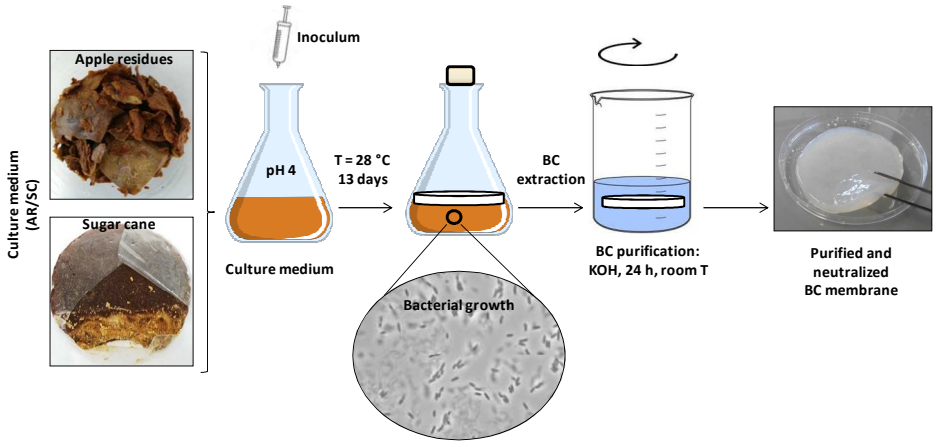

Figure 3.1 BC production process followed in this work.

3.3 RESULTS

3.3.1 Optimization of the culture medium for maximun BC production

As it has been previously reported, the yield of the BC production process depends on many factors such as pH, temperature, carbon source and relation of the surface area to the volume of substrate [2,3]. The cultivation time (13 days) was set taking into account the results obtained in previous work developed in our research group. In this previous study, BC was produced in a culture medium prepared with pineapple residues and sugar cane and BC production was analyzed at 7 and 13 days of cultivation [4]. The results showed that, in static conditions, the production increased 23% from the 7^{th} to 13^{th} day. Moreover, Castro et al. [1] reported that the optimum time for maximum cellulose production with this bacterial strain was from 8 to 13 days.

In order to study the BC production (expressed as g of dry BC per L of culture medium) using these residues, the first step was to adjust the ratio of sugars present in the AR/SC medium. For that, different quantities of sugar cane dissolved in water and apple residue juice, obtained from crushed and squeezed apple residues, were mixed. The production of BC in different culture media prepared varying the AR/SC ratio during 13 days at pH 4 and 28 °C was determined. Additionally, culture media with fresh apple peel from an apple of a commercial trademark and H-S standard media as control were prepared. **Table 3.1** gathers the production of BC in these different culture media.

Table 3.1 BC production in bacterial cultures prepared with different AR/SC ratios, H-S, AR and SC.

Culture	Apple residue/sugar cane ratio (w/w)	Production ($g\ L^{-1}$)
Fresh apple peel	1/2.3	1.50 ± 0.40
AR/SC (1)	1/2.3	1.40 ± 0.10
AR/SC (2)	0.5/2.8	2.00 ± 0.80
AR/SC (3)	2/1.3	1.20 ± 0.20
AR/SC (4)	1.5/2.3	2.50 ± 0.30
H-S	-	1.80 ± 0.60
Only AR	-	0.36 ± 0.01
Only SC	-	0.21 ± 0.06

The results suggest that the AR/SC mixture is suitable to be used for BC production with *K. medellinensis* as BC production was observed in all cases. BC production started to be observed between 72 and 96 h of cultivation due to the presence of a thin BC layer on the surface of the culture medium. It was observed that BC production in the media prepared with fresh apple peel and AR/SC (1) which were prepared with the same ratio was similar. Moreover, it can be noticed that in cultures AR/SC (2) and AR/SC (4) higher productions of BC were obtained than in the standard media (H-S). In previous works it has been reported that when glucose is the main carbon source, gluconic acid is produced during BC biosynthesis and this is not beneficial for BC production [5]. Keshk and Sameshima [6] reported that the presence of polyphenolic compounds with antioxidant nature in the culture medium prepared with non conventional carbon sources (lignosulphonate and sugar cane molasses) decreased the gluconic acid concentration leading to a higher BC production. As explained in chapter 1, cider apples are rich

in polyphenolic compounds with antioxidant properties, so the polyphenolic compounds which are probably present in the juice, may have influenced positively the BC production.

As control, cultures containing only AR and SC were also prepared. In both cases, BC production was observed although differences in the appearance and performance of the products were detected. In the case of the BC obtained from the culture prepared only with sugar cane, it showed a more viscous appearance while in the case of the BC obtained from the culture media prepared only with apple residues a more consistent and better formed membrane was observed. However, apple residue/sugar cane mixtures led to higher productions (**Table 3.1**) than only apple residues or only sugar cane, which means that is the combination of both nutrients which encourages the production of cellulose. Kurosumi et al. [7] investigated the BC production using fruit juices (apple, pineapple, orange, pear and grape) with and without the addition of nitrogen sources. They observed that in the case of the apple juice, BC yield was 19.5 times higher in the medium with nitrogen sources than in the medium without them. This could indicate that in the present work, the sugar cane enriched the apple juice with the nutrients that the apple may have not contain.

These results also suggest that the AR/SC ratio influences BC production. Differences in the BC production were observed depending on this ratio being optimal at 1.5/2.3 (AR/SC (4)). Additionally, in order to analyze the effect of AR content on BC production, three other AR/SC ratios were analyzed keeping constant the amount of sugar cane and increasing the amount of apple residue (3/2.3, 4.5/2.3 and 6/2.3) and maintaining the same conditions for BC biosynthesis. The results indicated that BC production was

slightly lower than in AR/SC (4), as it can be seen in **Figure 3.2**, so a decreasing tendency was observed when the apple residue content increased. In view of the results, AR/SC (4) medium was chosen as the optimum, so the subsequent characterization of this medium in terms of sugar and oxygen consumption was performed. Besides, the characterization of the BC membranes from this medium (AR/SC (4)) was performed.

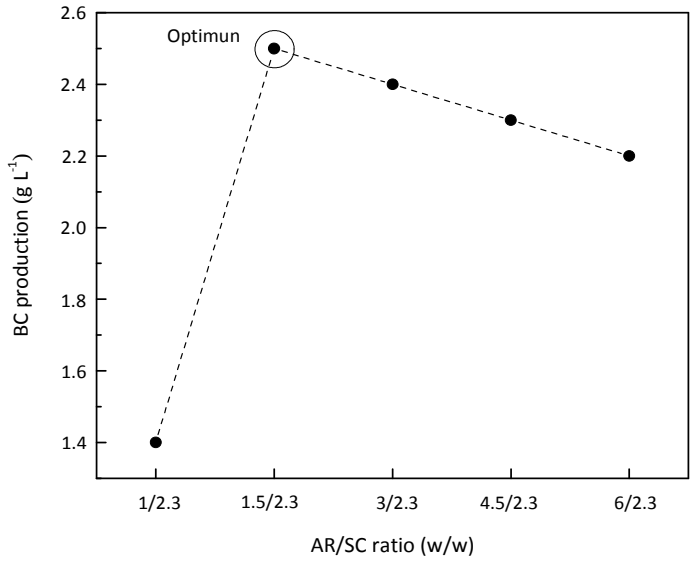

Figure 3.2 BC production in the cultures prepared with constant SC content and different AR contents.

Furthermore, BC biosynthesis is due to a four gene bcsABCD operon (bcsA, bcsB, bcsC and bcsD). Genes bcsA and bcsB are essential for the BC biosynthesis while genes bcsC and bcsD code proteins involved in the exporting of glucan molecules and pack them at the cell surface [8].

Therefore, it was of great interest to analyze if differences in the expression level of *bcs* operon in AR/SC versus H-S media were responsible of this different productivity. Total RNA of *K. medellinensis* cultures grown in AR/SC (4) and H-S media, at pH 4.0, was obtained and the relative changes of *bcsA* gene expression in H-S medium, when producing cellulose (after 7 days of culturing), respect to those obtained in AR/SC (4) medium (after 7 days of culturing) were calculated. It was found that the expression of *bcsA* mRNA was increased 1.5-fold times in AR/SC (4) medium respect to H-S medium. This result was in accordance and supported the results obtained in terms of BC production, as higher BC production was observed in AR/SC (4) medium than in H-S medium.

3.3.2 pH effect over cell growth and BC production

The pH of the growth medium is an important factor in the BC biosynthesis. Some authors found that for *Acetobacter xylinum*, the optimal pH interval is from 4 to 7 and temperature between 25 to 30 ^{o}C [9]. However, Kiziltas et al. [10] obtained the highest value of BC yield for a temperature of 28 ^{o}C and pH 8 using *Acetobacter xylinum* strain 23769. In this work, the culture media were prepared with cider apple residues. Among cider-specific apples, there are different varieties and each of them have certain levels of acid, tannin or sugars. In this case, the apple residue mixture resulted very acidic so it was of great interest to analyze the pH effect on the bacterial growth and BC production.

In this study, H-S medium was used as it is the most studied medium and it is used as a reference. Cells of *K. medellinensis* growing for 15 days at 30 ^{o}C, under static conditions, in H-S medium at pH 4.0, were used to inoculate

fresh liquid H-S adjusted at pH 4.0. After 15 days of incubation and under the conditions described above, the culture was able to produce BC pellicle with bacterial cells associated to the cellulose membrane. To release cells from the cellulose matrix and to obtain a uniform cell suspension, cultures producing cellulose were treated with cellulase [11]. These cultures were used to perform the following experiments.

To ascertain if the pH of the medium had any effect on the number of viable cells, cell viability was measured by plating of serial dilutions (10^{-2} to 10^{-6}) of the growing cells on H-S/agar medium adjusted at pH 4.0 or at pH 7.0. After that, plates were incubated at 30 ^{o}C for 32 h and total number of colonies/plate was counted. The obtained results are shown in **Table 3.2**.

Table 3.2 Colonies forming units (CFUs) obtained in H-S/agar plates at different pHs.

Dilution	CFUs/plate at pH 4.0	CFUs/plate at pH 7.0
10^{-2}	> 800	> 800
10^{-3}	102	5
10^{-4}	9	0
10^{-5}	1	0
10^{-6}	0	0

As it can be observed, the number of colonies forming units (CFUs) mL^{-1} obtained in plates with medium adjusted to pH 4.0 was 20 times higher than those obtained in plates with the medium adjusted at pH 7.0. The results demonstrated that acidic pH favoured cell viability under the tested conditions, which in this case was very convenient. Moreover, these results are in accordance with the ones reported by Castro et al. [1] with this

microbial strain since they observed a maximum BC production in acidic medium (pH 3.5).

3.3.3 Sugar consumption during BC biosynthesis

The concentrations of monosaccharides (glucose and fructose) and disaccharides (sucrose) in AR/SC medium were measured during BC biosynthesis. To evaluate the consumption of sugars, samples were taken at 0, 7 and 13 days of cultivation. **Figure 3.3** shows the mass of the three sugars (%) in the culture medium at 0, 7 and 13 days. The initial sugar composition of the medium was 5.2, 5.4 and 87.1 g L^{-1} of glucose, fructose and sucrose, respectively.

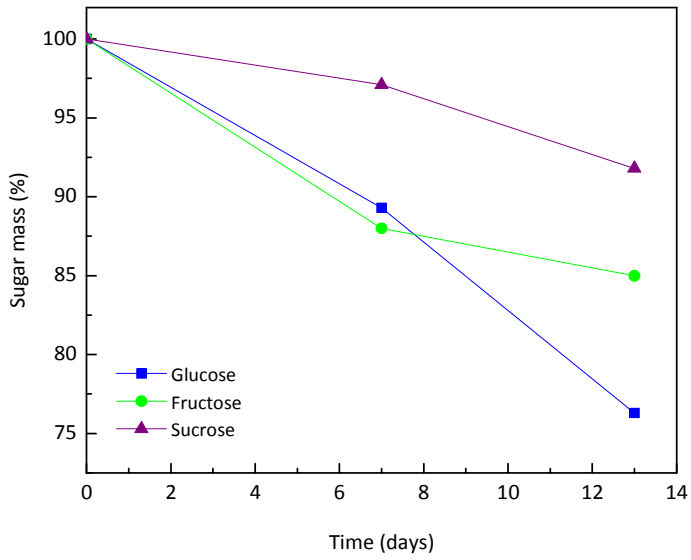

Figure 3.3 Variation of glucose, fructose and sucrose contents in the culture medium.

As it can be observed, there was a preferential consumption of glucose, as it was the most consumed sugar during 13 days, but all of them were metabolized simultaneously. Generally, glucose is the most consumed sugar in this type of bacteria and is consumed in the early stages of incubation. Moreover, BC yield from glucose-rich sources is higher than with other carbon sources [1,10,12]. This can be due to the fact that glucose is used for both, energy source and precursor for the assembly of the highly structured cellulose.

Castro et al. [1] reported that this bacterial strain was able to produce BC using different carbon sources, including fructose and sucrose. They observed that sucrose was the second most suitable carbon source for BC production after glucose. Keshk and Sameshima [12] tested the BC production using different carbon sources for *Gluconacetobacter xylinus* ATCC 10245 and observed that after 7 days of incubation, glucose was almost completely consumed while the consumption of fructose was <50%. They obtained high BC yield with glucose, followed by fructose and finally sucrose.

In the present work, the concentration of glucose decreased linearly from 5.2 to 3.9 g L^{-1}. In the case of the fructose, the decline was more pronounced in the first 7 days and then, little change was observed and something similar happened with the sucrose along the assay. This medium was rich in sucrose probably due to the sugar cane, while apple juice would have provided principally glucose and fructose. As described previously by other authors, when sucrose is the main carbon source, cellulose production starts later since it can not be transported through the cell membrane and needs to be hydrolized in the cell periplasm to glucose and fructose [13]. As

observed, sucrose was consumed at the same time as other sugars, so this may be the reason why in this study BC production started to be observed between 72 and 96 h of cultivation. Moreover, this is in accordance with the BC production results obtained with cultures prepared only with sugar cane and only with apple residues (**Table 3.1**). In the medium prepared only with apple residues, the BC membrane was more consistent than in the medium prepared only with sugar cane, probably because in the last, sucrose was the main carbon source and the bacteria needed longer time to metabolize it.

According to the results of **Figure 3.3**, no sugar depletion occurred in the medium after 13 days, but BC production after this period of time was practically null probably because of the production of inhibitory metabolites during the BC production such as glycolic and formic acids and others [10].

3.3.4 Oxygen consumption during BC biosynthesis

As explained in chapter 1, BC producer bacteria are strict aerobic, which means that the presence of oxygen during cultivation is a determining factor in BC production. In order to analyze the variation and consumption of oxygen in the cultures, Winkler method was used as explained in chapter 2, section 2.3.1.3.

Sample extractions of H-S and AR/SC media were carried out at 0, 2, 6, 8, 10 and 13 incubation days. The obtained results of concentration of dissolved oxygen (mg O_2 L^{-1}) with respect to cultivation time are displayed in **Figure 3.4**.

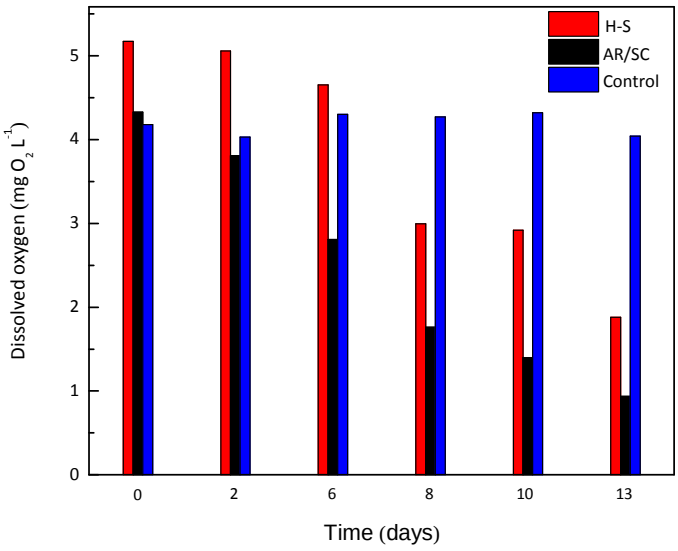

Figure 3.4 Dissolved oxygen at different cultivation days determined by Winkler method in H-S and AR/SC culture media and control.

The percentage reduction of dissolved oxygen (DO) was of 65% ± 2 in H-S medium and of 80% ± 2 in the AR/SC medium in 13 days. As control, the fermentation of the apple juice itself was considered as the cider production involves a natural fermentation of the apples. To analyze this, a medium without inoculum was prepared and the same procedure was followed to measure the dissolved oxygen over 13 days. No significant changes were detected in the oxygen consumption in this control medium (**Figure 3.4**). Dissolved oxygen values indicated that there was enough oxygen content in the medium to ensure bacterial activity as no depletion of oxygen occurred in 13 days.

3.3.5 Characterization of BC membranes

After the optimization and characterization of the AR/SC culture medium, a detailed characterization of the obtained BC membranes was performed and its properties were compared with the BC membranes obtained in commercial H-S culture medium.

3.3.5.1 Physicochemical characterization and crystallinity

Firstly, FTIR analysis of bacterial cellulose samples prepared from H-S, AR/SC, only sugar cane (SC) and only apple residues (AR) culture media was performed. The resultant spectra are shown in **Figure 3.5** where it can be observed the typical characteristic bands of cellulose I.

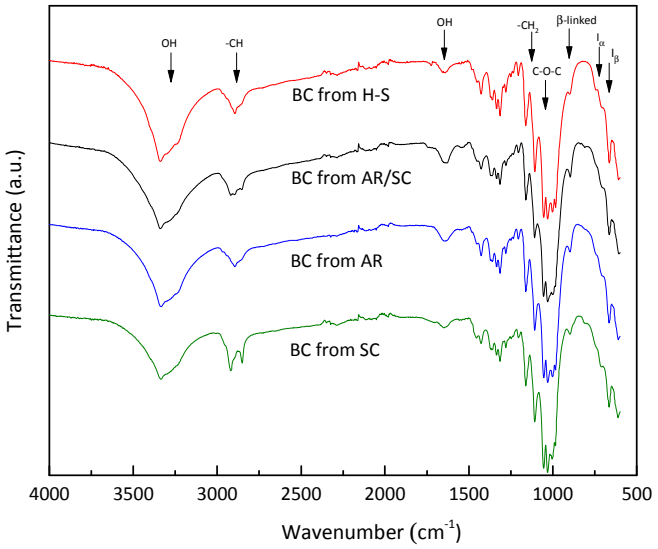

Figure 3.5 FTIR spectra of cellulose membranes from H-S, AR/SC, AR and SC culture media.

The bands around 3400 cm^{-1} correspond to OH cellulose stretching vibrations. The absorption bands at 2900-2880 cm^{-1} and 1460-1250 cm^{-1} are assigned to the CH and CH_2 stretching and bending vibrations, respectively. Furthermore, the bands at 1170-1050 cm^{-1} are associated with the vibrations of the C-O-C bond of the glycosidic bridges. The broad band at 897 cm^{-1} is characteristic of β-linked glucose based polymers. Finally, the band at around 1650 cm^{-1} is associated with the water absorbed by the cellulose [14].

These spectra show the characteristic bands of cellulose I allomorph as can be identified by the absorption bands at 1427 and 897 cm^{-1} [15]. As explained in chapter 1, the crystalline structure of cellulose I is a mixture of two distinct crystalline forms: cellulose I_α and I_β. Usually, in bacterial cellulose, the I_α structure is the dominant polymorph [16]. In this way, the bands at 750 and 710 cm^{-1} suggest the presence of cellulose I_α and I_β allomorph structures, respectively. The approximate percentage of I_β allomorph was estimated using the integrated areas of absorbance bands centered at 750 and 710 cm^{-1} **(Equation 2.11)**. It can be seen that the carbon source can affect the crystallization of cellulose I_α and I_β, being the percentage of I_β higher in the standard media than in the media prepared with non-conventional carbon sources (**Table 3.3**). Moreover the crystallinity indexes (CI^{IR}) were estimated from the ratio of the absorbance bands at 1427 and 897 cm^{-1} using the **Equation 2.10**. The results are gathered in the **Table 3.3.** The crystallinity of the BC obtained from the culture AR/SC increased with respect to the BCs obtained from cultures prepared only with sugar cane and only with apple residues. As discussed above, the different culture medium compositions have influenced the production and aspect of the obtained BC, and as expected, they have influenced the degree of order of

the polymer chains during BC biosynthesis which affects the crystallinity. Other authors have reported that the carbon sources and the additives can have an influence on the crystalline phase of the BC [17,18].

Table 3.3 CI^{IR}, approximate percentage of I_β allomorph and CI^{XRD} in different BC samples.

BC sample	CI^{IR}	I_β	CI^{XRD}
From H-S	2.30	0.59	0.87
From AR/SC	5.36	0.39	0.89
From AR	2.10	0.32	-
From SC	2.20	0.19	-

Additionally, the crystallinity of the BC from H-S and AR/SC media was also analyzed by X-ray diffraction. XRD patterns of the different BC samples are shown in **Figure 3.6**. The I_α one-chain triclinic unit cell presents three main peaks with Miller indices of (100), (010) and (110) while for I_β the Miller indices are defined as $(1\,\bar{1}\,0)$, (110) and (200) [19]. In this case, the patterns were indexed based on I_α, as it was considered more prevalent in BC. In both diffractograms two main peaks can be observed at 14.6° and 22.7°, which correspond to (100) and (110) crystallographic planes and are associated with cellulose I which agrees with the results of the FTIR spectra [20,21]. The CI^{XRD} were calculated using the **Equation 2.7**, taking into account that in this case, the maximum intensity would be the one of the (110) lattice diffraction.

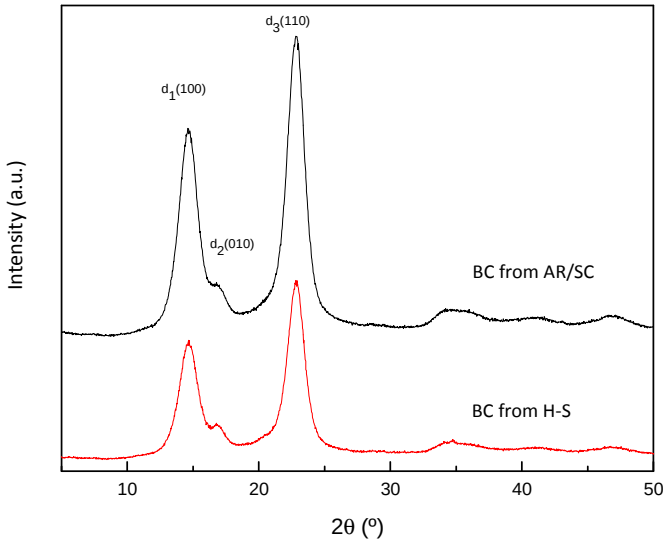

Figure 3.6 X-ray diffractograms of BC produced in AR/SC and H-S culture media.

As it can be observed in **Table 3.3**, BC from AR/SC medium presents a slightly higher crystalline index (CI^{XRD}) in comparison with BC from H-S medium which correlates with the results obtained from the FTIR analysis. As discussed below, this difference can be ascribed to the packing process during cellulose biosynthesis which seems more favoured in the AR/SC medium, resulting in cellulose with higher CI. Anyway, the values of CI obtained in this work are in the expected range for BC. Park et al. [22] determined the CI of celluloses from different nature by different techniques and bacterial cellulose prepared from *Gluconacetobacter hansenii* showed the higher CI in all cases. In the case of XRD method the CI (%) was 95. Shezad et al. [23] compared the BC produced in a commercial medium containing glucose as the main source (similar to H-S) and in a medium of waste from beer fermentation broth. They observed that the CI (%) of the BC obtained in the waste from beer fermentation was higher (80.8) than in the

commercial medium (78) and also the percentage of I_β was slightly higher in the commercial medium. This is in accordance with the results obtained in the present work.

3.3.5.2 Thermal stability

The thermal stability of the BC membranes was analyzed by thermogravimetric analysis (TGA). **Figure 3.7** shows the TGA and derivative TGA curves of the BC from HS and AR/SC media under a nitrogen atmosphere.

As it can be observed, both thermograms were very similar. The first initial loss below 120 °C is usually associated with a relatively small dTG peak and is assigned to the release of water (moisture) from the BC. As it can be observed, the degradation occurred in one step. The peaks of dTG curves in the range of 200-500 °C correspond to volatilization stages of thermally degraded cellulose such as depolymerisation, dehydration and decomposition of glycosidic units [10].

The temperature at 10 and 50% of mass loss (T_{10} and T_{50}, respectively), main dTG peak temperature and residue at 750 °C are summarized in **Table 3.4.** Both celluloses presented similar degradation temperatures and in the expected range. As it can be observed, the residue at 750 °C was slightly higher in the case of BC obtained in AR/SC medium.

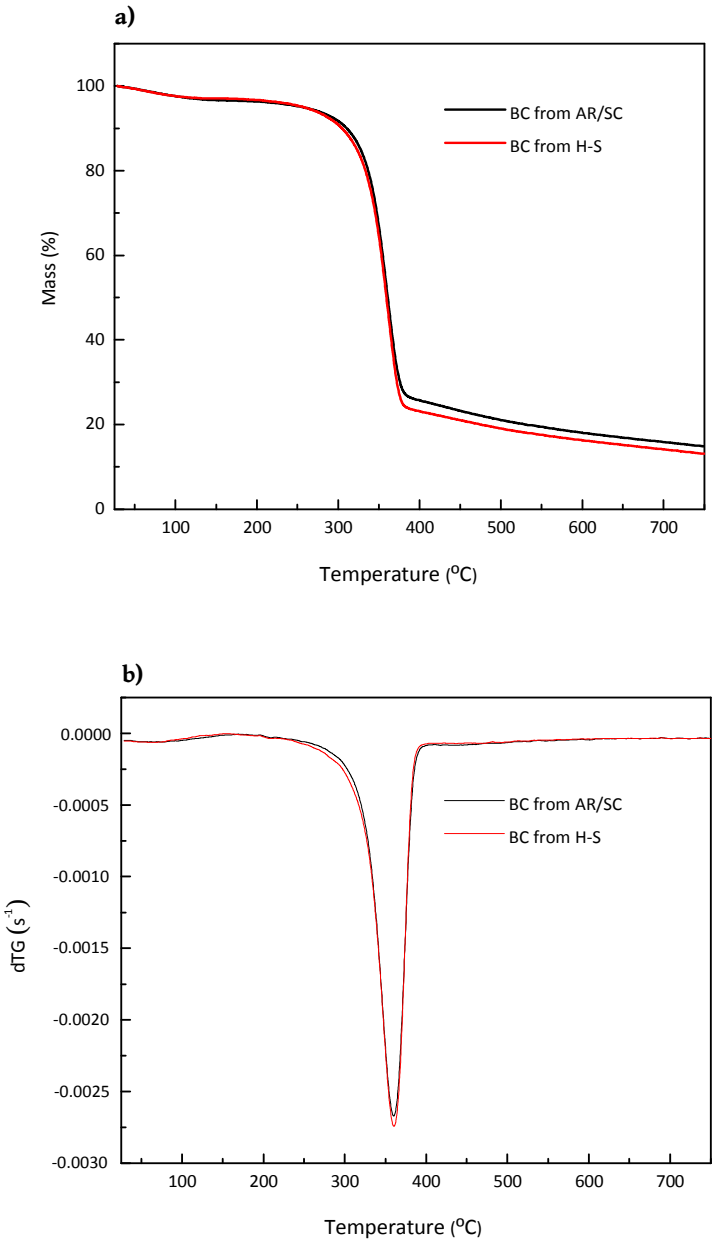

Figure 3.7 a) TGA and b) dTG curves of BC membranes obtained in H-S and AR/SC culture media.

Table 3.4 Temperature at 10 and 50% of mass loss (T_{10} and T_{50}), main dTG peak temperature and residue at 750 °C of BC biosynthesized in H-S and AR/SC culture media.

Sample	T_{10} (°C)	T_{50} (°C)	Main dTG peak temp. (ºC)	Residue at 750 °C (%)
BC from H-S	320	363	364	7.51
BC from AR/SC	316	364	360	10.18

3.3.5.3 Polymerization degree and morphological characterization

One important feature of cellulosic materials is the polymerization degree (PD), since a low PD can make the bacterial cellulose soluble in acidic or alkaline environments and make it less chemically resistant [24]. The PD was calculated through viscosity measurements using the **Equation 2.9** and the results are gathered in **Table 3.5**.

Table 3.5 Polymerization degree (PD), nanofiber diameter (d) and WHC of (air-dried, A-D, and freeze-dried, F-D) BC synthesized in H-S and AR/SC culture media.

BC sample	PD	d (nm)	WHC^{A-D} (%)	WHC^{F-D} (%)
From H-S	4000 ± 560	63 ± 6	162 ± 28	7218 ± 1121
From AR/SC	3500 ± 370	55 ± 6	165 ± 34	8194 ± 1226

Usually, the PD of BC depends on the culture conditions (fermentation time, carbon source, pH), but in this case similar values have been obtained, being the PD value of the BC produced from H-S slightly higher (**Table 3.5**). The PD values of BC are usually between 2000 and 6000 and the values obtained in this work are in the range [4,25,26].

Moreover, the topography of the surface of the BC membranes was analyzed by atomic force microscopy (AFM). **Figure 3.8** shows the AFM height and phase images of BC membranes obtained in AR/SC and H-S culture media.

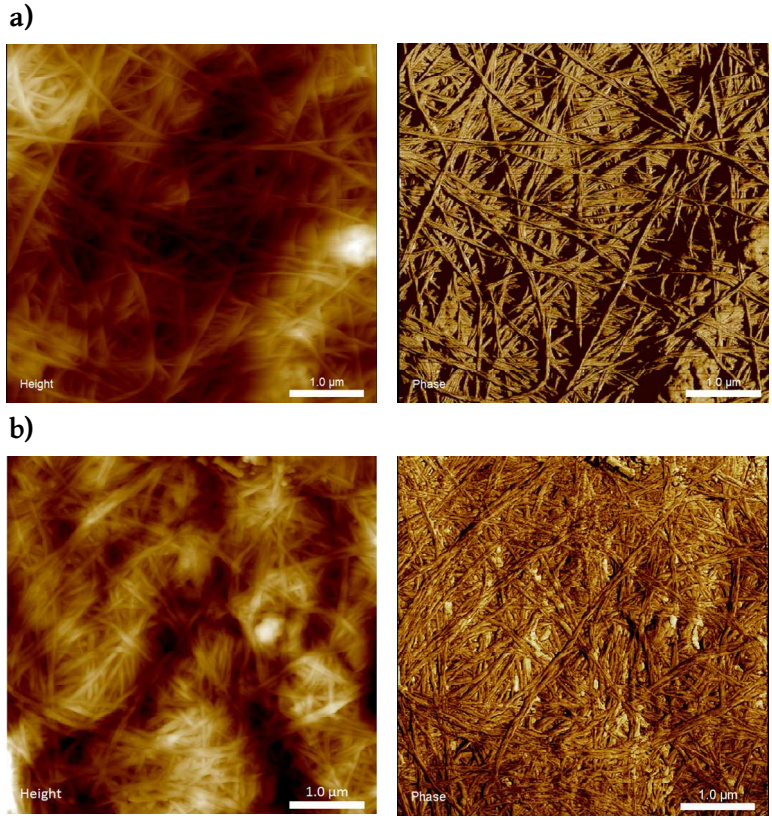

Figure 3.8 AFM height (left) and phase (right) images of BC membranes obtained in a) H-S and b) AR/SC culture media.

In **Figure 3.8** the typical 3D network-like structure of cellulose obtained from bacteria can be seen in both cases. Moreover, there is no preferential orientation of nanofibers in the membranes. This is the typical conformation of crystalline BC membranes. The diameter of the nanofibers (d) was measured from the AFM height profile images and the results are

shown in **Table 3.5**. As observed, the nanofibers of BC from H-S medium are slightly thicker than those from the AR/SC medium. The packaging process in AR/SC medium resulted in thinner nanofibers and the difference in their dimensions can have caused the increase in the number of nanofibers crossing each other.

In addition, the water holding capacity (WHC) or swelling capacity of the BC membranes in H-S and AR/SC media was measured. The WHC of the membranes was calculated using **Equation 2.16**. In this case, two drying methods were used to measure the WHC of the membranes since some authors confirmed that the porosity of the BC can be modified depending on the drying method [27]. The first drying method was freeze-drying (F-D) and the second one was hot air-drying (A-D). The obtained results are gathered in **Table 3.5**.

In the case of BC, BC matrix consists on reticulated nanofibrils forming a 3D network structure with air interstices in between with high water retention capacity. The porosity and surface area are the factors related with the WHC of cellulosic materials [28]. As it has been described by other authors, if there are plenty of spaces among the BC nanofibrils, then more water can penetrate and adsorb onto the material. This property is also related with the size of the fibrils. Ougiya et al. [29] reported that BC samples with thinner and longer nanofibers have high WHC.

Freeze-dried membranes (F-D) had higher porosity than hot air-dried ones (A-D) since the shrinkage of pores during drying can be prevented by this technique more effectively [30]. This fact can be easily observed in **Figure 3.9**, where SEM images of AR/SC freeze-dried and hot air-dried membranes are presented. The morphology of hot air-dried membrane showed a more

compacted matrix and thus, the pore size was smaller than in freeze-dried membrane. In this work, WHC values of the BC grown in H-S and AR/SC culture media were similar in each of the drying methods, as it can be observed from the results of **Table 3.5**, although the latter presented slightly higher WHC which probably was related to the size of the nanofibrils. Besides the values obtained in this work were slightly higher than those obtained by other authors for both freeze-dried and hot air-dried BC membranes using different feedstocks such as pineapple waste, by-product streams from biodiesel and confectionery industries or different bacterial strains such as *Gluconacetobacter xylinus* and *Gluconacetobacter europaeus* [4,17,27,31].

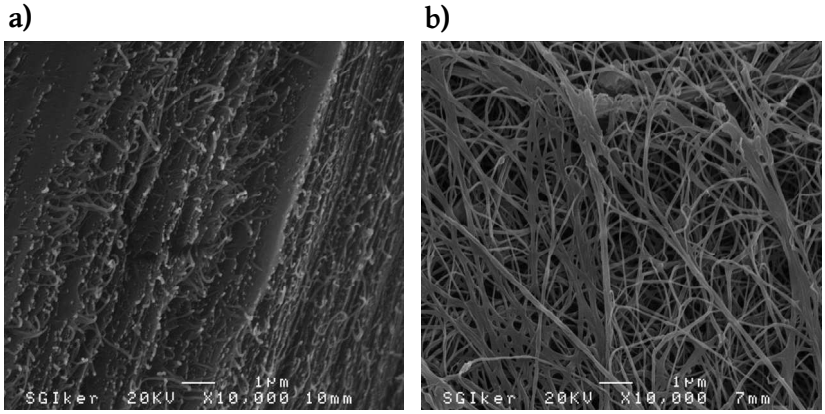

Figure 3.9 SEM images of AR/SC BC membranes, a) hot air-dried and b) freeze-dried.

3.3.5.4 Mechanical behavior

The mechanical behavior of BC membranes from AR/SC and H-S culture media was evaluated by tensile tests. Young's modulus (E), tensile strength

(σ_{max}) and elongation at break (ε_b) obtained from stress-strain curves are gathered in **Table 3.6**.

Table 3.6 Mechanical properties of BC biosynthesized in H-S and AR/SC culture media.

BC sample	E (MPa)	σ_{max} (MPa)	ε_b (%)
From H-S	9800 ± 360	95 ± 13	1.4 ± 0.2
From AR/SC	11250 ± 254	109 ± 18	1.7 ± 0.3

One of the most attractive features of BC is the outstanding mechanical performance attributed to the well-organized 3D nanonetwork structure formed through self assembly. BC is brittle, so low elongation at break and high modulus are usually observed. In the literature, several modulus and strength values can be found depending on the cultivation conditions and the subsequent treatment of the BC membranes. In this way, Young´s modulus and strength values ranging from 1-20 GPa and 70-200 MPa, respectively, can be found [32,33]. As it can be observed in **Table 3.6**, the values of this work are in the range.

As it can be seen, BC obtained from AR/SC medium presents better mechanical properties with higher modulus and tensile strength. As is well known, there is a great influence of the degree of crystallinity on the mechanical strength [34]. Hereby the higher value of the Young´s modulus of the BC obtained from AR/SC medium could be ascribed to its slightly greater crystallinity [35]. Moreover, a denser structure of the BC nanofibers can be related with a higher mechanical strength. As it has been observed in AFM images, BC from AR/SC medium presented a more reticulated structure

with thinner nanofibers (lower nanofiber diameter), factors which could have influence in the mechanical performance.

In any case, both membranes exhibited high mechanical properties. It has been reported that when BC membranes are subjected to compression, tensile strength increases since their compactness also increases [36,37]. In this case, the drying process of the membranes was carried out in compression between two Teflon plates in order to avoid the shrinkage of the samples, so this may have influenced positively the mechanical properties.

3.4 CONCLUSIONS

In this chapter, an effective culture method to produce bacterial cellulose was developed using by-products of the cider production from the Basque Country.

Different AR/SC ratios were used to produce BC, and in all cases BC production was observed confirming that AR/SC mixture was a suitable carbon source. In some experiments the BC production with AR/SC medium was higher than in H-S medium, which was ascribed to the possible polyphenolic compounds contained in the apple residue juice. The effect of pH on cell viability was tested and was demonstrated that acidic pH favored the growing of the cells and in consequence the BC production. The expression level of the operon *bcs* in AR and AR/SC media respect to standard H-S media was measured. The results indicated that in AR/SC medium the expression levels of *bcs*A gene, wich is the first gene of the *bcs* operon, was increased in 1.5-fold respect to the H-S medium. This result was

in agreetment with the fact that BC production in AR/SC medium was higher than in H-S medium. The AR/SC medium contained glucose, fructose and sucrose. Glucose was the most consumed sugar, although the three of them were assimilated simultaneously by the bacteria.

Additionally, BC membranes from AR/SC were characterized by several techniques and the properties were compared to the membranes obtained in H-S medium. BC from AR/SC presented slightly higher crystallinity, more reticulated structure and better mechanical performance than BC from H-S.

Therefore it can be concluded that, in general, the final properties of BC from AR/SC medium were better than the BC obtained in H-S medium. This process can be an alternative for the valorization of cider by-products by a biotechnological conversion into an added value product.

3.5 REFERENCES

[1] Castro, C., Zuluaga, R., Álvarez, C., Putaux, J.L., Caro, G., Rojas, O.J., Mondragon, I., Gañán, P. Bacterial cellulose produced by a new acid-resistant strain of *Gluconacetobacter* genus. Carbohydr. Polym. 89 (2012) 1033-1037.

[2] Pourramezan, G.Z., Roayaei, A.M., Quezelbash, Q.R. Optimization of culture conditions of bacterial cellulose production by *Azetobacter sp. 4B-2*. Biotechnology 8 (2009) 150-154.

[3] Zahan, K.A., Pa'e, N., Muhamad II. Monitoring the effect of pH on bacterial cellulose production and *Acetobacter xylinum* 0416 growth in a rotary discs reactor. Arab. J. Sce. Eng. 40 (2015) 1881-1885.

[4] Algar, I., Fernandes, S.C.M., Mondragon, G., Castro, C., Garcia-Astrain, C., Gabilondo N., Retegi, A., Eceiza, A. Pineapple agroindustrial residues for the production of high value bacterial cellulose with different morphologies. J. Appl. Polym. Sci. 132 (2015) 41237 (1-8).

[5] Chawla, P.R., Bajaj, I.B., Shrikant, A.S., Singhal, R.S. Fermentative production of microbial cellulose. Food. Technol. Biotechnol. 47 (2009) 107-124.

[6] Keshk, S., Sameshima, K. The utilization of sugar cane molasses with/without the presence of lignosulfonate for the production of bacterial cellulose. Applies Microbiol. Biotechnol. 72 (2006) 291-296.

[7] Kurosumi, A., Sasaki, C., Yamashita, Y., Nakamura, Y. Utilization of various fruit juices as carbon source for production of bacterial cellulose by *Acetobacter xylinum* NBRC 13693. Carbohydr. Polym. 76 (2009) 333-335.

[8] Römling, U., Galperin, M.Y. Bacterial cellulose biosynthesis: diversity of operons, subunits, products, and functions. Trends. Microbiol. 23 (2015) 545-557.

[9] Poyrazoglu, C. E., Biyik, H. Evaluation of different pH and temperatures for bacterial cellulose production in HS (Hestrin–Scharmm) medium and beet molasses medium. Afr. J. Microbiol. Res. 5 (2011) 1037-1045.

[10] Kiziltas, E.E., Kiziltas, A., Gardner, D.J. Synthesis of bacterial cellulose using hot water extracted wood sugars. Carbohydr. Polym. 124 (2015) 131-138.

[11] Florea, M., Hagemann, H., Santosa, G., Abbott, J., Micklem, C., Spencer-Milnes, X., de Arroyo Garcia, L., Paschou, D., Lazenbatt, C., Kong, D., Chughtai, H., Jensen, K., Freemont, P., Kitney, R., Reeve, B., Ellis, T. Engineering control of bacterial cellulose production using a genetic toolkit and a new cellulose-producing strain. PNAS. 113 (2016) E3431-E3440.

[12] Keshk, S., Sameshima, K. Evaluation of different carbon sources for bacterial cellulose production. Afr. J. Biotechnol. 4 (2005) 478-482.

[13] Mikkelsen, D., Flanagan, B.M., Dykes, G.A., Gidley, M.J. Influence of different carbon sources on bacterial cellulose production by *Gluconacetobacter xylinus* strain ATCC 53524. J. Appl. Microbiol. 107 (2009) 576-583.

[14] Belgacem, M.N., Gandini, A. (2008) Monomers, polymers and composites from renewable resources. Amsterdam: Elsevier Science.

[15] Castro, C., Zuluaga, R., Putaux, J.L., Caro, G., Mondragon, I., Gañán, P. Structural characterization of bacterial cellulose produced by *Gluconacetobacter swingsii sp*. from Colombian agroindustrial wastes. Carbohydr. Polym. 84 (2011) 96-102.

[16] Cerrutti, P., Roldán, P., Martínez-García, R., Galvagno, M.A., Vázquez, A., Foresti, M.L. Production of bacterial nanocellulose from wine industry residues: importance of fermentation time on pellicle characteristics. J. Appl. Polym. Sci. 133 (2016) 43109 (1-9).

[17] Saibuatong, O-A., Phisalaphong, M. Novo aloe vera–bacterial cellulose composite film from biosynthesis. Carbohydr. Polym. 79 (2010) 455-460.

[18] Jung, H.I., Jeong, J.H., Lee, O.M., Park, G.T., Kim, K.K., Park, H.C., Lee, S.M., Kim, Y.G., Son, H.J. Influence of glycerol on production and structural-physical properties of cellulose from *Acetobacter sp*. V6 cultured in shake flasks. Bioresour. Technol. 101 (2010) 3602-3608.

[19] French, A.D. Idealized powder diffraction patterns for cellulose polymorphs. Cellulose 21 (2014) 885-896.

[20] Xu, X., Liu, F., Jiang, L., Zhu, J.Y., Haagenson, D., Wiesenborn, D.P. Cellulose nanocrystals vs. cellulose nanofibrils: a comparative study on their microstructures and effects as polymer reinforcing agents. ACS. Appl. Mater. Interfaces. 5 (2013) 2999-3009.

[21] Sullivan, E.M., Moon, R.J., Kalaitzidou, K. Processing and characterization of cellulose nanocrystals/polylactic acid nanocomposite films. Materials 8 (2015) 8106-8116.

[22] Park, S., Baker, J.O., Himmel, M.E., Parilla, P.A., Johnson, D.K. Cellulose crystallinity index: measurement techniques and their impact on interpreting cellulose performance. Biotechnol. Biofuels. 3 (2010) 1-10.

[23] Shezad, O., Khan, S., Khan, T., Park, J.K. Physicochemical and mechanical characterization of bacterial cellulose produced with an excellent productivity in static conditions using a simple fed-batch cultivation strategy. Carbohydr. Polym. 82 (2010) 173-180.

[24] Laszkiewicz, B. Solubility of bacterial cellulose and its structural properties. J. Apply. Polym. Sci. 67 (1998) 1871-1876.

[25] Surma-Ślusarska, B., Presler, S., Danielewicz, D. Characteristics of bacterial cellulose obtained from *Acetobacter xylinum* culture for application in papermaking. Fibres. Text. East. Eur. 4 (2008) 108-111.

[26] Shi, Q.S., Feng, J., Li, W.R., Zhou, G., Chen, A.M., Ouyang, Y.S., Chen, Y.B. Effect of different conditions on the average degree of polymerization of bacterial cellulose produced by *Gluconacetobacter Intermedius BC-41*. Cellul. Chem. Technol. 47 (2013) 503-508.

[27] Zeng, M., Laromaine, A., Roig, A. Bacterial cellulose films: influence of bacterial strain and drying route on film properties. Cellulose 21 (2014) 4455-4469.

[28] Ul-Islam, M., Khan, T., Park, J.K. Water holding capacity and release properties of bacterial cellulose obtained by in situ and ex situ modification. Carbohydr. Polym. 88 (2012) 596-603.

[29] Ougiya, H., Watanabe, K., Matsumura, T., Yoshinaga, F. Relationship between suspension properties and fibril structure of disintegrated bacterial cellulose. Biosci. Biotechnol. Biochem. 62 (1998) 1714-1719.

[30] Tang, W., Jia, S., Jia, Y., Yang, H. The influence of fermentation conditions and post-treatment methods on porosity of bacterial cellulose membrane. World. J. Microbiol. Biotechnol. 26 (2010) 125-131.

[31] Tsouko, E., Kourmentza, C., Ladakis, D., Kopsahelis, N., Mandala, I., Papanikolaou, S., Paulokis, F., Alves, V., Koutinas, A. Bacterial cellulose production from industrial waste and by-product streams. Int. J. Mol. Sci. 16 (2015) 14832-14849.

[32] Gea, S., Reynolds, C.T., Roohpoura, N., Wirjosenton, B., Soykeabkaew, N., Bilotti, E. Peijs, T. Investigation into the structural, morphological, mechanical and thermal behaviour of bacterial cellulose after a two-step purification process. Bioresour. Technol. 102 (2011) 9105-9110.

[33] Tsouko, E., Kourmentza, C., Ladakis, D., Kopsahelis, N., Mandala, I., Papanikolaou, S., Paloukis, F., Alves, V., Koutinas, A. Bacterial cellulose production from industrial waste and by-product streams. Int. J. Mol. Sci. 16 (2015) 14832-14849.

[34] Krässig, H.A. (1993). Cellulose: structure, accessibility and reactivity. Pennsylvania: Gordon & Breach Science Publisher.

[35] Guhados, G., Wan, W., Hutter, J.L. Measurement of the elastic modulus of single bacterial cellulose fibers using atomic force microscopy. Langmuir 21 (2005) 6642-6646.

[36] Retegi, A., Gabilondo, N., Peña, C., Zuluaga, R., Castro, C., Gañan, P., de la Caba, K., Mondragon, I. Bacterial cellulose films with controlled microstructure–mechanical property relationships. Cellulose 1 (2010) 661-669.

[37] Cheng, K.C., Catchmark, J.M., Demirci, A. Effect of different additives on bacterial cellulose production by *Acetobacter xylinum* and analysis of material property. Cellulose 16 (2009) 1033-1045.

CHAPTER 4

BACTERIAL CELLULOSE/CHITOSAN MEMBRANES

4. BACTERIAL CELLULOSE/CHITOSAN MEMBRANES

4.1 INTRODUCTION

Nowadays, the search of advanced technologies for water purification is an important issue as it has to meet the requirements of the quality of the water either for human consumption or agricultural and industrial purposes. Concretely, the metal-mechanics industry (batteries, tanneries, fertilizers, etc) requires the use of heavy metals as raw materials, and the presence of these metals in aquatic environments with concentrations that exceed water quality criteria is an environmental problem. Heavy metals are not biodegradable and although some of them are essential for human health like copper, zinc or nickel, an excess in the intake of these, could cause serious health problems [1]. In particular, in the electrical, leather, fungicidal or paper industries wastewater streams containing copper ions are generated, which can cause serious environmental problems.

Membrane technology provides a promising alternative in the wastewater purification and reuse technologies because of its energy efficiency compared to other strategies such as coagulation-flocculation, ion exchange or chemical precipitation [2]. Although the membranes of major interest are polymeric, there is a need for improving some specific properties as selectivity, fouling, flux and resistance to chemical environment. Moreover, recently, research on water treatment materials has focused on the development of new eco-friendly materials which lead to non toxic or hazardous by-products [3]. In this context, biopolymers and biological materials such as nanocellulose, chitin and chitosan [4], starch derivatives [5], alginate, gelatin or seaweeds [6] have gained attention in heavy metal

ion adsorption applications due to their biodegradability, renewability and capacity to interact physically and/or chemically with a wide variety of molecules.

Nanocellulose materials have gained attention in recent years in wastewater cleaning area as they come from renewable sources and provide the advantage of the high specific surface area of the nanoscaled biomaterials with high mechanical performance [7]. Usually, chemical treatments are used to induce surface functionalities to nanocelluloses to interact with heavy metal ions. In this way, the capacity of chemically modified cellulose nanofibers and nanocrystals to remove heavy metals such as Ag^{+}, Cu^{2+} and Fe^{3+}/Fe^{2+} has been assessed [8-10]. Moreover, as BC has excellent mechanical properties even in wet state, it can be considered a good template to develop bionanocomposite membranes for heavy metal removal.

Another biopolymer extensively studied in the treatment of industrial wastewater for the elimination of heavy metals and dyes is the chitosan (Ch), (1→4)-2-amino-2-deoxy-β-D-glucan [11]. This biopolymer is derived from the deacetylation process of chitin which is the principal structural component of crustaceans, insects, fungi and yeasts. The industrial production of chitosan is mainly based on the chemical treatment of shells of various types of crustaceans (shrimp, crabs, lobsters) to obtain the chitin, and then the resulting chitin is deacetylated. When the chitin is deacetylated by more than 50%, chitosan is produced.

The interest of Ch derives from the ability to react in the chelation reaction of heavy metals since it presents highly reactive amino groups [12]. The chemical structure of Ch is shown in **Figure 4.1**. Ch has been used to develop composites with different conformations such as microspheres and

hydrogels with adsorption capacities for different heavy metals such as Cu^{2+}, Fe^{2+} and Pb^{2+}. Traditionally, glutaraldehyde has been used as a cross-linker of chitosan membranes with the aim of improving the mechanical properties and physical integrity of the membranes in addition to maximizing the adsorption capacity and varying the surface-area ratio. However, this strategy is limited due to its toxicity, so green alternatives are being considered [13-16].

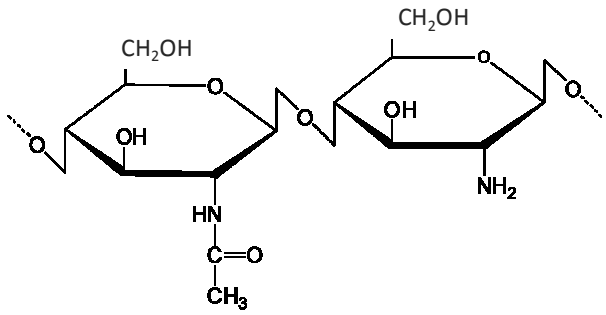

Figure 4.1. Chemical structure of chitosan.

In this chapter a new approach is explored for the design of novel, environmentally friendly membranes based on BC and Ch for water cleaning processes. For this purpose, the excellent mechanical properties in wet state of BC membranes have been taken in advantage to use it as a template, for the Ch as functional entity for the elimination of copper in wastewaters. BC/Ch membranes have been prepared through *ex situ* and *in situ* routes and the differences in the physicochemical and mechanical properties and morphology have been analyzed. Additionally, a comparative study of the copper removal capacity against the traditionally used glutaraldehyde crosslinked chitosan has been performed. Finally, the reusability of the membranes has been assessed.

4.2 EXPERIMENTAL

4.2.1 Preparation of BC/Ch membranes

BC/Ch membranes were obtained through two different routes: *in situ* and *ex situ*.

In the *ex situ* route, firstly, BC membranes were grown in the culture medium prepared with apple residues and sugar cane and purified, neutralized and stored at 5 °C in deionized water until utilization, as described in previous chapter 3. BC/Ch membranes were prepared by immersing BC wet membranes in two acid solutions (prepared with acetic acid 0.5% w/w) of different concentration, 0.6 and 1% (w/v) Ch, under stirring conditions at room temperature for 15 h. The obtained membranes by this route were designated as BC/Ch 0.6% *ex situ* and BC/Ch 1% *ex situ*.

BC/Ch membranes were prepared by *in situ* route by the addition of solutions of chitosan to obtain final concentrations of 0.50 and 0.75% (w/v) Ch into the culture medium. The culture medium was prepared as described previously, with a mixture of apple residues and sugar cane adjusted with acetic acid at pH 4. It was demonstrated that acidic pH favored cell viability and, in addition, this also helped to the dissolution of chitosan. Then, BC/Ch membranes were purified and neutralized with water as described in previously. Membranes obtained by this route were designed as BC/Ch 0.5% *in situ* and BC/Ch 0.75% *in situ*. The scheme of production process of both routes is depicted in **Figure 4.2**.

As a reference, BC membranes were also biosynthesized following the same procedure. Finally all biosynthesized membranes were freeze dried and pressed between aluminium plates in a compression molding machine at 10

Ton for 2 min at room temperature to obtain compacted membranes. All the samples were stored in a desiccator until use.

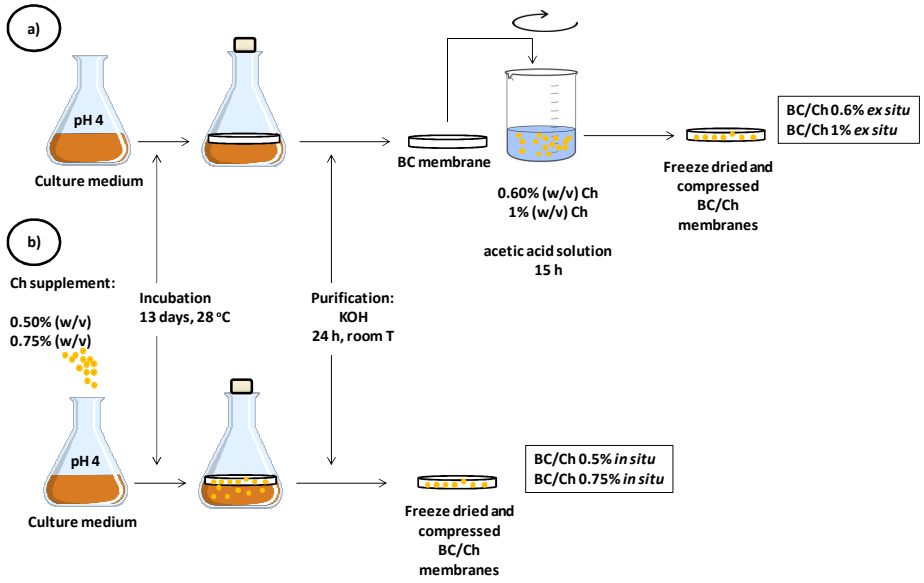

Figure 4.2 Scheme of the production of BC/Ch membranes, a) *ex situ* route and b) *in situ* route.

4.2.2 Preparation of glutaraldehyde crosslinked Ch membranes

Chitosan membranes were prepared by casting acid chitosan solution (1.0% (w/w) of chitosan in 0.5% (w/w) acetic acid solution) into Petri dishes. In order to remove the solvent, chitosan solution was placed at room temperature, until mass become constant. The obtained membranes were immersed in NaOH 1.0 M solution at 25 °C for 48 h and then washed with deionized water for 1 h. Glutaraldehyde crosslinking was performed immersing chitosan membranes in glutaraldehyde solution 0.25% (w/w) in

H_2O, at room temperature for 14 h. Afterwards, membranes were washed and kept in deionized water at 4 °C.

4.2.3 Evaluation of copper (II) ions adsorption and reusability of the membranes

Quantitative analysis of the adsorption capacity of Cu (II) ions by the glutaraldehyde crosslinked Ch membranes and *ex situ* and *in situ* prepared BC/Ch membranes was performed by the formation of the ammonia copper complex. When a small quantity of ammonia solution is added to a copper salt solution in aqueous medium, a precipitate is formed: copper hydroxide (**Equation 4.1**). If an excess of ammonia solution is added, the precipitate is dissolved and a very intense blue coloured complex is formed, ammonia copper complex (tetraamin copper (II)) (**Equation 4.2**).

$$Cu^{2+}(aq) + 2NH_3(aq) + 2H_2O\ (l) \leftrightarrow\ Cu(OH)_2(s) + 2NH_4^+(aq) \qquad \textbf{(4.1)}$$

$$Cu(OH)_2(s) + 4NH_3(aq) \leftrightarrow [Cu(NH_3)_4]^{2+}(aq) + 2OH^-(aq) \qquad \textbf{(4.2)}$$

Before the adsorption tests, solutions of different Cu (II) concentrations (50 and 250 mg L^{-1}) were prepared from $Cu(NO_3)_2{\cdot}3H_2O$. BC/Ch bionanocomposite membranes were cut into approximately 15 x 15 mm^2 pieces and then were incubated in 15 mL of Cu (II) solutions at pH 5.3 for 24 h at room temperature. After incubation, the remaining ion concentration was measured by UV absorption of the ammonia copper complex formed at 610 nm in a Ultraviolet-visible (UV-vis) spectrophotometer UV-3600/3100 from Shimadzu. For this analysis, 10 mL of the solution were taken, 1.5 mL of NH_3 solution were added and taken to a final volume of 15 mL with distillated

water. Standards with known concentrations of $Cu(NO_3)_2 \cdot 3H_2O$ were prepared to obtain the calibration curve. The initial standard solution of 500 mg L^{-1} was diluted in water to give 10, 50, 100, 150 and 250 mg L^{-1} solutions.

The copper removal efficiency (R) was calculated from **Equation 4.3**.

$$R\ (\%) = \frac{C_0 - C_{24h}}{C_0} \cdot 100 \qquad \textbf{(4.3)}$$

where C_0 and C_{24h} are the initial concentration and the concentration of copper in the solution after 24 h expressed in mg L^{-1}, respectively.

Additionally, to analyze the reusability of the bionanocomposite membranes, these were conducted to adsorption and desorption cycles. The membranes were cut in 15 x 15 mm^2 and immersed in two solutions of $Cu(NO_3)_2 \cdot 3H_2O$ at pH 5.3 at the initial concentrations of 50 and 250 mg L^{-1} for 24 h with magnetic stirring. After that, the bionanocomposite membranes were dried and introduced into a 10 mL of 10 mM ethylenediaminetetraacetic acid (EDTA) solution in order to desorb the copper loaded in the membranes. The mixture was stirred for 24 h and then bionanocomposite membranes were taken out and dried for subsequent re-adsorption studies. The remaining ion concentration of the solutions in each cycle was measured by UV-vis spectroscopy at 610 nm.

Two adsorption/desorption cycles were conducted to evaluate the reusability of these membranes for Cu (II) ions removal in water. The followed procedure is schematized in **Figure 4.3**.

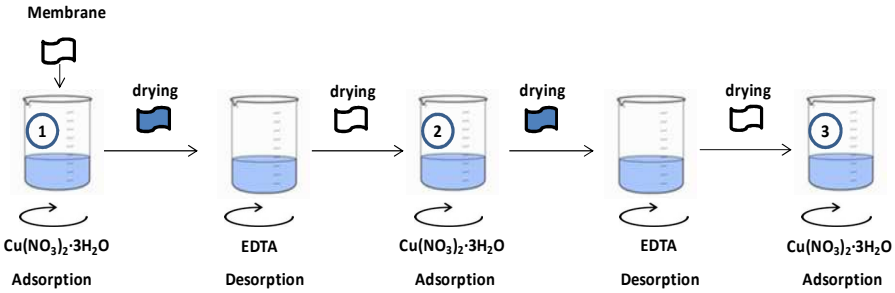

Figure 4.3 Schematic representation of adsorption and desorption cycles to analyze the reusability of the membranes.

4.3 RESULTS

4.3.1 BC/Ch membrane production

BC/Ch membranes prepared by two different routes, *in situ* and *ex situ*, were characterized. The differences between *ex situ* and *in situ* prepared membranes were noticeable at first sight as it can be observed in **Figure 4.4**. While the *ex situ* prepared membranes were very similar to the neat BC membranes, the *in situ* prepared membranes present darker colour with a different texture.

Figure 4.4 Digital images of freeze dried and compressed neat BC and BC/Ch membranes obtained by *in situ* and *ex situ* routes.

The addition of additives and other polymers to the culture media can alter the BC production. In the *in situ* route, BC productivity was affected depending on Ch content in the culture medium. The BC productivity was 1.60 ± 0.20 g L^{-1} without Ch addition, and decreased to 0.50 ± 0.03 and 0.45 ± 0.04 g L^{-1} for 0.5 and 0.75% Ch concentrations, respectively. This was indicative of the influence of Ch addition in BC production, which led to a decline in the yield with increasing Ch content. When the concentration of Ch was 0.5%, BC production was affected probably due to an increase of the viscosity of the culture medium. In the case of 0.75% concentration, it was difficult to dissolve the Ch in the culture medium. Predictably, adding more than 0.75% would have led to an inhibition of the cell growth and cellulose formation since it would have been complicated to dissolve properly the polymer. Phisalaphong and Jatupaiboon [17] prepared *in situ* BC/Ch composites using *A. Xylinus* bacterial strain. They also observed a strong inhibitory effect on the BC formation when the concentrations of chitosan of 30000 and 80000 molecular weights in the culture medium were higher than 0.75 % (w/v). In this case, a Ch of 6.4 x 10^5 molecular weight was used, so this would explain the decrease of BC production at high Ch concentrations. Taking these results into account, solutions of similar concentrations to the ones of the *in situ* route (0.5 and 0.75%) were chosen to impregnate the neat BC membranes for the *ex situ* route (0.6 and 1% of Ch).

4.3.2 Physicochemical characterization of BC/Ch membranes

Firstly, FTIR spectroscopy was used to analyze the functional groups and interactions between BC and Ch biopolymers in the membranes depending on the preparation route. The obtained FTIR spectra of the membranes

prepared by both routes, *in situ* and *ex situ*, are presented in **Figures 4.5** and **4.6**, respectively.

Pure chitosan shows characteristic bands at 1556 and 1646 cm^{-1} assigned to NH bending vibration in amides and amines groups and to carbonyl group (C=O) stretching vibration in amides, respectively and indicated with arrows in **Figures 4.5** and **4.6**. The broad band observed at 3200-3500 cm^{-1} is due to the contribution of different vibrations: the OH stretching vibration and the NH stretching vibration at 3347 cm^{-1} and 3270 cm^{-1}, respectively. The band at 1377 cm^{-1} is assigned to the CH_3 bending vibration. Moreover, the bands at 1100–1020 cm^{-1} are associated with the vibrations of the C–O–C bond of the glycosidic linkages. Finally, the band at 897 cm^{-1} is characteristic of β-glycosidic bond [18,19].

Cellulose and chitosan present a similar structure, so in the case of pure BC peaks assigned to the saccharide structure are also observed: 2900–2880 cm^{-1} (CH stretching vibrations), 1160 cm^{-1} (CH_2 bending vibrations), 1106 cm^{-1} (C-O-C glycosidic bonds) and 897 cm^{-1} (β-glycosidic bond). The broad band at around 3400 cm^{-1} is a characteristic band assigned to OH cellulose stretching vibrations.

Due to the chemical structure, chitosan and cellulose can present interactions through hydrogen bonds between the functional groups of both components. Significant differences can be observed between *in situ* and *ex situ* prepared bionanocomposites comparing **Figures 4.5** and **4.6**.

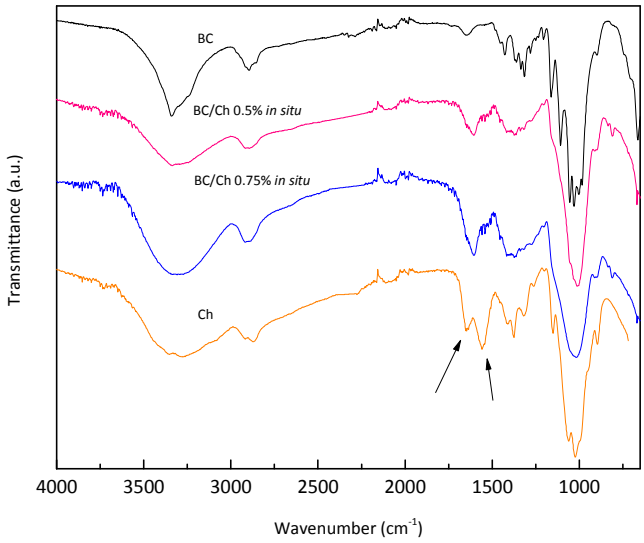

Figure 4.5 FTIR spectra of neat BC, neat Ch and BC/Ch *in situ* prepared membranes.

In the case of *in situ* prepared BC/Ch membranes, **Figure 4.5**, a band located at 1608 cm^{-1} is observed. This can be ascribed to the shifting of the carbonyl group band (1646 cm^{-1} in the pure chitosan) to a lower wavenumber, suggesting that BC functional groups are involved in hydrogen bonding interactions with those groups of the Ch. The band assigned to NH group bending vibration in amides and amines (1556 cm^{-1} in the pure chitosan) is not observed in the bionanocomposites probably because it is shifted to a higher wavenumber and is overlapped with the carbonyl group band. This was also observed in other works confirming the good miscibility of these two biopolymers [17,20]. Finally, it can also be observed the widening experienced by the OH cellulose stretching vibration band in the bionanocomposites because it is overlapped with the NH groups stretching vibration band of the Ch [21].

This study confirms that in the *in situ* prepared membranes hydrogen bonding interactions between BC-Ch are predominant. In the case of *ex situ* prepared membranes, **Figure 4.6**, the characteristic peaks of both cellulose and chitosan are observed confirming the presence of Ch into the BC membranes. However, the bands at 1556 and 1646 cm^{-1} of the pure chitosan remain practically in the same wavenumber in the bionanocomposites, suggesting that hydrogen bonding interactions between Ch-Ch are predominant.

These results suggest that the preparation route has an influence on the conformation of both biopolymers, and thus, affects the possible interactions between them.

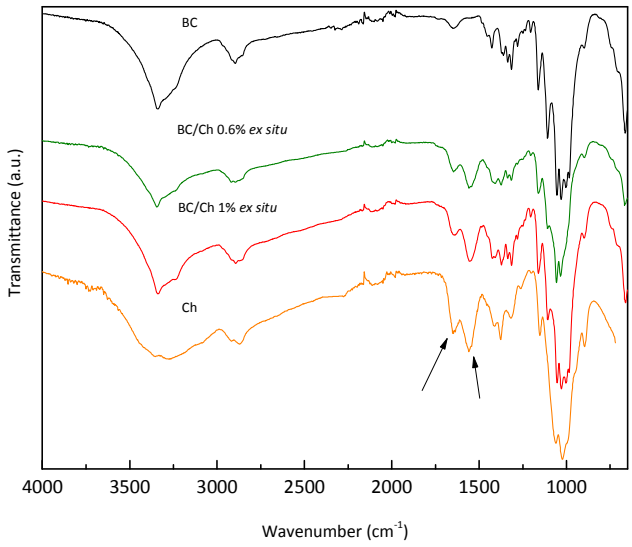

Figure 4.6 FTIR spectra of neat BC, neat Ch and BC/Ch *ex situ* prepared membranes.

4.3.3 Mechanical performance of BC/Ch membranes

The mechanical performance of neat BC and *in situ* and *ex situ* prepared BC/Ch bionanocomposite membranes was evaluated by tensile tests. Tensile test were carried out in dry and wet conditions, after soaking the membranes in water for 24 h. The study in wet state was performed from the point of view of the possible applications of the membranes as filtration supports which would imply moisture conditions. Young's modulus (E), tensile strength (σ_{max}) and elongation at break (ε_b) values obtained from stress-strain curves are gathered in **Figures 4.7**, **4.8** and **4.9**, respectively. The mechanical properties of the glutaraldehyde crosslinked chitosan are not presented due to the brittleness and fragility of the membranes.

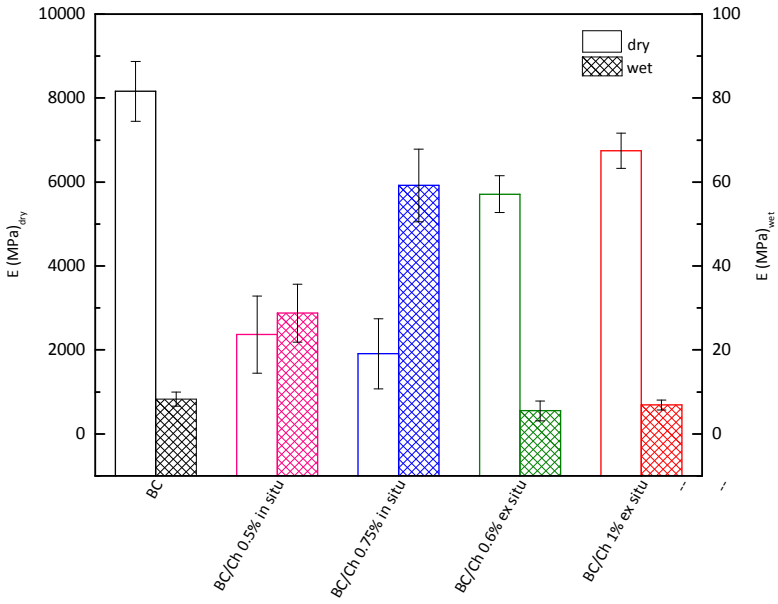

Figure 4.7 Young´s modulus of BC and BC/Ch bionanocomposite dry and wet membranes. (Left y-axys for dry samples and right y-axys for wet samples)

Water has plastifying effect, so in general, the tensile strength and modulus of wet cellulosic samples are lower compared to the dry samples and the opposite behavior is observed with the elongation at break [10,22,23]. In this case, this tendency was observed. BC presented excellent mechanical properties even in wet state due to the very crystalline tight 3D nanofiber structure formed during its biosynthesis, as commented in previous chapters.

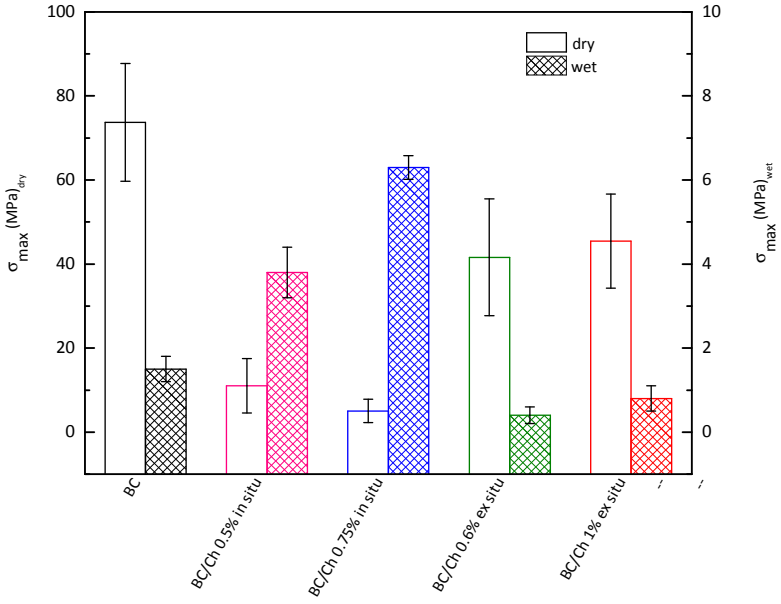

Figure 4.8 Tensile strength of BC and BC/Ch bionanocomposite dry and wet membranes. (Left y-axys for dry samples and right y-axys for wet samples)

Ex situ and *in situ* prepared bionanocomposite membranes showed the same behavior than neat BC, better mechanical properties in dry state than in wet state. In dry state, in both *in situ* and *ex situ* BC/Ch bionanocomposites, the incorporation of Ch to the BC led to a weakness of the nanofiber network

obtaining lower values of modulus and tensile strength compared to neat BC and similar elongation values. It was also observed that *ex situ* membranes exhibited more similar behavior to neat BC than *in situ* ones. This is related to changes in the crystallinity due to the packaging assembly of BC, which was disturbed by the incorporation of Ch into the culture medium during the biosynthesis as it will be discussed later. In wet state, *in situ* prepared membranes exhibited better mechanical performance than *ex situ* prepared ones and even neat BC. This suggested that the incorporation of Ch during BC biosynthesis through *in situ* method modified to a greater extent the structure of the BC membrane. These results indicated that the preparation route led to a very different interaction of the membranes with water and this will be discussed in the next section.

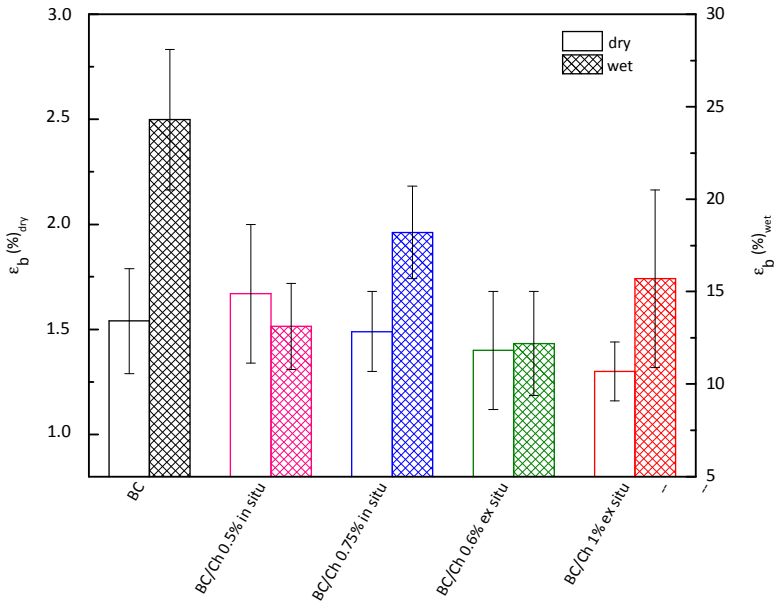

Figure 4.9 Elongation at break of BC and BC/Ch bionanocomposite dry and wet membranes. (Left y-axys for dry samples and right y-axys for wet samples)

Taking into account the moisture conditions of these bionanocomposites and the mechanical requirements to be used as filtration membranes, as BC/Ch 0.75% *in situ* and BC/Ch 1% *ex situ* membranes showed the best mechanical behavior in wet state, these two membranes were chosen from each preparation route for the subsequent analysis.

Moreover, in order to perform a more precise comparative study about the effect of membrane preparation route, the Ch content in both membranes was estimated by elemental analysis. It was found that the Ch content was 37 and 35 wt% for BC/Ch 1% *ex situ* and BC/Ch 0.75% *in situ* membranes, respectively. Therefore, although different preparation routes were used to prepare the membranes, similar Ch contents were obtained, which was more suitable to make the comparative study of the properties of both systems.

4.3.4 Water holding capacity of BC/Ch membranes

In order to understand the mechanical behavior of the membranes in wet state, the water holding capacity (WHC) of the membranes was determined. For this, membranes were immersed in water during 24 h at room temperature and WHC was calculated using **Equation 2. 16**. The obtained results are displayed in **Figure 4.10**.

In previous chapter 3, it has been explained that BC presents high WHC attributed to its morphological conformation and affinity with water due to the numerous hydroxyl groups present in its chemical structure. In this case, lower WHC values were obtained than in previous chapter 3, probably because these membranes were freeze dried and then compressed in a

molding machine, which led to certain closing of the pores obtaining compressed membranes.

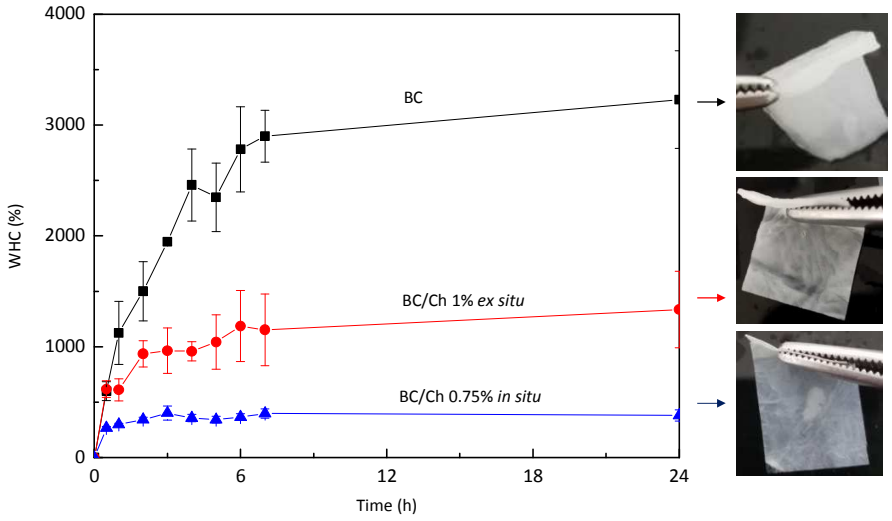

Figure 4.10 WHC and digital images of neat BC, BC/Ch 1% *ex situ* and BC/Ch 0.75% *in situ* membranes during 24 h of immersion in water.

As it can be observed in **Figure 4.10**, all the membranes present high WHC, but neat BC exhibits the highest WHC values. The WHC of the *in situ* membranes at 24 h was 3.5 times lower than the one of the *ex situ* membranes and 8.5 times lower than the one of the neat BC. This was ascribed to different absorption behavior and interaction of the membranes with water molecules depending on the preparation method used.

It was clear that *in situ* prepared membranes tended to interact to a lesser extent with water than *ex situ* prepared ones. As it has been observed in the FTIR analysis, *in situ* prepared membranes´ spectra showed that BC

functional groups interacted by hydrogen bonding with Ch groups. This means that probably there will be less OH groups available to interact with water molecules, affecting the swelling of the membranes. In the case of *ex situ* prepared membranes, Ch-Ch bonds were predominant, so BC will have more OH available to interact with water.

Therefore, these results correlate with the ones obtained by FTIR study and explain the different mechanical performance of the membranes in wet state. In the case of neat BC, higher water content led to higher plasticizing effect, obtaining lower modulus and tensile strength than in the *in situ* prepared sample which presented lower WHC, and consequently, a more rigid and brittle behavior. Other authors observed similar behavior on BC/Ch bionanocomposites, as the water sorption of BC decreased considerably by the incorporation of Ch and it was more pronounced when the amount of chitosan was higher [24].

4.3.5 Crystallinity of BC/Ch membranes

Additionally, the crystallinity of the neat BC and the two bionanocomposite membranes was analyzed by X-ray diffraction. XRD patterns of the different samples are shown in **Figure 4.11.** The crystallinity indexes (CI^{XRD}) were calculated using the **Equation 2.7** taking into account that the patterns were indexed based on I_{α}, so the maximum intensity would be the one of the (110) lattice diffraction, as explained in previous chapter 3.

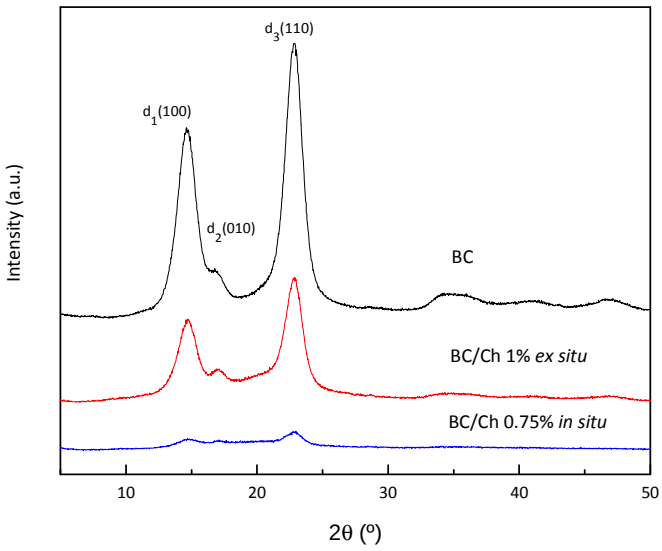

Figure 4.11 X-ray diffractograms of neat BC, BC/Ch 1% *ex situ* and BC/Ch 0.75% *in situ* bionanocomposites.

As it has been explained in previous chapter 3, BC is a semicrystalline material which displays excellent mechanical properties ascribed to its 3D conformation and high crystallinity. The two main peaks observed in the XRD pattern of neat BC (14.6° and 22.7°) which are related to cellulose I allomorph, were also observed in the case of *in situ* and *ex situ* bionanocomposite membranes, but with lower intensities. As expected, BC/Ch bionanocomposites exhibited lower crystallinities than neat BC. The crystallinity indexes calculated were 0.89, 0.77 and 0.45 for neat BC, BC/Ch 1% *ex situ* and BC/Ch 0.75% *in situ* membranes, respectively. *Ex situ* prepared membrane showed a decrease of the crystallinity index compared to the pure BC, but still presented a considerable crystallinity. Kim et al. [21] reported similar results for a BC/Ch *ex situ* prepared composite scaffold observing a decrease of crystallinity degree from 87% of the pure BC to 75%

of the BC/Ch composite. On the other hand, *in situ* prepared membrane also presented cellulose type I as characteristic peaks appeared in the same location, but the crystallinity was approximately the half of the neat BC. This was ascribed to the incorporation of Ch into the BC membrane during biosynthesis which altered the packing assembly of BC and thus, it reduced its crystallization.

Huang et al. [25] investigated the effect of introducing different substances into BC fermentation medium i. e. Tween 80, urea, fluorescent brightener, hydroxypropylmethyl cellulose and carboxymethyl cellulose. In all cases they observed a decrese of the CI^{XRD} compared to the neat BC, being more pronounced in the case of hydroxypropylmethyl cellulose and carboxymethyl cellulose. They ascribed this effect to the hindrance of BC crystallization by the adsorption of the additives on nanofibers which influenced BC nanofibers aggregating planes regarding the forming of ribbons. The results obtained in the present work confirmed that the incorporation of chitosan during the biosynthesis process modified the packaging assembly of the BC in a significant way so that the crystallinity was strongly affected and therefore, its mechanical properties.

Here it can be noted the different modification of the BC membrane depending on the route. Through *ex situ* route, Ch was introduced into the pores and also covered BC membrane, and this affected the crystallinity degree, while through *in situ* route Ch altered the packaging assembly of the BC to a greater extent and thus, the network structure.

4.3.6 Morphology and porosity of BC/Ch membranes

To compare the effect of the preparation route on the surface, conformation of the matrix and pore size of the membranes, BC/Ch 1% *ex situ* and BC/Ch 0.75% *in situ* bionanocomposites were analyzed by SEM and AFM. Moreover, a study of the specific surface area and pore size was performed by physical adsorption measurements using BET theory.

Images of SEM of the cross sections of different BC/Ch membranes are shown in **Figure 4.12**, where images x100, x2500 and x10000 are presented. SEM micrographs revealed the reticular 3D nanofiber network characteristic of BC in both bionanocomposites, but different compactness and density were observed. *In situ* prepared bionanocomposite showed thinner nanofibers that formed a more reticulated matrix while in the *ex situ* prepared bionanocomposite nanofibers were more loosely arranged forming cavities. In the augmented micrographs of the cross sections (x2500 and x10000), it can be seen the detailed structure of both membranes showing more compacted matrix in the case of *in situ* prepared bionanocomposite than in the *ex situ* one. Moreover, considering these images, the pore size seems more homogeneous in the case of *in situ* prepared membrane. *Ex situ* prepared membrane forms more heterogeneous network, which can be seen more detailed in the *ex situ* image x10000. Through the *ex situ* route, Ch was incorporated once the BC membrane was formed, so some Ch molecules penetrated BC nanofibers and some others were trapped into the BC network.

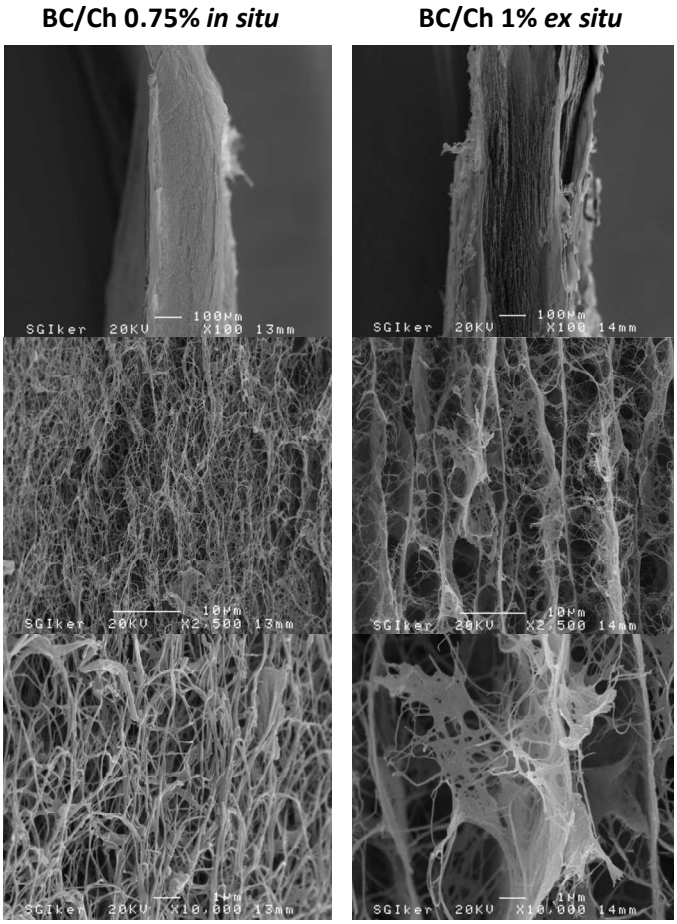

Figure 4.12 SEM images of cross sections of BC/Ch 0.75% *in situ* (left) and BC/Ch 1% *ex situ* (right) membranes.

In addition, topography of the surfaces and structure of the matrices was studied by AFM. The resultant images can be observed in **Figure 4.13,** where AFM height and phase images of the neat BC and different BC/Ch bionanocomposites are shown.

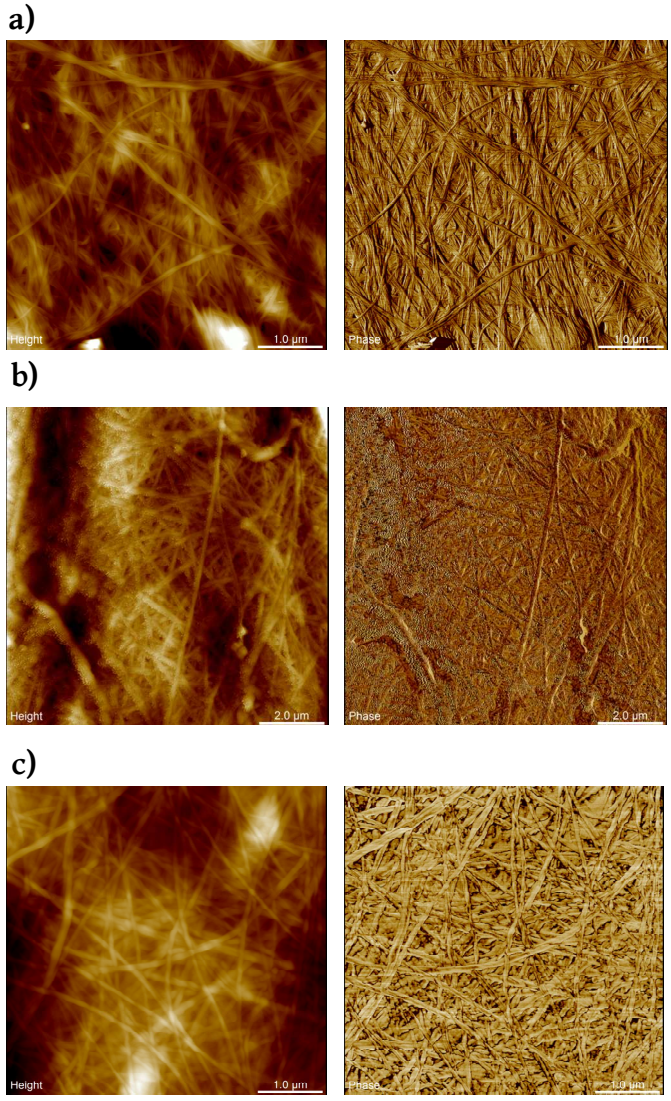

Figure 4.13 AFM height (left) and phase (right) images of a) neat BC, b) BC/Ch 0.75% *in situ* and c) BC/Ch 1% *ex situ* membranes.

Here, it can be observed that the incorporation of Ch into BC matrix results in a slightly different conformation depending on the preparation route

used. The surface morphology of the *ex situ* prepared bionanocomposite showed BC nanofibers recovered by Ch. In contrast, the presence of chitosan was less evident in the case of *in situ* prepared bionanocomposite because no aggregates or different structures to the nanofibers are observed. These results suggest that the incorporation of Ch through the *ex situ* route might have been more superficial, while through *in situ* route, a better inclusion in the BC membrane was achieved as the Ch incorporation took place during the packaging of the cellulose nanofibers during formation.

In filtration applications with membranes, the pore structure and volume are important features, since it is preferable to design membranes with a relatively uniform pore structure throughout the thickness which acts as a deep filter [26]. In this case, although the analysis of the morphology of the bionanocomposite membranes by SEM and AFM give an approximate idea of the pore size, physical adsorption (physisorption) was used to determine and quantify surface area, average pore diameter and total pore volume. The specific surface area of the samples was measured by Brunauer, Emmett and Teller (BET) method. The specific surface area of the materials is usually determined by physical adsorption of a gas on the surface of the solid and by calculating the amount of adsorbate gas corresponding to a monomolecular layer on the surface. Additionally, pore size distribution of the membranes was determined from adsorption data using the Barrett-Joyner-Halenda (BJH) method by means of Kelvin model of pore filling, which is the method used for porous materials.

The obtained results of specific surface area, average pore diameter and total pore volume are gathered in **Table 4.1**. As expected, all these parameters were higher in the case of neat BC than in the case of the

bionanocomposites due to the incorporation of chitosan molecules into both, surface and empty spaces of the BC membrane.

Table 4.1 Specific surface area, average pore width and total pore volume of neat BC and BC/Ch membranes.

Sample	BET specific surface area (m^2g^{-1})	Average pore diameter (nm)	Total pore volume (cm^3g^{-1})
BC	23.8	36.9	0.22
BC/Ch 1% *ex situ*	10.3	26.9	0.07
BC/Ch 0.75% *in situ*	9.8	33.4	0.08

The BET surface area of the neat BC membrane was 23.8 m^2 g^{-1}, which is very similar to a previous value reported with a freeze-dried nanofibrillated cellulose adsorbent (26.8 m^2 g^{-1}) [27]. In the case of the BC/Ch membranes no significant differences were observed between them. For all the membranes (BC and BC/Ch) the range of pore size distribution was 1-60 nm. The maximum distribution of pore diameter for the *in situ* and *ex situ* membranes was in the range 2-10 and 2-7 nm, respectively. These results confirm the suitability of these membranes as nanofiltration supports although the average pore diameter values obtained in this work are higher than some earlier results of bacterial cellulose membranes and its composites.

Ul-Islam et al. [28] observed average pore diameter values of 19 nm and 11.6 nm for neat BC and *ex situ* prepared BC-Ch membranes, respectively. Karim et al. [29] developed chitosan membranes with cellulose nanocrystals further stabilized by crosslinking with gluteraldehyde vapors with average pore diameters of 13-17 nm. Additionally, as observed, total pore volume of neat BC was higher than the one of the BC/Ch membranes, and this result correlates with the WHC, as the BC exhibited much higher WHC than BC/Ch membranes.

4.3.7 Copper (II) ions removal capacity and reusability

After the characterization of BC/Ch bionanocomposite membranes, it was observed that the pore size was in the range of nanofiltration supports, so a study was performed to analyze the possibility of using these membranes for heavy metal removal in aqueous solutions. Cu (II) ions removal capacity of BC/Ch bionanocomposite membranes was studied in static mode, at pH 5.3, at room temperature during 24 h.

The contact time, temperature and pH are factors that can affect the adsorption process of the membranes. Previous studies have revealed that the adsorption capacities of chitin and chitosan decrease when increasing the temperature from 25 to 45 °C. This indicates that the adsorption of copper is favored at lower temperatures because the adsorption process has exothermic nature [30]. For this reason, the study was performed at room temperature which is the common temperature of the water filtration processes. The optimal incubation time was set in 24 h. A preliminary study of the effect of incubation time revealed that the membranes were not saturated at shorter times than 24 h (12 h) and longer incubation times (48 h) did not led to a higher copper removal, probably due to the saturation of the membranes. Moreover, the study was conducted a pH 5.3, pH of the copper solution. This was not adjusted because there are several studies about chitosan and cellulosic materials which report that the greatest metal uptake is at pH 4-6 [10,29-31]. This is due to the fact that the adsorption process of the metal by chitosan is more efficient at slightly acidic pH. When the pH is very acidic (<pH 4), the amino groups of chitosan are easily protonated and an electrostatic repulsion effect between the adsorbent

surface and the positively charged ions is induced by the resultant NH_3^+. When the pH is above 6, precipitation of copper hydroxide occurs [32].

Two concentrations of cooper solutions were used, 50 mg L^{-1} and 250 mg L^{-1}, to test the Cu (II) removal capacity of the BC/Ch bionanocomposite membranes and also neat BC and glutaraldehyde crosslinked Ch membranes for comparison. Cu (II) ions removal efficiency results are gathered in **Table 4.2.**

Table 4.2 Cu (II) final concentration of the solutions after 24 h and Cu (II) ions removal efficiency (R) of glutaraldehyde crosslinked Ch, neat BC and BC/Ch membranes.

Sample	**Initial concentration**			
	50 mg L^{-1}		**250 mg L^{-1}**	
	C_{24h}	**R (%)**	**C_{24h}**	**R (%)**
crosslinked Ch	32 ± 3	36	141 ± 23	44
BC	49 ± 1	2	241 ± 0	3
BC/ Ch 1% *ex situ*	31 ± 3	39	161 ± 6	36
BC/ Ch 0.75% *in situ*	22 ± 3	55	136 ± 23	46

As it can be observed, the copper elimination capacity of the bionanocomposite membranes was in the range of the glutaraldehyde crosslinked chitosan membranes being higher in the case of *in situ* prepared ones. As BC posses a high water holding capacity, the BC/Ch bionanocomposite membranes were compressed to minimize the swelling of the nanofiber network in the water which can lead to close the pores. The Cu (II) ions removal study was also performed for neat BC and no metal removal capacity was observed. Usually, nanocellulose is subjected to chemical treatments to induce surface functionalities for metal removal or to modify the porosity [10,33]. The copper removal efficiencies of BC/Ch membranes of this work were similar, and in some cases higher, than the

ones obtained by other authors with similar systems. Karim et al. [10] obtained removal efficiencies of 13-19% in static mode with nanocellulose membranes coated with cellulose nanocrystals having sulphate or carboxyl surface groups. Wang et al. [34] developed a sugar cane cellulose-based adsorbent and obtained a Cu^{2+} removal efficiency of 41.2%. Steenkamp et al. [35] developed membranes of alumina/chitosan composites which could adsorb copper below the level of 1 mg L^{-1} with an initial concentration of 50 mg L^{-1}. However, the chitosan membrane was treated with NaOH and silica as a porogen to create pores. In this case, BC nanofiber network was used as a porous support for the attachment of chitosan which acted as the active phase for metal ion chelation. As it can be observed from **Table 4.2**, *in situ* prepared nanocomposite showed higher Cu^{2+} removal efficiency than *ex situ* prepared one, although Ch content in both of them was found to be similar (35 and 37% of Ch for *in situ* and *ex situ* membrane, respectively). The incorporation of Ch into the culture medium and thus, interactions between BC and Ch through *in situ* process led to a more homogeneous membrane with less tendency to swell in water. Probably, this homogeneity of the BC/Ch nanofiber network and the fact that water molecules did not close the pores, led to better Cu^{+2} - Ch interactions.

Moreover, the stability and reusability of filtration membranes are important features for industrial applications. Therefore, the reusability of the BC/Ch bionanocomposite membranes was studied. It is well known that EDTA (ethylenediaminetetraacetic acid) posses a strong complexing ability of metal ions in 1:1 metal-to-EDTA complexes, so in this case, EDTA was used for desorption of the metal ions loaded onto the membranes. Then, membranes were conducted to two adsorption-desorption cycles and the removal efficiency was calculated after each cycle (as indicated in **Figure**

4.3). The aspect and colour of the membranes before and after the Cu^{+2} absorption tests and after EDTA treatment for desorption of copper loaded in the membranes can be observed in **Figure 4.14**.

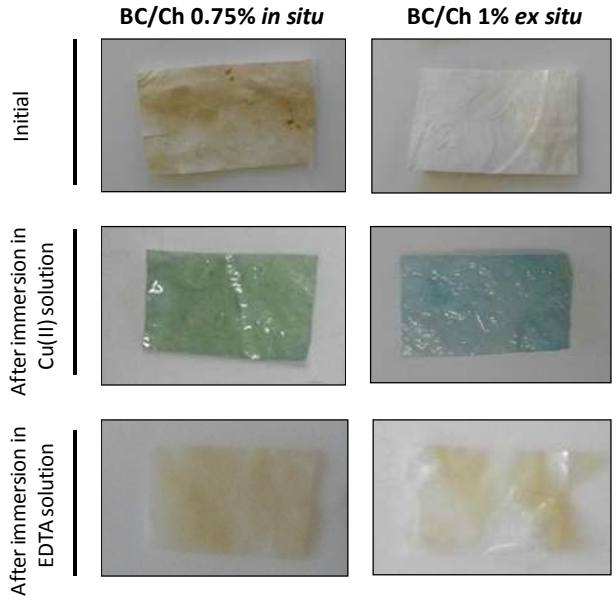

Figure 4.14 BC/Ch membranes before immersion, after 24 h in 250 mg L^{-1} Cu^{2+} and after 24 h immersed in EDTA solutions.

It is noticeable that after immersion in copper solutions, BC/Ch membranes turned a bluish-greenish dark colour and after immersion in EDTA solutions during 24 h, the membranes recovered practically their initial colour. This was indicative that the adsorbed metal had been successfully eliminated from the membranes and the EDTA-Cu^{2+} complex had been formed.

The results of membrane efficiency of Cu(II) ions removal obtained in adsorption-desorption cycles are shown in **Figure 4.15.** It can be observed that after two cycles, regenerated membranes still showed metal ion

removal capacity (they showed around 80% of copper removal efficiency after the second cycle), so this indicated that several cycles could be performed until the membranes lose their capacity to remove copper ions from water. Regardless of the preparation method used, *in situ* or *ex situ*, both membranes could be subjected to adsorption-desorption cycles.

These experiments proved that bionanocomposite membranes still retained the ability to remove Cu (II) ions from water after two re-adsorption cycles although it decreased with each cycle, so further optimization of the desorption process could be performed for even higher adsorption-desorption cyclic performance.

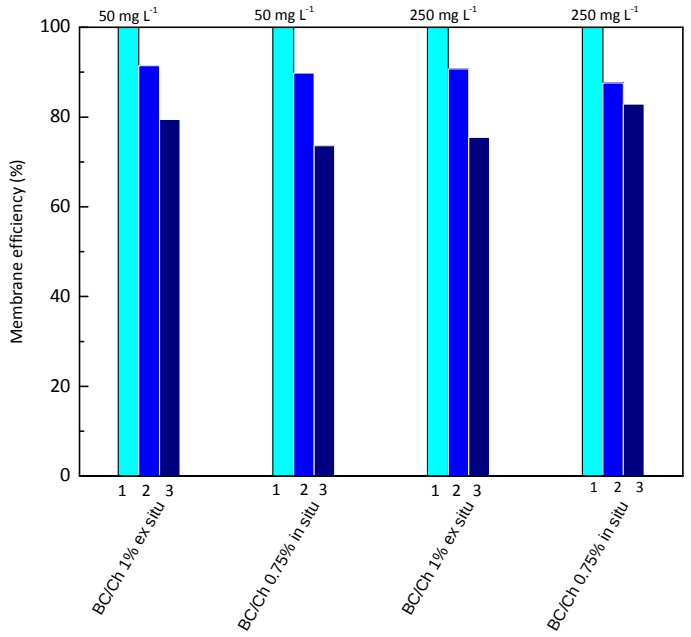

Figure 4.15 Cu (II) ions removal efficiency of the bionanocomposites after two regeneration cycles.

4.4 CONCLUSIONS

In this chapter the potential of the combination of the bacterial cellulose (BC) nanofibril network as a template and chitosan (Ch) as the active phase of the membranes prepared by two different preparation routes, *in situ* and *ex situ*, for the elimination of copper in wastewaters has been studied.

The *in situ* modified BC membranes were produced by the addition of different concentrations of Ch into the culture medium during BC biosynthesis, while *ex situ* modification was carried out by the immersion of BC membranes into Ch-acetic acid solutions. The two routes led to bionanocomposites with different physicochemical properties. The FTIR spectra revealed different interactions between both biopolymers. In the case of *in situ* membranes, predominant interactions between Ch and BC were observed while in the case of *ex situ* membranes, the characteristic peaks of both cellulose and chitosan were observed with no significant shiftings, suggesting less interactions between them. The crystallinity and the water holding capacity strongly related to the mechanical performance resulted to be very different depending on the preparation route. *In situ* prepared membranes showed better mechanical performance in wet state than *ex situ* and neat BC membranes, due to the lower interaction with water molecules. This was analyzed by a swelling study, where it was confirmed that *in situ* prepared membrane had a WHC 3.5 times lower than the one of the *ex situ* membrane and 8.5 times lower than the one of the neat BC. Moreover, the crystallinity of BC/Ch membranes decreased with respect to the neat BC. The incorporation of Ch during the biosynthesis process by the *in situ* route, modified the packaging assembly of the BC in a significant way and therefore, the crystallinity was strongly affected. The morphological

characterization by SEM and AFM revealed a more homogenous reticulated structure with the addition of Ch during BC biosynthesis, suggesting a better inclusion of Ch into BC matrix through *in situ* route. The surface area and pore diameter and volume of BC/Ch membranes were determined by BET analysis and all of them resulted lower compared to the neat BC due to the filling of the pores and compaction by the Ch.

Finally, the cooper removal capacity of these novel membranes was analyzed in two solutions with different copper concentrations and compared to that of the traditionally glutaraldehyde crosslinked Ch membranes, showing higher removal efficiency in the case of *in situ* prepared membranes. Although the prepared membranes resulted to have similar compositions, 35 and 37%wt of Ch for *in situ* and *ex situ* membranes, respectively, the incorporation of the Ch into the BC matrix through *in situ* route led to a more homogenous network with less tendency to swell in water and therefore, to a better interaction with the cooper ions. Moreover the reusability of the membranes was assessed and after two cycles a decrease of less than 20% of the removal efficiency was observed. Therefore, these results suggest the possibility of producing fully biobased reusable filtering membranes for removal of copper from wastewater.

4.5 REFERENCES

[1] Zare, E.N., Motahari, A., Sillanpää, M. Nanoadsorbents based on conducting polymer nanocomposites with main focus on polyaniline and its derivatives for removal of heavy metal ions/dyes: A review. Environ. Res. 162 (2018) 173-195.

[2] Kamal, O., Pochat-Bohatier, C., Sanchez-Marcano, J. Development and stability of gelatin cross-linked membranes for copper (II) ions removal from acid waters. Sep. Purif. Technol. 183 (2017) 153-161.

[3] Deshpande, K. Adsorptive removal of metal ions from water using functionalized biomaterials. Recent. Pat. Biotechnol. 11 (2017) 155-170.

[4] Liu, Z., Wang, Liu, H., Jiang, Y., Yu,G., Mu, X., Wang, X. Magnetic cellulose-chitosan hydrogels prepared from ionic liquids as reusable adsorbent for removal of heavy metal ions. Chem. Comm. 48 (2012) 7350-7352.

[5] Li, Y.J., Xiang, B., Ni, Y.M. Removal of Cu (II) from aqueous solutions by chelating starch derivatives. J. Appl. Polym. Sci. 92 (2004) 3881-3885.

[6] Ajjabi, L.C., Chouba, L. Biosorption of Cu^{2+} and Zn^{2+} from aqueous solutions by dried marine green macroalga Chaetomorpha linum. J. Environ. Manage. 90 (2009) 3485-3489.

[7] Jamshaid, A., Hamid, A., Muhammad, N., Naseer, A., Ghauri, M., Iqbal, J., Rafiq, S., Shah, N.S. Cellulose-based materials for the removal of heavy metals from wastewater-an overview. ChemBioEng Reviews 4 (2017) 240-256.

[8] Maatar, W., Boufi, S. Poly(methacylic acid-co-maleic acid) grafted nanofibrillated cellulose as a reusable novel heavy metal ions adsorbent. Carbohydr. Polym. 126 (2015) 199-207.

[9] Wang, F., Pan, Y., Cai, P., Guo, T., Xiao, H. Single and binary adsorption of heavy metal ions from aqueous solutions using sugarcane cellulose-based adsorbent. Bioresour. Technol. 241 (2017) 482-490.

[10] Karim, Z., Claudpierre, S., Grahn, M., Oksman, K., Mathew, A. Nanocellulose based functional membranes for water cleaning: Tailoring of mechanical properties, porosity and metal ion capture. J. Membr. Sci. 514 (2016) 418-428.

[11] Zhang, L., Zeng, Y., Cheng, Z. Removal of heavy metal ions using chitosan and modified chitosan: A review. J. Mol. Liq. 214 (2016) 175-191.

[12] Krajewska, B. Diffusion of metal ions through gel chitosan membranes. React. Funct. Polym. 47 (2001) 37-47.

[13] Beppu, M.M., Vieira, R.S., Aimoli, C.G., Santana, C.C. Crosslinking of chitosan membranes using glutaraldehyde: Effect on ion permeability and water absorption. J. Membran. Sci. 301 (2007) 126-130.

[14] Schiffman, J.D., Schauer, C. L. Cross-linking chitosan nanofibers. Biomacromolecules 8 (2007) 594-601.

[15] Mitra, T., Sailakshmi, G., Gnanamani, A. Could glutaric acid (GA) replace glutaraldehyde in the preparation of biocompatible biopolymers with high mechanical and thermal properties. J. Chem. Sci. 126 (2014) 127–140.

[16] Beauchamp, R., St Clair, M.B., Fennell, T., Clarke, D., Morgan, K., Karl, F. A critical review of the toxicology of glutaraldehyde. Crit. Rev. Toxicol. 22 (1992) 143-174.

[17] Phisalaphong, M., Jatupaiboon, N. Biosynthesis and characterization of bacteria cellulose–chitosan film. Carbohydr. Polym. 74 (2008) 482-488.

[18] Amaral, I.F., Granja, P.L., Barbosa, M.A. Chemical modification of chitosan by phosphorylation: an XPS, FT-IR and SEM study. J Biomater. Sci. Polym. Ed. 16 (2005) 1575-1593.

[19] Xie, W., Xu, P., Wang, W., Liu, Q. Preparation and antibacterial activity of a water-soluble chitosan derivative. Carbohydr. Polym. 50 (2002) 35-40.

[20] Stefanescu, C., Daly, W.H., Negulescu, I.I. Biocomposite films prepared from ionic liquid solutions of chitosan and cellulose. Carbohydr. Polym. 87 (2012) 435-443.

[21] Kim, J., Zhijiang, C., Lee, H.S., Choi, G.S., Lee, D.H., Jo, C. Preparation and characterization of a bacterial cellulose/chitosan composite for potential biomedical application. J. Polym. Res. 18 (2011) 739-744.

[22] Nge, T.T., Nogi, M., Yano, H., Sugiyama, J. Microstructure and mechanical properties of bacterial cellulose/chitosan porous scaffold. Cellulose. 17 (2010) 349-363.

[23] Wu, T., Farnood, R., O'Kelly, K., Chen, B. Mechanical behaviour of transparent nanofibrillar cellulose-chitosan nanocomposite films in dry and wet conditions. J. Mech. Behav. Biomed. 32 (2014) 279-286.

[24] Li, G., Nandgaonkar, A., Habibi, Y., Krause, W., Wei, Q., Lucia, L. An environmentally benign approach to achieving vectorial alignment and high microporosity in bacterial cellulose/chitosan scaffolds. RSC. 7 (2017) 13678-13688.

[25] Huang, H-C., Chen, L-C., Lin, S-B., Hsu, C-P., Chen, H-H. *In situ* modification of bacterial cellulose network structure by adding interfering substances during fermentation. Bioresour. Technol. 101 (2010) 6084-6091.

[26] Geise, G., Lee, H-S., Miller, D., Freeman, B., Mcgrath, J., Paul. D. Water purification by membranes: the role of polymer science. J. Polym. Sci. B. Polym. Phys. 48 (2010) 1685-1718.

[27] Gebald, C., Wurzbacher, J.A., Tingaut, P., Zimmermann, T., Steinfeld, A. Amine-based nanofibrillated cellulose as adsorbent for CO_2 capture from air. Environ. Sci. Technol. 45 (2011) 9101-9108.

[28] Ul-Islam, M., Khan, T., Park, J. K. Water holding and release properties of bacterial cellulose obtained by in situ and ex situ modification. Carbohydr. Polym. 88 (2012) 596– 603.

[29] Karim, Z., Mathew, A., Grahn, M., Mouzon, J., Oksman, K. Nanoporous membranes with cellulose nanocrystals as functionalentity in chitosan: Removal of dyes from water. Carbohydr. Polym. 112 (2014) 668-676.

[30] Labidi, A., Salaberria, A., Fernandes, S., Labidi, J., Abderrabba, M. Adsorption of copper on chitin-based materials: Kinetic and thermodynamic studies. J. Taiwan. Inst. Chem. Eng. 65 (2016) 140–148.

[31] Xiao, M., Hu, J. Cellulose/chitosan composites prepared in ethylene diamine/potassium thiocyanate for adsorption of heavy metal ions. Cellulose 24 (2017) 2545-2557.

[32] Aman, T., Kazi, A.A., Sabri, U.M., Bano, Q. Potato peels as solid waste for the removal of heavy metal copper (II) from waste

water/industrial effluent. Colloids. Surf. B. Biointerfaces 63 (2008) 116-121.

[33] Mautner, A., Maples, H.A., Sehaqui, H., Zimmermann, T., de-Larraya, U.P., Mathew, A.P., Lai, C.Y., Li, K., Bismarck, A. Nitrate removal from water using a nanopaper ion-exchanger. Environ. Sci.: Water Res. Technol. 2 (2016) 117-124.

[34] Wang, F., Pan, Y., Cai, P., Guo, T., Xiao, H. Single and binary adsorption of heavy metal ions from aqueous solutions using sugarcane cellulose-based adsorbent. Biores. Technol. 241 (2017) 482-490.

[35] Steenkamp, G.C., Keizer, K., Neomagus, H.W.J.P., Krieg, H.M. Copper (II) removal from polluted water with alumina/chitosan composite membranes. J. Membr. Sci. 197 (2002) 147-156.

CHAPTER 5

BACTERIAL CELLULOSE/POLYURETHANE NANOCOMPOSITES

5. BACTERIAL CELLULOSE/POLYURETHANE NANOCOMPOSITES

5.1 INTRODUCTION

In this chapter, BC membranes were used for the preparation of BC/polyurethane nanocomposites with water-activated shape memory properties which could be suitable for applications in the biomedical field.

In this way, currently, smart materials with the ability to recover their original shape after being deformed in a temporary shape under the application of external stimulus are in the focus of research [1]. These materials are known as shape memory polymers (SMPs) and the external stimulus can be temperature, water, pH, light, etc. Polyurethane (PU)-based thermoplastic polymers possess shape memory properties based on transition temperatures (glass transition or melting temperature) and also can be thermo-moisture responsive, since the water absorbed upon immersion has a strong influence in their properties [2]. This means that these materials can be activated upon immersing into water. This interesting feature opens new possibilities for the application of PU and their nanocomposites in the biomedical field for the development of implants, drug delivery carriers, vascular stents, etc. allowing to minimizing invasive surgeries [3].

Among PUs, the development of waterborne polyurethanes (WBPU) has experienced an increase because their use does not imply the use of organic solvents, thus reducing the amount of volatile organic compounds released to the atmosphere [4]. Moreover, WBPU dispersions present low viscosities

and good film forming ability with strong adhesion and large flexibility. In addition, these matrixes in aqueous dispersion present good affinity with hydrophilic nanoentities and nanoreinforcements, such as polysaccharides [5]. Among polysaccharides, cellulose is the most abundant organic biopolymer that exists naturally. Nanocellulose is widely used as a nanoentity for production of advanced nanostructured materials, since the use of nanocelluloses as reinforcements leads to an enhancement of some properties, especially, mechanical properties. Nanocelluloses possess active hydroxyl groups which can interact by hydrogen bonding with the macromolecular chains of WBPU matrixes leading to an increased dispersion, reinforcement and interfacial adhesion [6]. However, in order to obtain advanced nanocomposites, a proper dispersion of the nanoentity in the WBPU matrix must be achieved.

Furthermore, nanocellulose can be considered a good substrate material for water-activated shape memory materials due to its surface´s hydroxyl groups and intermolecular hydrogen bonds. Song et al. [7] developed a cellulose based water-activated shape memory composite with sisal cellulose nanofibers and graphene oxide which reached a shape recovery ratio nearly of 100%.

As it has been discussed in chapter 1, with its interesting spatial configuration of 3D nanofiber network, BC can be considered an interesting material for the development of a wide range of nanocomposites for applications in several fields. The use of the BC nanofiber membrane as a nanoreinforcement could be an interesting possibility to counteract the difficulty to obtain a good dispersion of nanofibers in polymer matrixes.

Moreover, due to its biocompatibility, BC has proven to have interesting properties for *in vivo* and *in vitro* applications in the biomedical field [8-10].

Therefore, in this chapter, water-activated nanocomposites based on WBPU and BC were developed. BC membranes were embedded into WBPU dispersion to produce nanocomposites with improved stiffness and favourable effects on the shape memory properties. The interactions between components, morphology and thermal, thermomechanical and mechanical properties were investigated. In order to evaluate the potential applications of these nanocomposites in the biomedical field, the *in vitro* biocompatibility was studied by cytotoxicity and cell adhesion assays. Additionally, water-activated shape memory properties were analyzed by fold-deploy shape memory test.

5.2 EXPERIMENTAL

5.2.1 Preparation of BC/WBPU nanocomposites

Firstly, BC membranes were grown in the culture medium prepared with apple residues and sugar cane as described in the previous chapter 3. Then, BC membranes were purified, thoroughly washed with running water until a complete neutralization and stored at 5 °C in deionized water until utilization.

BC/WBPU nanocomposites were prepared by immersing BC wet membranes in 50 mL of the commercial WBPU dispersion (Impraperm DL 3746) under stirring conditions at room temperature for different times, 5, 30, 60 and 120 min, and then were dried at room temperature for 4 days in order to obtain transparent nanocomposite films. The as prepared BC/WBPU

nanocomposites were designated: BC/WBPU5, BC/WBPU30, BC/WBPU60 and BC/WBPU120. The schematic preparation of BC/WBPU nanocomposites is depicted in **Figure 5.1**. As a reference, a neat WBPU film was prepared by casting the WBPU dispersion and dried in the same conditions as the nanocomposites. Additionally, neat BC films were prepared by drying the BC membranes between Teflon plates in an oven at 55 °C for two days. Finally, all the samples were stored in a desiccator until use.

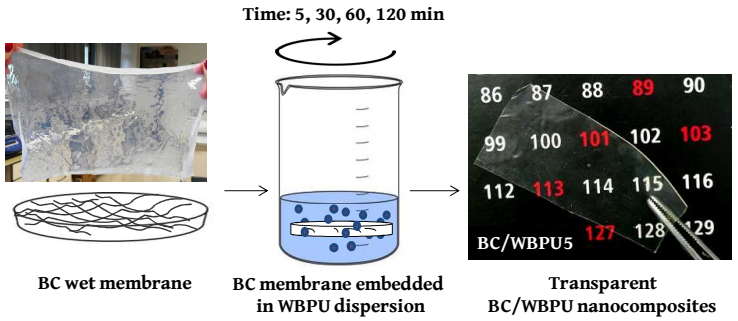

Figure 5.1 The scheme of preparation of BC/WBPU nanocomposites.

5.2.2 Shape memory behavior test

The shape memory effect was investigated by fold-deploy shape memory test [11,12]. Samples (30 x 10 mm^2) were immersed in a water bath at 60 °C inside closed containers and folded (φ_d) by applying external constant force. Then, samples were cooled down in an ice water bath under the external force to fix the temporary shape. This force was then removed after holding for several minutes and a marginal recovery occurred (φ_1) and the bending angle became fixed (φ_f). Finally, the specimens were immersed in water at 40 °C and the change of the angle with time (φ_t) was recorded using a video

camera. The shape fixity ratio (R_f) and the shape recovery ratio (R_r) were calculated from **Equation 5.1** and **5.2**, respectively.

$$R_f(\%) = \frac{\varphi_f}{180^\circ} \cdot 100 = \frac{180^\circ - \varphi_1}{180^\circ} \cdot 100 \quad \textbf{(5.1)}$$

$$R_r(\%) = \frac{\varphi_t - \varphi_1}{180^\circ - \varphi_1} \cdot 100 \quad \textbf{(5.2)}$$

The measure of the bending test angles was carried out through an open source image-processing program, ImageJ. Each system was tested in triplicate in order to calculate the standard deviation. The shape memory study procedure is indicated in **Figure 5.2**, where the temperatures of each phase are presented: T_s (storage temperature), T_d (deformation temperature), T_f (fixation temperature) and T_r (recovery temperature).

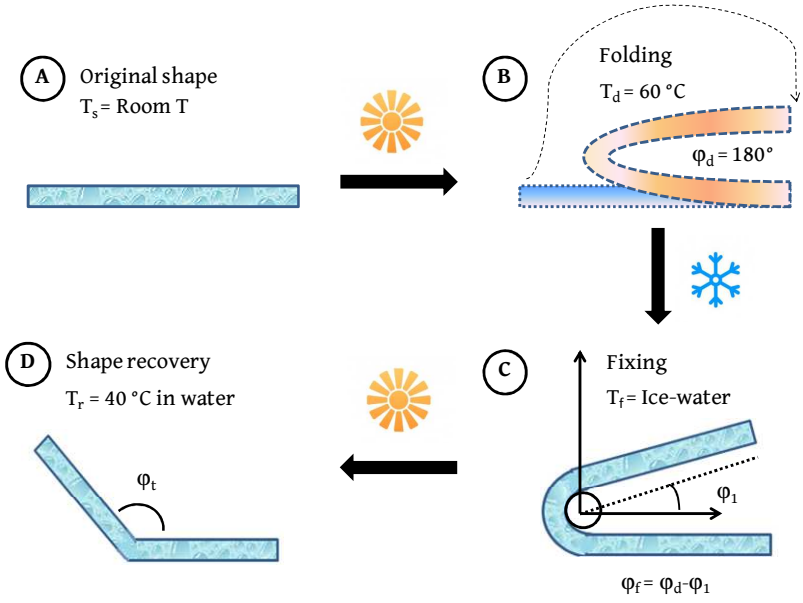

Figure 5.2 Fold-deploy shape memory test procedure.

5.3 RESULTS

5.3.1 Characterization of BC/WBPU nanocomposites

5.3.1.1 Composition and morphology

Firstly, the effect of the impregnation time of the WBPU dispersion into BC membranes in the morphology and thickness of the resulting BC/WBPU nanocomposites was analyzed. As it can be observed in **Table 5.1**, there is a direct relationship between the impregnation time and the thickness of the nanocomposites. As the impregnation time increased, the thickness of the nanocomposite was greater, which suggestes that the quantity of WBPU in the BC/WBPU nanocomposite was higher.

Table 5.1 Thickness of neat BC, neat WBPU and BC/WBPU nanocomposites and BC content.

Sample	Thickness (mm)	BC (wt%)
BC	0.04 ± 0.01	100
BC/WBPU5	0.22 ± 0.05	1.8 ± 0.1
BC/WBPU30	0.33 ± 0.05	-
BC/WBPU60	0.35 ± 0.07	-
BC/WBPU120	0.42 ± 0.05	0.6 ± 0.1
WBPU	0.43 ± 0.17	0

In order to estimate the composition of the nanocomposites, the amount of BC was determined in the BC/WBPU5 and BC/WBPU120 nanocomposites, which were the membranes prepared with the largest and the shortest immersion times. For this, consecutive extractions with N,N-dimethylformamide (DMF, purchased from Sigma-Aldrich) were carried out for a week to ensure the complete removal of the WBPU from the BC membrane. This fact was confirmed by FTIR analysis of the resultant dried BC samples, as no characteristic bands corresponding to the WBPU were

observed in the FTIR spectra of the dried samples. Then DMF was eliminated from the extract in a rotary evaporator (100 mbar, 97 °C).

The amount of BC in the nanocomposites was estimated using two variables: through the weight difference between the initial nanocomposite and the BC after the elimination of WBPU, and though the weight difference between the WBPU/DMF and the collected WBPU after DMF removal from the flask. Each system was measured in duplicate and it was estimated that BC/WBPU5 contained a 1.8 ± 0.1 wt% of BC while BC/WBPU120 contained 0.6 ± 0.1 wt% of BC (**Table 5.1**).

These results confirmed that the nanocomposites contained high amount of WBPU, probably due to the high affinity between BC and WBPU and the BC porous structure. In this way, the porous structure of the BC nanofiber network and the nanometric size of WBPU particles (87.1 ± 0.3 nm) in water probably favoured the penetration and coating of the BC structure.

Additionally, the fact that the polyurethane was water based was an important feature. This also facilitated the diffusion and impregnation of the WBPU particles into the BC wet membrane as both components are hydrophilic. Some preliminary experiments were performed with dry BC membranes and the results confirmed that the impregnation was more effective in the case of using wet membranes. This was probably due to the fact that the BC membranes were already swollen, which led to a greater diffusion of the WBPU nanoparticles though the BC membranes at the studied time intervals.

This fact was confirmed by SEM analysis. **Figure 5.3** shows the microstructure of the cross section of the neat BC membrane and BC/WBPU5 nanocomposite (x250 and x1000).

As it can be seen, BC presented the typical compacted layered structure with nanofibrous texture [13,14]. In the case of the nanocomposite, the presence of the BC was not appreciated due to the high amount of WBPU resulting in an increase of film thickness and making very complicated to observe the last into the nanocomposites by SEM.

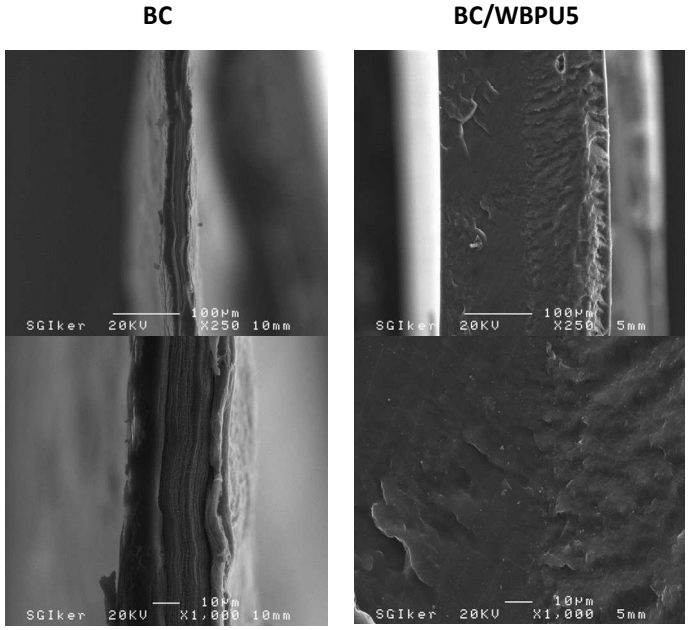

Figure 5.3 SEM images of cross sections of BC membrane and BC/WBPU5 nanocomposite.

As it can be observed in **Figure 5.1**, BC/WBPU nanocomposites exhibited excellent transparency. It has been previously reported that the nanofiber

papers are translucent due to the effect of the light diffraction at the interface between the cellulose nanofibers and the air interstices between them [15]. The 3D nano-sized fiber network of the BC with air interstices in between makes it very opaque, so the transparency of the nanocomposites implies that these gaps may had been completely filled and the surface had been coated by the WBPU. This was also observed in a previous work developed in our research group in which BC membranes were impregnated with poly(lactic acid) (PLA). Interaction between BC and PLA was improved by the addition of a small amount of polyethylene glycol (PEG). In that previous work BC/PLA-PEG nanocomposites were prepared by the immersion of BC wet membranes in solutions of different concentrations of PLA-PEG and the final nanocomposites contained 89-96 wt% of BC. The PLA-PEG film was fully transparent and the BC/PLA-PEG nanocomposites showed an increase of transparency due to the filling of the interstices of the BC membranes by the PLA-PEG. However, PLA is hydrophobic (static contact angle 78°), so BC and PLA showed poor compatibility and thus, the impregnation was less effective.

These results would confirm that as the polyurethane used in the present work was water based, BC and WBPU presented strong affinity, leading to nanocomposites with high amount of the last.

5.3.1.2 Physicochemical characterization

To identify the possible interactions between BC and WBPU in the nanocomposites, FTIR spectroscopy analysis was carried out. In **Figure 5.4**, the FTIR spectra of neat BC, neat WBPU and BC/WBPU5 are shown.

The neat WBPU showed the typical bands of the repetitive urethane group (-NHCOO-). The band located at 3440 cm^{-1} corresponds to stretching vibration of N-H bond and the band at 1530 cm^{-1} is assigned to the in-plane bending vibration of N-H. The bands at 2920 and 2850 cm^{-1} are associated to stretching vibration of C-H. The characteristic band about 1730 cm^{-1} is related with the urethane C=O group. The band at 1259 cm^{-1} corresponds to asymmetric stretching vibration of C-O [5,16].

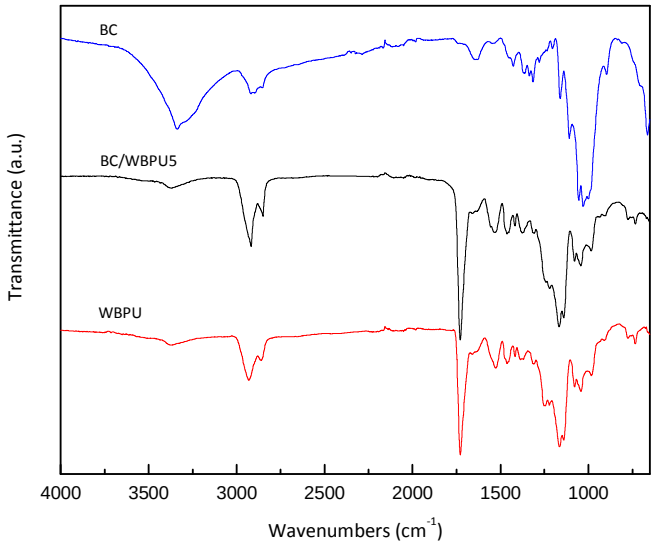

.Figure 5.4 FTIR spectra of the neat BC, neat WBPU and BC/WBPU5.

In the case of BC membrane, as explained in previous chapters 3 and 4, the broad band around 3340 cm^{-1} corresponds to OH stretching vibration, the absorption bands at 2900-2880 corresponds to CH stretching vibration and the band at 1430 cm^{-1} to CH_2 bending vibration. The bands at 1160 and 1108 are associated to C-O-C bond of the glycosidic bonds and the band at 898

cm^{-1} is characteristic of β-linked glucose based polymers. Finally, the band at 1646 cm^{-1} is associated with the water absorbed by the cellulose.

In the nanocomposite spectrum, the peaks of the BC are not observed due to the high content and coating of WBPU. Moreover, FTIR spectra of the neat WBPU and the nanocomposite were very similar, with small differences in the intensities of the characteristic bands. As described in other works, these differences can be analyzed through the second derivative study [17]. Therefore a second derivative spectroscopy analysis was carried out and the resultant spectra are shown in **Figure 5.5**.

The second derivative spectra in the range of 1500-900 cm^{-1} were almost identical for the two samples, as observed in **Figure 5.5** a). However, significant differences were found in the OH stretching vibration region in the range 3500-3290 cm^{-1} as showed in **Figure 5.5** b). Here it can be clearly find a shift in the bands at 3495, 3486, 3421, 3411, 3338, 3320 and 3301 cm^{-1} in the case of the nanocomposite.

Guo et al. [17] analyzed the hydrogen bonding interactions of poly(3-hydroxybutyrate) and poly(4-vinylphenol) blends through the second derivative spectra. They observed bands in this region which were shifted in the case of the blend to higher wavenumbers with respect to the neat components and they attributed this to intermolecular hydrogen bonding. In this case, everything indicates that new hydrogen bonding interactions between BC and WBPU have been formed in the nanocomposite.

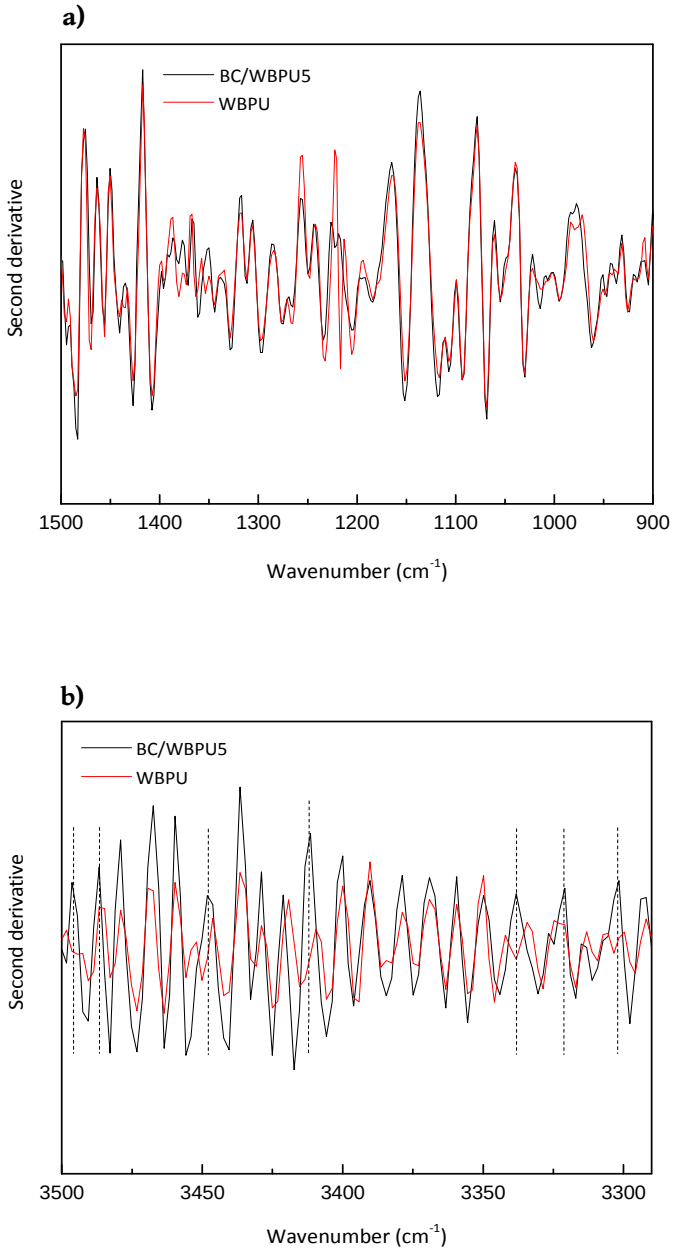

Figure 5.5 Second derivatives of neat WBPU and BC/WBPU5 a) around 1500-900 cm^{-1} and b) around 3500-3290 cm^{-1}.

5.3.1.3 Mechanical performance

The mechanical behavior of neat BC, neat WBPU, and BC/WBPU nanocomposites was evaluated by tensile tests, and their Young's modulus (E), tensile strength (σ_{max}) and elongation at break (ε_b) are gathered in **Table 5.2**.

Table **5.2** Mechanical properties of neat BC, neat WBPU and BC/WBPU nanocomposites.

Sample	E (MPa)	σ_{max} (MPa)	ε_b (%)
BC	7120.3 ± 421.3	116.9 ± 17.0	2.5 ± 0.3
BC/WBPU5	41.4 ± 5.1	11.6 ± 2.9	464.3 ± 31.8
BC/WBPU30	28.7 ± 3.5	9.7 ± 1.7	582.8 ± 76.0
BC/WBPU60	25.1 ± 3.8	10.3 ± 2.7	711.5 ± 77.1
BC/WBPU120	15.2 ± 2.8	10.1 ± 1.4	697.3 ± 68.7
WBPU	7.2 ± 1.7	9.2 ± 2.5	917.7 ± 96.4

As commented in previous chapters, due to the conformation of the 3D structure of the interconnected nanofibers formed during the biosynthesis, BC exhibits an outstanding high modulus. The high content of WBPU in the nanocomposites was evident taking into account the results obtained in the mechanical properties.

The commercial WBPU used in this work exhibited a remarkable elastomeric behavior and the prepared BC/WBPU nanocomposites presented a high elongation at break, with elongation values superior to 400% in all cases. It was observed a decline in elongation at break of the nanocomposites with shorter impregnation times probably due to the slightly higher content of BC, although still maintained the elastomeric behavior of the WBPU.

In addition, the Young's modulus experienced an important improvement with respect to the neat WBPU, suggesting the effectiveness of the reinforcing effect of the BC membrane. The improvement in the tensile strength in presence of BC was less accused than in the modulus. The BC/WBPU5 nanocomposite (~1.8 wt% BC) presented 26% of improvement in tensile strength and 475% of increase in Young´s modulus compared to neat WBPU and the BC/WBPU120 nanocomposite (~0.6 wt% BC) experienced 10% of improvement in tensile strength and 110% of increase in Young´s modulus compared to neat WBPU. This fact could be due to the good interfacial interactions between both polymers as it has been observed in the FTIR results [18]. Wu et al. [19], prepared nanocomposite films from a two-component waterborne polyurethane with 0.5, 1, 1.5, and 2 wt% contents of nanofibrillated cellulose (NFC). They observed enhancement in the modulus (from 194 MPa to 388 MPa) and tensile strength (from 7.4 MPa to 13.8 MPa) up to 1% of nanofiller with respect to the neat polyurethane and they ascribed this behavior to the uniform dispersion and interfacial bonding of the NCF with the polyurethane. However, the increase of the NFC content led to a decline of the mechanical performance attributed to the self aggregation of NFC. Furthermore, elongation at break of the nanocomposite films decreased with the increase of NFC content.

In the present work, the randomly oriented nanofiber membrane of BC is completely embedded in the WBPU so the good wetting and adhesion between both components could have led to the superior mechanical properties. Moreover, in this case the use of the whole BC membrane counteracts the difficulties to obtain a better dispersion of nanofibers. In view of these results, 5 min of impregnation would be enough time to obtain stiffer yet elastomeric nanocomposites.

5.3.1.4 Thermal and thermomechanical properties

Additionally, the thermal and thermomechanical properties of BC/WBPU nanocomposites were analyzed. For these studies, BC/WBPU5 and BC/WBPU120 were chosen since these were the nanocomposites with higher and lower content of BC, and the results were compared to those obtained for the neat BC and neat WBPU.

Thermal transitions of neat BC, neat WBPU and BC/WBPU nanocomposites were analyzed by differential scanning calorimetry (DSC) and the obtained thermograms are gathered in **Figure 5.6**.

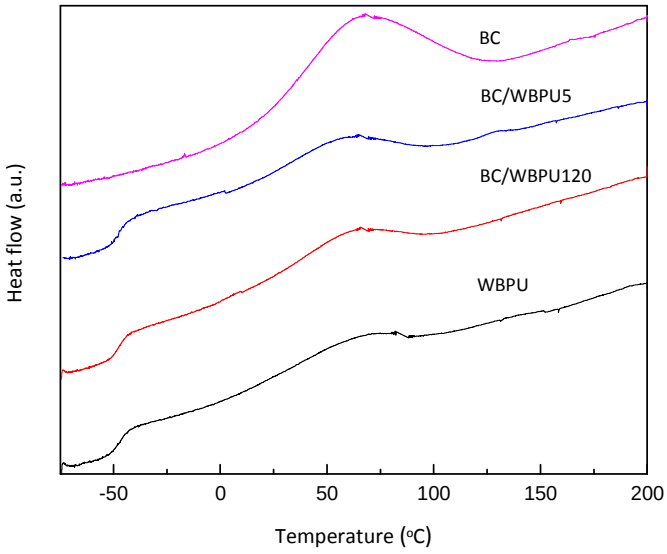

Figure 5.6 DSC thermograms of neat BC, neat WBPU and BC/WBPU120 and BC/WBPU5 nanocomposites.

In the case of neat BC, an endothermic transition is observed in the temperature range of 35-120 °C. This can be ascribed to the dehydration process of cellulose [20]. In the case of WBPU and the nanocomposites, the presence of two transitions was observed. The one at low temperature (from -70 to -40 °C) was associated to glass transition (T_g) of the soft segment of WBPU and the second one at higher temperature (in the range of 50-120 °C), an endothermic peak, associated to melting process (T_m). The values of glass transition temperature (T_g), melting temperature (T_m) and melting enthalpy (ΔH_m) are gathered in **Table 5.3**. No significant changes were observed in the case of T_g and T_m between WBPU and the nanocomposites. However, it can be noted that the melting enthalpy increased with BC content. This suggested that the presence of BC in the WBPU may have induced a nucleating effect, favouring its crystallization.

Table 5.3 Thermal properties of neat WBPU and BC/WBPU nanocomposites.

Sample	T_g (°C)		T_m (°C)	ΔH_m (J g^{-1})	T_{10} (°C)	T_{50} (°C)
WBPU	-48.2*	-44.6**	64.2	12.3	335	370
BC/WBPU120	-46.6*	-43.7**	65.4	15.4	326	358
BC/WBPU5	-47.6*	-42.8**	63.9	19.9	325	354

T_g values measured by DSC (*) and DMA (**).

In addition, thermal stability of neat BC, neat WBPU and BC/WBPU nanocomposites was studied by TGA. Besides, this study was used to corroborate that the last transition observed in the range of 50-120 °C was not related to the evaporation process of possible water content present in the WBPU and BC/WBPU nanocomposites. The TG curves are shown in **Figure 5.7**.

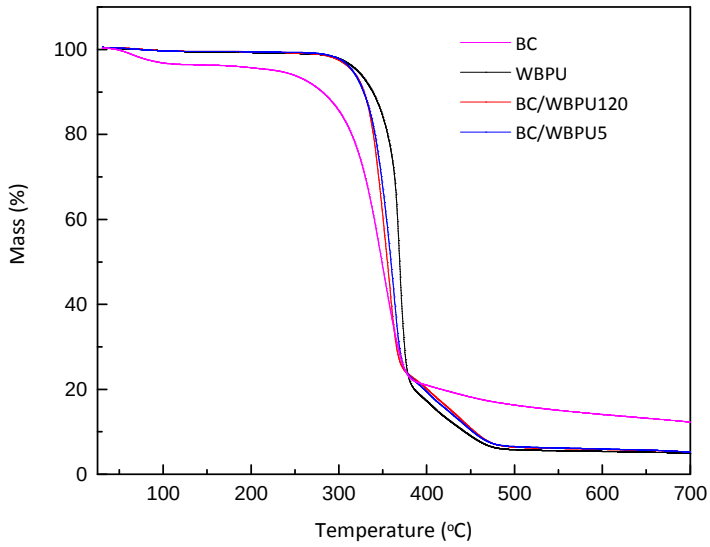

Figure 5.7 TGA curves of neat BC, neat WBPU and BC/WBPU120 and BC/WBPU5 nanocomposites.

In the case of neat BC, the first initial mass loss below 150 °C is usually associated to the release of water while the volatilization of thermally degraded cellulosic compounds is in the range of 200-500 °C, as described in previous chapter 3. As it can be observed, the neat WBPU does not contain water, nor the BC/WBPU nanocomposites as no mass loss is observed up to temperatures around 300 °C. The presence of BC induces to an earlier degradation in the nanocomposites, since as it can be observed the corresponding TG curves of the nanocomposites are shifted towards lower temperatures compared to the neat WBPU. The temperature at 10 and 50% of mass loss (T_{10} and T_{50}, respectively) are shown in **Table 5.3**, where it can be observed a decrease of around 10 °C in the case of the temperature at 10% mass loss of the nanocomposites with respect to the neat WBPU.

Finally, the thermomechanical behavior of the different samples was studied by dynamic mechanical analysis (DMA). The evolution of storage modulus (E´) and Tan Delta (Tan δ) curves as a function of temperature are shown in **Figure 5.8** a) and b), respectively.

In the case of the neat BC, a drop in the storage modulus and a maximum in the Tan δ in the range of -10 to 50 °C was observed, associated to the presence of water into the structure that acts as plasticizer which was in agreement with the TGA analysis. This was also observed by other authors [21].

Compared to neat WBPU, both nanocomposites showed higher storage modulus on all temperature range. In the glassy state, at very low temperature (from -100 to -40 °C), neat BC presented the highest E´ value (5700 MPa) while the neat WBPU presented the lowest value (1040 MPa) and, as it can be observed, BC/WBPU nanocomposites showed intermediate E´ values between neat components. Similar E´ values were observed for both nanocomposites, 1900 and 1920 MPa for BC/WBPU5 and BC/WBPU120, respectively. As the temperature increased, the storage modulus of the neat WBPU and both nanocomposites showed a significant decrease associated with the glass transition temperature. In the case of neat WBPU, the modulus kept decreasing with temperature in the rubbery region due to the thermoplastic nature of the material, while in the BC/WBPU nanocomposites the drop was reduced due to the effect of BC network into the WBPU. This effect was also observed by other authors in a polyurethane elastomer reinforced with 0.5, 1 and 5 wt% of cotton cellulose nanocrystals [22]. They ascribed this effect to the increase of the cross-linked density of the elastomer through polyurethane-cellulose interactions.

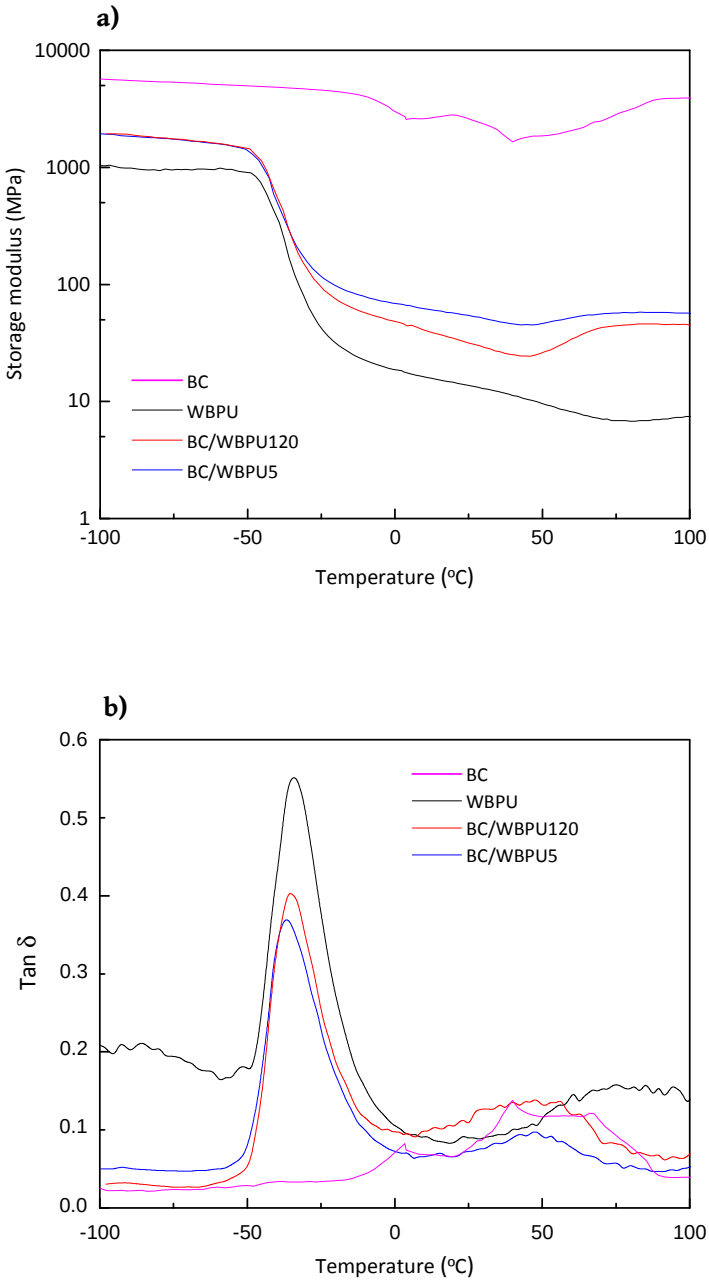

Figure 5.8 a) Storage modulus and b) Tan δ of neat BC, neat WBPU and BC/WBPU120 and BC/WBPU5 nanocomposites.

In the present work, a slightly increase of the modulus above 50 °C was observed in the case of the nanocomposites. Around the T_m of the WBPU, the polymer mobility could favour the formation of interactions between BC and WBPU, and therefore, a slight increase in the modulus.

5.3.2 Biocompatibility

In order to evaluate the possible application of these nanocomposites in the biomedical field, cell viability, proliferation and adhesion were analyzed.

On the one hand, short-term cytotoxicity assays were carried out. BC/WBPU5 nanocomposite was chosen for the study since it was the system which presented the better mechanical properties. Neat BC was also analyzed as reference. The cytotoxicity test results are presented in **Figures 5.9** and **5.10**.

Figure 5.9 shows the absorbance versus incubation time for the positive (polyvinyl chloride, PVC) and negative (high density polyethylene, HDPE) controls, as well as for the neat BC and BC/WBPU5. As it can be observed, both BC and BC/WBPU5 nanocomposite displayed nontoxic cell growth, similar to the negative control.

The cell proliferation with respect to the negative control as a function of the incubation time is represented in **Figure 5.10**. It was observed that the viability of the L929 cells cultured in the extracted media of both, neat BC and BC/WBPU5 was significantly higher than the established acceptance limit of 70% of this value. Consequently, the obtained results are good indication when thinking on the future biomedical application of the studied polymers.

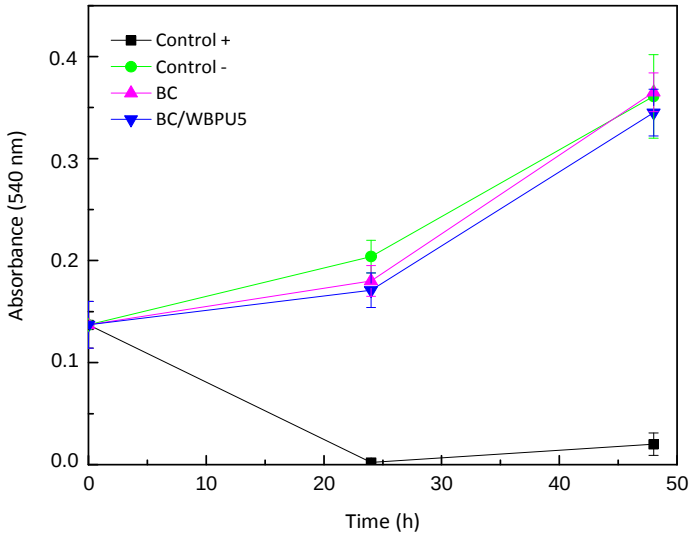

Figure 5.9 Absorbance at 540 nm versus incubation time of a positive control, negative control, neat BC and BC/WBPU5.

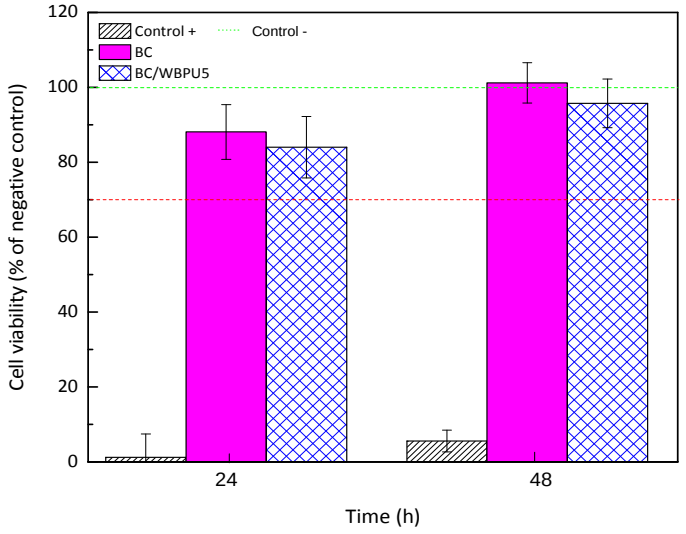

Figure 5.10 Viability of L-929 murine fibroblast cells as function of incubation time.

In addition, long-term cell adhesion test were carried out by Live/Dead assays. **Figure 5.11** shows the fluoresce confocal microscopy images (x20) where Calcein-AM shows cell viability (green) and ethidium homodimer-1 non-viable cells (red). As it can be observed, significant cellular adhesion and proliferation were found for both, neat BC and BC/WBPU5 nanocomposite. There is a large number of adherent cells that show viability (green), and a shortage of dead cells (red). The culture reached the monolayer in 72 h, showing adhesion and stable growth until day 14. In the last stage (C and F), the number of non-viable cells increased, probably due to the high density of the culture. The cells responded in a similar manner to both materials, so since the composition of the materials directly affects cell viability and adhesion, it is concluded that both BC and BC/WBPU bionanocomposites are biocompatible materials.

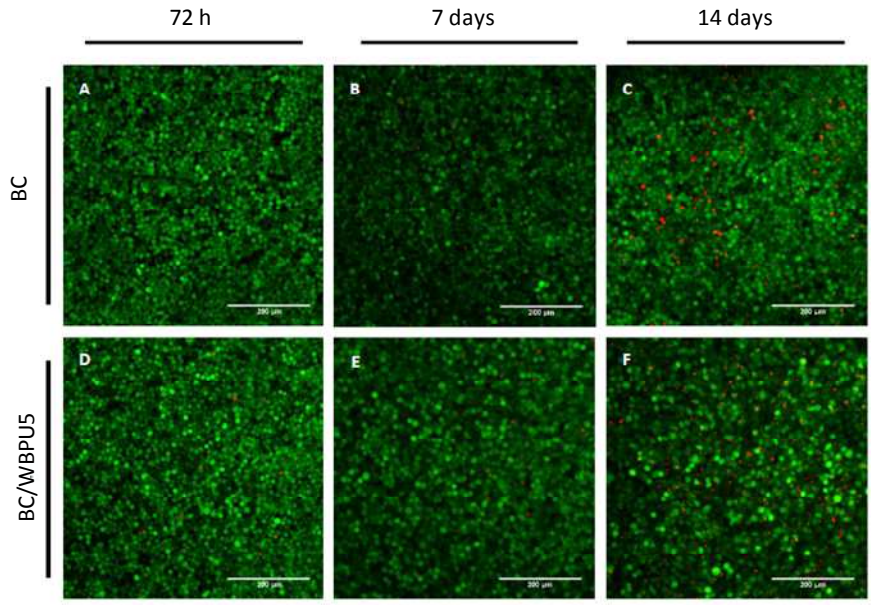

Figure 5.11 Adhesion and viability of L929 cells on BC (A-C) and BC/WBPU5 (D-F).

5.3.3 Water-activated shape memory properties

The shape memory properties, namely shape fixity ratio (R_f) and the shape recovery ratio (R_r), of the neat WBPU and two nanocomposites (5 min and 120 min of impregnation) were analyzed according to fold-deploy test procedure schematized in **Figure 5.2**.

The shape recovery process in water as function of time of the neat WBPU and BC/WBPU nanocomposites can be observed in **Figure 5.12** and the results of shape recovery ratio in water along time are shown in **Figure 5.13**. All the results are gathered in **Table 5.4**.

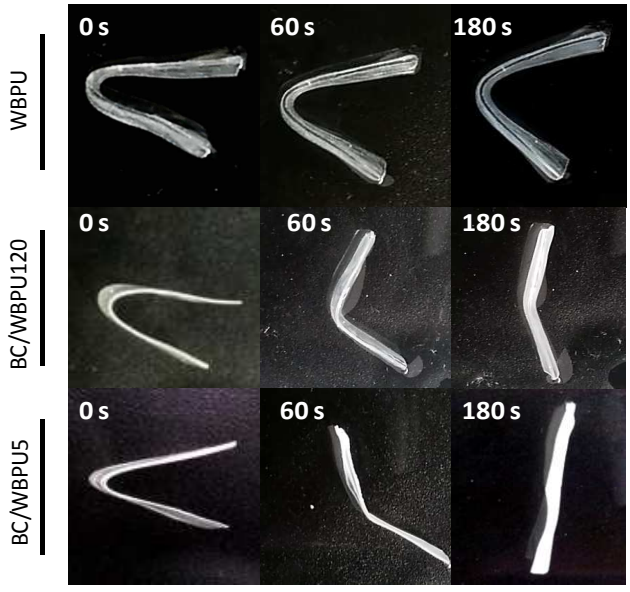

Figure 5.12 Shape recovery process in water of the neat WBPU and BC/WBPU120 and BC/WBPU5 nanocomposites.

T**able 5.4** Marginal recovery angle (φ_1), shape fixity (R_f) and recovery (R_r) ratios and maximun water uptake for neat WBPU and BC/WBPU5 and BC/WBPU120 nanocomposites.

Sample	φ_1 (°)	R_f(%)	R_r (%)$_{3min}$	R_r (%)$_{final}$	Maximun water uptake (%)
WBPU	43.7 ± 4.8	75.7 ± 2.7	33.4 ± 9.6	73.0 ± 3.5	49.2 ± 0.8
BC/WBPU120	32.7 ± 4.7	81.8 ± 2.7	72.0 ± 5.1	78.2 ± 8.4	33.5 ± 6.4
BC/WBPU5	26.6 ± 4.6	86.0 ± 5.5	92.8 ± 6.3	94.5 ± 7.2	30.1 ± 6.8

The R_f of the samples summarized in **Table 5.4**, suggested that the shape fixity ability was enhanced with the presence of BC. This behavior has been also observed in other works involving polyurethane matrixes reinforced with nanocelluloses and it can be ascribed to the presence of the numerous hydroxyl groups of the BC nanonetwork [23,24]. These can contribute to the formation of hydrogen bonds between BC and WBPU, resulting in a higher rigidity, increasing the modulus of the material and thus, favouring the fixity of the material´s shape respect to the neat WBPU [25].

Moreover, these results were in accordance to the ones obtained in the mechanical and thermomechanical analysis where it was observed that the storage modulus of the nanocomposites were higher with the presence of BC. According to Ratna and Karger-Kocsis [26] a high glass state modulus will provide the material with high fixity during simultaneous cooling and unloding.

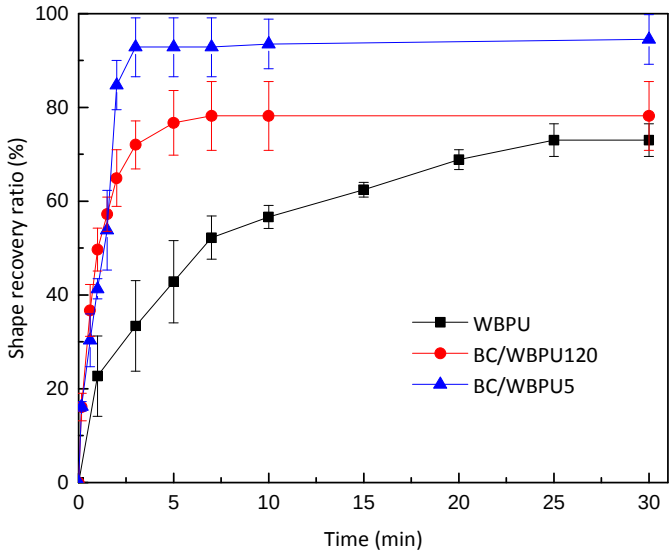

Figure 5.13 Shape recovery ratio in water of neat WBPU and BC/WBPU120 and BC/WBPU5 nanocomposites.

Taking into account that these nanocomposites could have applications in the biomedical field, once the shape of the nanocomposites is fixed, these should be capable to recover the original shape inside the human body. Therefore, considering the possible application of these nanocomposites in medical devices triggered by human body liquids, the shape recovery was analyzed in water at 40 °C. This was set taking into account that the suitable recovery temperature must be slightly higher than body temperature (>37 °C) but not too high so as not to damage the normal cells and tissues [11].

As it can be observed in **Figure 5.13**, the incorporation of the BC also induced to a faster recovery process due to its hydrophilic nature. The water molecules diffused through the nanocomposite and the hydrogen bonds between water and BC hydroxyl groups made the film become softer, so the

recovery of the original shape was faster [24]. In 3 min, the BC/WBPU5 recovered 92.8 ± 6.3% of the original shape, while BC/WBPU120 recovered 72.0 ± 5.1% and neat WBPU only 33.4 ± 9.6%. In the case of the neat WBPU needed 25-30 min to recover 73.0 ± 3.5% of the original shape.

Additionally to the presence of BC, the chemical structure and thickness of the nanocomposites as well as the movement of molecular architecture had influence on the shape memory recovery.

Huang et al. [27] reported that the R_r in moisture induced recovery is lower than in thermally induced recovery. In moisture induced recovery systems, there is a strong dependency on the sample size because the water absorption is easier on the sample´s surface, so the saturation is faster than inside the material. This means that thin films are more suitable for moisture induced recovery systems than bulky materials [27]. In this case, it was observed (**Table 5.1**) that as impregnation time increased, the thickness of the nanocomposite increased (0.22 ± 0.05 and 0.42 ± 0.05 mm for BC/WBPU5 and BC/WBPU120 nanocomposites, respectively) and this could have had an influence on the shape memory properties. BC/WBPU5 presented the fastest recovery and was the thinnest nanocomposite, so these results correlated with this fact. Song et al. [7] also reported that when the material presents a well arrayed layered structure the movement of water molecules in the matrix after immersion in water is favoured. As it was observed in SEM images (**Figure 5.3**), BC presented a layered structure so this fact could have helped to the recovery process in the nanocomposites.

On the other hand, the temperature at which the test was performed may have helped to the recovery of the shape. As it has been previously reported,

the increase of the temperature leads to a weakening of the hydrogen bonding, so the system will have greater recovery capacity [28]. The effect of the temperature can also be important if the recovery temperature is higher than any transition. As it was observed in the DSC thermograms (**Figure 5.6**), the second transition of the WBPU started around 40 °C, so in this case as the test was performed below the transition temperature, everything indicated that the phenomenon of shape recovery was mainly caused by water and the effect of temperature would be minimal.

The results suggest that these materials could be suitable to develop rapid responsive materials with applications in different fields such us in sensors, artificial muscles, self-expandable stents or devices involving minimally invasive surgery in the human body.

In view of the results of the shape memory test, it was interesting to analyze the water holding capacity (WHC) of neat WBPU and BC/WBPU nanocomposites, since the shape recovery was predictably related to the absorption of water. In order to analyze the influence of the presence of BC in the nanocomposites in the water intake, neat WBPU and BC/WBPU5 and BC/WBPU120 nanocomposites were immersed in water at room temperature for a certain time and the WHC was calculated using the **Equation 2.16**. The obtained results are compiled in **Figure 5.14**.

As it has been observed in previous chapters 3 and 4, BC presents a high water holding capacity (WHC) ascribed to its conformation and affinity with water due to the numerous hydroxyl groups present in its structure. The obtained results confirmed that water uptake increased rapidly in the presence of BC up to 1 hour of immersion in the case of BC/WBPU nanocomposites.

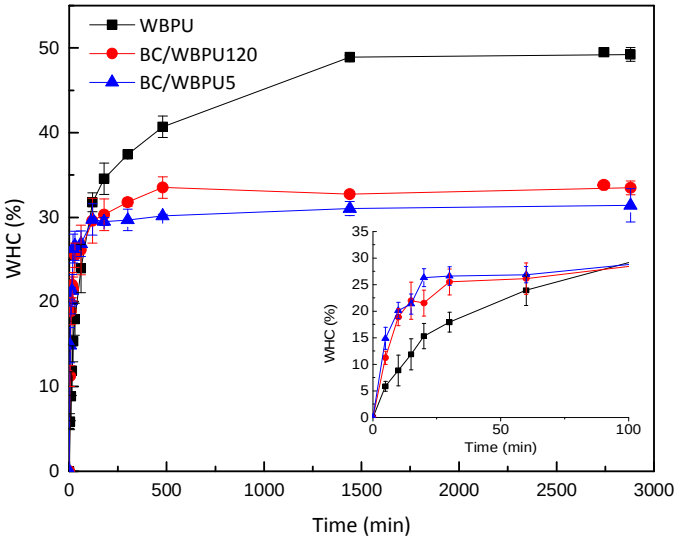

Figure 5.14 WHC of neat WBPU and BC/WBPU120 and BC/WBPU5 nanocomposites.

After that moment, BC/WBPU nanocomposites started to approach equilibrium, and after 2 h of immersion the equilibrium was reached. The water uptake of the neat WBPU was slower and the equilibrium was reached between 24 and 48 h of immersion. As it can be observed in **Table 5.3**, it can be concluded that the presence of BC induced to a faster water uptake, but limited the water content allowed in the nanocomposite. This suggested that hydrogen bonding interactions between BC and WBPU (seen in the FTIR study) led to the presence of less -OH available to interact with water molecules [29]. This could be a positive feature, since absorbed water can accumulate in the interface between components in blends leading to a delamination [30]. These results corroborated the ones obtained in the shape memory test since the nanocomposites absorbed more water at shorter times (which would induce a decrease of T_g) and thus, they presented greater recovery and at lower times.

5.4 CONCLUSIONS

In this chapter, flexible, transparent and biocompatible nanocomposites with enhanced water-activated shape memory properties were prepared by the combination of BC membranes and WBPU dispersions with potential applications in the biomedical field.

BC wet membranes were immersed in WBPU dispersions for different times and the BC membranes resulted totally embedded and coated by the WBPU, suggesting the good affinity of both polymers due to their hydrophilic nature. Additionally, the FTIR study revealed interactions between BC and WBPU. Mechanical test showed that the elastomeric properties of the WBPU were maintained in the nanocomposites, but an improvement of the modulus and strength of the nanocomposites with respect to the neat WBPU was observed. This suggested the effective reinforcement of the BC membrane and was confirmed by DMA analysis, where it was observed that the storage modulus of the nanocomposites was higher on all temperature range compared to the pure WBPU. The *in vitro* biocompatibility and cell adhesion tests of the nanocomposites showed non-toxic behavior making them suitable for biomedical applications. Furthermore, water-activated shape memory properties were analyzed by fold-deploy test method. The results revealed an improvement of the shape fixity ability and faster recovery process with the presence of BC. The BC/WBPU5 recovered 92.8 ± 6.3% of the original shape in 3 min, while for the same time period BC/WBPU120 recovered 72.0 ± 5.1% and neat WBPU only 33.4 ± 9.6%. This could be due to the faster diffusion of the water molecules through the nanocomposite and the hydrogen bonding between water and BC hydroxyl groups.

5.5 REFERENCES

[1] Hager, M.D., Bode, S., Weber, C., Schubert, U. S. Shape memory polymers: Past, present and future developments. Prog. Polym. Sci. 49-50 (2015) 3-33.

[2] Sun, W., Huang, M. Thermo/moisture responsive shape-memory polymer for possible surgery/operation inside living cells in future. Mater. Des. 31 (2010) 2684-2689.

[3] Small, W., Singhal, P., Wilson, T. S., Maitland, D.J. Biomedical applications of thermally activated shape memory polymers. J. Mater. Chem. 20 (2010) 3356-3366.

[4] Zhou, X., Li, Y., Fang, C., Li, S., Cheng, Y., Lei, W., Meng, X. Recent advances in synthesis of waterborne polyurethane and their application in water-based ink: a review. J. Mater. Sci. Technol. 31 (2015) 708-722.

[5] Santamaria-Echart, A., Ugarte, L., García-Astrain, C., Arbelaiz, A., Corcuera, M.A., Eceiza, A. Cellulose nanocrystals reinforced environmentally-friendly waterborne polyurethane nanocomposites. Carbohydr. Polym. 151 (2016) 1203-1209.

[6] Solanki, A., Das, M., Thakore, S. A review on carbohydrate embedded polyurethanes: An emerging area in the scope of biomedical applications. Carbohydr. Polym. 181 (2018) 1003-1016.

[7] Song, L., Li, Y., Xiong, Z., Pan, L., Luo, Q., Xu, X., Lu, S. Water-induced shape memory effect of nanocellulose papers from sisal cellulose nanofibers with graphene oxide. Carboydr. Polym. 179 (2018) 110-117.

[8] Picheth, G.F., Pirich, C. L., Sierakowski, M. R., Woehl, M. A., Sakakibara, C. N., Fernandes de Souza, C., Martin, A.A., da Silva, R., Alves de Freitas, R. Bacterial cellulose in biomedical applications: A review. Int. J. Biol. Macromol. 104 (2017) 97-106.

[9] Wu, J., Zheng, Y., Song, W., Luan, J., Wen, X., Wu, Z., Chen, X., Wang, Q., Guo, S. In situ synthesis of silver-nanoparticles/bacterial cellulose composites for slow-released antimicrobial wound dressing. Carbohydr. Polym. 102 (2014) 762-771.

[10] Kim, J., Cai, Z., Chem Y. Biocompatible bacterial cellulose composites for biomedical application. J. Nanotechnol. Eng. Med. 1 (2010) 1-7.

[11] Cai, Y., Jiang, J-S., Zheng, B. Xie, M-R. Synthesis and properties of magnetic sensitive shape memory Fe_3O_4/Poly(ε-caprolactone)-polyurethane nanocomposites. J. Appl. Polym. Sci. 127 (2013) 49-56.

[12] Liu, Y., Han, C., Tan, H., Du, X. Thermal, mechanical and shape memory properties of shape memory epoxy resin. Mat. Sci. Eng. A. 527, (2010) 2510-2514.

[13] Bodin, A., Bäckdahl, H., Fink, H., Gustafsson, L., Risberg, B., Gatenholm, P. Influence of cultivation conditions on mechanical and

morphological properties of bacterial cellulose tubes. Biotechnol. Bioeng. 97 (2006) 425-434.

[14] Klemm, D., Schumann, D., Udhardt, U., Marsch, S. Bacterial synthesized cellulose-artificial blood vessels for microsurgery. Prog. Polym. Sci. 26 (2001) 1561-1603.

[15] Nogi, M., Iwamoto, S., Nakagaito, S.N., Yano. H. Optically transparent nanofiber paper. Adv. Mater. 21 (2009) 1595-1598.

[16] Jiao, L., Xiao, H., Wang, Q., Sun, J. Thermal degradation characteristics of rigid polyurethane foam and the volatile products analysis with TG-FTIR-MS. Polym. Deg. Stab. 98 (2013) 2687-2696.

[17] Guo, L., Sato, H., Hashimoto, T., Ozaki, Y. FTIR study on hydrogen-bonding interactions in biodegradable polymer blends of poly(3-hydroxybutyrate) and poly(4-vinylphenol). Macromolecules 43 (2010) 3897-3902.

[18] Alemi, B., Shodja, H.M. Effective shear modulus of solids reinforced by randomly oriented-/aligned-elliptic multi-coated nanofibers in micropolar elasticity. Compos. Part B. Eng. 143 (2018) 197-206.

[19] Wu, G-m., Liu, G-f., Chen, J., Kong, Z-w. Preparation and properties of thermoset composite films from two-component waterborne polyurethane with low loading level nanofibrillated cellulose. Prog. Org. Coat. 106 (2017) 170-176.

[20] Ciolacu, D., Ciolacu, F., Popa, V.I. Amorphous cellulose-structure and characterization. Cellul. Chem. Technol. 45 (2010) 13-21.

[21] Figueiredo, A.G.P.R., Figueiredo, A.R.P., Alonso-Varona, A., Fernandes, S.C.M., Palomares, T., Rubio-Azpeitia, E., Barros-Timmons, A., Silvestre, A.J.D., Neto, C.P., Freire, C.S.R. Biocompatible bacterial cellulose-poly(2-hydroxyethyl methacrylate) nanocomposite films. Biomed. Res. Int. 2013 (2013) 1-14.

[22] Pei, A., Malho, J-M., Ruokolainen, J., Zhou, Q., Berglund, L.A. Strong nanocomposite reinforcement effects in polyurethane elastomer with low volume fraction of cellulose nanocrystals. Macromolecules 44 (2011) 4422-4427.

[23] Luo, H., Hu, J., Zhu, Y. Tunable shape recovery of polymeric nano-composites. Mater. Lett. 65 (2011) 3583-3585.

[24] Zhu, Y., Hu, J., Luo, H., Young, R.J., Deng, L., Zhang, S., Fan, Y., Ye, G. Rapidly switchable water-sensitive shape-memory cellulose/elastomer nano-composites. Soft. Matter. 8 (2012) 2509-2517.

[25] Wang, Y., Cheng, Z., Liu, Z., Kang, H., Liu, Y. Cellulose nanofibers/polyurethane shape memory composites with fast water-responsivity. J. Mater. Chem. B. 6 (2018) 1668-1677.

[26] Ratna, D., Karger-Kocsis, J. Recent advances in shape memory polymers and composites: a review. J. Mater. Sci. 43 (2008) 254-269.

[27] Huang, W.M., Yang, B., Zhao, Y. Ding, Z. Thermo-moisture responsive polyurethane shape-memory polymer and composites: a review. J. Mater. Chem. 20 (2010) 3367-3381.

[28] Yildirim, E., Yurtsever, M., Yilgor, E., Yilgor, I., Wilkes, G.L. Temperature-dependent changes in the hydrogen bonded hard segment network and microphase morphology in a model polyurethane: experimental and simulation studies. J. Polym. Sci. Part B. 56 (2018) 182-192.

[29] Popescu, M-C., Dogaru, B-I., Popescu, C-M. The influence of cellulose nanocrystals content on the water sorption properties of bio-based composite films. Mater. Des. 132 (2017) 170-177.

[30] Lyu, S.P., Untereker, D. Degradability of polymers for implantable biomedical devices. Int. J. Mol. Sci. 10 (2009) 4033-4065.

CHAPTER 6

MEDIUM-CHAIN-LENGTH POLYHYDROXYALKANOATE BIOSYNTHESIS

6. MEDIUM-CHAIN-LENGTH POLYHYDROXYALKANOATE BIOSYNTHESIS

6.1 INTRODUCTION

Polyhydroxyalkanoates (PHAs), biopolyesters that can be synthesized by numerous microorganisms, can be considered a green alternative to the petroleum-derived plastics. The main drawback or limitation for the scale up production of these biopolymers is the cost of the raw materials and carbon sources. For this reason, the use of inexpensive carbon substrates such as agro-industrial wastes and by-products as feedstock, is in the focus of research.

In this chapter the feasibility of producing medium-chain-length polyhydroxyalkanoates (mcl-PHAs) with *Pseudomonas putida* KT 2440 using cider by-products and the possibility to increase the PHA production by different strategies have been explored. The first part of the work which consists on the polymer biosynthesis experiments, was performed during an international internship in a research group in the School of Chemical Engineering and Analytical Science at The University of Manchester. This group works in the development and optimization of biosynthetic pathways to produce PHAs via bacteria using by-products and wastes [1,2]. Moreover, the biosynthesized polymer was extracted from the biomass and the solvent casted film was characterized. Characteristic chemical groups, monomeric composition and chemical structure of the mcl-PHA were determined. In addition, molecular weight and thermomechanical properties were evaluated to assess the suitability of using the obtained PHA in different fields.

6.2 EXPERIMENTAL

6.2.1 Media preparation for mcl-PHA biosynthesis

In this study *Psedomonas putida* KT2440 (*P. putida*) bacterial strain was acquired from The Leibniz Institute DSMZ, Germany. Master and working stocks were created from the lyophilized cells as per instruction provided by the supplier, and stored at -80 °C prior to reactivation and use in experiments.

For the preparation of inocula, cells from cryo-storage were reactivated using nutrient agar plates (Sigma Aldrich, UK) prior to each experiment. A single colony of *P. putida* from the petri dish was used to inoculate 10 mL of minimal medium (synthetic medium described below), which was grown at 30 °C at 200 rpm for 24 h. These inoculated and grown 10 mL were transferred to 100 mL of identical medium (10% v/v) in Erlenmeyer flasks, incubated as above and used to inoculate the apple waste juice media (10% of the working volume).

The minimal medium formulation contained per litre: 2.90 g $Na_3C_6H_5O_7{\cdot}2H_2O$ as carbon source and 7.50 g K_2HPO_4, 3.70 g KH_2PO_4, 2.38 g Na_2HPO_4, 0.89 g NH_4Cl (salts) [3]. The pH was adjusted to 7.1 with 1 M NaOH. This medium was autoclaved and subsequently supplemented with filter sterilized 1 mL L^{-1} of 0.2 g L^{-1} $MgSO_4{\cdot}7H_2O$ solution and filter sterilized 1 mL L^{-1} mineral trace element (MT) stock solution. The MT solution was prepared with 1 M HCl which contained 2.78 g L^{-1} $FeSO_4{\cdot}7H_2O$, 1.47 g L^{-1} $CaCl_2{\cdot}2H_2O$, 1.98 g L^{-1} $MnCl_2{\cdot}4H_2O$, 2.81 g L^{-1} $CoSO_4{\cdot}7H_2O$, 0.17 g L^{-1} $CuCl_2{\cdot}2H_2O$, 0.29 g L^{-1} $ZnSO_4{\cdot}7H_2O$ and 0.2 g L^{-1} $MgSO_4{\cdot}7H_2O$. Sterile conditions were maintained throughout the experiments, and all the stock solutions used were either sterile filtered

using 0.45 μm NalgeneTM Rapid-Flow™ membrane filtration units (Thermo Fisher, UK) or autoclaved.

The apple medium was prepared with crushed and squeezed apple residues in a commercial blender with distilled water at room temperature with different solid:liquid ratios indicated in the next 6.2.2. section. Then it was filtered and centrifuged for 10 min at 7000 rpm to remove the solids. After that, the apple waste juice was supplemented with salts and MT solution to provide the other elements required for cellular growth (N, P, S, etc.). Salts were added directly to the juice to obtain the enriched apple residue juice: 7.50 g K_2HPO_4, 3.70 g KH_2PO_4, 2.38 g Na_2HPO_4 and 0.89 g NH_4Cl. The pH was adjusted to 7.1 with 1 M NaOH. Afterwards, the apple waste enriched medium was sterilized by filtration using 0.45 μm NalgeneTM Rapid-Flow™ membrane filtration units (Thermo Fisher, UK). Finally, filter sterilized $MgSO_4$ and MT were supplemented as above.

A control medium was prepared to compare the PHA production and total biomass over time with the apple juice media. The control medium for shake flask experiments contained 3 g L^{-1} and 10 g L^{-1} of commercial glucose and fructose, respectively, as carbon sources. These sugars and concentrations were chosen to mimic the most concentrated apple juice medium obtained. The pH was adjusted as above before autoclaving. Then, the medium was supplemented with sterile salts, filter sterilized $MgSO_4$ and MT as above.

6.2.2 Shake flask experiments

All the experiments were conducted in duplicate in 1 L Erlenmeyer shake flasks with a working volume of 200 mL. The cultures were incubated at 30 °C in an orbital shaker at 200 rpm.

The first experiment was conducted to confirm the capability of *P. putida* to utilize these residues to produce PHAs and check for cell growth inhibitory effects. For this, different apple waste (AW) to water (W) ratios were used to prepare juices with different concentration of sugars and determine the optimum ratio for the maximum PHA production. Total nitrogen (TN), glucose and fructose concentration and optical density were measured during 72 h of cultivation. PHA concentration was checked at the 72 h mark. Additionally, a control culture prepared with commercial glucose and fructose was also tested.

The second experiment was carried out in shake flasks in order to establish a batch feeding strategy to maximize the PHA production. More concentrated apple juice was prepared with the best AW:W ratio obtained from the first experiment. 20 mL of the same apple juice with salts were supplemented in each culture at different cultivation times in order to increase the PHA production (experiments A, B and C). In experiment A the extra feed was added at 12 h of fermentation, in experiment B, the extra feed at 24 h of fermentation and in experiment C, the extra feed was added at 48 h of fermentation. Total nitrogen, glucose and fructose concentration and optical density were measured during 96 h of cultivation. PHA concentration was quantified at the 96 h mark.

6.2.3 Maximun growth rate, PHA production and yield coefficients

The time-dependent increase in the microbial population in a closed system is refered to as a gowth curve. A typical growth curve for a bacterial population is shown in **Figure 6.1**.

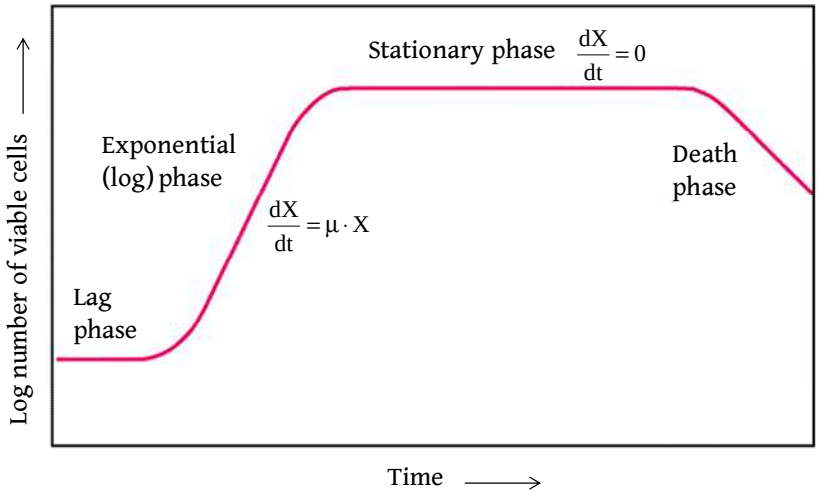

Figure 6.1 Typical growth curve of bacterial population.

Different growth phases can be observed within a growth curve: lag phase, the exponential or log phase, the stationary phase, and the death phase. The lag phase is thought to be due to the physiological adaptation of the cell to the culture conditions and the growth rate is practically zero. The exponential phase is characterized by a period of the exponential growth- the most rapid growth possible under the conditions present in the batch system. Mathematically cell growth during the exponential phase can be described using the following **Equation 6.1**:

$$\frac{dX}{dt} = \mu \cdot X \qquad \textbf{(6.1)}$$

where X is the number or mass of cells (mass/volume), t is time, and μ is the specific growth rate constant ($time^{-1}$).

The stationary phase in a batch culture can be defined as a state of no net growth and finally, the death phase is characterized by a net loss of culturable cells.

The maximum growth rate (μ_{max}) is an important parameter in modelling microbial growth under batch conditions and its calculation is based on the inflection of the slope of the growth curse in the exponential phase. In the case of the maximum growth rates, although PHA content over time was not analyzed, the PHA did not start producing until there was a nitrogen limitation in the medium. According to this data and the results of nitrogen consumption in the experiments, optical density (OD) data until 12 h of fermentation was used for the calculation of the growth rates, which was equivalent to the cell growth as no PHA had been produced.

The PHA proportion of total biomass was evaluated at the end of the fermentation process and the results are expressed (1) as a concentration, mass of PHA per litre of fermentation broth ($g\ L^{-1}$), and (2) as a percentage of total biomass (PHA (%)), using the **Equation 6.2**. The total biomass was estimated as dry cell weight (DCW).

$$\text{PHA}\quad(\%) = \frac{\text{PHA produced}}{\text{total biomass}} \cdot 100 \qquad \textbf{(6.2)}$$

The yield coefficient of cell biomass ($Y_{X/S}$) was determined based on the amount of active biomass produced (the mass of produced cells) (ΔX) per total mass substrate (glucose + fructose) consumed (ΔS) (**Equation 6.3**).

$$Y_{X/S} = \frac{\Delta X}{\Delta S} = \frac{\text{mass cells produced}}{\text{mass substrate consumed}} = \frac{DCW_{final} - DCW_0 - \text{PHA produced}}{\text{mass substrate consumed}} \left(\frac{g}{g}\right) \quad \textbf{(6.3)}$$

where DCW_{final} is the dry cell weight at the end of the fermentation and DCW_0 is the initial dry cell weight.

The product yield coefficient ($Y_{P/S}$) was calculated based on the amount of PHA produced at the end of the fermentation per total mass substrate consumed (ΔS) (**Equation 6.4**).

$$Y_{P/S} = \frac{\text{PHA produced}}{\Delta S} = \frac{\text{mass product produced}}{\text{mass substrate consumed}} \left(\frac{g}{g}\right) \quad \textbf{(6.4)}$$

6.2.4 Polymer extraction from biomass and purification

PHA was extracted from the bacterial biomass using the method developed by Jiang et al. [4]. The recovery process was based in three steps. Firstly, pretreatment of the biomass, then Soxhlet extraction with acetone and finally purification of the PHA with methanol.

Firstly, about 2 g of dried biomass were vortex mixed with 40 mL of methanol for 5 min at room temperature to make the PHA more pure, accessible and soluble for the extraction step. The methanol treated biomass was then centrifuged for 5 min at 7000 rpm and then dried at 40 °C. The pretreatment was followed by Soxhlet extraction with 120 mL acetone for 5 h. Then, the solution was concentrated by rotary evaporation at 40 °C.

Finally, the acetone containing bioplastic solution was added drop-wise into cold methanol (acetone:methanol 1:10 (v/v)) under agitation. After bioplastic precipitation, the solution was centrifuged at 9000 rpm for 30 min. The liquid was carefully eliminated with a syringe and the plastic was dissolved with chloroform and finally dried at room temperature in a Teflon plate to obtain the PHA films. These films were stored in a desiccator until use.

6.3 RESULTS

The main objective of this chapter was to assess the feasibility of using not pretreated cider by-products as the sole carbon source for the production of PHAs by *P. putida* KT2440. Shake flask experiments were carried out to analyze the possibility of increasing the polymer concentration and accumulation by producing the most suitable media for fermentation and finally, the extraction and characterization of the PHA produced was performed in order to examine its possible film applications in different fields.

6.3.1 mcl-PHA production

In the first experiment, apple waste juice fermentation media were prepared using different apple waste to water ratios (AW:W) and were analyzed in terms of sugar content. The AW:W ratios used were 0.4:1, 1:1 and 1.5:1. The apple waste juices were analyzed by HPLC, and found to contain a mixture of mainly glucose and fructose, the latter being the main carbohydrate present (**Table 6.1**).

Table **6.1**. Initial glucose, fructose and total nitrogen concentrations and C/N ratio for the different AW:W juices and control media.

		AW:W		
	Control	**0.4:1**	**1:1**	**1.5:1**
Glucose (g L^{-1})	3	1.2	2.5	1.8
Fructose (g L^{-1})	10	3.7	7.5	3.3
Nitrogen (g L^{-1})	0.2	0.2	0.2	0.2
C/N (mol/mol)	27	13	23	11

It was found that an AW:W ratio either below or above 1:1 resulted in a decrease of the quantity of carbohydrates extracted. In the case of the 1.5:1 ratio, it seemed that there was not enough water to extract the sugars during juice preparation, suggesting that much unextracted soluble waste would be left. Therefore, in this case the optimum ratio for the highest extraction of carbohydrates was 1:1. For the fermentation experiments control cultures were prepared with commercial glucose and fructose with the similar concentrations obtained in the apple waste juice prepared with 1:1 ratio as a reference. Initial glucose, fructose and total nitrogen concentrations and C/N ratios in each media are indicated in **Table 6.1**.

In this way, both glucose and fructose have proven to be adequate substrates for *Pseudomonas* strains [5]. Davis et al. [6] used glucose as sole carbon source to achieve high cell density in fed batch bioprocesses. Escapa et al. [7] compared the growth of *P. putida* KT2440 on different carbon sources i.e. acetate, citrate, pyruvate, succinate, gluconate, glucose, fructose and glycerol in flask experiments and they obtained the highest biomass yield on fructose. Moreover, mixtures of both sugars have been tested for PHA production and it was found that high cell density and high PHA amount in the biomass could be obtained using carbohydrates as the sole carbon source reaching a 63% of mcl-PHA accumulation using fed batch

strategies in bioreactors [8]. This suggests that cider by-products can be suitable substrates for fermentation with *P. putida* KT2440.

All shake flask experiments were done in duplicate and total nitrogen, glucose and fructose concentration and cell biomass were measured during 72 h of cultivation and average values are displayed in **Figure 6.2**. PHA content was measured at the end of the fermentation (72 h). Through the OD measurements (in red) bacterial growth + PHA accumulation were monitored.

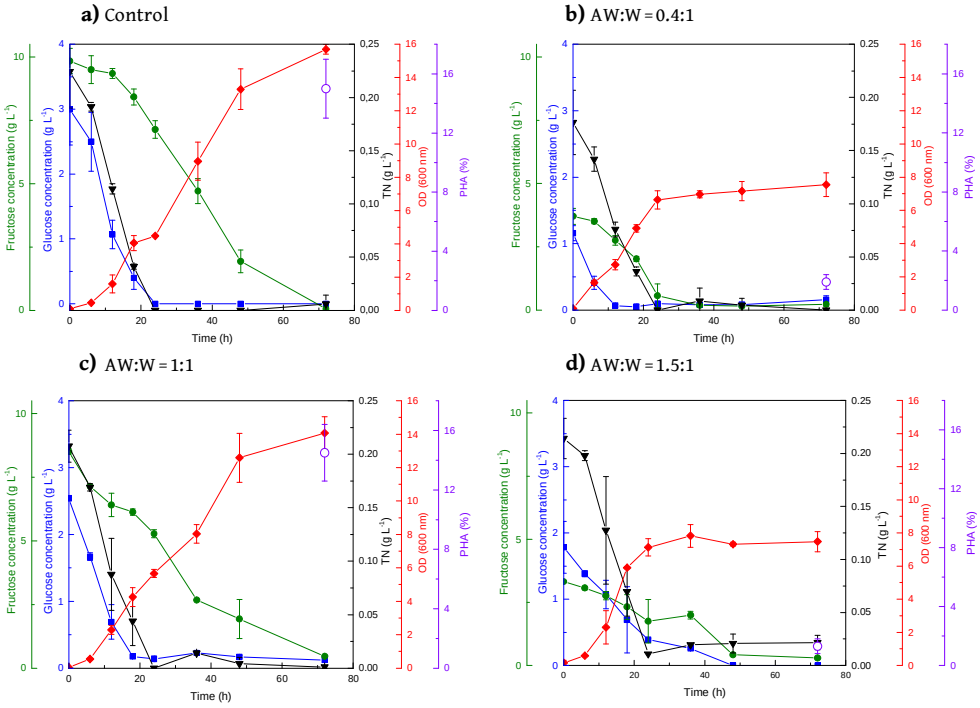

Figure 6.2 Evolution of *P. putida* KT2440 in a) control, b) 0.4:1 AW:W ratio, c) 1:1 AW:W ratio and d) 1.5:1 AW:W ratio. (♦OD (600 nm), ▼TN, ●fructose, ■glucose, ○PHA (%)).

As it can be seen in **Figure 6.2**, *P. putida* bacterium was able to grow in the apple waste juice media with different sugar concentrations, with minimal inhibitory effects being observed (as it can be seen from OD results). As commented in previous chapter 1, cider apples are rich in polyphenolic compounds which are retained in the pomace and show antioxidant activity. In some cases, their presence can have inhibitory effects on the microbial growth of *P.putida* KT2440, as it was observed in the case of other fruit pomaces by Follonier et al. [9]. They observed complete inhibition of the cell growth at high concentrations of cherry hydrolyzed pomace, while no significant changes in the growth of the cells was detected for apricot and grape pomaces. They ascribed this, to the presence of polyphenols with antimicrobial activity in the cherry pomace.

In the present work the phenolic compounds which were probably present in the juice, do not seem to have negatively affected the fermentation since both total biomass and PHA concentrations were reasonable and in the expected range. This could be due to the method used to extract the sugars of the apple pomace, since water at room temperature was used, and the phenolic compounds are usually extracted using organic solvents or thermal treatments. Therefore, probably the prepared apple waste juices did not contain high concentrations of polyphenols and thus, the bacterial growth was not affected.

The control medium contained a slightly larger amount of carbohydrates than the medium prepared with 1:1 ratio and therefore, that led to a slightly higher OD and PHA concentration. The sugar consumption pattern was virtually the same in all the cultures. Glucose uptake was faster than fructose uptake leading to a depletion of glucose, followed by fructose, but

as expected, higher sugar concentration led to higher OD. This behavior agreed with the data obtained in other works. Löwe et al. [10] observed the same trend with *P. putida* growing in a mixture of equal parts of glucose and fructose. Diniz et al. [8] observed preferential consumption of glucose by *P. putida* IPT 046 when fed glucose and fructose mixtures.

Nitrogen exhaustion was reached in 24 h in all cases. It has been previously reported that production of PHAs requires nutrient limitation depending on the substrate used. *P. putida* KT2440 is able to produce PHA under no nutrient limitations when octanoate is used as carbon source. However, in the case of using non-related precursors as carbon sources for PHA production, two factors are required for PHA accumulation in *P. putida* KT2440: a simultaneous nitrogen limitation with an excess of carbon source [11].

In the apple waste juice prepared with 1:1 ratio and in the control media (**Figure 6.2** a) and c)), glucose was depleted between 18 and 24 h of fermentation, but OD values continued increasing until 72 h of fermentation due to the presence of fructose. In the apple waste juice prepared with 0.4:1 and 1.5:1 ratios, the sugar concentration was much lower, so depletion occurred sooner and consequently the OD experienced a stop after 24 h of fermentation (**Figure 6.2** b) and d)). Almost no PHA synthesis was detected in *P. putida* grown on the media prepared with 0.4:1 and 1.5:1 ratios, likely due to their being insufficient carbon source remaining by the 24 h mark. However, in the control and the media prepared with 1:1 ratio, 15 ± 2.5 and 14.5 ± 2.5 % of PHA accumulation was obtained, respectively. These results suggest that glucose was consumed during the growth of *P. putida*, while fructose was used by the bacteria mainly for PHA biosynthesis.

In this experiment, maximum values of total weight at 72 h (DCW) (3.7 ± 0.47 g L^{-1}), PHA yield (0.39 ± 0.02 g L^{-1}) and PHA accumulation (14.5 ± 1.9 %) were obtained with AW:W ratio of 1:1. Therefore, after analyzing the effect of different AW:W ratios on the growth of *P. putida*, 1:1 ratio was chosen as the working ratio for a second experiment.

6.3.2 Fed-batch strategies for maximun mcl-PHA production

In the second experiment, batch feeding strategy (addition of extra feed) was employed in order to increase the PHA production using the same apple waste juice medium supplemented with salts.

For these fed-batch experiments, new apple waste medium was prepared with 1:1 AW:W ratio. In this second experiment a total carbohydrate concentration of 15 ± 3 g L^{-1} was obtained with these cider by-products, in contrast to the first experiment, where the carbohydrate concentration with 1:1 ratio was 10 g L^{-1}. The higher concentration of sugars compared to the previous batch was attributed to the heterogeneity of the apple waste. The new apple waste juice was enriched with salts as explained in section 6.2.1.

The extra feed was added into the culture media at different cultivation times in order to analyze the influence of the addition of this extra feed on bacterial growth and PHA accumulation. In the experiment A, the extra feed was added at 12 h of cultivation, i.e. early stage of bacterial growth and before nitrogen depletion. In the experiment B, the extra feed was added at 24 h of cultibation, which according to previous experiments was the onset time of nitrogen depletion. Finally, in experiment C the extra feed was added at 48 h of cultibation, i.e. after nitrogen depletion and final stage of bacterial growth. Each experiment was conducted in duplicate and total

nitrogen, glucose and fructose concentration and cell biomass were measured during 96 h of cultivation.

The results are displayed in **Figure 6.3**, where the horizontal dotted lines indicate the cultivation times at which the extra feed was added.

In these experiments the cultivation time was extended to 96 h. Taking into account that in these experiments the media contained slightly higher concentration of sugars, and that extra feed was being added, it was decided to extend the cultivation time, assuming that the stationary phase would arrive somewhat later than in the previous experiments. Biomass and product yields, as well as specific growth rate and maximum PHA content (at 96 h) were calculated and the results are shown in **Table 6.2**.

Table 6.2. PHA accumulation and growth kinetic parameters determined in apple waste cultures prepared with 1:1 (AW:W) ratio following batch feeding strategy at different cultivation times.

	Experiment		
	A	**B**	**C**
μ_{max} **(h^{-1})**	0.24 ± 0.01	0.24 ± 0.01	0.25 ± 0.01
$Y_{X/S}$ **(g g^{-1})**	0.28 ± 0.02	0.31 ± 0.05	0.18 ± 0.10
$Y_{P/S}$ **(g g^{-1})**	0.11 ± 0.02	0.09 ± 0.02	0.07 ± 0.02
$DCW^{96\ h}$ (g L^{-1})	4.33 ± 0.57	4.02 ± 0.21	3.75 ± 0.07
$PHA^{96\ h}$ (g L^{-1})	1.10 ± 0.04	0.93 ± 0.10	0.80 ± 0.10
$PHA^{96\ h}$ (%)	25.50 ± 2.30	22.90 ± 2.50	21.30 ± 2.30

μ_{max}, maximum specific growth rate; $Y_{X/S}$, yield coefficient of biomass on substrate (glucose+fructose) conversion to biomass; $Y_{P/S}$, yield coefficient of substrate conversion to PHA.

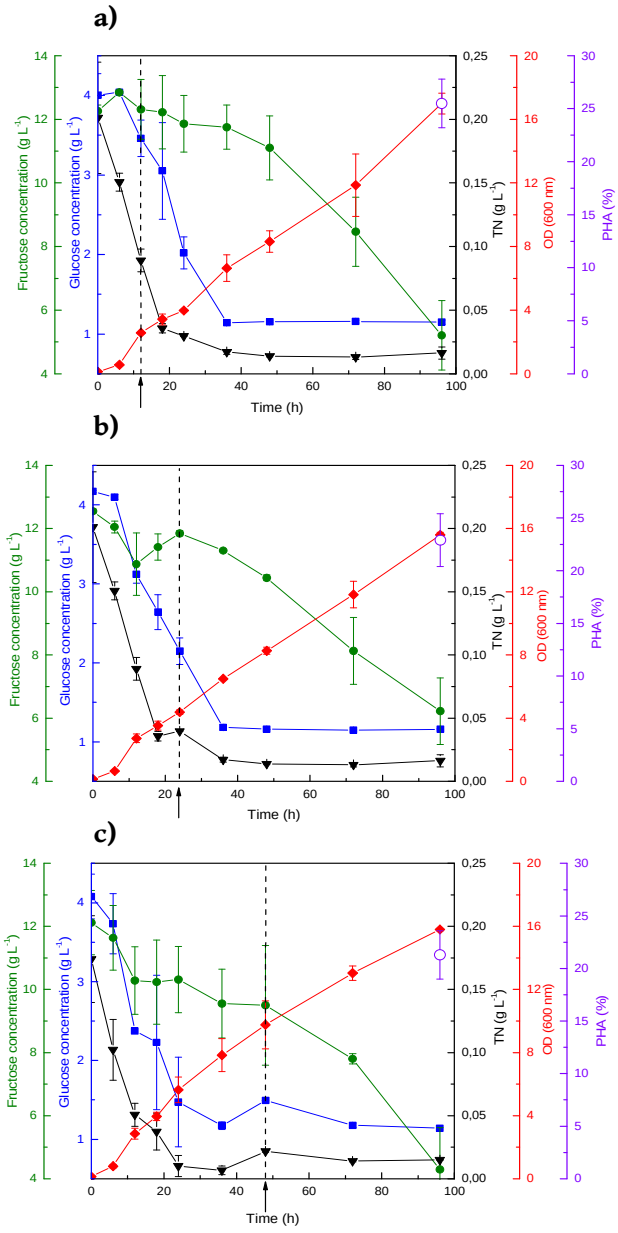

Figure 6.3 Evolution of *P. putida* KT2440 in apple waste media after 96 h following a batch feeding strategy. **a)** experiment A, **b)** experiment B and **c)** experiment C (dotted lines indicate the cultivation times at which the extra feed was added) (♦OD (600 nm), ▼TN, ●fructose, ■glucose, ○PHA (%)).

PHA content and yield tended to be higher when the addition of the extra feed was made during the early stages of bacterial growth. This could be due to the fact that the most active growth of microorganisms occurred before 20 h of fermentation so the greater availability of substrate and nutrients at this stage possibly stimulated the production of higher cell concentrations with concurrent PHA storage.

Although in these experiments initial carbohydrate concentrations were higher than in the previous experiments, it can be concluded that a fed batch cultivation could provide the solution to give a higher final product concentration. This experiment could help to design a strategy for a future optimization of the process in a bioreactor since different feeding strategies can be followed to increase the cell biomass and volumetric productivity [6]. Follonier et al. [9] obtained a polymer accumulation of 23.3% using Solaris grape hydrolyzed pomace and waste frying oil in bioreactor experiments with *P. resinovorans*. They used a two step fermentation process, starting with the grape hydrolized pomace as a growth substrate enriched with salts and adding the waste frying oil as a mcl-PHA precursor. In the present work, when the extra feed was added at 12 h of fermentation a total PHA accumulation of 25.5 ± 2.3% was obtained at 96 h of cultivation. In this case no PHA precursors were added to increase the production of the polymer and no pre-treatment of the raw material was performed, so the results indicate that cider by-products are a promising raw material for PHA production.

In terms of sugar consumption, fructose uptake was slower than glucose uptake, but both were metabolized simultaneously, as observed in the

previous experiment. Glucose concentration was reduced by 72-73 % while fructose concentration was reduced between 58 and 64 %.

The maximum growth specific rates obtained in this work (μ_{max} 0.24-0.25) were lower than the values obtained by Follonier et al. [9] using hydrolyzed pomaces of different fruits i.e. apricots, cherries and grapes (μ_{max} 0.85-0.60) and Borrero-de Acuña et al. [12] using glucose as carbon source ((μ_{max} 0.56) for *P. putida* KT2440. Diniz et al. [8] obtained maximum specific growth rates on glucose (0.63-0.65) and fructose (0.26-0.20) with total glucose and fructose concentrations between 10 and 20 g L^{-1} in bioreactor experiments with *P. putida* IPT 046.

In this context, Sawyer et al. [13] reported that when species of *Pseudomonas* were grown in fructose as the main or sole carbon source, high doubling times (the period of time required for the bacterial population to double in size or value) were observed compared to other carbon sources, such as succinate. This indicates that growth rate on fructose is lower than on glucose, i.e. the bacteria grow faster when glucose is the main carbon source. In this work, everything indicates that glucose has been the main sugar for the bacterial growth, but a small fraction of fructose has also been consumed in the early stages of the fermentation process so this probably had an effect in the growth rates leading to lower values compared to other works.

However, the yield values of biomass ($Y_{X/S}$) and PHA production ($Y_{P/S}$) of this work (**Table 6.2**) resulted in the range of the ones obtained by Borrero-de Acuña et al.[12] with *P. putida* KT2440 and some *P. putida* mutant strains for the improvement of PHA production using glucose as sole carbon source in

batch cultures. They obtained values of $Y_{X/S}$ between 0.21 and 0.25 and $Y_{P/S}$ values between 0.05 and 0.11. These results contribute to support the assumption that in this work the bacterial growth is mainly derived from glucose and that the substrate conversion to PHA derives from the fructose consumption after nitrogen depletion.

The results obtained in this work prove that using only waste-derived media as carbon source, i.e. by-products of cider production, which consist of a heterogeneous mixture of sugars, is a viable solution for an acceptable production of PHA.

6.3.3 Characterization of the PHA

Biosynthesised PHA was extracted as described previously and characterized by different techniques to evaluate its possible applications in different fields. As it can be observed in **Figure 6.4**, the PHA film was optically transparent with yellowish colour.

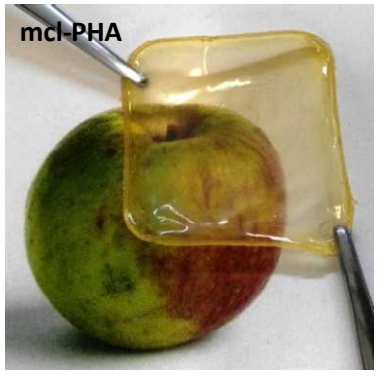

Figure 6.4 Digital image of extracted mcl-PHA.

6.3.3.1 Identification of the functional groups of the PHA

The major functional groups present in the purified PHA structure were characterized by FTIR spectroscopy and the spectrum is shown in **Figure 6.5**.

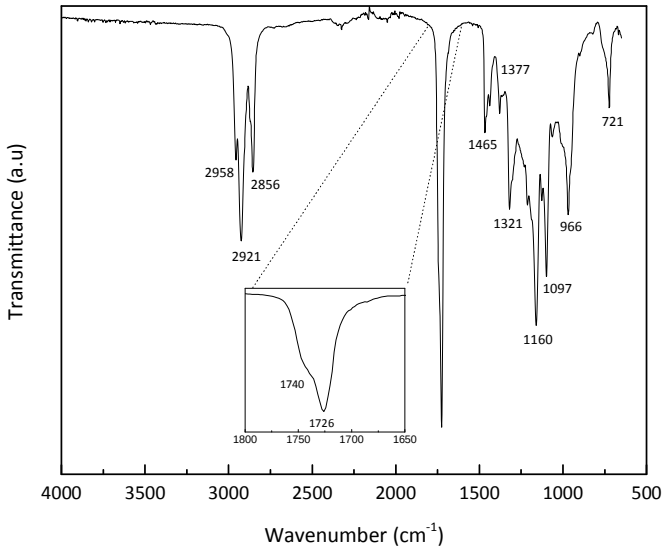

Figure 6.5 FTIR spectrum of the purified PHA biosynthesized by *P. putida* KT2440.

The FTIR spectrum shows the typical bands of the polyester structure. The bands at 2958, 2921 and 2856 cm^{-1} are associated to aliphatic C-H. The strong band at 1740-1726 cm^{-1} is a characteristic peak of PHAs and corresponds to carbonyl of ester group (C=O) stretching vibration. The intensity and position of the carbonyl group are related to changes in the crystallinity of the PHA. The band shifts from a broad shoulder centered at 1740 cm^{-1} (related with the free C=O), to stronger and sharper peak at 1726 cm^{-1} (related to the hydrogen bonding C=O), which are assigned to amorphous

and crystalline phases, respectively [14]. The bands at 1465 and 1377 cm^{-1} are assigned to CH_2 and CH_3 bending vibrations, respectively. In the region 1330-1000 cm^{-1} (1321, 1160 and 1097 cm^{-1}) appears the stretching vibration of the C-O-C bonds. Finally, the band at 966 corresponds to C-C stretching vibration and the band at 721 cm^{-1} is associated with the contribution of more than four CH_2 units at the side chain [15,16].

6.3.3.2 Monomeric composition of the PHA

GC–MS analysis was used to identify PHA monomer composition of the 3-hydroxyalkanoate methyl esters prepared by total methanolysis and compared with standards. **Figure 6.6** displays the resultant chromatogram and the molar composition (%) of each monomer is gathered in **Table 6.3**.

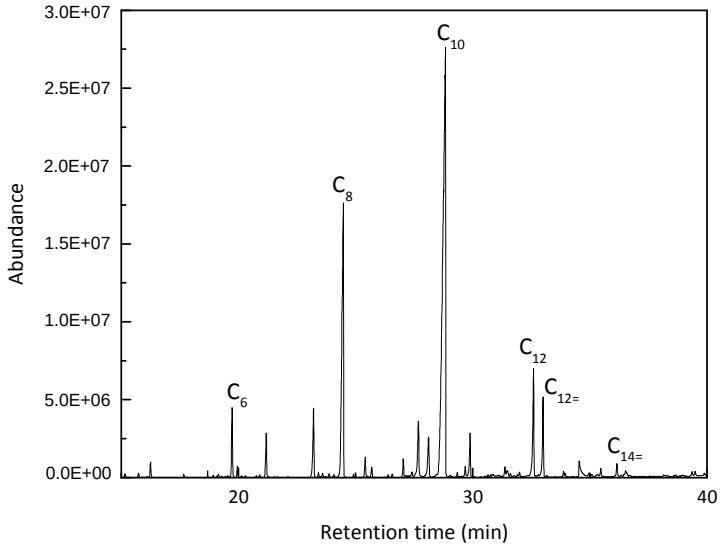

Figure 6.6 Gas chromatogram of purified mcl-PHA copolymer.

As it can be observed, the synthesized PHA is composed by 3-hydroxyhexanoate (3HH, C_6), 3-hydroxyoctanoate (3HO, C_8), 3-hydroxydecanoate (3HD, C_{10}), 3-hydroxydodecanoate (3HDD, C_{12}), 3-hydroxydodecenoate (3HDD, $C_{12=}$) and traces of 3-hydroxytetradecenoate (3HTD, $C_{14=}$). 3HD is the predominant compound of this polymer, followed by 3HO.

Table 6.3 PHA monomeric molar composition (%) determined by GC-MS.

Monomer	mol (%)
3HH (C6)	3.19
3HO (C8)	23.43
3HD (C10)	60.90
3HDD (C12)	6.94
3HDD (C12=)	4.76
3HTD (C14=)	0.77

The monomeric composition was the typical observed by other authors using sugars as carbon source and *Pseudomonas* strains [5,17]. The composition of unsaturated monomers 3HDD ($C_{12=}$) and 3HTD ($C_{14=}$) was established by comparing their mass spectra with that reported in the literature [5,17-20]. The position of the double bonds is discussed below and established taking into account the results of ^{13}C and ^{1}H NMR analysis.

6.3.3.3 Chemical structure

The chemical structure of the mcl-PHA was investigated using carbon (^{13}C) and proton (^{1}H) NMR analysis and the resultant spectra are gathered in **Figure 6.7** a) and b), respectively. Both NMR peak assignments were carried out comparing these results with previously literature reported by other authors [5,17,19,21,22].

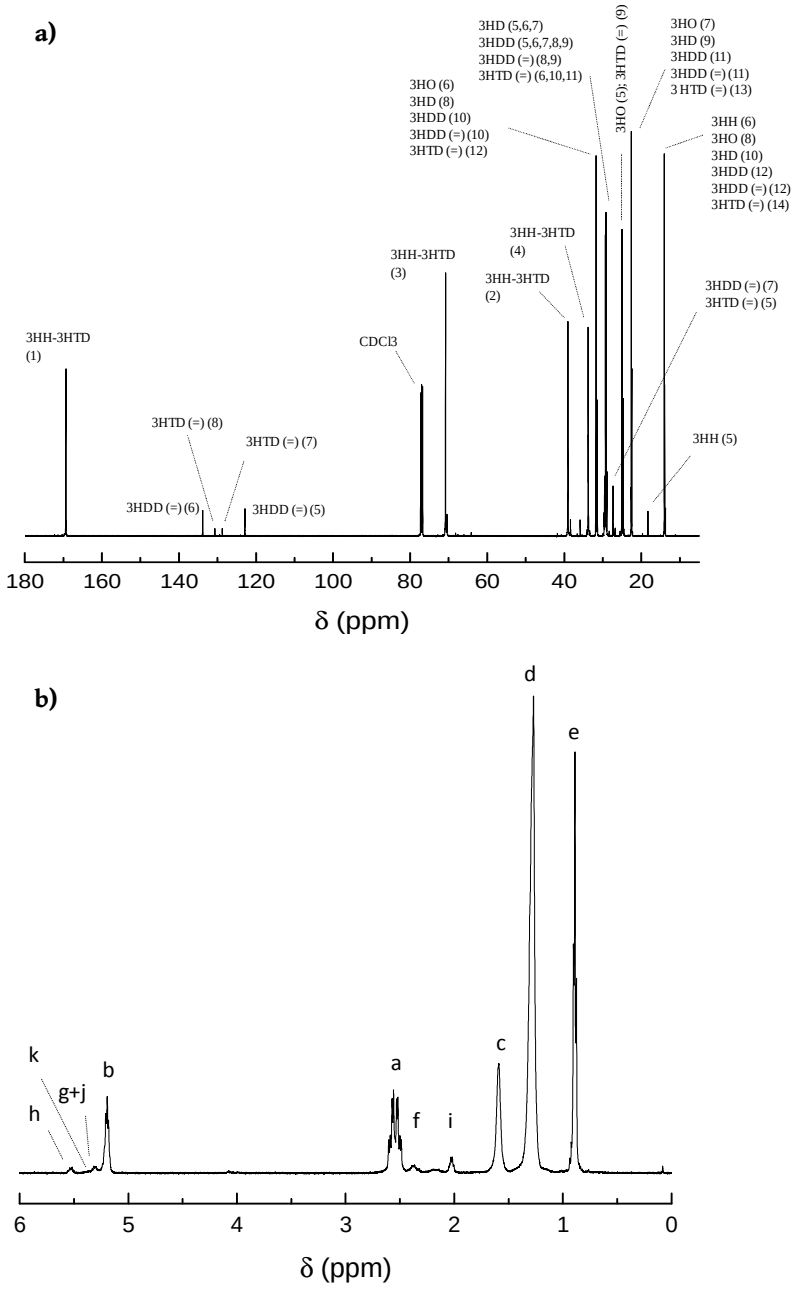

Figure 6.7 a) ^{13}C NMR spectrum and b) ^{1}H NMR spectrum of mcl-PHA synthesized by *P. putida* KT2440.

Figure 6.7 a) displays the ^{13}C NMR spectrum of the PHA produced. The detailed 13C NMR chemical resonance signals and their corresponding carbon positions are represented in **Table 6.4.**

Table 6.4. ^{13}C NMR chemical shifts of mcl-PHA synthesized by *P. putida* KT2440.

Carbon	3-Hydroxyalkanoate monomers					
	3HH (C6)	3HO (C8)	3HD (C10)	3HDD (C12)	3HDD (C12=)	3HTD (C14=)
	δ (ppm)					
1	169.3	169.3	169.3	169.3	169.3	169.3
2	38.3	39.0	39.0	39.0	39.0	39.1
3	70.4	70.4	70.4	70.4	70.5	71.0
4	35.8	33.8	33.8	33.8	33.7	33.7
5	18.2	25.0	29.3	29.3	122.9	26.6
6	13.7	31.3	29.5	29.5	133.8	29.1
7		22.4	29.3	29.5	27.2	128.7
8		13.7	31.4	29.5	29.6	130.6
9			22.4	29.3	29.4	24.6
10			13.7	31.7	31.8	28.9
11				22.4	22.5	29.6
12				13.7	13.9	31.8
13						22.6
14						14.0

The chemical shift assigned to the major anomeric carbon (C_1) was detected at 169.35 ppm for all monomers. In the same way, all the monomers were sharing similar chemical shifts for C_2 (around 39-38 ppm), C_3 (around 70-71 ppm) and C_4 (around 33-36 ppm). The methyl groups located at the end of the chains of the monomers correspond to the chemical shifts detected between 13-14 ppm. The chemical shifts located between 120 and 140 ppm indicate the presence of unsaturated carbons. Two major signals at 122.9 and 133.8 ppm can be observed which are assigned to olefinic carbons. These correspond to the double bond between C_5 and C_6, respectively, in the side chains of 3HDD units. Additionally, two minor olefinic signals are observed

at 128.7 and 130.6 ppm, corresponding to the localization of the double bond between C_7 and C_8 of 3HTD units.

Additionally, ^{1}H NMR spectrum is shown in **Figure 6.7** b). The protons next to carboxyl and hydroxyl groups (a and b) are assigned to the signals centered at 2.54 and 5.19 ppm, respectively. The first CH_2 of the saturated alkane chain (c) corresponds to the signal centered at 1.59 ppm. Weak signals at 5.54, 5.52, 5.37 and 5.30 ppm confirm the presence of side chains containing the -CH=CH- sequences. Finally, the remaining protons of methylene (d) and methyl (e) groups are assigned to the peaks centered at 1.27 and 0.88 ppm, respectively.

The sequence structure proposed for the mcl-PHA produced by *Pseudomonas putida* KT2440 in cider apple residues is represented in **Figure 6.8**, where the carbons and protons are indicated with numbers and letters, respectively.

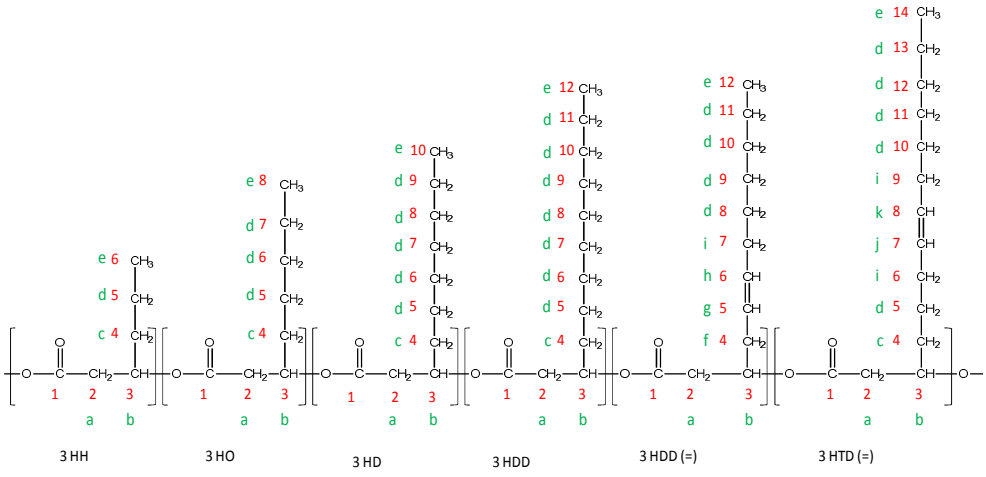

Figure 6.8 Representative sequence structure of mcl-PHA synthesized by *P. putida* KT2440.

6.3.3.4 Molecular weight

Molecular weight of the PHA copolymer were determined by GPC. Weight average molecular weight ($\overline{M}_w$) and number average molecular weight ($\overline{M}_n$) of the obtained PHA were 4.7×10^4 and 2.1×10^4, respectively, and the polydispersity index (PI) was 2.2 (all of them referred to monodisperse polystyrene standards).

It has been previously reported that the molecular weight of the PHAs depends on four factors which are (1) concentration of PHA synthase, (2) occurrence of the chain transfer reaction, (3) catalytic activity of PHA synthase and (4) simultaneous degradation of PHA during biosynthesis [23,24]. The molecular weight values obtained in this work are slightly lower than those obtained by other authors using *Pseudomonas* strains and sugars as carbon source [17,19] and similar to others obtained using *Pseudomonas* strains and glycerol as the main substrate [15,22]. Nevertheless, it should be noted that the eluent used for the molecular weight measurements influences the values obtained and in three of the four cases chloroform was used as the elution solvent, while in this case THF was used.

The molecular weight is directly related to the mechanical strength, so usually for thermoplastic polymers such as PHB, high molecular weight is preferred. Nevertheless, mcl-PHAs which present lower molecular weights, have potential applications in the biomedical field such as the development of polymeric nanoparticles for the delivery of active compounds in the human body, as well as coatings, adhesive materials or biding agents for polymers [25-27].

6.3.3.5 *Thermal, thermomechanical and mechanical properties*

The thermal analysis of the mcl-PHA was performed by DSC, and the resultant thermogram is shown in **Figure 6.9.** This mcl-PHA was semicrystalline biopolymer. In **Figure 6.9** the presence of two transitions can be observed, one associated to the amorphous region (glass transition, T_g= -42 °C) and second one associated to the crystalline region (melting process, T_m= 46.8 °C and ΔH_m= 20.2 J g^{-1}).

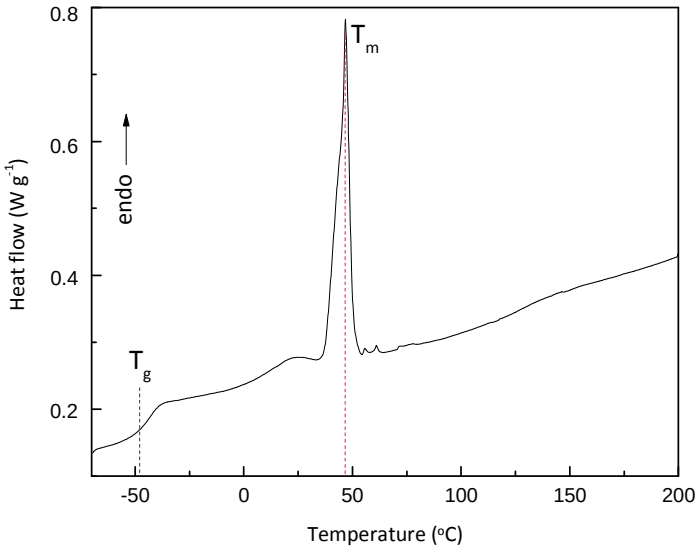

Figure 6.9 DSC thermogram of mcl-PHA.

The obtained results are very similar to the ones obtained by Sánchez et al. [17] with a mcl-PHA produced by *Pseudomonas putida* IPT 046 with a similar monomeric composition than the one obtained in this work. Moreover, this result was in accordance with the result obtained in the FTIR spectrum, where bands associated to the crystallinity of the biopolymer were observed

(**Figure 6.5**). Generally, the crystallization of mcl-PHAs is slow and some copolymers do not crystallize at all, so no T_m is observed [28]. The production of amorphous biopolymers can be ascribed to the incorporation of unsaturated monomers and long chains, factors which can perturb the packing for crystallization [22]. It is worth mentioning that for *in vivo* applications in the biomedical field, the enzymes that degrade PHB are more efficient for the polymer in its amorphous state. For this reason, mcl-PHAs are more suitable than PHB, which has high crystalline nature.

Moreover, the thermomechanical behavior of the mcl-PHA film was studied by dynamic mechanical analysis (DMA). The analysis of the evolution of storage modulus (E´) and Tan Delta (Tan δ) as a function of temperature was performed and the results are shown in **Figure 6.10**.

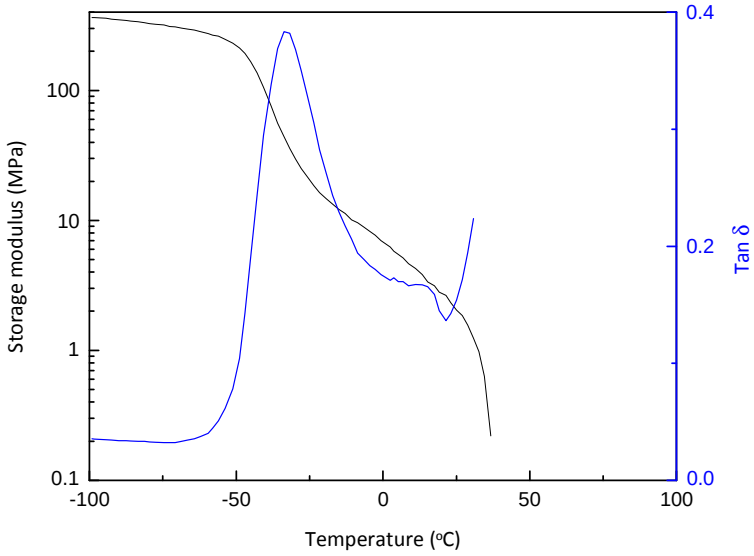

Figure 6.10 Storage modulus and Tan δ of mcl-PHA.

As it can be observed, at low temperatures the PHA shows high E´ (~ 360 MPa) in the glassy state. At higher temperatures, a continuous decrease in E´ happens related to the glass transition region and Tan δ curve shows a maximum which is related to the mechanical relaxation (α) of the PHA, associated with the glass transition temperature (T_g= -32 °C) [29]. The E´ value at room temperature is low, so this mcl-PHA is a very soft, elastic and slightly sticky material. With these features, this mcl-PHA could be suitable to use in coatings and in adhesives.

Finally, the mechanical performance of the mcl-PHA was analyzed by tensile tests. Young's modulus (E), tensile strength (σ_{max}) and elongation at break (ε_b) obtained from stress-strain curves are gathered in **Table 6.5.** mcl-PHAs are usually elastomeric materials, which present low crystallinity, low tensile strength and high elongation at break. As it can be observed, the biosynthesized PHA shows the typical mechanical behavior of mcl-PHAs. It has been previously reported that mcl-PHAs containing high amounts of 3HO monomer and other long chain monomers present modulus values from 11-17 MPa and elongation at break in the range of 250-400% [28,30]. In contrast to mcl-PHAs, scl-PHAs such as PHB, displays higher crystallinity and it is a malleable thermoplastic material with a modulus of 3.5 GPa, a tensile strength of 40 MPa and elongation at break of 6%. Generally, mcl-PHAs are used in blends with PHB to improve its processability and increase its elongation at break [28].

Table 6.5 Mechanical properties of the mcl-PHA.

E (MPa)	**σ_{max} (MPa)**	**ε_b (%)**
12.3 ± 2.9	3.1 ± 0.5	264.8 ± 16.6

6.4 CONCLUSIONS

In this chapter the technical feasibility of using cider by-products from the Basque Country for the biosynthesis of mcl-PHA by *P. putida* KT2440 bacterial strain was demonstrated.

The raw material contained glucose and fructose, both of which could be utilised in PHA production. Shake flask experiments revealed a high bacterial growth and biopolymer accumulation at higher sugar contents, reaching a PHA concentration of 1.1 g L^{-1} at a PHA accumulation of 25.5 % with the addition of extra feed at 12 h of fermentation. Further, the biosynthesized PHA was extracted from the biomass and monomer composition, chemical structure, molecular weight, thermal, thermomechanical and mechanical properties were analyzed. The polymer was found to be a mcl-PHA with a composition of different monomers containing from 6 to 14 carbons with saturated and unsaturated chains. This composition resulted in an elastomeric behavior, being the material soft, elastic and sticky at room temperature with potential applications in the biomedical field as well as in adhesives, or coatings. Although further bioprocess engineering development would be required to make the process industrially viable, cider by-products have been proven to be promising carbon source for mcl-PHA production, which in turn could be used in the processing of value-added products.

6.5 REFERENCES

[1] Guzmán, F.; Winterburn, J. Effect of limonene on the heterotrophic growth and polyhydroxybutyrate production by *Cupriavidus necator* H16. Bioresour. Technol. 221 (2016) 336-343.

[2] Yousuf, R.G.; Winterburn, J. Date seed characterisation, substrate extraction and process modelling for the production of polyhydroxybutyrate by *Cupriavidus necator*. Bioresour. Technol. 222 (2016) 242-251.

[3] Lageveen, R. G., Huisman, G.W., Preusting, H., Katelaar, P., Eggink, G., Witholt, B. Formation of polyesters by Pseudomonas oleovorans: effect of substrates on formation and composition of poly-(R)-3-hydroxyalkanoates and poly-(R)-3-hydroxyalkenoates. Appl. Environ. Microbiol. 54 (1998) 2924-2932.

[4] Jiang, X., Ramsay, J. A., Ramsay, B.A. Acetone extraction of mcl-PHA from *Pseudomonas putida* KT2440. J. Microbiol. Methods. 67 (2006) 212–219.

[5] Huijberts, G., Eggink, G., de Waard, P., Huisman, G.W., Witholt, B. *Pseudomonas putida* KT2442 cultivated on glucose accumulates Poly(3-hydroxyalkanoates) consisting of saturated and unsaturated monomers. Appl. Environ. Microbiol. 58 (1992) 536-544.

[6] Davis, R., Duane, G., Kenny, S.T., Cerrone, F., Guzik, M.W., Babu, R.P., Casey, E., O´Connor, K.E. High cell density cultivation of *Pseudomonas*

putida KT2440 using glucose without the need for oxygen enriched air supply. Biotechnol. Bioeng. 112 (2015) 725-733.

[7] Escapa, I.F., del Cerro, C., García, J.L., Prieto, M.A. The role of GlpR repressor in *Pseudomonas putida* KT2440 growth and PHA production from glycerol. Environ. Microbiol. 15 (2013) 93-110.

[8] Diniz, S.C., Taciro, M.K., Gomez, J.G.C., Pradella, J.G.C. High-cell-density cultivation of *Pseudomonas putida* IPT 046 and medium-chain-length polyhydroxyalkanoate production from sugarcane carbohydrates. Appl. Biochem. Biotechnol. 119 (2004) 51-70.

[9] Follonier, S., Goyder, M.S., Silvestri, A-C., Crelier, S., Kalman, F., Riesen, R., Zinn, M. Fruit pomace and waste frying oil as sustainable resources for the bioproduction of medium-chain-length polyhydroxyalkanoates. Int. J. Biol. Macromol. 71 (2014) 42–52.

[10] Löwe, H., Schmauder, L., Hobmeier, K., Kremling, A., Pflüger-Grau, K. Metabolic engineering to expand the substrate spectrum of *Pseudomonas putida* toward sucrose. Microbiology Open. 6 (2017) e00473.

[11] Follonier, S., Panke, S., Zinn, M.A. Reduction in growth rate of *Pseudomonas putida* KT2442 counteracts productivity advances in medium-chain-length polyhydroxyalkanoate production from gluconate. Microb. Cell. Fact. 10 (2011) 25.

[12] Borrero-de Acuña, J.M., Bielecka, A., Häussler, S., Schobert, M., Jahn, M., Wittmann, C., Jahn, D., Poblete-Castro, I. Production of medium chain length polyhydroxyalkanoate in metabolic flux optimized Pseudomonas putida. Microb. Cell. Fact. 13 (2014) 88.

[13] Sawyer, M.H., Baumann, P., Baumann, L., Berman, S.M., Cánovas, J.L., Berman, H. Pathways of D-fructose catabolism in species of *Pseudomonas*. Arch. Microbiol. 112 (1977) 49-55.

[14] Kansiz, M., Domínguez-Vidal, A., McNaughton, D., Lendl, B. Fourier-transform infrared (FTIR) spectroscopy for monitoring and determining the degree of crystallisation of polyhydroxyalkanoates (PHAs). Anal. Bioanal. Chem. 388 (2007) 1207-1213.

[15] Sathiyanarayanan, G., Bhatia, S. K., Song, H-S., Jeon, J-M., Kim, J., Lee, Y.K., Kim, Y-G., Yang, Y-H. Production and characterization of medium-chain-length polyhydroxyalkanoate copolymer from Arctic psychrotrophic bacterium *Pseudomonas sp.* PAMC 28620. Int. J. Biol. Macromol. 97 (2017) 710-720.

[16] Larrañaga, A., Fernández, J., Vega, A., Etxeberria, A., Ronchel, C., Adrio, J.L., Sarasua, J.R. Crystallization and its effect on the mechanical properties of a medium chain length polyhydroxyalkanoate. J. Mech. Behav. Biomed. Mater. 39 (2014) 87-94.

[17] Sánchez, R. J., Schripsema, J., da Silva, L. F., Taciro, M. K., Jose G.C., Pradella, J. G.C., Gomez, J.G.C. Medium-chain-length polyhydroxyalkanoic acids (PHAmcl) produced by *Pseudomonas putida* IPT 046 from renewable sources. Eur. Polym. J. 39 (2003) 1385-1394.

[18] Kang, D-K., Lee, C-R., Lee, S.H., Bae, J-H., Park, Y-K., Rhee, Y. H., Sung, B. H., Sohn, J-H. Production of polyhydroxyalkanoates from sludge palm oil using *Pseudomonas putida* S12. J. Microbiol. Biotechnol. 27 (2017) 990-994.

[19] Kato, M., Bao, H.J., Kang, C.K., Fukui, T., Doi, Y. Production of a novel copolyester of 3-hydroxybutyric acid and medium-chain-length 3-hydroxyalkanoic acids by *Pseudomonas sp.* 61-3 from sugars. Appl. Microbiol. Biotechnol. 45 (1996) 363-370.

[20] Lee, E.Y., Choi, C.Y. Gas chromatography-mass spectrometric analysis and its application to a screening procedure for novel bacterial polyhydroxyalkanoic acids containing long chain saturated and unsaturated monomers. J. Ferment. Bioeng. 4 (1995) 408-414.

[21] Pappalardo, F., Fragalà, M., Mineo, P. G., Damigella, A., Catara, A. F., Palmeri, R., Rescifina, A. Production of filmable medium-chain-lenght polyhydroxyalkanoate produced from glycerol by *Pseudomonas Mediterranea*. Int. J. Biol. Macromol. 65 (2014) 89-86.

[22] Muangwong, A., Boontip, T., Pachimsawat, J., Napathorn, S. C. Medium chain length polyhydroxyalkanoates consisting primarily of

unsaturated 3-hydroxy-5-cis-dodecanoate synthesized by newly isolated bacteria using crude glycerol. Microb. Cell. Fact. 15 (2016) 1-17.

[23] Reddy, M. V., Mawatari, Y., Onodera, R., Nakamura, Y., Yajima, Y., Chang, Y-C. Polyhydroxyalkanoates (PHA) production from synthetic waste using *Pseudomonas pseudoflava*: PHA synthase enzyme activity analysis from P. pseudoflava and P. Palleronii. Biores. Technol. 234 (2017) 99–105.

[24] Tsuge, T. Fundamental factors determining the molecular weight of polyhydroxyalkanoate during biosynthesis. Polym. J. 48 (2016) 1051-1057.

[25] Ward, P.G., Roo, G., O'Connor, K.E. Accumulation of polyhydroxyalkanoate from styrene and phenylacetic acid by Pseudomonas putida CA-3. Appl. Environ. Microbiol. 71 (2005) 2046-2052.

[26] Panaitescu, D.M., Lupescu, I., Frone, A.N., Chiulan, I., Nicolae, C. A., Tofan, V., Stefaniu, A., Somoghi, R., Trusca, R. Medium chain-length polyhydroxyalkanoate copolymer modified by bacterial cellulose for medical devices. Biomacromolecules 18 (2017) 3222-3232.

[27] Ishak, K.A., Annuar, M.S.M. Phase inversion of medium-chain-length poly-3-hydroxyalkanoates (mcl-PHA)-incorporated nanoemulsion:

effects of mcl-PHA molecular weight and amount on its mechanism. Coll. Polym. Sci. 294 (2016) 1969-1981.

[28] R. Rai, T. Keshavarz, J.A. Roether, A.R. Boccaccini, I. Roy, Medium chain length polyhydroxyalkanoates, promising new biomedical materials for the future. Mater. Sci. Eng. R. Rep. 72 (2011) 29-47.

[29] Cognet-Georjon, E., Mechin, F., Pascault, J. P. New polyurethanes based on 4,4-diphenylmethane diisocyanate and 1,4:3,6 dianhydrosorbitol, 2. Synthesis and properties of segmented polyurethane elastomers. Macromol. Chem. Phys. 197 (1996) 3593-3612.

[30] R. Rai, J.A. Roether, J.C. Knowles, N. Mordan, V. Salih, I.C. Locke, M.P. Gordge, A. McCormick, D. Mohn, W.J. Stark, T. Keshavarz, A.R. Boccaccini, I. Roy, Highly elastomeric poly(3-hydroxyoctanoate) based natural polymer composite for enhanced keratinocyte regeneration. Int. J. Polym. Mater. 66 (2017) 326-335.

CHAPTER 7

STIFF AND HYDROPHOBIC NANOPAPERS WITH ANTIOXIDANT CAPACITY

7. STIFF AND HYDROPHOBIC NANOPAPERS WITH ANTIOXIDANT CAPACITY

7.1 INTRODUCTION

Nowadays, sustainable packaging is an important issue due to the environmental concerns. In the food packaging area, biopolymers are considered very promising alternative to synthetic materials, as they offer improved properties coupled with eco-friendly attributes. Moreover, "active packaging" is in the focus of research. This novel technology is based on the design of packaging materials with material components that release or absorb substances from or into the packaged food or the surrounding environment in order to extend the shelf-life and maintain or improve the condition of packaged food. In recent years, the number of investigations related to the extraction of natural plant and fruit extracts and their addition to coatings and packaging materials has been increased in order to obtain packaging materials with antioxidant capacity.

In the field of food packaging, paper-based materials are regarded as a suitable option as paper is completely renewable and recyclable. Moreover, in the production of packages and bags, paper is an important material because it can be considered a suitable alternative to replace synthetic plastics. However, paper-based material presents some disadvantages compared to plastic, i.e. it is less durable and non water resistant. The hydrophilic nature of cellulose makes it very sensitive to moisture and it presents high water vapour transmission rates. Therefore, paper sheets can be externally filled with various additives and coatings or can be chemically modified and functionalized.

In this context, the application of nanotechnology in the papermaking science offers the possibility to produce paper with improved properties and performance in terms of hydrophobicity, strength, barrier properties and processing. In fact, nanopapers fabricated from cellulose nanofibers show interesting features such as high strength, thermal stability, optical transparency and good oxygen barrier properties due to the strongly reduced penetration of oxygen molecules through the highly entangled fibrillar structure. These enhanced properties would not be achieved using the traditional microsized pulp papers [1]. Indeed, bacterial cellulose can be considered a nanopaper with high mechanical properties due to its 3D conformation and high crystallinity. Due to its interesting properties, the use of bacterial cellulose in packaging related applications has also been investigated. In fact, BC has been previously used to reinforce papers and cellulosic surfaces [2,3] and bacterial cellulose nanocrystals (BCNCs) have been used as reinforcing fillers for edible films [4]. Cellulose nanocrystals have attracted a great deal of interest in such applications, due to its highly crystalline nature, high aspect ratio, low cost, renewability and biodegradability.

This chapter consists on the preparation of BC-based films for food related applications with improved mechanical properties, hydrophobicity and antioxidant properties. For this purpose, firstly, bacterial cellulose nanocrystals were isolated from previously biosynthesized BC membranes in chapter 3. The study of the effect of two acid hydrolysis treatments on the morphology and thermal properties of BCNCs was performed. The aim of this study was the optimization of the isolation conditions of BCNCs in order to obtain a high crystalline material with an acceptable thermal stability and high aspect ratio for applications in the nanocomposites field. After the

isolation of BCNCs with suitable properties, the effective improvement of the paper quality in terms of mechanical strength was studied by the infiltration of the BCNCs into the BC membrane structure in order to obtain a stiffer nanopaper (BC/BCNC nanopapers).

Then, the reinforced BC/BCNC nanopapers were coated with the medium-chain-length polyhydroxyalkanoate (mcl-PHA) synthesized in chapter 6, in order to study the effect of the coating on the hydrophobicity and transparency required for food packaging films (BC/BCNC/PHA films).

Finally, apple extracts with antioxidant capacity were extracted from cider by-products by Soxhlet extraction and were incorporated in different quantities in the mcl-PHA coating in order to develop films with antioxidant capacity for active food packaging (BC/BCNC/PHA-extract). Therefore, firstly a study was undertaken to provide information related to the free radical scavenging capacity of the extracted cider waste extracts using different solvents. After the evaluation of the antioxidant capacity of the obtained extracts, the most suitable ones were chosen to be incorporated to the PHA coatings. The effect of the incorporation of the extracts on the mechanical and thermal properties of the films as well as hydrophobicity, opacity and oxygen barrier properties was analyzed and also the antioxidant capacity of the prepared films was evaluated.

7.2 ISOLATION OF BACTERIAL CELLULOSE NANOCRYSTALS

The first part of this chapter consists on the isolation of BCNCs from BC membranes. Two acid hydrolysis treatments were used and the crystallinity, morphology and thermal stability of the BCNCs were analyzed. The ones

with most suitable characteristics were chosen to be infiltrated into BC membranes in order to obtain stiffer nanopapers.

7.2.1 Experimental

BC membranes were biosynthesized as explained in chapter 3. *Komagataeibacter medellinensis CECT 8140*, obtained from the Spanish Type Culture Collection (CECT), was used in a culture media containing a mixture of apple residues and commercial sugar cane at pH 4, at 28 °C, for 13 days, in static conditions. Then BC membranes were purified, neutralized and stored at 5 °C in deionized water until utilization, as described in previous chapter 3.

Firstly, BC membranes were mechanically desintegrated in a blender and the gel-like material was vacuum filtered to remove most of the adsorbed water. In order to hydrolyze the amorphous regions, the cellulosic material was treated with sulphuric acid 64% (wt) in a cellulose/acid ratio of approximately 4.5 g L^{-1}, at 45 °C with stirring for two different periods of time, 90 min and 24 h to obtain the BC nanocrystals.

After the hydrolisis, the obtained suspensions were diluted with deionized water to stop the process and washed using 4 centrifuge cycles at 4500 rpm for 20 min. The resulting suspensions were then dialyzed (in Spectra/Por^{R} 6 MWCO 8000 dialysis membranes) against ultrapure water for 5 days to remove any remaining free acid until the collecting medium water reached almost neutral pH. Finally, BCNC suspensions were freeze dried and stored in a dessicator until use. The isolated BCNCs were designated as BCNC 90 min and BCNC 24 h. A scheme of the hydrolysis process is shown in **Figure 7.1**.

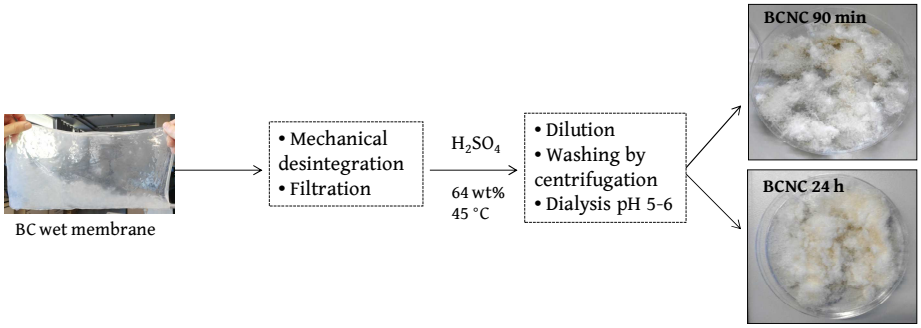

Figure 7.1 Scheme of BC acid hydrolysis process to isolate BCNCs.

7.2.2 Results

BCNCs were obtained by acid hydrolysis of BC membranes. This treatment consists on the digestion of significant fraction of amorphous domains and thus, the obtaining of a highly crystalline material (**Figure 7.2**). HCl and H_2SO_4 are the most commonly used acids for the hydrolysis of cellulose, and in this case H_2SO_4 was chosen. When H_2SO_4 is used, the produced cellulose nanocrystals are easily dispersible in water since during hydrolysis sulfate groups are introduced on the surface of the nanocrystals [5].

Usually, for BC longer hydrolysis times (from 1 h to 69 h) are required than for plant cellulose (usually from 30 to 60 min) due to the highly crystalline ribbon-shaped bundles formed during the biosynthesis process which hinders the acid penetration. For this reason, two hydrolysis times were chosen for the isolation of nanocrystals (90 min and 24 h) and the effects of hydrolysis time on the crystallinity, thermal stability and dimensions of the BCNCs was studied.

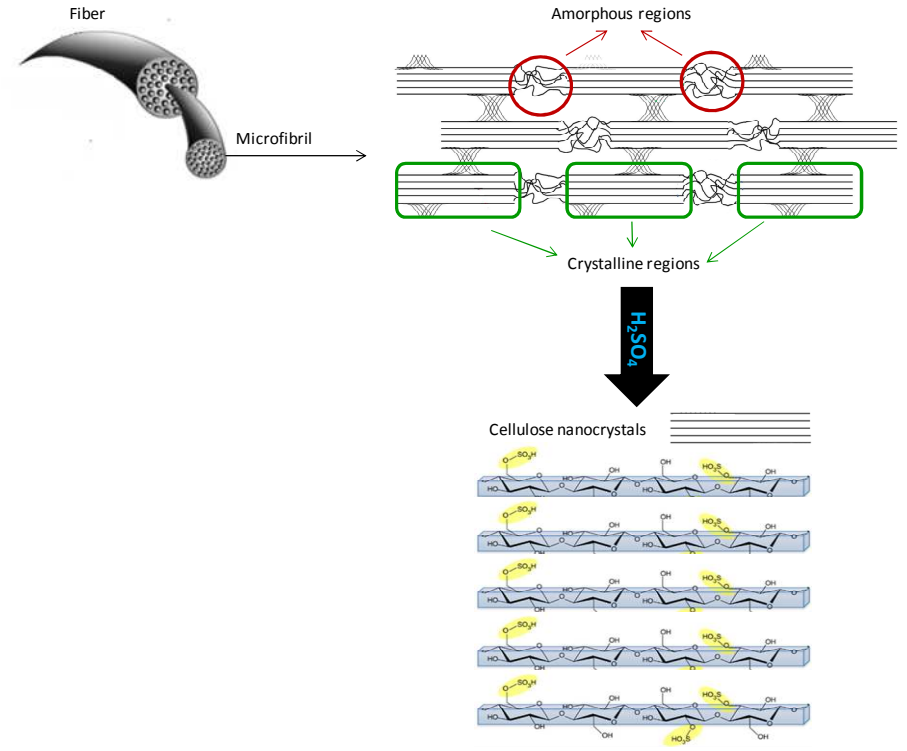

Scheme 7.2 Schematic process of cellulose nanocrystals isolation.

7.2.2.1 Crystallinity and physicochemical characterization of BCNCs

In order to analyze the effect of the hydrolysis time on the crystallinity of the obtained BCNCs, X-ray diffraction was carried out. **Figure 7.3** shows the X-ray diffraction patterns of BC membrane and BCNCs. The crystallinity index (CI^{XRD}) values were calculated from **Equation 2.7** taking into account that the patterns were indexed based on I_α, so the maximum intensity would be the one of the (110) lattice diffraction. Crystallite size ($L_{h,k,l}$) values were calculated from **Equation 2.8.** The results are gathered in **Table 7.1**. As it

can be observed from the results, the acid hydrolysis treatment affected the crystallinity of the initial BC and thus, the associated parameters.

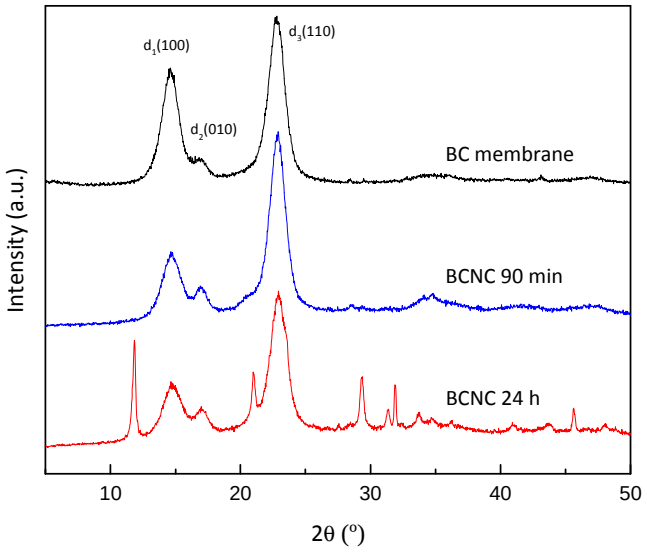

Figure 7.3 X-ray diffraction patterns of BC and BCNCs.

Table 7.1 Crystallinity index, crystallite size and I_β allomorph of BC membrane and BCNCs isolated using different acid hydrolysis times.

Sample	CI^{XRD}	$L_{h,k,l}$ (nm)	I_β
BC	0.80	2.0	0.39
BCNC 90 min	0.86	5.3	0.77
BCNC 24 h	0.85	6.2	0.80

As discussed in the previous chapter 3, the cellulose produced by bacteria corresponds to cellulose I polymorph, and concretely I_α is usually the predominant. As it can be observed in **Figure 7.3**, all the samples exhibit the

three main peaks for the I_α one-chain triclinic unit cell which correspond to the Miller indices of (100), (010) and (110) [6]. There may be slight variations between the crystallinity of the BC samples due to the biosynthesis process, the culture medium or the bacteria. In the case of BC membrane, the obtained crystallinity index is in the expected range (**Table 7.1**).

The X-ray diffraction pattern of the BCNCs treated for 90 min was very similar to the one of the BC membrane. In contrast, in the case of the BCNCs treated for 24 h the appearance of new peaks at 12.0, 21.0, 29.4 and 31.8 was observed. These new peaks were assigned to cellulose II [7,8]. As it has been previously reported, alkali and acid treatments result in a structural transformation from cellulose I to II because during these processes the form of the crystalline lattices is changed [9,10].

As it can be observed in **Table 7.1**, both acid hydrolysis led to an increase of the crystallinity of the initial BC membrane, being the CI^{XRD} of both BCNCs very similar. Usually, the hydrolysis time is a determining factor in the final crystallinity of the nanocrystals because if the hydrolysis is too short there may not be major changes in the crystallinity of the material, while too long reaction times may lead to a decrease in the crystallinity due to the digestion of the crystalline domains [11]. In this work, 90 min of reaction time was enough to cause an acceptable increase on the crystallinity and the increase of the hydrolysis time from 90 min to 24 h did not significantly change the crystallinity of the BCNCs.

Regarding the crystallite size, it experienced a significant increase in BCNC samples with respect to the one of BC membrane. These results agreed with the ones obtained in other works. Xu et al. [9] observed larger crystallite size in cellulose nanocrystals than in cellulose nanofibrils. Maiti et al. [12]

also observed the same trend comparing the apparent crystallite size of cotton and nanocellulose obtained from cotton by acid hydrolysis. They attributed this change in crystallite size to two factors that occur during acid hydrolysis: (1) the degradation of smaller crystallites and (2) the growth of the defective crystallites. As it can be observed from the results of the **Table 7.1**, this phenomenon is more intense as the hydrolysis time increases.

In addition, FTIR analysis of BC membrane and BCNCs was also carried out and the resultant spectra are shown in **Figure 7.4**.

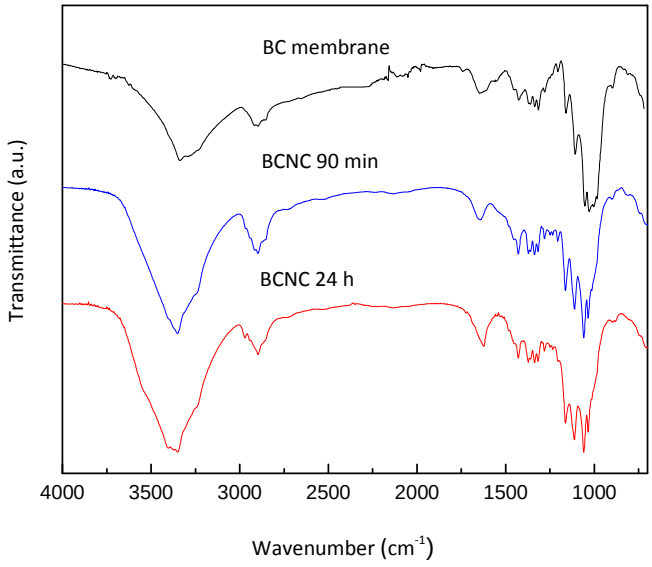

Figure 7.4 FTIR spectra of BC membrane and BCNCs.

The spectra showed the typical bands of cellulosic materials: bands around 3400 cm^{-1} (OH cellulose stretching vibrations), bands at 2900-2880 cm^{-1} (CH stretching vibrations), bands at 1460-1250 cm^{-1} (CH_2 vibrations), bands at

1170-1050 cm^{-1} (C-O-C bond of the glycosidic linkages), the band at 897 cm^{-1} (characteristic of β-linked glucose based polymers) and the band at around 1650 cm^{-1} (associated with the water absorbed by the cellulose).

As it can be noticed, a sharpening of the bands centred at 3400 was observed in the case of BCNCs spectra. Changes in these bands confirmed the increase of the crystallinity of the BCNCs with respect to the BC [11]. The most indicative feature of the crystallinity change was the sharpening of the broad band between 3000-3700 cm^{-1}, which corresponds to OH hydrogen bonding. These results were in accordance with the XRD results.

Moreover, in the FTIR spectrum of the BCNCs treated for 24 h, a shoulder or broadening of the band at 897 cm^{-1} was observed to lower wavenumber. This band is assigned to the β-glucosidic linkage for the cellulose I structure and the shifting of this band to lower wavenumber is indicative of the crystal transformation from cellulose I to II [13]. This result was in accordance to the one obtained in the XRD, were peaks associated to cellulose II were observed.

Additionally, the approximate percentage of I_β allomorph was estimated using the integrated areas of absorbance bands centered at 750 and 710 cm^{-1} and the results are gathered in **Table 7.1**. In this case, it can be noted that the percentage of I_β considerably increased with the acid hydrolysis, being similar with both acid hydrolysis treatments. It has been previously reported that I_α is metastable and can be converted into I_β by annealing (heat treatment), so the acid treatment at 45 °C would have induced a change of the crystal phase [14].

7.2.2.2 Thermal stability of BCNCs

The thermal stability of BC membrane and BCNCs was analyzed by thermogravimetric anaysis and TGA and dTG curves in a nitrogen atmosphere are displayed in **Figure 7.5** a) and b), respectively.

As described in previous chapter 3, in cellulosic samples the mass loss around 100 °C is attributed to water loss, while the main dTG peaks between 200-500 °C correspond to degradation processes of cellulose.

In the case of BCNCs, a mass loss in the 100-250 °C temperature range was observed. Other authors observed the same trend and they ascribed this mass loss to direct solid-to-gas phase transitions catalyzed by surface sulphate groups [15]. In the present work, in the case of BCNCs, the thermal degradation started at lower temperatures than in the BC membrane and occurred over a broader temperature range.

The temperature at 10 and 50% of mass loss (T_{10} and T_{50}, respectively), main dTG peak temperature, residue at 750 °C and sulphur content obtained by elemental analysis (EA) and conductiometric titration (CT) are shown in **Table 7.2.**

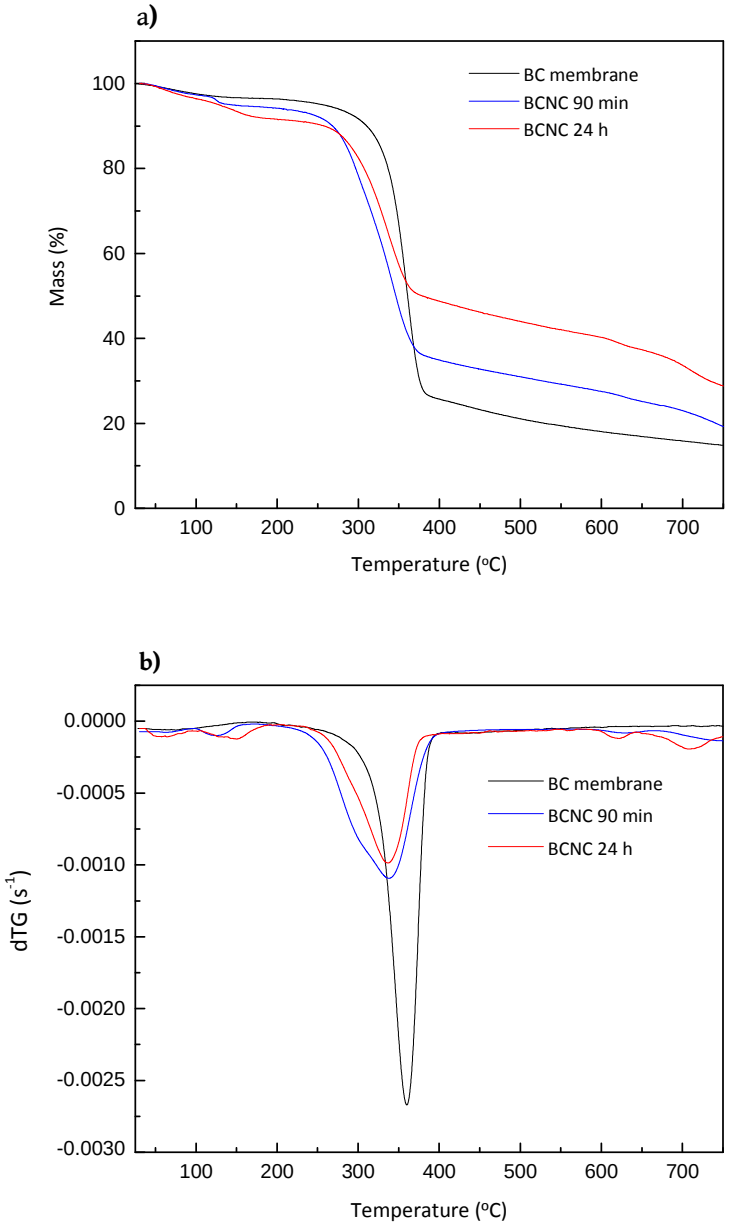

Figure 7.5 a) TGA and **b)** dTG curves of BC membrane and BCNCs.

Table 7.2 Temperature at 10 and 50% of mass loss (T_{10} and T_{50}), main dTG peak temperature, residue at 750 °C and sulphur content of BC membrane and BCNCs.

Sample	T_{10} (°C)	T_{50} (°C)	Main dTG peak temp. (°C)	Residue at 750 °C (%)	S^{EA} (%)	S^{CT} (%)
BC membrane	310	361	362	14.3	-	-
BCNC 90 min	268	346	338	19.6	2.5	3
BCNC 24 h	258	-	335	28.2	5.0	6

At 10% of mass loss, the degradation temperatures of BCNCs 90 min and 24 h were 42 and 52 °C lower than the one of the neat BC, respectively. At 50% of mass loss the degradation temperature of BCNC 90 min was 15 °C lower than the neat BC. The degradation temperature at 50% mass loss of BCNC 24 h was not included, since at that point, the residue was already formed so it would not be a real degradation temperature value. These results were in accordance to previously reported ones and this was ascribed to the attachment of sulphate groups into the BCNCs [11,16]. The highly sulphated regions are more accessible, so the degradation starts earlier. Also the main degradation temperatures were 24 and 27 °C lower in the BCNCs 90 min and 24 h respectively, compared to neat BC.

Moreover, the concentration of sulphate groups increased with the hydrolysis time being the double when the hydrolysis time increased from 90 min up to 24 h. In this way, the amount of char residue at 750 °C was remarkably larger in the case of the BCNCs (practically the double of the BC membrane in the case of BCNCs obtained in 24 h of hydrolysis). Indeed sulphuric acid facilitates the formation of char residue since it is a dehydration catalyst [11].

7.2.2.3 Morphological characterization of BCNCs

The morphology of isolated BCNCs was studied by AFM. AFM images are shown in **Figure 7.6** and dimensions (cross-section and length) obtained from the AFM images from at least 50 measurements, are gathered in **Table 7.3**.

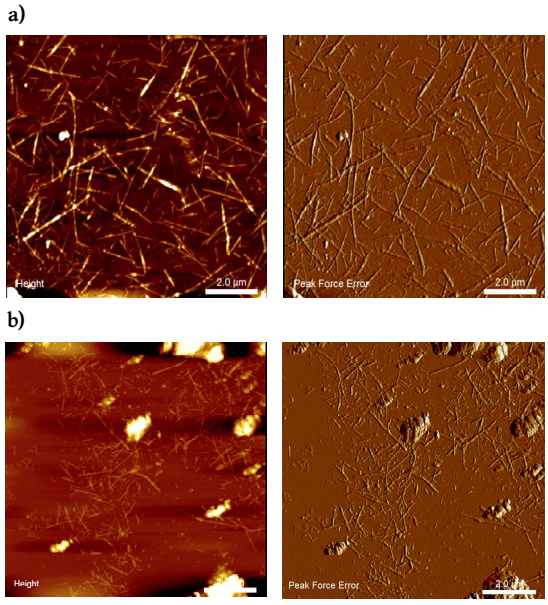

Figure 7.6 AFM height (left) and peak force (right) images of BCNCs, a) 90 min and b) 24 h.

Table 7.3 Dimensions of the nanofibers of BC membrane and BCNCs prepared with different acid hydrolysis times.

Sample	Cross-section (nm)	Length (nm)	Aspect ratio (L/D)
BC	55 ± 10	1000-2000	-
BCNC 90 min	53 ± 17	741 ± 269	17.0 ± 3.1
BCNC 24 h	50 ± 14	428 ± 136	10.0 ± 2.0

As it can be observed from the results, changes in the cross-section and especially, in the length were induced by varying the acid hydrolysis time, which were more accused when increasing the hydrolysis time from 90 min up to 24 h.

In general, longer hydrolysis times lead to shorter nanocrystals. However, BC nanocrystals with different sizes and L/D values can be obtained depending on various factors such as the state of the BC membranes (dry or wet), the acid used and its concentration, the hydrolysis time or the temperature. In this work some preliminary experiments were performed using dried BC samples and it was found that the hydrolysis suspension was more homogeneous and the BCNCs size was smaller in the case of using wet membranes. Martinez-Sanz et al. [11] used hydrolysis times of 2 h, 48 h and 69 h to treat dried and freeze-dried BC membranes. They reported that after 2 h, the hydrolysis suspension was not completely homogeneous so they needed longer hydrolysis times probably due to the initial state of the membranes.

Also it has been reported that to choose the most adequate BCNCs as nanoreinforcement for a polymeric matrix, the aspect ratio must be taken into account. For this application, higher aspect ratios are preferred. Martinez-Sanz et al. [11] obtained L/D values ranging from 52.26 to 23.33 using more severe conditions for BC hydrolysis (longer hydrolysis times (2, 48 and 69 h) and higher temperature (50 °C)). Vasconcelos et al. [17] also obtained higher L/D values using more concentrated H_2SO_4 for the hydrolysis of BC membranes. George and Siddaramaiah [18] obtained BC nanocrystals with L/D value of 15 using hydrochloric acid at boiling

conditions for 4 h for wet BC membranes. In the present work, the shortest acid treatment provided the BCNCs with the highest aspect ratio.

7.2.3 Conclusions

In this first part of the chapter, bacterial cellulose nanocrystals were successfully isolated from BC membranes. Two hydrolysis times, 90 min and 24 h, were used to obtain BCNCs and their crystallinity, thermal stability and morphology were determined. In view of the results, both acid hydrolysis treatments led to BCNCs with superior crystallinity index, but significantly lower thermal stability compared to BC due to the attachment of the sulphate groups into the BCNCs´ surface. The crystallinity index of BCNCs was similar for both treatments. An increase of the crystallite size and the appearance of new peaks in XRD difractogram assigned to cellulose II were observed with 24 h of hydrolysis. The BCNCs retained their chemical structure but the I_α crystalline structure changed to I_β with the hydrolysis treatment. The BCNCs obtained in 90 min of acid hydrolysis presented higher aspect ratio than the ones obtained in 24 h, so for the application as nanoreinforcements, BCNCs 90 min would be the ones with better characteristics. Taking this into account, BCNC 90 min were chosen for the posterior infiltration into BC membranes.

7.3 EXTRACTION AND ANTIOXIDANT CAPACITY OF APPLE WASTE EXTRACTS

In the second part of the chapter, natural extracts with antioxidant capacity were obtained from cider by-products with the objective of their use in active food packaging films. A study was undertaken to provide information

related to the free radical scavenging capacity of the obtained natural extracts.

Soxhlet method was chosen for the extraction. On the one hand, this is a method in which no posterior filtration is needed as in the case of other methods such as maceration, and on the other hand, high yields are usually obtained. Karabegovic et al. [19] compared different extraction methods for cherry laurel fruits i.e. microwave and ultrasound assisted extractions, classical extraction and Soxhlet extraction, and they found that Soxhlet extraction achieved the highest yield.

Acetone and ethanol 80%, two food safe solvents, were chosen for the extraction. Ethanolic and acetonic extracts were then subjected to a deffating process. First were deffated with n-hexane in order to remove waxes, fats, pigments and other metabolites that may interfere with extraction of flavonoids and then, the residual was extracted with ethyl acetate to isolate less polar flavonoids (isoflavones, flavanones, flavonols) [20-22]. As it has been previously reported, the antioxidant activity is strongly influenced by factors such as processing treatment and pH of the medium. In other works it has been observed that the antioxidant activity of the extracts is higher at neutral or alkaline pH conditions [23-25]. Schieber et al. [26] proposed a fractionation of apple pomace extract in pH 7.0 and pH 1.5 since catechin, epichatechin and procyanidins are not detectable following acidic extraction. In the present work, firstly acetone was used as solvent. Once the antioxidant capacity of the acetonic extracts was analyzed, it was decided to use another solvent (ethanol (80%)). Since the results indicated that the neutral pH extract was the one with higher antioxidant capacity, the ethanolic extract was adjusted to pH 7.

Then, the antioxidant capacity of the different extracts was analyzed by four different methods: DPPH radical scavenging assay, ferric reducing antioxidant power assay (FRAP), ABTS radical scavenging assay and total phenolic content method (TPC). After the evaluation of the antioxidant capacity, the thermal stability and physicochemical characterization of the extracts was performed in order to choose the most suitable ones for the addition to the mcl-PHA coatings.

7.3.1 Experimental

Natural extracts were obtained by solvent extraction of the apple pomace derived from the cider production using a Soxhlet extractor.

Firstly, the apple pomace was dried in an oven (110 °C) for ~24 h and milled to powder with a crusher. Two different solvents were used to perform the antioxidant extraction: acetone and ethanol (80%). The extraction was carried out in a Soxhlet apparatus for a period of 120 min (approximate ratio 1:10 (g dry matter: mL^{-1} solvent)). The liquid extract was concentrated by a rotary vacuum evaporator (40 °C) and then resuspended in water. This suspension was defatted with hexane two times in order to remove fats, waxes, pigments and other metabolites that may interfere with the extraction of flavonoids.

After the defatting with hexane, one fraction of the aqueous solution was adjusted to pH 7.0 with NaOH and the other to 1.5 with H_3PO_4 in the case of acetone extraction. These extracts were identified as AE7 and AE1.5. In the case of the ethanolic extract this was adjusted to pH 7.0 and was identified as EE7.

Finally a liquid-liquid extraction with ethyl acetate using a separating funnel was performed two times and the extracts were evaporated by a rotary vacuum evaporator to dryness (80 °C). All the samples were stored in a desiccator (in darkness) until use. The solvent extraction procedure followed in this work is shown in **Figure 7.7**.

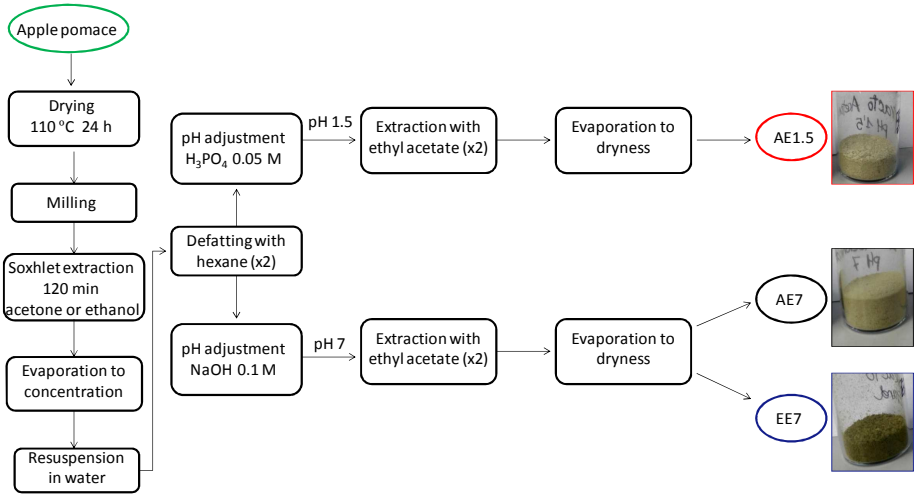

Figure 7.7 Scheme of the extraction procedure.

7.3.2 Results

7.3.2.1 Antioxidant activity of the extracts

Phenolic content and antioxidant capacity of the obtained extracts were analyzed depending on different variables of the process such as solvent and pH adjustment before ethyl acetate extraction. **Table 7.4** gathers the results obtained for antioxidant activity and polyphenolic content of cider apple extracts measured through DPPH, FRAP, ABTS and TPC methods, described in chapter 2, section 2.3.9.

Table 7.4 Antioxidant capacity of apple waste extracts measured by TPC, FRAP, DPPH and ABTS techniques.

Sample	TPC (mg GA/g extract)	FRAP (mg TE/g extract)
AE1.5	18.2 ± 1.5	20.0 ± 2
AE7	22.8 ± 1.2	34.0 ± 2
EE7	55.1 ± 2.3	43.0 ± 3
Sample	**DPPH (mg TE/ g extract)**	**ABTS (mg TE/g extract)**
AE1.5	5.5 ± 0.9	30.0 ± 2.0
AE7	12.7 ± 0.3	63.5 ± 1.1
EE7	20.0 ± 1.3	77.9 ± 1.3

The extraction yield (2.5 % for EE7) was also higher than that obtained with acetone (1.6 and 2.1 % for AE1.5 and AE7, respectively). These yields were calculated as function of the amount of apple residues extracted in the Soxhlet and the amount of solid extracts obtained at the end of the process. It can be noted that low yield values have been obtained due to the extraction process followed, which has many intermediate steps.

Even though there can be found research works about apple pomace extracts, results are not often comparable due to differences on samples (variety or ripeness of the fruits), solvents, sample size, extraction procedures, presentation of results (on fresh or dry basis of apple, extract, etc.).

Reis et al. [27] used a fractionation method to extract polyphenolic compounds from apple pomace involving a first extraction with water, followed by a second extraction with acetone or methanol. They performed the optimization of the extraction process with both solvents through a central composite rotatable design and they obtained TPC values ranging from 46-1711 mg GA/g dry extract for the methanolic extracts and 43-319 mg GA/g dry extract for the acetonic extracts. The antioxidant capacity of

the extracts can vary depending on the extraction process, solvent, temperature, time and other variables, so in this case a further optimization of the process could result in higher antioxidant capacities.

Finally, as it can be observed in **Figure 7.7**, significant differences on the colour of the extracts was observed. Indeed, it seems that there is a relationship between colour and antioxidant capacity, as the darker the extract is, the higher antioxidant capacity presents. Some authors have also noticed direct correlations between polyphenol content and colour in other extracts [28,29].

7.3.2.2 Physicochemical characterization of the extracts

In apple extracts two main families of polyphenolic compounds are present: flavonoids and phenolic acids and among the latter in particular, hydroxycinnamate derivatives (i.e. chlorogenic acid or caffeoylquinic acid and feruloylquinic acid) [30]. Flavonoids share a common structure consisting of 2 aromatic rings that are bound together by 3 carbon atoms that form an oxygenated heterocycle. These are divided into 6 subclasses as a function of the type of heterocycle involved: flavonols, flavones, isoflavones, flavanones, anthocyanidins and flavanols (catechins and proanthocyanidins).

As it can be observed in **Figure 7.8,** the FTIR spectra of the apple waste extracts showed the characteristic absorption bands of the chemical groups present in flavonoids and hydroxycinnamic acids, i.e., OH groups (phenols and alcohols) at 3400 cm^{-1}, C=O group of ketone at 1700 cm^{-1}, benzene rings around 3000 cm^{-1} (aromatic C-H stretching), 1600-1500 cm^{-1} (aromatic C=C

stretching), 1300-1000 cm^{-1} (aromatic C-H in plane bending) and 700-800 cm^{-1} (aromatic C-H out of plane bending) and cyclic ether at 1150-1050 cm^{-1} (C-O single bond stretching).

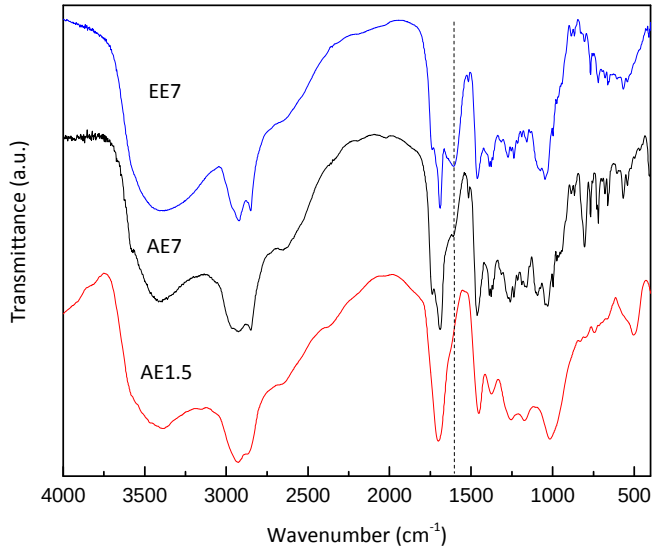

Figure 7.8 FTIR spectra of extracts obtained from cider by-products.

Figure 7.9 shows the chemical structure of polyphenolic compounds usually contained in apple extracts [27].

Between samples no significant differences were observed. In the case of the EE7 extract, a characteristic band was observed around 1600 cm^{-1} suggesting the presence of more aromatic compounds than in other samples. It has been previously reported that aqueous ethanol mixtures can dissolve a wider range of polyphenols while aqueous acetone mixtures are good solvent systems for the extraction of polar antioxidants, so the recovery of

polyphenolic compounds can slightly vary depending on the solvent used [31].

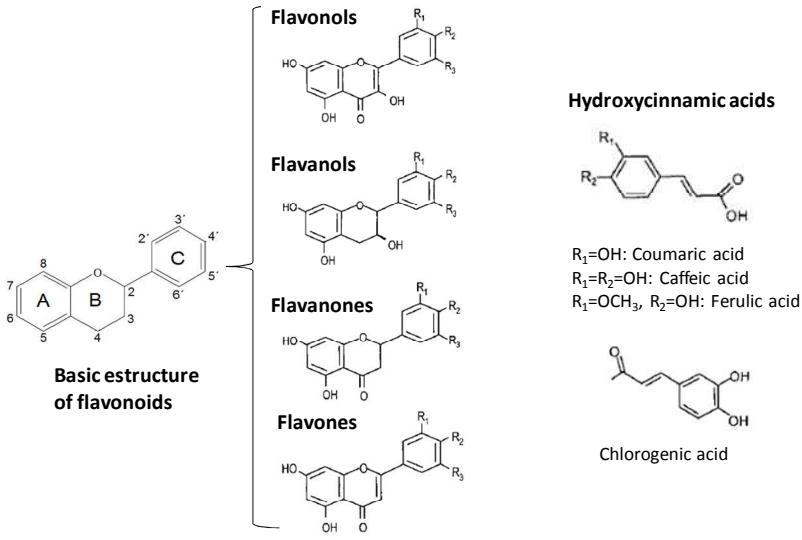

Figure 7.9 Structure of some flavonoids and hydroxycinnamic acids usually present in apple extracts [27].

7.3.2.3 Thermal stability of the extracts

For application in food products and cosmetics, natural antioxidants should satisfy several requirements such as stability to heat processing and effectiveness for at least 1 year at a temperature between 25 and 30 °C. The presence of atmospheric oxygen and high temperatures can cause various chemical changes and loss of antioxidants [32]. In order to study the thermal stability of apple waste extracts TGA measurements were carried out under nitrogen and oxygen atmosphere. **Figure 7.10** shows the TGA and dTG curves of the apple waste extracts.

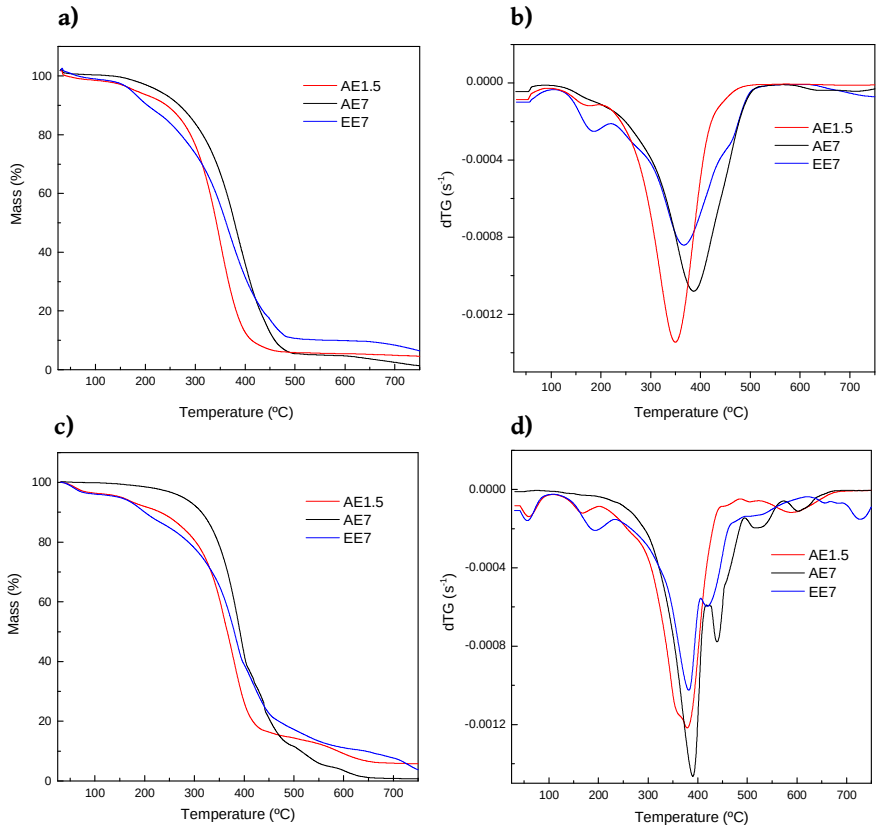

Figure 7.10 a) TGA and b) dTG curves in nitrogen atmosphere and c) TGA and d) dTG curves in oxygen atmosphere of apple pomace extracts.

As it can be observed, all the extracts presented different thermal zones which were reflected in distinct mass losses in the TG curves. This confirmed the presence of different compounds and complex structures. Usually the mass loss around 100-200 °C is related to preliminary oxidation steps and elimination of volatile fractions. In the case of EE7 and AE1.5 the presence of volatile fractions was noticeable, however in the case of AE7 the degradation occurred in one step (under nitrogen) and two steps (under

oxygen) and no volatiles were observed. AE7 was the most stable extract under both, nitrogen and oxygen atmospheres, since as it can be observed, the degradation started later, at higher temperatures. In the case of EE7, the degradation occurred over a broader temperature range and in more degradation steps, probably due to the presence of more compounds than in the other two samples. These results confirmed the fact that the ethanol might have dissolved and extracted a higher number of pholypenolic compounds which in turn has been reflected in the greater antioxidant capacity.

7.3.3 Conclusions

In this second part of the chapter, natural polyphenols from cider by-products were extracted by a Soxhlet extraction with acetone or ethanol. The solvent extraction was followed by the adjustment of the pH to 7.0 and 1.5 in the case of acetonic extract and pH 7.0 in ethanolic extract, and finished with a liquid-liquid extraction with ethyl acetate. The results indicated that pH and solvent had a great influence on the colour and antioxidant capacity of the extracts. Ethanol was the most suitable solvent since extracts exhibited the highest antioxidant activity and polyphenol content values. Although the polyphenolic composition of the extracts was not determined, TGA and FTIR results indicated the presence of a wider range of pholyphenolic compounds in the case of ethanolic extract. These results indicate that apple pomace from the cider production can be used as a source of antioxidant compounds with applications in different fields such as cosmetics or food packaging materials. In view of the results, ethanolic extracts were chosen for the development of BC-based films with antioxidant properties.

7.4 BC-BASED FILMS WITH ANTIOXIDANT CAPACITY

The third part of this chapter consists on the preparation of BC-based films for food related applications with improved mechanical properties as well as hydrophobicity and antioxidant properties. For this purpose, bacterial cellulose nanocrystals obtained in the first part of this chapter (BCNC 90 min) were incorporated into the BC membranes by infiltration (BC/BCNC). Then, the reinforced nanopapers were coated with the medium-chain-length polyhydroxyalkanoate (mcl-PHA) synthesized in chapter 6, with different contents of ethanolic extracts (EE7) obtained in the second part of this chapter. After the preparation of the nanocomposites, the morphological, mechanical and thermal characterization was performed. Taking into account the possible applications of these films in the food packaging field, hydrophobicity, opacity and oxygen barrier properties were analyzed. Finally, the antioxidant capacity of the films was assessed.

7.4.1 Experimental

7.4.1.1 Preparation of BC/BCNC nanopapers

Firstly, aqueous suspesions of 0.25 wt% of freeze-dried BCNCs obtained in the first part of the chapter (BCNC 90 min) were prepared (**Figure 7.11**). To assure the proper dispersion of the nanocrystals, the suspensions were magnetically stirred 24 h and then, sonicated in ice bath for 1 h. Subsequently, BC wet membranes were infiltrated (vacuum filtered) with these suspensions in a Büchner funnel. These suspensions were filtered four consecutive times until the filtered BCNC suspensions became clear, indicating that most of the nanocrystals had been incorporated into the BC membrane. Finally, BC/BCNC infiltrated nanopapers were dried at 60 °C for

three days in an oven between Teflon plates in order to avoid the shrinkage and then compressed at 10 Ton for 2 min at room temperature. The approximate BCNCs content in the BC nanopapers was calculated by weight difference between the initial weight of BCNCs and the weight of BCNCs after infiltration and elimination of water from the final aqueous suspension in an oven. This resulted in an approximate 34 %wt of BCNCs in the BC membranes. This system was designated as BC/BCNC. As a reference, neat BC wet membranes were conducted to the same drying and compressing procedure.

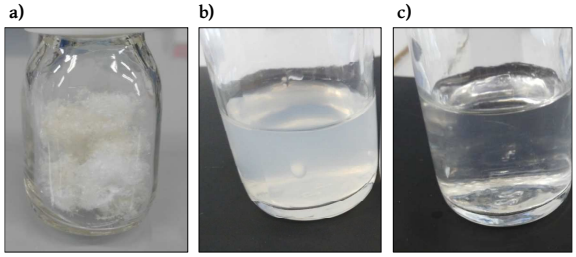

Figure 7.11 a) Freeze dried BCNCs, b) BCNC initial aqueous suspension and c) BCNC final aqueous suspension after four consecutive filtration cycles.

7.4.1.2 Preparation of BC/BCNC/PHA-extract films

Nanocomposites were prepared by coating previously dried BC/BCNC nanopapers with mcl-PHA dissolved in acetone. Firstly, dried BC/BCNC nanopapers were immersed in mcl-PHA solution in acetone to obtain approximately 70 %wt of PHA in the nanocomposites. These films are designated as BC/BCNC/PHA. The films were prepared by solvent casting in Teflon molds and dried at room temperature during 4 days to eliminate the solvent. Moreover, films with different content of apple extracts were prepared. For this, apple extracts were dissolved together with PHA in

acetone and the BC/BCNC nanopapers were immersed into PHA-extract solutions. Films with 1, 3 and 5% wt (respect to the PHA) of apple extracts were prepared and were designated as BC/BCNC/PHA-Xe, where X is referred to the extract weight content in the PHA coating. All the films were prepared by solvent casting in Teflon molds and dried at room temperature during 4 days to eliminate the solvent. Digital images of the films can be observed in **Figure 7.12**, where it can be noted that as the extract content increased, the films became darker. The PHA-extract content was calculated by weight difference between the initial BC/BCNC nanopapers and final BC/BCNC/PHA-extract nanocomposites. The compositions of the different systems are indicated in **Table 7.5**. All the samples were kept in a desiccator until use.

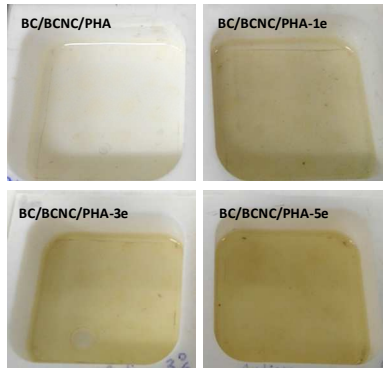

Figure 7.12 Digital images of BC/BCNC/PHA films with different extract contents.

Table 7.5 Designation and composition of different systems (wt%).

Sample	BC (%)	BCNC (%)	PHA (%)	Extracts (%)
BC	100.0	-	-	-
BC/BCNC	66.0	34.0	-	-
BC/BCNC/PHA	17.0	9.0	74.0	-
BC/BCNC/PHA-1e	20.5	8.8	70.0	0.7
BC/BCNC/PHA-3e	19.0	8.9	70.0	2.1
BC/BCNC/PHA-5e	16.9	7.5	72.0	3.6

7.4.2 Results

7.4.2.1 Morphology and mechanical performance of BC/BCNC nanopapers

To assess the incorporation of the BCNCs into BC membrane AFM was used to analyze the morphology of the surface and images are shown in **Figure 7.13**.

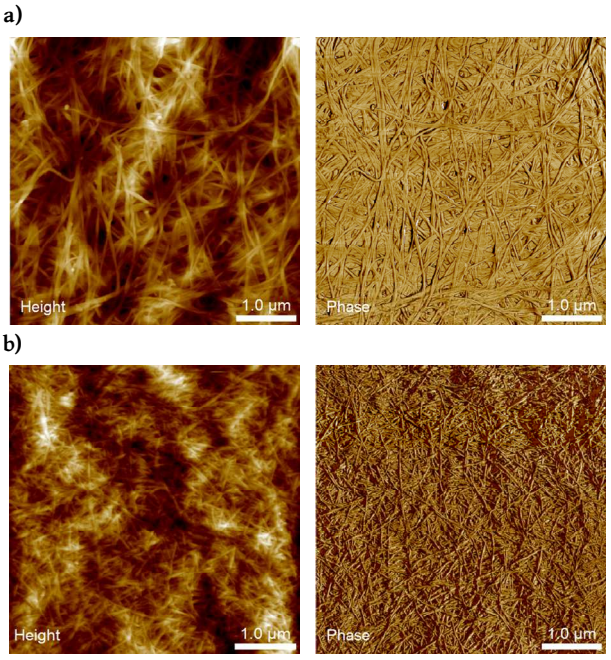

Figure 7.13 AFM height (left) and phase (right) images of a) BC and b) BC/BCNC nanopapers.

As it can be observed, the incorporation of BCNCs resulted in a more dense structure as dense regions of BCNCs occupy the spaces between large nanofibers of BC. These AFM images suggest that the BC surface is covered by the BCNCs. Therefore, it seems that the BC sheet shows a more

continuous structure and becomes more compact with the incorporation of BCNCs.

In this work the effective improvement of the nanopaper quality in terms of mechanical strength was analyzed by the infiltration of the BCNCs in the BC structure. The effect of the incorporation of BCNCs to the BC membrane was studied by tensile tests and Young's modulus (E), tensile strength (σ_{max}) and elongation at break (ε_b) were obtained from stress-strain curves.

From the mechanical point of view, the incorporation of BCNCs led to an improvement of ~11% of the modulus (from 7151 MPa for neat BC to 8067 MPa for BC/BCNC nanopapers) and ~37% of the tensile strength (from 116 MPa for neat BC to 159 MPa for BC/BCNC nanopapers). The elongation at break was also increased ~44% (**Table 7.6**).

The improvement of the tensile properties depends on the affinity between the matrix and the nanoreinforcement and the homogeneous dispersion or non agglomeration of the last. In many cases, high concentrations of nanoreinforcement do not induce an improvement of the mechanical properties. For example, Luong et al. [33] prepared graphene/amine-modified nanofibrillated cellulose nanocomposites with 0.1–10 wt% content of graphene and they observed improvement in tensile properties except for the 10 wt% graphene loading. They ascribed this phenomenon to the agglomeration of graphene in the composite. Lavoine et al. [34] studied the effect on the mechanical properties of two microfibrillated cellulose (MFC) coatings in papers and they observed that the modulus values of the MFC-coated papers were lower than the one of the base paper. They ascribed this

effect, among other things, to the possible non-homogeneous coating of the MFC and the low penetration of MFC suspensions into the paper structure.

In this context, BC membranes have been previously impregnated with dispersions containing other polymers and reinforcing agents. Ul-Islam et al. [35] developed nanocomposites with 25, 40 and 45 wt% content of montmorillonite (MMT) nanoparticles to reinforce BC membranes. They observed an improvement of the tensile strength (22-38%) and modulus (35-42%) with respect to the neat BC due to hydrogen bonding interactions, although the highest MMT loading did not provide the highest improvement due to the agglomeration of the nanoparticles. Feng et al. [36] observed an improvement of 10% and 20% in the modulus and tensile strength, respectively, of BC films containing 5 wt% of graphene oxide (GO) prepared by mixing aqueous solutions of BC and GO. They ascribed this improvement to the proper dispersion of GO on the BC matrix and the hydrogen bonding interactions between GO and BC.

In this work, BC membranes with 34 wt% of BCNCs were obtained, which is a high amount of BCNCs, and the improvement of the tensile properties was probably the result of: (1) the suitable filling of the interstices between the nanofibers of the 3D network of the BC sheet by the BCNCs and (2) the strong hydrogen bonding formation between the nanofiber matrix and the BCNCs due to the presence of strongly interacting surface hydroxyl groups.

The improvement has been acceptable since although the incorporation of the BCNCs seems more superficial (as seen in AFM images) a fraction of BCNCs would have penetrated the BC structure. These results suggest that the infiltration method used in this work was appropriate to obtain stiffer BC reinforced nanopapers with high amount of BCNCs.

7.4.2.2 Characterization of BC/BCNC/PHA-extract films

7.4.2.2.1 Physicochemical properties

Once the BC/BCNC stiffer nanopaper was prepared and characterized, the characterization of the BC/BCNC/PHA-extract films was performed. The characteristic functional groups and hydrogen bonding interactions in the nanocomposites were analyzed by Fourier transform infrared spectroscopy. The FTIR spectra of different films are shown in **Figure 7.14**.

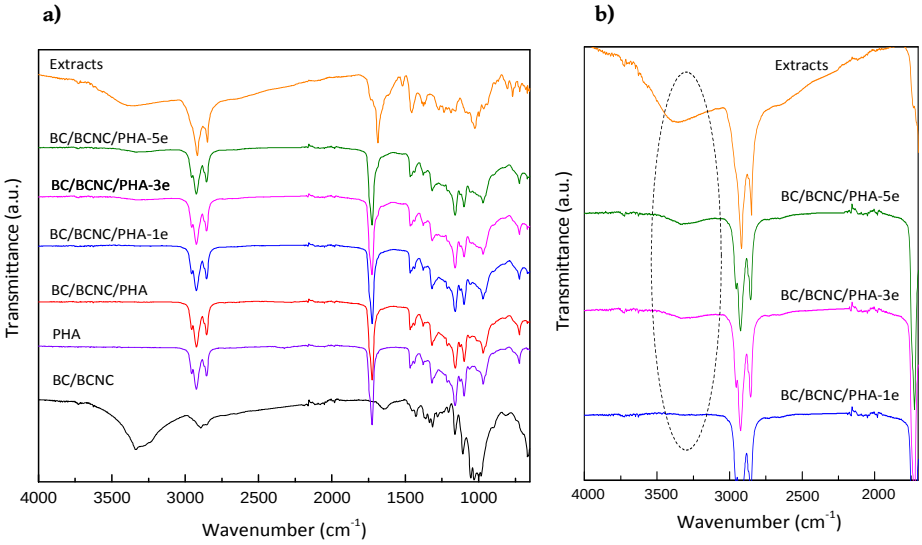

Figure 7.14 a) FTIR spectra of different systems and b) amplification of the FTIR spectra in the range 4000-1700 cm^{-1}.

The FTIR spectra of the BC/BCNC/PHA film and neat PHA were very similar. Moreover, no characteristic bands corresponding the BC or BCNCs were observed in the BC/BCNC/PHA spectrum, suggesting that the PHA had completely coated the structure of the BC/BCNC nanopaper.

Moreover, FTIR patterns of BC/BCNC/PHA film and the films with extracts were very similar, with no visible change in the peak intensities and wavenumbers shift indicating no relevant changes in chemical or physical interactions. The most significant change that can be appreciated with the addition of extracts was in the range of 3000-3500 cm^{-1}. As it can be observed in the augmented image in **Figure 7.14** b), the OH band centered at 3370 cm^{-1} of the apple extracts assigned to these groups of the polyphenolic compounds, widens and becomes more intense when increasing the amount of extracts in the films and slightly shifted to lower wavenumbers. This confirmed the presence of extracts in PHA coatings of BC/BCNC nanopapers and the possible interactions of the OH groups of the extracts with the matrix. Li et al. [37] observed a widening and sharpening of bands between 3250 cm^{-1} to 3600 cm^{-1} due to the incorporation of natural extracts to the gelatine matrix and attributed this to the intramolecular and intermolecular hydrogen bonding formation of OH groups contained in the extracts with the matrix.

7.4.2.2.2 Mechanical performance

The effect of the incorporation of PHA and PHA-apple extract coatings to BC/BCNC nanopapers on the mechanical performance of the films was analyzed by tensile tests. Young's modulus (E), tensile strength (σ_{max}) and elongation at break (ε_b) of neat BC, BC/BCNC nanopaper, neat PHA, and nanocomposite films obtained from stress-strain curves are summarized in **Table 7.6**. As it can be observed from the results of the **Table 7.6**, an important standard deviation value was obtained in some cases which can

be related to intrinsec material variability: multicomponent material (up to 4), bacterial derived polymers and preparation of the samples.

Table 7.6 Mechanical properties of different systems.

Sample	E (MPa)	σ_{max} (MPa)	ε_b (%)
PHA	12.3 ± 2.9	3.1 ± 0.5	264.8 ± 16.6
BC	7151.5 ± 215.3	116.9 ± 17.0	2.5 ± 0.3
BC/BCNCs	8067.7 ± 913.5	159.6 ± 53.4	3.6 ± 1.1
BC/BCNCs/PHA	1215.7 ± 159.6	23.2 ± 4.7	4.6 ± 1.8
BC/BCNCs/PHA-1e	1290.7 ± 261.7	31.9 ± 6.1	3.3 ± 0.4
BC/BCNCs/PHA-3e	1040.4 ± 99.7	25.3 ± 11.1	3.7 ± 1.4
BC/BCNCs/PHA-5e	430.5 ± 54.5	24.0 ± 5.9	6.9 ± 1.1

As explained in the previous chapter 6, the mcl-PHA exhibits adhesive properties and a remarkable elastomeric behavior with low tensile strength and high elongation at break. These features make it suitable for coatings.

On the contrary, BC and BC/BCNC nanopapers present high stiffness with high modulus values. In this case, BC/BCNC nanopaper was completely coated by the PHA as it has been observed in the FTIR spectra of the BC/BCNC/PHA film. Taking into account the high amount of PHA in the films (**Table 7.5**), it can be concluded that the mechanical performance of the nanocomposites was improved with respect to the neat PHA. The Young´s modulus of the neat PHA film, 12.3 MPa, increased to 1215.7 MPa for BC/BCNC/PHA film, and similarly, the tensile strength (3.1 MPa for neat PHA) increased to 23.2 MPa. However, the elongation at break experienced a significant drop. The BC/BCNC/PHA nanocomposite experienced 650% of improvement in tensile strength, 9700% of increase in Young´s modulus and 98% decrease in elongation at break compared to neat PHA.

Similar behavior was also observed in a previous work developed in our research group with BC/PLA-PEG films for food packaging applications. In that case, BC content in the nanocomposites was higher than in the present work, practically over 90 % for all systems. Therefore, BC/PLA-PEG nanocomposites maintained the strength and stiffness of the BC. In the case of the nanocomposite with lowest BC content (89%wt) an enhancement of the modulus of 600% and strength of 100% was observed with respect to the PHA-PEG blend. Moreover, Zhijiang et al. [38] with poly(3-hydroxybutyrate-co-4-hydroxybutyrate)/BC composites (50:50 weight ratio) and Zhijiang and Guang [39] with BC/PHB composites (50:50 weight ratio) also obtained improvements in modulus and strength and drops in elongation at break with the incorporation of BC into the matrix.

However, although in the present work BC content was lower than in all those previous works, the incorporation of BC in the mechanical performance of the PHA was more pronounced. This can be explained because scl-PHAs (PHB and copolymers) and PLA are stiffer and more brittle plastic materials than mcl-PHAs, which often display latex-to resin-like properties [40].

As commented in the introduction, until date, PHB has been widely used in food packaging field and the literature regarding mcl-PHA nanocomposite production for food related applications is scarce, but mcl-PHAs could be interesting for storage of goods like foods under freezing conditions as they present low glass transition temperatures.

In the present work, the mechanical properties obtained for the BC/BCNC/PHA film are in the range of some other polymers of interest for food packaging, such as PHB, PLA or PS. In **Table 7.7** some values of

mechanical properties has been included from literature for comparison [41].

Table 7.7 Mechanical properties of some polymers of interest in food packaging [41].

Polymer	E (MPa)	σ_{max} (MPa)	ε_b (%)
PHB	1700-3500	40	3-6
PHBV	700-2900	30-38	20
PLA	1200-2700	28-50	7-9
PCL	400	16	120-800
PP	1700	35-40	150
PS	1600-3100	12-50	3-4

On the other hand, the incorporation of apple extracts to the system originated a decrease in the modulus and strength with respect to the film without extracts. In the case of BC/BCNC/PHA-1e film, no significant differences were observed. However, the increase of the amount of extracts to 3 and 5% led to a drop in the stiffness of the films, especially with 5% content. This could be ascribed to the non homogenous dispersion or plastifying effect of the extracts in the coatings. In fact, the decrease in the tensile strength is a common trend observed in systems containing natural additives which becomes more noticeable with the content of the additive. However, it must be taken into account that the BC/BCNC/PHA-5e presented lower BC/BCNC content than other films and this could had an influence on the stiffness of the film.

Riaz et al. [42] also observed this effect in systems of chitosan containing apple peel polyphenols and it was attributed to the interruption of the ordered crystalline structure formation in the chitosan matrix by the polyphenols which led to a weakening of the intermolecular hydrogen

bonding. Ramos et al. [43] related the changes in the mechanical performance of polypropylene films with carvacrol and thymol (phenolic monoterpenes and isomers contained in thyme and oregano essential oils) to the plastifying effect caused by the addition of both additives to the polymer matrix. Li et al. [34] explained that when the amount of natural extracts in gelatine-based films increased, these extracts induced to the formation of heterogeneous and discontinuous areas producing low tensile strength.

7.4.2.2.3 Wettability, opacity and barrier properties

It is commonly known that cellulose has poor water resistance due to its hydrophilic nature and this might be a problem since the material may lose physical integrity and mechanical strength by absorbing water during distribution and storage. There are several alternatives to solve this problem. On the one hand, surface functionality of cellulose can be modified with reagents by the incorporation of groups which are reactive with OH cellulose groups. On the other hand, the paper´s surface can be modified using coatings to vary the wettability or hydrophobicity.

PHAs posses an intrinsic hydrophobicity, so the effect of the incorporation of PHA and PHA-extract coatings to BC/BCNC nanopapers was analyzed by static water contact angle (WCA) measurements. **Figure 7.15** shows the wetting of a water droplet on the surface of some samples and **Table 7.8** gathers WCA results.

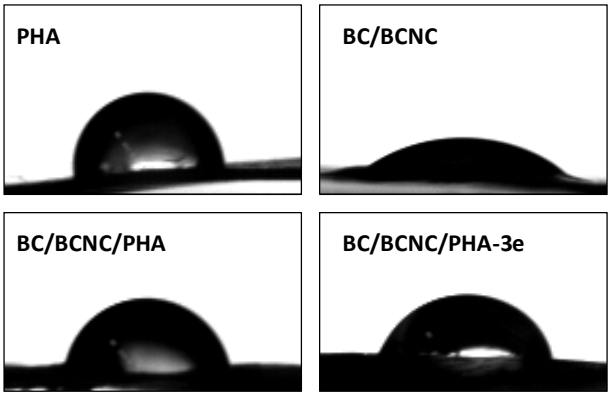

Figure 7.15 Image of a water droplet on the surface of some samples.

Table 7.8 Water contact angle (WCA), opacity (O) and oxygen permeability (OP) of different systems.

Sample	WCA (°)	O (Abs mm^{-1})	OP (cm^3 mm m^{-2} $day^{-1}atm^{-1}$)
PHA	87.5 ± 5.2	1.1 ± 0.2	-
BC	32.4 ± 2.3	24.1 ± 0.3	-
BC/BCNCs	29.4 ± 2.3	21.9 ± 0.4	1.4
BC/BCNCs/PHA	71.1 ± 3.9	4.8 ± 0.7	4.8
BC/BCNCs/PHA-1e	69.6 ± 5.1	5.2 ± 0.4	-
BC/BCNCs/PHA-3e	66.6 ± 4.5	5.7 ± 0.4	3.3
BC/BCNCs/PHA-5e	68.2 ± 3.2	5.9 ± 0.3	-

Low contact angle values, ranging from 0° to 30°, are characteristic from highly hydrophilic surfaces such as glass or mica, while high contact angle values, between 70° and 90°, are indicative of hydrophobic surfaces.

In the case of neat BC, as it has been previously seem in chapters 3 and 4, it possesses a high water holding and absorbing capacity, so the drop of water was absorbed quickly. Moreover, the infiltration of BCNCs to BC membranes did not significantly change the hydrophilicity of the surface. The WCA values indicate that the surface turned slightly more hydrophilic with the

presence BCNCs. This can be ascribed to the presence of more hydroxyl groups due to the presence of BCNCs in the surface which can interact more easily with water molecules [44].

In contrast, the WCA value of the PHA (87.5°) was indicative of a hydrophobic material and it was in the range of the ones reported in the literature for PHAs [45,46]. As it can be observed, the incorporation of the PHA coating to BC/BCNC nanopapers significantly increased the hydrophobicity of the surface from 29.4° to 71.1° suggesting that the BC/BCNC nanopaper had been almost completely coated by the PHA.

Nevertheless, the incorporation of extracts to the PHA coating led to a slight decrease of the WCA respect to PHA without extracts. This was expected, as the polyphenolic compounds contained in the apple extracts present significant hydrogen bonding capacity, enabling it to interact with practically any hydrophilic material or water. These results correlated with the ones obtained in the FTIR spectra, where a widening of the -OH band was observed with the incorporation of the extracts to the coating. BC/BCNC/PHA-extract films resulted to be much more hydrophobic than the neat BC and BC/BCNC nanopapers, therefore the integrity of the films against water was enhanced with the PHA-extract coating.

Moreover, the opacity is an important parameter for film appearance, so the opacity (O) of the different systems was analyzed by UV-vis and calculated using the **Equation 2.15**. The results are gathered in **Table 7.8**. High values of O indicate higher degree of opacity and consequently, lower transparency.

As it has been observed in **Figure 6.4**, the biosynthesized mcl-PHA had a yellowish colour but it was quite transparent. In contrast, BC/BCNC film was very opaque due to the effect of the light diffraction at the interface between the cellulose fibers and air interstices. As it can be observed from the results of the **Table 7.8**, the coating of the PHA led to a significant change in the opacity of the BC/BCNC film. The opacity value was 4.5 times lower in the case of BC/BCNC/PHA film compared to the one of BC/BCNC nanopaper. The film became much more transparent due to the filling of the gaps and interstices by the PHA. This effect was previously observed in chapter 5, where the BC membrane had been totally embedded and coated by the WBPU and thus, the increase of the transparency in the BC/WBPU nanocomposite was evident. As expected, opacity values of the BC/BCNC/PHA-extract films slightly increased with extract content (**Figure 7.12**). As observed in the second part of this chapter, the EE7 extracts had a strong green dark colour so the change in opacity is attributed to the content of extracts. This is a common trend observed in systems containing natural antioxidants such as apple peel polyphenols or tea polyphenols [42,47].

Furthermore, good barrier properties of films are important features in functional aspects of packaging materials for achieving a long self life for the packaged food. The active protection of oxygen-sensitive food products is an important issue, so the incorporation of natural antioxidants to the package is an interesting alternative due to their ability to reduce oxidative radicals [48]. In this way, the barrier properties of BC/BCNC, BC/BCNC/PHA and BC/BCNC/PHA-3e films were analyzed through gas permeation measurements with O_2 and the results are shown in **Table 7.8**. BC/BCNC/PHA-3e film was chosen to analyze the effect of the addition of

apple waste extracts to the mcl-PHA coating on the oxygen permeability of the film. The neat PHA film was not measured due to the configuration of the equipment used, which caused the breaking of the PHA films.

As it can be observed, BC/BCNC film showed very low oxygen permeability. This could be ascribed to the conformation of the nanofibrous membrane which creates a tortuous path for oxygen [49]. On the other hand, the incorporation of the mcl-PHA hydrophobic coating to the BC/BCNC nanopaper led to an increase of the oxygen permeability. It has been previously reported that PHB and poly(3-hydroxybutyrate-co-3-hydroxyvalerate) (PHBV) exhibit approximate oxygen permeability values in the range of 2-10 and 5-14 cm^3 mm m^{-2} $day^{-1}atm^{-1}$, respectively and these values are slightly better than the ones of PLA (15-25 cm^3 mm m^{-2} $day^{-1}atm^{-1}$), PCL (20-200 cm^3 mm m^{-2} $day^{-1}atm^{-1}$) and other plastic materials used in food packaging [41].

In view of the results, it can be concluded that the oxygen permeability value obtained for the BC/BCNC/PHA film would be in the range of the ones obtained with other PHAs and plastics. Moreover, the incorporation of apple extracts led to a decrease of the oxygen permeability compared to the film without extracts. This confirmed that the presence of polyphenolic compounds present in the mcl-PHA coating had a positive effect on the barrier properties of the films and could provide protection to oxygen-sensitive food products.

Gonçalves et al. [50] also observed that the gas barrier properties i.e. carbon dioxide and oxygen permeation properties, of PLA films could be improved with the incorporation of natural and synthetic antioxidants, although they concluded that these gas permeation properties were dependent of the

compatibility between the polymer matrix and the antioxidant incorporated as well as the content of antioxidant added.

7.4.2.2.4 Thermal stability

The thermal stability of the different systems was analyzed by TGA. **Figure 7.16** a) displays the TGA curves of BC/BCNC nanopaper, neat PHA and extracts and **Figure 7.16** b) shows the TGA curves of the BC/BCNC/PHA-extract films.

As it can be observed in **Figure 7.16** a), except BC/BCNC nanopaper, neat PHA and extracts showed more than one degradation stage.

In the case of the neat PHA, this showed an onset decomposition temperature around 207 °C. At 270 °C, around 50% mass reduction was observed and complete degradation of PHA occurred at 500 °C. The TGA curve was similar to other PHAs reported in the literature [51,52].

In contrast, the BC/BCNC nanopaper, the mass loss around 100 °C was attributed to water loss. This system was the most stable with an onset decomposition temperature around 300 °C. As it has been previously reported, the thermal stability is related to the crystalline structure. As BC/BCNC nanopaper is so crystalline, more energy (heat) is required to break the higher crystalline structure than the one of the PHA.

Finally, in the case of the extracts, degradation occurred in various steps probably due to the variety of polyphenolic compounds present in the extracts. Moreover, the degradation started at lower temperature than in the case of the neat PHA and BC/BCNC nanopaper.

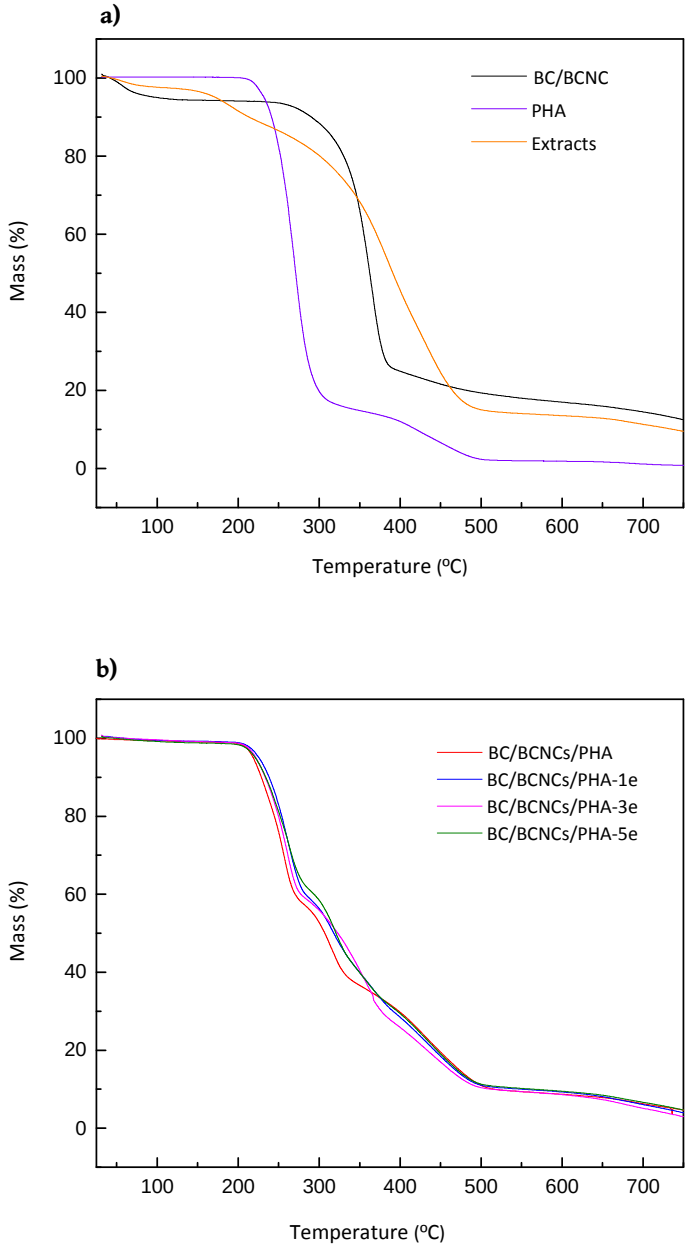

Figure 7.16 a) TGA curves of BC/BCNC, neat PHA and extracts and b) TGA curves of BC/BCNC/PHA-extract films.

In the case of BC/BCNC/PHA and BC/BCNC/PHA-extract systems (**Figure 7.16** b)) the degradation followed a multistep decomposition probably due to the degradation of the different components. All samples presented a mass loss around 257-263 °C (probably related to the PHA) another one around 320-350 °C (probably related to the BC/BCNC and the extracts) and a final mass loss around 400 °C (related to the PHA and less volatile extracts). The temperature at 10 and 50% of mass loss (T_{10} and T_{50}, respectively) and residue at 750 °C are shown in **Table 7.9**. It was observed that the extracts conferred higher thermal stability to the films as the temperatures were shifted a few degrees towards higher values with respect to the film without extracts (BC/BCNC/PHA). Usually the incorporation of antioxidants increases thermal stability of polymers [53,54], although it does not happen in all cases.

Table 7.9 Temperature at 10 and 50% of mass loss (T_{10} and T_{50}) and residue at 750 °C of the different systems.

Sample	T_{10} (°C)	T_{50} (°C)	Residue at 750 °C (%)
Extracts	213	391	9.4
BC/BCNCs/PHA-5e	234	323	4.6
BC/BCNCs/PHA-3e	233	323	2.9
BC/BCNCs/PHA-1e	238	317	3.9
BC/BCNCs/PHA	228	307	4.6
PHA	241	270	0.7
BC/BCNC	290	363	11.1

7.4.2.2.5 Antioxidant capacity

Finally, the antioxidant capacity of the films was evaluated by two of the four methods previously used to evaluate the antioxidant capacity of the

extracts. In this case ABTS and DPPH methods were used, which assay the capacity of scavenge free radicals.

In ABTS method, the reduction of blue-green ABTS radical colored solution by hydrogen-donating antioxidant is measured by the disappearance of its characteristic absorption band at 734 nm from the UV-vis spectrum. The colour of the standard solutions (5, 10, 15, 30 and 50 mg L^{-1} trolox) and solutions containing the dissolved neat extracts and BC/BCNC/PHA-extract films in ABTS are shown in **Figure 7.17**. As it can be observed, there was a colour change in the solutions containing BC/BCNC/PHA-extract films, suggesting antioxidant capacity.

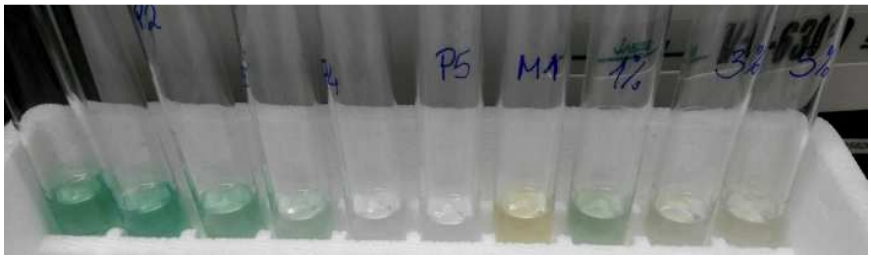

Figure 7.17 ABTS solutions after incubation 40 min at room temperature. From left to right: trolox standards (5, 10, 15, 25, 30 and 50 mg L^{-1}), apple extracts, BC/BCNC/PHA-1e, BC/BCNC/PHA-3e and BC/BCNC/PHA-5e.

DPPH is a stable free radical that is dissolved in methanol and its purple colour shows a characteristic absorption band at 517 nm. Antioxidant molecules scavenge the free radical by hydrogen donation and the colour from the DPPH assay solution becomes light yellow resulting in a decrease in absorbance. The colour of the standard solutions (5, 10, 25, 30, 50 and 100 mg L^{-1} trolox) and solutions containing the dissolved neat extracts and BC/BCNC/PHA-extract films DPPH can be observed in **Figure 7.18**. In this

case the colour change in the solutions containing the films is less noticeable, but it can be seen that there has been a reaction.

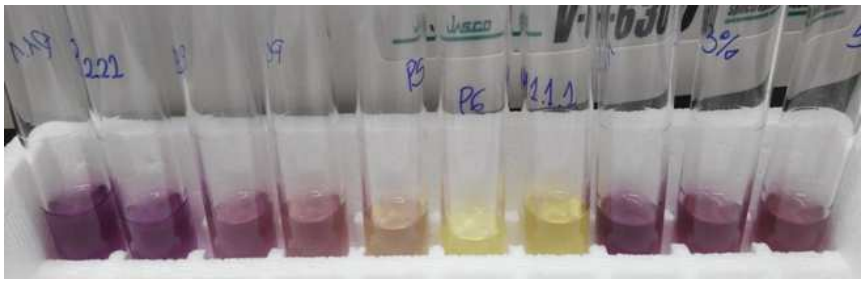

Figure 7.18 DPPH solutions after incubation 30 min at room temperature. From left to right: trolox standards (5, 10, 25, 30, 50 and 100 mg L^{-1}), apple extracts, BC/BCNC/PHA-1e, BC/BCNC/PHA-3e and BC/BCNC/PHA-5e.

The results of radical scavenging activity are indicated as % inhibition of the DPPH and ABTS using the **Equations 2.18** and **2.19**, respectively and are shown in **Figure 7.19**. As it can be observed, all the films showed DPPH and ABTS scavenging activity. As reported by other authors, the antioxidant activity detected by the ABTS assay is higher than the one of the DPPH assay since high pigmented and hydrophilic antioxidants are better reflected by ABTS assay [55]. The free radical scavenging activity increased with extract content in the films.

Riaz et al. [42] also observed the same trend in chitosan films containing apple peel polyphenols, although they obtained higher scavenging activities against ABTS and DPPH with lower antioxidant contents (0.25-1 %). In that case, they observed that the native film of chitosan exhibited antioxidant capacity without the addition of polyphenolics. In this case, the BC/BCNC/PHA film did not show antioxidant activity so all the antioxidant

activity of the final films would be attributed only to the presence of extracts.

Ferreira et al. [56] evaluated the antioxidant capacity of chitosan films containing grape pomace extracts and they obtained lower values of ABTS and DPPH scavenge capacity than the ones obtained in this work. This indicates that apple peel is a suitable source of antioxidants for food related applications.

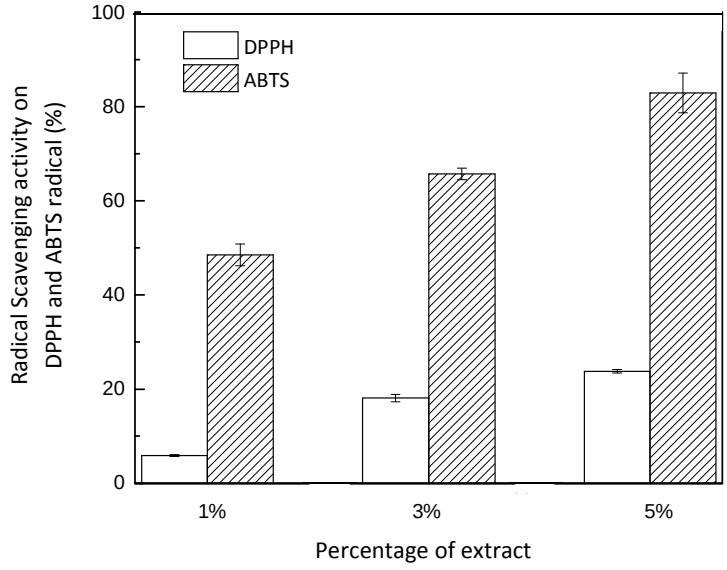

Figure 7.19 Scavenging activities of BC/BCNC/PHA-extract films on DPPH and ABTS radicals.

7.4.3 Conclusions

In this third part of the chapter, BC-based hydrophobic films with antioxidant properties for food related applications were developed. Firstly,

BC membranes were reinforced by infiltration of BCNCs into the nanofiber network leading to an improvement of 25.5 % and 6.1 % in the modulus and tensile strength of BC membranes, respectively. Then, an hydrophobic coating was added to the BC/BCNC nanopapers based on the previously biosynthesized mcl-PHA with elastomeric and adhesive properties. High amount of PHA was coated in the system and the BC/BCNC/PHA nanocomposite experienced an improvement in tensile strength, increase in Young´s modulus and decrease in elongation at break compared to neat PHA. Moreover, the hydrophobicity and transparency of the films was significantly enhanced with the incorporation of the PHA coating. Additionally, coatings with different amounts of apple extracts were prepared. Moreover, BC/BCNC/PHA-extract films resulted to be much more hydrophobic than the neat BC and BC/BCNC nanopapers. The oxygen permeability of the films improved with the presence of extracts and also the thermal stability. Finally, the antioxidant capacity of the films was analyzed and the results obtained in this work, suggest that the incorporation of apple extracts in the PHA coating contributed to enhance the scavenge free radical capacity of the films and that the degree of antioxidant capacity is proportional to the amount of the antioxidant additives added.

7.5 REFERENCES

[1] Samyn, P., Barhoum, A., Öhlund, T., Dufresne, A. Review: nanoparticles and nanostructured materials in papermaking. J. Mater. Sci. 53 (2018) 146-184.

[2] Santos, S.M., Carbajo, J.M., Gómez, N., Ladero, M., Villar, J.C. Paper reinforcing by in situ growth of bacterial cellulose. J. Mater. Sci. 52 (2017) 5882–5893.

[3] Campano, C., Merayo, N., Negro, C., Blanco, A. Low-fibrillated bacterial cellulose nanofibers as a sustainable additive to enhance recycled paper quality. Int. J. Biol. Macromol. 114 (2018) 1077-1083.

[4] George, J., Siddaramaiah. High performance edible nanocomposite films containing bacterial cellulose nanocrystals. Carbohydr. Polym. 87 (2012) 2031-2037.

[5] Pirich, C.L., de Freitas, R.A., Woehl, M.A., Picheth, G.F., Petri, D.F.S., Sierakowski, M.R. Bacterial cellulose nanocrystals: impact of the sulphate content on the interaction with xyloglucan. Cellulose 22 (2015) 1773-1787.

[6] French, A.D. Idealized powder diffraction patterns for cellulose polymorphs. Cellulose 21 (2014) 885–896.

[7] Oh, S.Y., Yoo, D.I., Shin, Y., Kim, H.C., Kim, H.Y., Chung, Y.S., Park, W.H., Youk, J.H. Crystalline structure analysis of cellulose treated with sodium
hydroxide and carbon dioxide by means of X-ray diffraction and FTIR spectroscopy. Carbohydr. Res. 340 (2005) 2376-2391.

[8] Sullivan, E.M., Moon, R.J., Kalaitzidou, K. Processing and characterization of cellulose nanocrystals/polylactic acid nanocomposite films. Materials 8 (2015) 8106-8116.

[9] Xu, X., Liu, F., Jiang, L., Zhu, J. Y., Haagenson, D., Wiesenborn, D.P. Cellulose nanocrystals vs. cellulose nanofibrils: a comparative study on their microstructures and effects as polymer reinforcing agents. Appl. Mater. Interfaces. 5 (2013) 2999-3009.

[10] Yue, Y., Han, G., Wu, Q. Transitional properties of cotton fibers from cellulose I to cellulose II structure. Bioresources 8 (2013) 6460-6471.

[11] Martínez-Sanz, M., Lopez-Rubio, A., Lagaron, J.M. Optimization of the nanofabrication by acid hydrolysis of bacterial cellulose nanowhiskers. Carbohydr. Polym. 85 (2011) 228-236.

[12] Maiti, S., Jayaramudu, J., Das, K., Reddy, S.M., Sadiku, R., Ray, S.S., Liu, D. Preparation and characterization of nano-cellulose with new shape from different precursor. Carbohydr. Polym. 98 (2013) 562-567.

[13] Yue, Y., Han, G., Wu, Q. Transitional properties of cotton fibers from cellulose I to cellulose II structure. Bioresources 8 (2013) 6460-6461.

[14] Nishiyama,Y., Sugiyama, J., Chanzy, H., Langan, P. Crystal structure and hydrogen bonding system in cellulose I_α from synchrotron X-ray and neutron fiber diffraction. J. Am. Chem. Soc. 125 (2003) 14300-14306.

[15] Lu, P., Hsieh, Y-L. Preparation and properties of cellulose nanocrystals: Rods, spheres, and network. Carbohydr. Polym. 82 (2010) 329-336.

[16] Roman, M., Winter, W.T. Effect of sulphate groups from sulphuric acid hydrolysis on the thermal degradation behaviour of bacterial cellulose. Biomacromolecules 5 (2004) 1671-1677.

[17] Vasconcelos, N.F., Feitosa, J.P.A., da Gama, F.M.P., Morais, J.P.S., Andrade, F.K., Filho, M. M., Rosa, M. F. Bacterial cellulose nanocrystals produced under different hydrolysis conditions: Properties and morphological features. Carbohydr. Polym. 155 (2017) 425-431.

[18] George, J., Siddaramaiah. High performance edible nanocomposite films containing bacterial cellulose nanocrystals. Carbohydr. Polym. 87 (2012) 2031-2037.

[19] Karabegovic, I.T., Stojicevic, S.S., Velickovic, D.T., Todorovic, Z.B., Nikolic, N. C. Lazic, M.L. The effect of different extraction techniques

on the composition and antioxidant activity of cherry laurel (*Prunus laurocerasus*) leaf and fruit extracts. Ind. Crops. Prod. 54 (2014) 142–148.

[20] Aguilar, E., Bonilla, P. Antioxidant activity and immunological of flavonoids isolated from leaves of *Smallanthus sonchifolius* (yacon). Ciencia e Investigación 12 (2009) 15-23.

[21] Cao, X., Wang, C., Pei, H. Sun, B. Separation and identification of polyphenols in apple pomace by high-speed counter-current chromatography and high-performance liquid chromatography coupled with mass spectrometry. J. Chromatogr. A. 1216 (2009) 4268–4274.

[22] Pérez-Nájera V.C., Lugo-Cervantes, E.C., Gutiérrez-Lomelí. M. Del-Toro-Sánchez, C.L. Extraction of phenolic compounds from lime peel (*Citrus limetta Risso*) and antioxidant activity determination. Biotecnia XV. 3 (2013) 18-22.

[23] Arabshahi-D, S., Devi, V., Urooj, A. Evaluation of antioxidant activity of some plant extracts and their heat, pH and storage stability. Food. Chem. 100 (2007) 1100-1105.

[24] Azizah, A.H., Ruslawat, N.M., SweeTee, T. Extraction and characterization of antioxidants from cocoa by-products. Food. Chem. 64 (1999) 199-202.

[25] Yen, G.C., Duh, P.D. Antioxidant properties of methanolic extracts from peanut hulls. J. Am. Oil. Chem. Soc. 70 (1993) 383-386.

[26] Schieber, A., Keller, P. Carle, R. Determination of phenolic acids and flavonoids of apple and pear by high-performance liquid chromatography. J. Chromatogr. A. 910 (2001) 265-273.

[27] Reis, S.F., Rai, D.K., Abu-Ghannam, N. Water at room temperature as a solvent for the extraction of apple pomace phenolic compounds. Food. Chem. 135 (2012) 1991-1998.

[28] Bucic-Kojic, A., Planinic, M., Tomas, S., Jakobek, L. Seruga, Marijan. Influence of solvent and temperature on extraction of phenolic compounds from grape seed, antioxidant activity and colour of extract. Int. J. Food. Sci. Tech. 44 (2009) 2394-2401.

[29] Woffenden, H.M., Ames, J.M., Chandra, S. Relationships between antioxidant activity, color, and flavor compounds of crystal malt extracts. J. Agric. Food Chem. 49 (2001) 5524-5530.

[30] Manach, C., Scalbert, A., Morand, C., Remesy, C. Jimenez, L. Polyphenols: Food sources and bioavailability. Am. J. Clin. Nutr. 79 (2004) 727–747.

[31] Alothman, M., Bhat, R., Karim, A.A. Antioxidant capacity and phenolic content of selected tropical fruits from Malaysia, extracted with different solvents. Food. Chem. 115 (2009) 785-788.

[32] Taghvaei, M., Jafari, S.M. Application and stability of natural antioxidants in edible oils in order to substitute synthetic additives. J. Food. Sci. Technol. 52 (2013) 1272–1282.

[33] Luong, N.D., Pahimanolis, N., Hippi, U., Korhonen, J.T., Ruokolainen, J., Johansson, L-S., Nam, J-D., Seppälä, J. Graphene/cellulose nanocomposite paper with high electrical and mechanical performances. J. Mater. Chem. 21 (2011) 13991-13998.

[34] Lavoine, N., Desloges, I., Khelifi, B., Bras, J. Impact of different coating processes of microfibrillated cellulose on the mechanical and barrier properties of paper. J. Mater. Sci. 49 (2014) 2879-2893.

[35] Ul-Islam, M., Khan, T., Park, J.K. Nanoreinforced bacterial cellulose-montmorillonite composites for biomedical applications. Carbohydr. Polym. 89 (2012) 1189-1197.

[36] Feng, Y., Zhang, X., Shen, Y., Yoshino, K., Feng, W. A mechanically strong, flexible and conductive film based on bacterial cellulose/graphene nanocomposite. Carbohydr. Polym. 87 (2012) 644-649.

[37] Li, J-H., Miao, J., Wu, J-L., Chen, S-F., Zhang, Q-Q. Preparation and characterization of active gelatin-based films incorporated with natural antioxidants. Food. Hydrocoll. 37 (2014) 166-173.

[38] Zhijiang, C., Chengwei, H., Guang, Y. Poly(3-hydroxybutyrate-co-4-hydroxybutyrate)/bacterial cellulose composite porous scaffold: Preparation, characterization and biocompatibility evaluation. Carbohydr. Polym. 87 (2012) 1073-1080.

[39] Zhijiang, C., Guang, Y. Optical nanocomposites prepared by incorporating bacterial cellulose nanofibrils into poly(3-hydroxybutyrate). Mater. Lett. 65 (2011) 182-184.

[40] Muhr, A., Rechberger, E.M., Salerno, A., Reiterer, A., Schiller, M., Kwiecień, M., Adamus, G., Kowalczuk, M., Strohmeier, K., Schober, S., Mittelbach, M., Koller, M. Biodegradable latexes from animal-derived waste: Biosynthesis and characterization of mcl-PHA accumulated by *Ps. citronellolis*. React. Funct. Polym. 73 (2013) 1391–1398.

[41] Plackett, D., Siro, I. Polyhydroxyalkanoates (PHAs) for food packaging. In book: Multifunctional and nanoreinforced polymers for food packaging. (2011) 498-526.

[42] Riaz, A., Lei, S., Akhtar, H.M.S., Wan, P., Chen, D., Jabbar, S., Abid, M., Hashim, M.M., Zeng, X. Preparation and characterization of chitosan-based antimicrobial active food packaging film incorporated with apple peel polyphenols. Int. J. Biol. Macromol. 114 (2018) 547–555.

[43] Ramos, M., Jiménez, A., Peltzer, M., Garrigós, M.C. Characterization and antimicrobial activity studies of polypropylene films with

carvacrol and thymol for active packaging. J. Food. Eng. 109 (2012) 513-519.

[44] George, J., Ramana, K.V., Bawa, A.S., Siddaramaiah. Bacterial cellulose nanocrystals exhibiting high thermal stability and their polymer nanocomposites. Int. J. Biol. Macromol. 48 (2011) 50-57.

[455] Zhao, C., Li, J., He, B., Zhao, L. Fabrication of hydrophobic biocomposite by combining cellulosic fibers with polyhydroxyalkanoate. Cellulose 24 (2017) 2265-2274.

[46] Andreotti, S., Franzoni, E., Esposti, M.D., Fabbri, P. Poly(hydroxyalkanoate)s-based hydrophobic coatings for the protection of stone in cultural heritage. Materials 11 (2018) 165-191.

[47] Wang, L., Dong, Y., Men, H., Tong, J., Zhou, J. Preparation and characterization of active films based on chitosan incorporated tea polyphenols. Food Hydrocoll. 32 (2013) 35-41.

[48] Bonilla, J., Talón, E., Altarés, I., Vargas, M., Chiralt, A. Effect of the incorporation of antioxidants on physicochemical and antioxidant properties of wheat starch-chitosan films. J. Food. Eng. 118 (2013) 271-278.

[49] Aulin. C., Gällstedt, M., Lindström, T. Oxygen and oil barrier properties of microfibrillated cellulose films and coatings. Cellulose 17 (2010) 559-574.

[50] Gonçalves, C.M.B., Tomé, L.C., Garcia, H., Brandão, L., Mendes, A.M., Marrucho, I.M. Effect of natural and synthetic antioxidants incorporation on the gas permeation properties of poly(lactic acid) films. J. Food. Eng. 116 (2013) 562-571.

[51] Ray, S., Prajapati, V., Patel, K., Trivedi, U. Optimization and characterization of PHA from isolate *Pannonibacter phragmitetus* ERC8 using glycerol waste. Int. J. Biol. Macromol. 86 (2016) 741-749.

[52] Shrivastav, A., Mishra, S.K., Mishra, S. Polyhydroxyalkanoate (PHA) synthesis by *Spirulina Subsalsa* from Gujarat coast of India. Int. J. Biol. Macromol. 46 (2010) 255-260.

[53] Singh, S., Gaikwad, K.K., Lee, Y.S. Antimicrobial and antioxidant properties of polyvinyl alcohol bio composite films containing seaweed extracted cellulose nano-crystal and basil leaves extract. Int. J. Biol. Macromol. 107 (2018) 1879-1887.

[54] Zhang, G., Nam, C., Petersson, L., Jambeck, J., Hillborg, H., Chung, T.C.M. Increasing polypropylene high temperature stability by blending polypropylene-bonded hindered phenol antioxidant. Macromolecules 51 (2018) 1927-1936.

[55] Floegel, A., Kimb, D-O., Chungc, S-J., Koo, S.I., Chun, O.K. Comparison of ABTS/DPPH assays to measure antioxidant capacity in popular antioxidant-rich US foods. J. Food. Compost. Anal. 24 (2011) 1043-1048.

[56] Ferreira, A.S., Nunes, C., Castro, A., Ferreira, P., Coimbra, M.A. Influence of grape pomace extract incorporation on chitosan films properties. Carbohydr. Polym. 114 (2014) 490-499.

CHAPTER 8

GENERAL CONCLUSIONS, FUTURE WORK AND PUBLICATIONS

8. GENERAL CONCLUSIONS, FUTURE WORK AND PUBLICATIONS

8.1 GENERAL CONCLUSIONS

The goal of this work was the integral utilization of cider by-products from the Basque Country to obtain value added materials for advanced applications. For this purpose, different biosynthesis processes for biopolymer production via bacterial fermentation i.e. bacterial cellulose and polyhydroxyalkanoates, have been developed using these residues as carbon source and BC-based nanocomposites have been prepared.

In this way, the optimal culture conditions to produce BC using apple residues and sugar cane (AR/SC) were investigated. Different AR/SC ratios were used to prepare the culture media for BC production and in all cases BC production was observed confirming that AR/SC mixture was a suitable carbon source. The study of the effect of pH on cell viability confirmed that acidic pH favored the growing of the cells and in consequence, the BC production. BC membranes were characterized and exhibited a strong 3D reticulated structure with high crystallinity and excellent mechanical properties making them suitable for a range of applications in different fields.

In addition, BC membranes were used as a template for the development of different nanocomposites with tailored properties with potential applications in different areas: water cleaning processes, biomedicine and food packaging.

BC membranes were modified by *ex situ* and *in situ* routes with chitosan (Ch) to develop water cleaning membranes for copper removal in wastewaters. Two routes led to different interactions between both biopolymers, packaging assembly, morphology and consequently, different properties. The crystallinity and the water holding capacity strongly related to the mechanical performance resulted to be very different depending on the preparation route. Through the *in situ* route, better mechanical performance in wet state was obtained due to the lower interaction with water molecules, while lower mechanical performance in dry state was observed due to a lower crystallinity. The incorporation of Ch during the biosynthesis process by the *in situ* route modified the packaging assembly of the BC in a significant way and therefore, the crystallinity was strongly affected. The morphological characterization revealed a more homogenous reticulated structure with the addition of Ch during BC biosynthesis, suggesting a better inclusion of Ch into BC matrix through *in situ* route while the incorporation of Ch through *ex situ* route seemed more superficial. Finally the copper removal capacity of the *in situ* and *ex situ* membranes was assessed and compared to that of the glutaraldehyde crosslinked Ch. *In situ* prepared membranes showed the highest copper removal capacity and this was ascribed to the more homogenous network with less tendency to swell in water and therefore, to a better interaction with the cooper ions. Finally the reusability of the membranes was confirmed.

Moreover, biocompatible water-activated shape memory nanocomposites were prepared by the immersion of wet BC membranes into waterborne polyurethane (WBPU) dispersions for biomedical applications. The good affinity of both polymers led to a complete embedding and coating of the BC by the WBPU. Nanocomposites with high amount of WBPU were obtained, so

the elastomeric properties of the WBPU were maintained in the nanocomposites, but an improvement of the modulus and strength was observed confirming the effective reinforcement of the BC membrane. The *in vitro* biocompatibility and cell adhesion tests of the nanocomposites showed non-toxic behavior making them suitable for biomedical applications. Finally, the water-activated shape-memory test revealed a great improvement of the shape fixity ability and faster recovery process with the presence of BC.

Furthermore, the feasibility of using cider by-products to produce medium-chain-length polyhydroxyalkanoates (mcl-PHAs) was investigated. Different apple residues/water ratios were used to prepare juices with different concentrations of sugars and determine the optimum ratio for the maximum PHA production. Apple residues contained two main residual sugars, glucose and fructose, being the last the main sugar present. Sugar consumption pattern revealed that both sugars were metabolized simultaneously, but glucose was consumed faster than fructose. These results suggested that glucose was used mainly for bacterial growth while substrate conversion to PHA derived from the fructose consumption. Different batch feeding strategies were used to maximize the PHA production and it was found that an acceptable PHA content could be produced. The biosynthesized PHA was extracted from biomass and characterized and was found to be a mcl-PHA with a composition of different monomers containing from 6 to 14 carbons with saturated and unsaturated chains. This composition resulted in an elastomeric behavior, being soft, elastic and sticky at room temperature with potential applications in adhesives or coatings.

Finally, BC-based films with improved mechanical properties and hydrophobicity and antioxidant properties were prepared for food related applications. Firstly, bacterial cellulose nanocrystals (BCNCs) were obtained by different acid hydrolysis treatments and characterized in order to choose the most suitable ones as nanoreinforcements. Then, apple extracts were obtained by Soxhlet extraction of the cider by-products and their antioxidant capacity was evaluated to use them as additives in active food packaging applications. BCNCs were incorporated into the BC membranes by infiltration and the mechanical properties were improved. In addition, the previously synthesized mcl-PHA was applied as an hydrophobic coating in the reinforced BC/BCNC sheets. The mechanical performance was affected, but the hydrophobicity and transparency of the films were enhanced with the mcl-PHA coating. Finally, different cider-waste extracts were added into the mcl-PHA coating in order to obtain films with antioxidant capacity. The incorporation of apple extracts in the PHA coating contributed to enhance the oxygen permeability and thermal stability of the films with respect to the films without extracts. Finally, the scavenge free radical capacity of the films was evaluated and it was observed that the degree of antioxidant capacity was proportional to the amount of the antioxidant additives added.

8.2 FUTURE WORK

Based on this work and with the aim of following with the research in this field, different challenges are proposed, which would complete this work and provide suitable outlines for future frameworks:

- Production of BC in different shapes for different applications. In static cultivation BC can be obtained in different structures and

shapes depending on the container used. It is possible to obtain tubular form BC for blood vessels in biomedical applications. Experiments in this area could be performed and modifications of the tubular BC could be carried out. In addition, different *in situ* and *ex situ* modifications could be performed in dynamic cultures with different polymers or additives in order to obtain modified BC spheres for advanced applications in drug delivery or biomedicine.

- Replace the sugar cane in the culture medium with another waste rich in sugars such as grape pomace from wine industry, glycerol or residual streams from food industries. These residues could be used in combination with apple residues to optimize the BC production.

- Scale up the production of mcl-PHA in bioreactors. In this work, shake flask experiments were carried out in order to optimize a set of conditions. To perform a process on an industrial scale firstly the developed system should be reproduced in a laboratory scale bioreactor where the conditions and different parameters could be controlled.

- Identification of apple extracts composition and polyphenolic profile in order to understand their influence on the final properties of the developed films and their antioxidant effect. In addition, migration or release tests of the antioxidants could be performed to analyze this effect on the packaging and packaged food.

- Development of different extraction routes for obtaining apple extracts without the use of solvents. Use of other techniques, for

example microwave assisted extraction or ultrasound assisted extraction.

8.3 LIST OF PUBLICATIONS AND COMMUNICATIONS

8.3.1 List of publications

Authors	Leire Urbina, Arantxa Eceiza, María Ángeles Corcuera, Aloña Retegi
Title	Stiff and hydrophobic nanopapers with antioxidant properties for food packaging applications
Journal	Under preparation
Year	2019

Authors	Leire Urbina, Ana Alonso, Arantxa Eceiza, María Ángeles Corcuera, Aloña Retegi
Title	Hybrid and biocompatible bacterial cellulose/waterborne polyurethane nanocomposites with water-activated shape memory properties
Journal	Materials and Design (Under review)
Year	2018
Impact factor	4.525
Rank	53/285 Materials science, multidisciplinary (JCR 2017)

Authors	Carlos del Cerro, Ana María Hernández-Arriaga, Leire Urbina, Arantxa Eceiza, María Auxiliadora Prieto
Title	Genome sequence and characterization of the bcs clusters for the production of nanocellulose from the low pH resistant strain Komagataeibacter medellinensis ID13488
Journal	Microbial Biotechnology (Under review)
Year	2018
Impact factor	3.913
Rank	33/161 Biotechnology & Applied Chemistry (JCR 2017) 34/126 Microbiology (JCR 2017)

Authors	Leire Urbina, Phavit Wongsirichot, María Ángeles Corcuera, Nagore Gabilondo, Arantxa Eceiza, James Winterburn, Aloña Retegi
Title	Application of cider by-products for medium chain length polyhydroxyalkanoate production by *Pseudomonas putida* KT2440
Journal	European Polymer Journal, 108, pp. 1-9
Year	2018
Impact factor	3.741 (JCR 2017)
Rank	12/87 Polymer Science (JCR 2017)

Authors	Leire Urbina, Olatz Guaresti, Jesús Requies, Nagore Gabilondo, Arantxa Eceiza, María Ángeles Corcuera, Aloña Retegi
Title	Design of reusable novel membranes based on bacterial cellulose and chitosan for the filtration of copper in wastewaters
Journal	Carbohydrate Polymers, 193, pp. 362-372
Year	2018
Impact factor	5.158 (JCR 2017)
Rank	2/71 Chemistry, Applied (JCR 2017) 6/57 Chemistry, Organic (JCR 2017) 7/87 Polymer Science (JCR 2017)

Authors	Leire Urbina, Ana María Hernández-Arriaga, Arantxa Eceiza, Nagore Gabilondo, María Ángeles Corcuera, María Auxiliadora Prieto, Aloña Retegi
Title	By-products of the cider production: an alternative source of nutrients to produce bacterial cellulose
Journal	Cellulose, 133-28, pp. 43669(1)-43669(10)
Year	2017
Impact factor	3.809 (JCR 2017)
Rank	1/21 Materials Science, Paper & Wood (JCR 2017) 1/24 Materials Science, Textiles (JCR 2017) 11/87 Polymer Science (JCR 2017)

Authors	Leire Urbina, Itxaso Algar, Clara García-Astrain, Nagore Gabilondo, Alba González, María Ángeles Corcuera, Arantxa Eceiza, Aloña Retegi
Title	Biodegradable composites with improved barrier properties and transparency from the impregnation of PLA to bacterial cellulose membranes
Journal	Journal of Applied Polymer Science, 24-5, pp. 2071-2082
Year	2016
Impact factor	1.86 (JCR 2016)
Rank	36/86 Polymer Science (JCR 2016)

8.3.2 List of communications

Authors	Leire Urbina, Phavit Wongsirichot, Tamara Calvo-Correas, María Ángeles Corcuera, Arantxa Eceiza, James Winterburn, Aloña Retegi
Title	Sustainable production of polyhydroxyalkanoates from cider waste
Congress	10th ECNP International Conference on Nanostructured Polymers and Compostites
Participation	Poster
Year	2018
Place	Donostia- San Sebastian, Spain

Authors	Leire Urbina, Gabriel Arner, Nagore Gabilondo, Arantxa Eceiza, María Ángeles Corcuera, Aloña Retegi

Title	Two different routes for the preparation of bacterial cellulose/chitosan filtration membranes for copper removal in wastewaters
Congress	8th World Congress on Biopolymers and Bioplastics
Participation	Oral presentation
Year	2018
Place	Berlin, Germany

Authors	Leire Urbina, Phavit Wongsirichot, María Ángeles Corcuera, Nagore Gabilondo, Arantxa Eceiza, James Winterburn, Aloña Retegi
Title	Sagardogintza hondakinen bideragarritasuna bioplastikoa lortzeko bakterioen hartziduraren bitartez
Congress	Materialen Zientzia eta Teknologia IV. Kongresua (MZT IV)
Participation	Poster
Year	2018
Place	Donostia-San Sebastian, Spain

Authors	Leire Urbina, Olatz Guaresti, Nagore Gabilondo, Arantxa Eceiza, María Ángeles Corcuera, Aloña Retegi
Title	Design of new membranes based on bacterial cellulose and chitosan for the filtration of heavy metals in water wastes

Congress	4th International Conference on Biobased Materials and Composites (ICBMC 2017)
Participation	Flash presentation and poster
Year	2017
Place	Nantes, France

Authors	Leire Urbina, Ana María Hernández-Arriaga, Arantxa Eceiza, Nagore Gabilondo, María Ángeles Corcuera, María Auxiliadora Prieto, Aloña Retegi
Title	Subproductos de la elaboración de la sidra: fuente de nutrientes alternativa para la producción de celulosa bacteriana
Congress	I Jornadas Doctorales de la UPV/EHU
Participation	Presentación oral y poster. Premio al mejor poster presentado en la sesión de Ingeniería y Arquitectura
Year	2016
Place	Bilbao, Spain

Authors	Leire Urbina, Ana María Hernández-Arriaga, Arantxa Eceiza, Nagore Gabilondo, María Ángeles Corcuera, María Auxiliadora Prieto, Aloña Retegi
Title	Valorization of cider industry wastes by means of their use in the biosynthesis of bacterial cellulose
Congress	15th International Symposium on Biopolymers (ISBP 2016)
Participation	Poster

Year	2016
Place	Madrid, Spain

Authors	Leire Urbina, Arantxa Eceiza, María Ángeles Corcuera, Aloña Retegi
Title	Balio erantsidun nanoerrefortzuak: sagardogintza hondakinen ustiapenetik lortutako zelulosa nanokristalak
Congress	Materialen Zientzia eta Teknologia III. Kongresua (MZT III)
Participation	Poster
Year	2016
Place	Markina-Xemein, Spain

Authors	Leire Urbina, María Auxiliadora Prieto, María Ángeles Corcuera, Nagore Gabilondo, Arantxa Eceiza, Aloña Retegi
Title	By-products of the cider production: a potential source of nutrients to produce bacterial cellulose
Congress	5th International Conference of Biobased and Biodegradable Polymers (BIOPOL 2015)
Participation	Poster
Year	2015
Place	Donostia-San Sebastian, Spain

Authors	Leire Urbina, Itxaso Algar, Alba González, Arantxa Eceiza, Nagore Gabilondo, María Ángeles Corcuera, Aloña Retegi

Title	Biodegradable composites with improved optical and barried properties from the impregntacion of PLA to bacterial cellulose membranes
Congress	3rd International Meeting on Material/Bioproduct Interaction (MATBIM 2015)
Participation	Poster
Year	2015
Place	Zaragoza, Spain

Authors	Leire Urbina, Itxaso Algar, Kizkitza González, Arantxa Eceiza, Aloña Retegi
Title	Bionanocomposites obtained from renewable resources
Congress	5th Workshop Green Chemistry and Nanotechnologies in Polymer Chemistry (Biopurfil 2014)
Participation	Poster
Year	2014
Place	Donostia-San Sebastian, Spain

Authors	Leire Urbina, Itxaso Algar, Kizkitza González, Arantxa Eceiza, Aloña Retegi
Title	Iturri berriztagarrietatik eratorriko bionanokonpositeak
Congress	Materialen Zientzia eta Teknologia II. Kongresua (MZT II)
Participation	Poster
Year	2014
Place	Donostia-San Sebastian, Spain

ANNEXES

LIST OF TABLES

Chapter 3: Bacterial cellulose biosynthesis

Chapter 4: Bacterial cellulose/chitosan membranes

Chapter 5: Bacterial cellulose/polyurethane nanocomposites

Chapter 6: Medium-chain-length polyhydroxyalkanoate biosynthesis

Chapter 7: Stiff and hydrophobic nanopapers with antioxidant capacity

LIST OF FIGURES

Chapter 1: Introduction

Chapter 2: Materials and characterization techniques

Chapter 3: Bacterial cellulose biosynthesis

Chapter 4: Bacterial cellulose/chitosan membranes

Chapter 5: Bacterial cellulose/polyurethane nanocomposites

LIST OF ABBREVIATIONS

BC	Bacterial cellulose
PHA	Polyhydroxyalkanoate
mcl-PHA polyhydroxyalkanoate	Medium-chain-length
scl-PHA	Short-chain-length polyhydroxyalkanoate
UDPGlc	Uridine diphosphoglucose
CNF	Cellulose nanofibers
CNC	Cellulose nanocrystals
BCNC	Bacterial cellulose nanocrystals
PEG	Polyethylene glicol
PVA	Poly(vinyl alcohol)
PHB	Poly(3-hydroxybutyrate)
AR	Apple residue
SC	Sugar cane
H-S	Hestrin and Schramm
Ch	Chitosan
MMW	Medium molecular weight
DD	Degree of deacetylation
EDTA	Ethylenediaminetetraacetic acid
WBPU	Waterborne polyurethane

DO	Dissolved oxygen
OD	Optical density
DCW	Dry cell weight
TN	Total nitrogen
GPC	Gel permeation chromatograpy
PI	Polydispersity index
GC-MS	Gas chromatograpy-mass spectrometry
XRD	X-ray diffraction
CI	Crystallinity index
PD	Polymerization degree
CED	Cupriethylendiamine
FTIR	Fourier transform infrared spectroscopy
^{1}H NMR	Proton nuclear magnetic resonance
^{13}C NMR	Carbon nuclear magnetic resonance
BET	Brunauer, Emmett and Teller
BHJ	Barrett-Joyner-Halenda
EA	Elemental analysis
CT	Conductiometric titration
UV-vis	Ultraviolet visible
O	Opacity
DSC	Differential scanning calorimetry

TGA	Thermogravimetric analysis
dTG	Derivative thermogravimetric curve
DMA	Dynamic mechanical analysis
WCA	Water contact angle
WHC	Water holding capacity
AFM	Atomic force microscopy
SEM	Scanning electron microscopy
OP	Oxygen permeability
PBS	Phosphate buffered saline
ppm	Parts per million
DPPH	2,2-Diphenyl-1-picrylhydrazyl
Trolox	6-Hydroxy-2,5,7,8-tetramethylchroman-2-carboxylic acid
TE	Trolox equivalents
FRAP	Ferric reducing antioxidant power
TPTZ	2,4,6-Tripyridyl-S-triazine
ABTS	2,2´-Azinobis(3-ethylbenzothiazoline-6-sulfonic acid
TPC	Total phenolic content
GA	Galic acid
K. medellinensis	*Komagataeibacter medellinensis*
CFUs	Colony forming units

A. xylinus	*Acetobacter xylinus*
SMPs	Shape memory polymers
DMF	N,N-Dimethylformamide
PLA	Poly(lactic acid)
NFC	Nanofibrillated cellulose
PVC	Polyvinyl chloride
HDPE	High-density polyethylene
P. putida	*Pseudomonas putida*
AW:W	Apple waste to water ratio
3HH	3-hydroxyhexanoate
3HO	3-hydroxyoctanoate
3HD	3-hydroxydecanoate
3HDD	3-hydroxydodecanoate
3HTD	3-hydroxytetradecenoate
AE	Acetonic extract
EE	Ethanolic extract
PCL	Polycaprolactone
PS	Polystyrene
PHVB	Poly(3-hydroxybutyrate-co-3-hydroxyvalerate)
PP	Polypropylene

LIST OF SYMBOLS

V	Volume
N	Normality
$\bar{M}_w$	Weight average molecular weight
$\bar{M}_n$	Number average molecular weight
λ	Wavelength
I	Intensity
$L_{h,k.l}$	Crystallite size
β	Width of half heigh of selected peak in X-ray
θ	Angle of incidence of the X-ray
k	Scherrer constant
σ	Surface tension
ϖ	Contact angle
η	Viscosity
K	Constant of Staudinger-Mark-Houwink equation
A	Area
Abs	Absorbance
T	Temperature
r	Radius

P	Pressure
W	Weight
q	Thickness
T_g	Glass transition temperature
T_m	Melting temperature
ΔH_m	Melting enthalpy
σ_{max}	Maximum stress
E	Young's modulus
ε_b	Elongation at break
E´	Storage modulus
Tanδ	Tangent of phase angle
C	Concentration
R (%)	Removal efficiency
φ_d	Folding angle
φ_1	Marginal recovery angle
φ_t	Angle change with time
φ_f	Fixing angle
t	Time
μ	Specific growth
X	Mass cells
Y	Yield coefficient

S	Substrate
L/D	Length/diameter

Bacterial derived biopolymers, i.e. bacterial polysaccharides, such as bacterial cellulose (BC) and bacterial polyesters, such as polyhydroxyalkanoates (PHAs) represent an important group of bipolymers with a wide range of applications. One of the major challenges to address in bacterial derived biopolymer technology is to find suitable carbon sources as substrates that are cheap and do not compete with food production for achieving large scale industrial applications.

In this work, by-products from cider production have been used as a cheap and sustainable carbon substrate for the biosynthesis of BC and PHAs. Additionally, the extraction of polyphenolic compounds from cider by-products has been performed to develop films with antioxidant properties. The obtained biopolymers have been characterized and used for the preparation of materials with tailored properties for specific applications in different fields.

The proposed approach would imply the integral use and valorization of cider by-products to obtain low-cost and environmentally-friendly materials for advanced applications.